Investigations and Modelling of Flank Modifications of Spur Gears by Pulsed Electrolytic Dissolution Process

Ph.D. Thesis

By

Vivek Rana

Department of Mechanical Engineering

Indian Institute of Technology Indore

May 2023

Investigations and Modelling of Flank Modifications of Spur Gears by Pulsed Electrolytic Dissolution Process

A Thesis

Submitted in partial fulfillment of the requirements for the award of the degree

of

DOCTOR OF PHILOSOPHY

By

Vivek Rana

(Roll No. 1806103001)

Department of Mechanical Engineering

Indian Institute of Technology Indore

May 2023

Indian Institute of Technology Indore

Candidate's Declaration

I hereby certify that the work which is being presented in the thesis entitled **Investigations and Modelling of Flank Modifications of Spur Gears by Pulsed Electrolytic Dissolution Process** in the partial fulfillment of the requirements for the award of the degree of **DOCTOR OF PHILOSOPHY** and submitted in the **Department of Mechanical Engineering, Indian Institute of Technology Indore**, is an authentic record of my own work carried out during the time period from **Aug 2018 to May 2023** under the supervision of **Prof. Neelesh Kumar Jain,** Department of Mechanical Engineering, IIT Indore and **Dr. Sunil Pathak,** Senior Researcher, Hilase Center, Czech Academy of Sciences, Praha and Assistant Professor, Czech Technical University, Praha

The matter presented in this thesis has not been submitted by me for the award of any other degree of this or any other institute.

Vivek Rana

Vivek Rana

This is to certify that the above statement made by the candidate is correct to the best of our knowledge.

18th May 2023	**18th May 2023**
(Prof. Neelesh Kumar Jain)	**(Dr. Sunil Pathak)**
Signature of thesis supervisor #1 with date	Signature of thesis supervisor #2 with date

----

Vivek Rana has successfully given his Ph.D. Oral Examination held on **4th September 2023**

4th Sep 2023	**4th Sep 2023**
(Prof. Neelesh Kumar Jain)	**(Dr. Sunil Pathak)**
Signature of thesis supervisor #1 with date	Signature of thesis supervisor #2 with date

----

Acknowledgement

First and foremost, I would like to thank my thesis supervisors **Prof. Neelesh Kumar Jain and Dr. Sunil Pathak** for providing me with the opportunity to complete my PhD thesis at **Indian Institute of Technology Indore**. As my supervisors, they have constantly forced me to remain focused towards achieving my goal. Their observations and comments helped me to establish the overall direction of the research and to move forward with investigation in depth. I am very grateful for their patience, motivation, enthusiasm, and immense knowledge in advanced machining processes and especially in Gear Engineering that taken together, make them as great mentors.

I express my deep gratitude to my PSPC members **Prof. Anand Parey** and **Dr. Eswara Prasad Korimilli** for their guidance and cooperation. I am grateful to the faculty members of the Department of Mechanical Engineering for providing the essential facilities and guidance. I want to thank past scholar of the Advance Manufacturing Processes Lab **Dr. Mayur Sawant, Dr. Pravin Kumar, Dr. Vishal Kharka** for sharing their knowledge and expertise during my entire research work. I would also like to thank and express my gratitude towards my fellow PhD students **Pankaj Kumar, Bhavesh Chaudhary and Pradyumn Kumar Arya** for motivating me and helping me during the tough phases of my research. I would also like to thank my all friends of IIT Indore for their help, company, and comments despite of their busy schedules. I am thankful to **the Sophisticated Instrumentation Center (SIC**), **Advanced Manufacturing Processes (AMP) Lab,** and **Central Workshop** of **IIT Indore**. I express my gratitude to **Prof. Anand Parey, Prof. Rajneesh Misra, Prof. Suman Mukhopadhyay** for providing various characterization and testing facilities. I am also thankful to Lab staff of Mechanical Engineering Labs and Central Workshop especially **Dr. Anand Petare**, **Sh. Deepak Rathore**, **Sh. Vinay Mishra, Sh. Santosh Sharma**, **Sh. Sandeep Gour, Sh. Rishiraj Chouhan**, **Sh. Satish Kaushal, Sh. Umakant Sharma, Sh. Pawan Chohuan, Sh. Deepak Dhepte, and Sh. Balkishan Vishwakarma** for their cooperation in fabrication of my experimental apparatus.

I express my sincere gratitude to **Department of Science and Technology, Govt. of India** for providing me the DST-INSPIRE fellowship (IF180641) to pursue my doctoral studies.

Vivek Rana

Dedicated

to

My Family and Friends

Abstract

Gears find wide applications in automobiles, aviation, railroad drives, marine transmissions, machine tools, construction equipment, agricultural machines, computer peripherals, helicopters, etc. Service life, functional performance, transmission efficiency, load-carrying capacity, and wear resistance of gear can be improved, its running noise and vibrations can be reduced, and the adverse effect of shaft misalignment can be mitigated by providing different flank modifications i.e., tip relief, root relief, end relief, profile crowning, and lead crowning to its flank surfaces. The intricate design of gears makes providing the above-mentioned flank modifications a challenging task. Researchers used conventional contact type processes such as gear hobbing, gear honing, gear grinding, gear skiving, and gear shaving to provide different gear flank modifications. In the present research, an innovative apparatus and five cathode gears were conceptualized and developed for non-contact flank modifications of anodic workpiece gear by the Pulsed Electrolytic Dissolution (PED) process and describe their imparting mechanisms. Continuous rotary motion was provided to the cathode gears. Constant reciprocating velocity was provided to anodic workpiece gear for its profile crowning, tip relieving, and root relieving, whereas lead crowning needed variable reciprocating velocity. No reciprocating velocity is required for end relieving. The intended functioning of the developed cathode gears was confirmed through experimental investigation. It revealed that the developed cathode gears not only provided the intended flank modification but also reduced flank surface roughness and completely removed the hob cutter marks and cracks from the flank surfaces of the modified spur gear. Imparted flank modifications are found to increase with voltage and modification duration. Root relieving required 20 minutes as modification duration, which is more than other flank modifications, which is 12 minutes. Analytical models for different flank modifications are developed and required to develop relation for the volume of material removed using Faraday's law of electrolysis, and some common assumptions were made in the development of analytical models. The developed analytical models for tip relief, root relief, end relief, and lead crowning were validated by conducting 12 experiments for each model (i.e., a total of 48 experiments) by varying applied voltage, pulse-on time, and pulse-off time at four levels each according to OFAT approach and 12 experiments to study effects of pulse-on time, pulse-off time, and applied voltage for profile crowning (PC) using OFAT approach were performed. The Comparative study of the functional performance parameters in terms of single flank roll testing, double flank roll testing, and measurement of noise and vibrations was done by comparing eight modified spur gears with unmodified gears. These spur gears were modified using innovatively developed five cathode gears and apparatus by imparting them four flank modifications (i.e., tip relief, end relief, profile crowning, lead crowning) individually and their four selected combinations. End relieved spur gear showed maximum reductions in noise and vibrations by 5 dBA and 3.77 $m/s^{2,}$ respectively for 1200 rpm speed at 5 N and 20 N load. The reduction in the amount of noise and vibrations of modified gears increases with rotary speed. Lead crowned gear showed maximum reductions of 146 μm in total transmission error, 109 μm in total composite error, and 102 μm in radial runout. End relieved gear showed maximum reductions of 37 μm in tooth-to-tooth and 139 μm longwave transmission errors. Tip relieved, and tip and root relieved gear showed a maximum reduction of 121 μm in tooth-to-tooth composite error.

This work proves that the developed non-contact process can effectively impart different flank modifications individually and their combinations to spur gears without any twist error. Lead crowning, end relieving, tip relieving, and tip and root relieving are the main flank modifications that significantly improve the functional performance characteristics of spur gears. It will result in enhanced operating performance and service life, which will help their manufacturers and end-users.

List of Patent and Publications

(A) Patent

1. **A Cathode Tool for Gear Tooth Flank Modification by Electrochemical Machining,** Inventors: Vivek Rana, Neelesh Kumar Jain, Sunil Pathak, Indian Patent Application No. 202221016570 [Filed on 24th March 2022; Published on 6th May 2022; First Examination Report (FER) filed on 21st Sep 2022]

(B) Published Journal Papers

1. **Vivek Rana,** Neelesh Kumar Jain, Sunil Pathak **(2023), "**Investigations on tip relieving of spur gears by non-contact process", **Materials and Manufacturing Processes,** https://doi.org/10.1080/10426914.2023.2176877 **(Impact Factor: 4.78)**
2. **Vivek Rana,** Neelesh Kumar Jain, Sunil Pathak **(2023),** "Improving functional performance characteristics of spur gears through flank modifications by non-contact advanced finishing process" **The International Journal of Advanced Manufacturing Technology,** 124, 5-6, 1787-1811, https://doi.org/10.1007/s00170-022-10566-9 **(Impact factor: 3.56)**
3. **Vivek Rana**, Anand Petare, Neelesh Kumar Jain, **(2023),** "Sound intensity analysis of straight bevel gears finished by using AFF process" **Manufacturing Technology Today**, 22(2), 42-29, https://doi.org/10.58368/MTT.22.2.2023.42-49
4. **Vivek Rana**, Anand Petare, Neelesh Kumar Jain, Anand Parey **(2022)**, "Using abrasive flow finishing process to reduce noise and vibrations of cylindrical and conical gears", **Proceedings IMechE, Part B: Journal of Engineering Manufacture,** 236(10), 1341-1354, https://doi.org/10.1177/09544054221075875 **(Impact Factor: 2.759)**

(C) Published Book Chapter

5. **Vivek Rana**, Anand C. Petare, Neelesh Kumar Jain **(2020) "Advances in Abrasive Flow Finishing"** Chapter 7 In *Advances in Abrasive Based Machining and Finishing Processes* (Editors: S. Das, G. Kibria, B. Doloi, B. Bhattacharyya), Springer, Cham, pp. 147-181, Print ISBN: 978-3-030-43311-6, **DOI:** https://doi.org/10.1007/978-3-030-43312-3_7, ebook ISBN: 978-3-030-43312-3,

(D) Publications from Collaborative Work

6. Bhavesh Chaudhary, Mahesh Patel, Neelesh Kumar Jain, Jayaprakash Muruges, **Vivek Rana (2023)** "Friction stir powder additive manufacturing of multi-track depositions of Al 6061 alloy for cladding and 3D printing applications" accepted in **JOM: The Journal of The Minerals, Metals & Materials Society (TMS) (Impact factor: 2.6)**
7. Vishal Kharka, **Vivek Rana**, Neelesh Kumar Jain, Kapil Gupta **(2022)** "Performance characteristics of spur gears hobbed under MQL, flood lubrication and dry lubrication environments" **Lubricants,** 10, Article ID: 230, https://doi.org/10.3390/lubricants10100230 **(Impact factor: 3.58)**

(E) Journal papers under review

8. **Vivek Rana,** Neelesh Kumar Jain, Sunil Pathak **(2023),** "Design and development of cathode gears for non-contact flank modification of spur gears" 1st revised version under review since Aug 2023 in **Materials and Manufacturing Processes,** (Manuscript ID: LMMP-2023-0849) **(Impact Factor: 4.78)**
9. **Vivek Rana,** Neelesh Kumar Jain, Sunil Pathak **(2023),** "Mathematical modelling and validation of twist-free lead crowning of spur gears by pulsed electrochemical flank modification process", 1st revised version under review since Sep 2023 in **The International Journal of Advanced Manufacturing Technology,** (Manuscript ID: JAMT-D-23-02423) (**Impact factor: 3.56)**
10. **Vivek Rana,** Neelesh Kumar Jain, Sunil Pathak **(2023),** "Development of analytical models for tip, root and end relieving of spur gears by pulsed electrochemical finishing process" **CIRP Journal of Manufacturing Science and Technology,** 2nd revised version under review since July 2023 in **(**Manuscript ID: CIRPJ-D-23-00122R2**)** **(Impact factor: 4.8)**

Table of Contents

Details	Page No.

List of Figures ………………………………………………………………... **xxi**

List of Tables …………………………………………………………………. **xxv**

Nomenclature……………………………………………………………………. **xxvii**

Abbreviations……………………………………………………………………. **xxxv**

Chapter 1: Introduction …………………………………………………….. **1-10**

1.1 Types of Gear Flank Modifications …………………………………….. 1

1.2 Flank Modifications Along Gear Profile ……………………………….. 2

1.2.1 Tip and Root Relief ……………………………………….................... 2

1.2.2 Profile Angle Modification …………………………………………….. 2

1.2.3 Profile Crowning …………………………………….......................... 3

1.3 Flank Modifications Along Gear Flank Surface ……………………….. 3

1.3.1 End Relief ……………………………………................................... 3

1.3.2 Helix Angle Modification ……………………………………………… 3

1.3.3 Flank or Lead Crowning ……………………………………............... 3

1.3.4 Triangular End Reliefs ………………………………………………… 3

1.3.5 Flank Twist ……………………………………................................... 4

1.4 Gear Flank Modifications by Contact Type Processes …………………. 4

1.4.1 Flank Modifications by Gear Grinding …………………………………. 4

1.4.2 Flank Modifications by Gear Shaving …………………………….…. 6

1.4.3 Flank Modifications by Gear Honing ………………………………… 7

1.4.4 Flank Modifications by Gear Skiving ……………………………….... 7

1.4.5 Flank Modifications by Gear Hobbing ……………………………….. 8

1.5 Gear Flank Modifications by Non-Contact Type Process ……………… 8

1.5.1 Advantages of Electrolytic Dissolution Process……………………….. 9

1.5.2 Disadvantages of Electrolytic Dissolution Process…………….......... 9

1.6 Organization of the Thesis ……………………………………………… 9

Chapter 2: Review of Past Works and Research Objectives ………………. 11-20
2.1 Past Work on Gear Flank Modifications by Contact Type Processes …... 11
2.1.1 Past Work on Flank Modifications by Gear Grinding …………………… 11
2.1.2 Past Work on Flank Modifications by Gear Shaving ………………….... 12
2.1.3 Past Work on Flank Modifications by Gear Honing …………………..... 12
2.1.4 Past Work on Flank Modifications by Gear Skiving …………………… 16
2.1.5 Past Work on Flank Modifications by Gear Hobbing …………………… 16
2.2 Past Work on Non-Contact Flank Modifications of Gears ……………... 16
2.3 Past Work on Effects of Flank Modifications on Gear Performance …… 17
2.4 Identified Research Gaps ……………………………………………….. 17
2.5 Research Objectives …………………………………………………….... 18
2.6 Research Methodology …………………………………………………... 18
Chapter 3: Development of Apparatus and Cathode Gears ………………... 21-39
3.1 Development of Apparatus for Non-Contact Flank Modification ………. 21
3.1.1 Flank Modification Chamber …………………………………………… 24
3.1.2 Drive System for Anodic Workpiece Gear and Cathode Gear …………... 24
3.1.3 Power Supply System …………………………………………………… 24
3.1.4 Electrolyte Supply and Recycling System ……………………………….. 24
3.2 Development of Cathode Gears and their Flank Modification Mechanisms 25
3.2.1 Cathode Gear for Tip Relief ……………………………………………… 27
3.2.2 Cathode Gear for Root Relief …………………………………………… 29
3.2.3 Cathode Gear for End Relief …………………………………………… 31
3.2.4 Cathode Gear for Profile Crowning ………………………………....... 32
3.2.5 Cathode Gear for Lead Crowning …………………………………….. 34
3.3 Development of Single Flank Roll Tester ………………………………. 36
3.4 Specifications and Material of Workpiece Gear ………………………… 39

Chapter 4: Development of Analytical Models for Flank Modifications ….. 41-63
4.1 Assumptions ………………………………………………………………... 41
4.2 Development of Model for Tip Relief ……………………………………... 41
4.2.1 Volumetric MRR during Tip Relieving ………………………………….. 42
4.2.2 Effects of Continuous Reciprocation of Workpiece Gear and Pulsed DC Power Supply ………………………………………………………………… 44
4.2.3 Analytical Model for Tip Relief ………………………………………... 46
4.3 Development of Model for Root relief …………………………………….. 48
4.3.1 Volumetric MRR during Root Relieving …... 49
4.3.2 Analytical Model for Root Relief ………………………………………... 50
4.4 Development of Model for End Relief ……………………………………... 52
4.4.1 Volumetric MRR During End Relieving…………………………………. 54
4.4.2 Analytical Model for End Relief …………………………………………. 55
4.5 Development of Model for Lead Crowning ………………………………... 55
4.5.1 Volumetric MRR During Lead Crowning ………………………………. 56
4.5.2 Effects of Variable Reciprocation of Workpiece Gear and Pulsed DC Power Supply …………………………………………………………….. 57
4.5.3 Analytical Model for Lead Crowning …………………………………….. 62
Chapter 5: Experimentation ……………………………………………… 65-74
5.1 Planning and Design of Experiments ……………………………………… 65
5.2.1 Stage-1 Experiments: Confirm Functioning of the Developed Cathode Gears and Apparatus …………………………………………………………. 65
5.2.2 Stage-2 Experiments: Effects of PED Process Parameters on Tip Relief 66
5.2.3 Stage-3a Experiments: Validation of the Developed Analytical Models and Effects of PED Process Parameters on Profile Crowning 66
5.2.4 Stage-3b Experiments: Effects of Workpiece Gear Material Hardness …... 67
5.3 Evaluation of the Responses ………………………………………………… 68
5.3.1 Measurement of Flank Modification Value ……………………………… 68
5.3.2 Measurement of Volumetric MRR ……………………………………….. 69
5.3.3 Measurement of Roughness of Workpiece Gear Flank Surfaces ………… 69
5.3.4 Evaluation of Morphology of Workpiece Gear Flank Surfaces …………... 69
5.4 Stage 4 Experiments: Comparative Study of Functional Performance Parameters of Flank Modified and Unmodified Workpiece Gears ……………... 70
5.4.1 Evaluation of Parameters from Single Flank Roll Testing ……………… 71
5.4.2 Evaluation of Parameters from Double Flank Roll Testing ……………… 71
5.4.3 Measurement of Running Noise and Vibrations ………………………….. 73

Chapter 6: Results and Analysis …………………………………………… **75-131**
6.1 Functioning Confirmation of Developed Cathode Gears and Apparatus … 75
6.2 Effects of PED Process Parameters on Tip Relief …………….................. 84
6.3 Validation of the Developed Analytical Models ………………………… 91
6.4 Effects of PED Parameters on Profile Crowing ……………………….. 99
6.5 Analysis of Surface Roughness and Morphology ……………............. 101
6.6 Effects of Workpiece Gear Material Hardness …………………………… 108
6.7 Comparative Study of Functional Performance Parameters of Flank Modified and Unmodified Workpiece Gears ………………………………………. 110
6.7.1 Analysis of Single Flank Roll Testing Results …………………………… 110
6.7.2 Analysis of Double Flank Roll Testing Results ………………………... 115
6.7.3 Analysis of Running Noise and Vibrations ……………………………….. 120
Chapter 7: Conclusions and Scope for the Future Work …………………… **133-137**
7.1 Significant Achievements ……………………………………………… 133
7.2 Conclusions ………………………………………………………………. 133
7.2.1 Developed Cathode Gears and Apparatus ………………………………… 133
7.2.2 Parametric Study for Tip Relief and Profile Crowning ………………….. 134
7.2.3 Developed Analytical Models …………………….............................. 134
7.2.4 Surface Finish and Morphology ……………………………................... 135
7.2.5 Influence of Workpiece Gear Material Hardness ……………………….. 135
7.2.6 Comparative Study of Functional Performance Parameters …………….. 136
7.3 Directions for the Future Work ……………………………………….... 137
References **……………………………………………………………………...** **139-143**
Appendix-A: Spur Gear Geometry Relations Used in Development of Analytical Models for Tip/Root/End Relief and Lead Crowning ……………… **145-152**
A1: Geometry Relations Used in Developing Analytical Model for Tip Relief …… 145
A2: Geometry Relation Used in Developing Analytical Model for Root Relief …… 147
A3: Geometry Relations Used in Developing Analytical Model for End Relief …... 149
A4: Expressions for Lead Crowning Time at Different Positions of the Anodic Workpiece Gear During its Downward/Upward Reciprocating Motion ……… 150

Appendix-B: Results of Microgeometry Measurement ………………………….. **153-174**

B1: For Validation of the Developed Analytical Model for Tip Relief …………….. 153

B2: For Validation of the Developed Analytical Model for Root Relief …………… 157

B3: For Validation of the Developed Analytical Model for End Relief ……………. 161

B4: For Validation of the Developed Analytical Model for Lead Crowning ………. 165

B5: For Effects of PED Process Parameters on Profile Crowning …………………. 169

B6: For Effects of Workpiece Gear Material Hardness …………………………….. 173

Appendix-C: Details of the Equipment Used in Evaluation of the Responses….. **175**

Appendix-D: Arduino Code for Single Flank Roll Testing ……………………. **181**

List of Figures

Figure Number and Captions

Figure Number and Captions	Page No.
Fig. 1.1: Benefits of flank modifications of a gear.	1
Fig. 1.2: Different types of flank modifications of a gear **(ISO 21771)**.	2
Fig. 1.3: Schematic showing concept of different types of gear flank modifications: (a) Tip and root relief, (b) Profile angle modification, (c) Profile crowning, (d) End relief, (e) Helix angle modification, (f) Lead crowning, (g) Triangular end relief, and (h) Flank twist.	2
Fig. 1.4: Schematic of helical gear flank modifications by form grinding process using 5-axis CNC machine.	5
Fig. 1.5: Gear flank modifications by generative gear grinding using dish-shaped wheels: (a) 15/20° position for imparting tip and root relief, and (b) 0° position to impart lead crowning.	6
Fig. 1.6: Schematic of helical gear flank modifications by gear shaving process: (a) meshing of shaving cutter and workpiece gear, and (b) auxiliary mechanism to provide lead crowning (Hsu et *al.*, 2019).	7
Fig. 1.7: Schematic of helical gear flank modifications by external gear honing process.	7
Fig. 1.8: Schematic of flank modifications of an internal gear by gear skiving process.	8
Fig. 1.9: Schematic of spur gear flank modification by hobbing process.	8
Fig. 2.1: Flow chart for past work on flank modification of gears.	11
Fig. 2.2: Flow chart of the research methodology used in the present work to achieve the identified research objectives.	19
Fig. 3.1: Apparatus developed for flank modification of a workpiece gear by pulsed electrolytic dissolution process: (a) schematic, (b) photograph of apparatus, and (c) photograph of flank modification chamber showing relative positioning of the developed cathode gears and workpiece gear.	22
Fig. 3.2 Electrical connection between power supply and shafts mounting workpiece and cathode gears through carbon brush.	25
Fig. 3.3: Manufacturing processes used for different portions of cathode gear for tip relief.	27
Fig. 3.4: Developed cathode gear *for non-contact tip relieving* of an anodic workpiece gear and its imparting mechanism: (a) schematic diagram, (b) photograph, (c) design details of its single tooth, (d) minimum IEG at start of meshing of left-flank tip of anodic workpiece gear tooth with non-conductive portion of cathode gear tooth, (e) new position of IEG after slight rotation of gears, (f) left-flank tip of anodic workpiece gear tooth disengaging with the non-conductive portion of the cathode gear.	29
Fig. 3.5: Developed cathode gear for *non-contact root relieving* of a anodic workpiece gear and its mechanism: (a) schematic diagram, (b) photograph, (c) design details of its single tooth, (d) occurrence of minimum IEG outside the base circle at the start of meshing of right-flank of the workpiece gear with tip of non-conductive portion of the cathode gear, (e) new position of IEG after slight rotation of gears, (f) disengagement of right-flank of workpiece gear tooth from tip of non-conductive portion of the cathode gear tooth.	30
Fig. 3.6: Developed cathode gear for *non-contact end relieving* of an anodic workpiece gear by PED process: (a) schematic of engagement of cathode and anode gears along with enlarged view of their teeth meshing, (b) schematic of cathode gear, (c) photograph of developed cathode gear.	32
Fig. 3.7: Developed cathode gear for *non-contact profile crowning* of a anodic workpiece gear and its mechanism: (a) schematic diagram, (b) photograph, (c) design of its single tooth, (d) minimum IEG at start of meshing of right-flank root of anodic workpiece gear	34

tooth with tip of non-conductive portion of cathode gear, (e) increase in IEG from addendum circle to pitch circle of the cathode gear, (f) decrease in IEG from pitch circle to base circle diameter of cathode gear, (g) right-flank tip of anodic workpiece gear disengaging with non-conductive portion of cathode gear.

Fig. 3.8: Developed cathode gear for non-contact *lead crowning* of an anodic workpiece gear and its mechanism: (a) schematic diagram, (b) photograph, (c) design details of its single tooth, (d) anodic workpiece gear starts moving downward when the bottom end of face width of anodic workpiece gear is above conductive portion of the cathode gear, (e) anodic workpiece gear meshing conductive portion of the cathode gear at midpoints of their face widths, (f) top end of face width of anodic workpiece gear reaches below conductive portion of the cathode gear, (g) variation in reciprocating velocity of anodic workpiece gear with distance travelled. 36

Fig. 3.9: Schematic of working principle of single flank roll testing. 37

Fig. 3.10: Developed single flank roll tester: (a) Photograph, and (b) its sample results. 38

Fig. 3.11: CAD drawing of workpiece gear and its specifications. 39

Fig. 4.1: Non-contact *tip relieving* of anodic workpiece gear by PED process: (a) schematic of meshing with the developed cathode gear, and (b) instantaneous area of anodic workpiece gear tooth *'A_{ttr}'* that will be modified by conductive portion of the developed cathode gear. 42

Fig. 4.2: Variation of fraction of total face width *'b(t)'* of anodic workpiece gear tooth while meshing with conductive portion of the cathode gear during its reciprocating motion: (a) different meshing positions, and (b) trapezium shaped variation of *'b(t)'* with time, and (c) concept of pulsed DC power superimposed with trapezium shaped variation of '*b(t)'*. 45

Fig. 4.3: Effect of non-contact *tip relieving* by the PED process on flank surface of anodic workpiece gear tooth: (a) change in its involute profile, (b) enlarged view used to compute area of *GEHG,* and (c) volume of material removed. 47

Fig. 4.4: *Non-contact root relieving* of anodic workpiece gear by PED process: (a) schematic of meshing with the developed cathode gear, and (b) instantaneous area of anodic workpiece gear tooth *'A_{trr}'* that will be modified by conductive portion of the developed cathode gear. 49

Fig. 4.5: Effect of non-contact *root relieving* by the PED process on flank surface of anodic workpiece gear tooth: (a) change in its involute profile, (b) enlarged view used to compute area of *RQAR,* and (c) volume of material removed. 51

Fig. 4.6: Non-contact *end relieving* of anodic workpiece gear by PED process: (a) schematic of meshing with the developed cathode gear, (b) instantaneous area of anodic workpiece gear tooth which will be modified *'A_{ter}'*, and (c) volume of material removed from one end of anodic workpiece gear tooth. 53

Fig. 4.7: Non-contact *lead crowning* of anodic workpiece gear by PED process: (a) schematic of meshing with the developed cathode gear, (b) instantaneous area of anodic workpiece gear tooth which will be modified *'A_{tlc}'*. 56

Fig. 4.8: Sequence of events in non-contact *lead crowning* of anodic workpiece gear by PED process: (a) relative position of workpiece gear face width with respect to conducting portion of the cathode gear, (b) change in reciprocating velocity of workpiece gear with the distance travelled by it, (c) change in fraction of total face width of workpiece gear *'b(t)'* with lead crowing time *'t'*, (d) combined effect of change *b(t)'* and use of pulsed DC power. 59

Fig. 4.9: Volume of material removed in lead crowning of anodic workpiece gear by PED process: (a) single tooth, (b) top land geometry of lead crown gear, and (c) shape of lead crowning. 63

Fig. 5.1 Measurement of value of flank modification on CNC gear metrology machine. 69

Fig. 5.2: Direction of trace for measurement of surface roughness parameters. 70
Fig. 5.3: Double flank roll testing of cylindrical gears: (a) photograph of in-house developed apparatus; and (b) its sample results. 72
Fig. 5.4: Photograph of the test-rig used for measurement of noise and vibrations of unmodified and flank modified workpiece gears. 74
Fig. 6.1: Photographs of anodic workpiece gear (a) before any flank modification i.e., unmodified, (b) after tip relieving, (c) after root relieving, (d) after end relieving, (e) after lead crowning, and (f) after profile crowning. 76
Fig. 6.2: Charts for anodic workpiece gear showing its microgeometry along profile direction: ($\mathbf{a_1}$ and $\mathbf{a_2}$) before and after its tip relieving, ($\mathbf{b_1}$ and $\mathbf{b_2}$) before and after its root relieving, and ($\mathbf{c_1}$ and $\mathbf{c_2}$) before and after profile crowning; and microgeometry charts for anodic workpiece along its lead direction ($\mathbf{d_1}$ and $\mathbf{d_2}$) before and after its end relieving, and ($\mathbf{e_1}$ and $\mathbf{e_2}$) before and after its lead crowning. 81
Fig. 6.3: Concept for different types of tips, roots, and profile of a hobbed spur gear: (a) negative tip, (b) positive tip, (c) both negative and positive tip, (d) negative root, (e) positive root, (f) both negative and positive root, and (g) negative and positive involute profile. 83
Fig. 6.4: Change in the imparted average values of tip and root relief and their associated volumetric material removal rate (MRR) with the modification duration. 84
Fig. 6.5: Change in value of tip relief provided to workpiece spur gear and associated volumetric material removal rate with (a) tip relieving duration, (b) electrolyte concentration, (c) electrolyte temperature, (d) electrolyte flow rate, and (e) rotational speed of cathode gear. 87
Fig. 6.6: Change in percentage reduction in surface roughness parameters with (a) modification duration, (b) electrolyte concentration, (c) electrolyte temperature, (d) electrolyte flow rate, and (e) rotational speed of cathode gear. 89
Fig. 6.7: Measurement of overvoltage: (a) Photograph of electrochemical cell with the working, reference, and counter/auxiliary electrodes dip in the electrolyte solution, and (b) Tafel curve used to obtain the value of overvoltage. 93
Fig. 6.8: An illustration of measurement of pulse form and actual values of pulse-on and pulse-off times supplied to the PED process during tip, root, end relieving, and lead crowning of anodic workpiece gear. 94
Fig. 6.9: Change in analytical model predicted and experimental values of tip relief, root relief, end relief, and lead crowning with (a) applied voltage, (b) pulse-on time, and (c) pulse-off time. 98
Fig. 6.10: Topography of flank surface of anodic workpiece gear corresponding to Exp No. 3 in Table 6.5: (a) before its lead crowning i.e., unmodified or hobbed condition, (b) after its twist-free lead crowning by the developed cathode gear and apparatus through PED process. 99
Fig. 6.11: Change in values of profile crowning of workpiece spur gear and associated volumetric MRR with the applied voltage, pulse-on time, and pulse-off time. 101
Fig. 6.12: Surface roughness profiles of left and right flanks of anodic workpiece gear before and after lead crowning by the PED process (Exp. No. 4 in Table 6.7) for randomly chosen (a) tooth no.1, and (b) tooth no. 2. 104
Fig. 6.13: Change in experimental values of percentage reductions in maximum height *'PRRy'* and in arithmetical average roughness *'PRRa'* of tip relieved, root relieved, end relieved, profile crowned, and lead crowned anodic workpiece gear by the PED process with (a) applied voltage, (b) pulse-on time, and (c) pulse-off time. 105
Fig. 6.14: Surface morphology of a workpiece gear flank surfaces: (a) before any flank modification, and after its (b) tip relieving (corresponding to Exp. No. 6 in Table 6.7), (c) root relieving (corresponding to Exp. No. 10 in Table 6.7), (d) end relieving (corresponding 107

to Exp. No. 10 in Table 6.7), (e) profile crowning (corresponding to Exp. No. 6 in Table 6.7), and (f) lead crowning (corresponding to Exp. No. 7 in Table 6.7).

Fig. 6.15: Results of single flank roll testing for workpiece spur gear: (a_1) left flank (LF) and (a_2) right flank (RF) of workpiece spur gear before any flank modification i.e., unmodified gear, (b_1) LF and (b_2) RF of tip relieved gear, (c_1) LF and (c_2) RF of end relieved gear, (d_1) LF and (d_2) RF of lead crowned gear, (e_1) LF and (e_2) RF of profile crowned gear, (f_1) LF and (f_2) RF of tip and root relieved gear, (g_1) LF and (g_2) RF of tip and end relieved gear, (h_1) LF and (h_2) RF of tip, root, end relieved gear, and (i_1) LF and (i_2) RF of profile and lead crowned gear. 113

Fig. 6.16: Results of double flank roll testing of workpiece spur gear: (a) before any flank modification, and after imparting it: (b) tip relief, (c) end relief, (d) lead crowning, (e) profile crowning, (f) tip and root relief, (g) tip and end relief, and (h) tip, root, and end relief, and (i) profile and lead crowning. 118

Fig. 6.17: Example of time domain signal in frequency domain using FFT for obtaining the value of vibration at gear mesh frequency (GMF) at 1200 rpm and 20 N applied load for workpiece gear with: (a) unmodified, (b) tip relief, (c) end relief, (d) lead crowning, (e) profile crowning, (f) tip and root relief, (g) tip and end relief, and (h) tip, root, and end relief, and (i) profile and lead crowning. 122

Fig. 6.18: Variation in sound pressure levels of unmodified and 8 modified workpiece gears with applied load for test gear speed of (a) 300 rpm, (b) 600 rpm, (c) 900 rpm, and (d) 1200 rpm. 127

Fig. 6.19: Variation in RMS value of vibrations of unmodified and 8 modified workpiece spur gears with applied load for workpiece gear speed of (a) 300 rpm, (b) 600 rpm, (c) 900 rpm, and (d) 1200 rpm. 128

Fig. 6.20: Variation in values vibrations of unmodified and 8 modified workpiece spur gears with applied load at GMF for test gear speed of (a) 300 rpm, (b) 600 rpm, (c) 900 rpm, and (d) 1200 rpm. 129

List of Tables

Table Number and Captions — Page No.

Table 1.1: Capabilities and limitations of conventional contact-type processes for gear flank modifications **(Jain and Petare, 2017).** 4

Table 2.1: Summary of the past work on gear flank modifications by contact type processes. 13

Table 2.2: Details of research methodology and experiments used to meet research objectives of the present work. 20

Table 3.1: Functions and specifications of different components used in the apparatus. 23

Table 3.2: Details of the materials selected for different components of the apparatus along with their selection criteria. 25

Table 3.3 Specifications of the developed five cathode gears for non-contact flank modifications of anodic spur gear. 26

Table 3.4: Specifications of the components used in development of single flank roll tester. 37

Table 4.1: Expressions for different time instants in downward and upward stroke of anodic workpiece gear in its non-contact tip or root relieving by PED process. 45

Table 4.2: Expressions for lead crowning time at different positions of the anodic workpiece gear during its downward/upward reciprocating motion in its non-contact lead crowning by PED process. 61

Table 5.1: Values of fixed and variable parameters used in studying the effects of PED process parameters on non-contact tip relieving of the workpiece spur gear. 66

Table 5.2: Values of fixed and variable parameters used in validation of the developed analytical models. 67

Table 5.3: Values of PED process parameters used in studying the effects of hardness of workpiece gear material. 68

Table 5.4: Values of variable parameters of PED process used in imparting different flank modifications and their combinations to workpiece spur gear. 71

Table 6.1: Results of experiments performed to confirm functioning of the developed cathode gears and apparatus for non-contact flank modifications of spur gears by the PED process. 75

Table 6.2: Average value of tip relief, material removal rate, and surface roughness parameters for different parametric combinations of the PED process. 85

Table 6.3: Values of different constant parameters used in the developed analytical models to predict the values of tip, root, end relief, and lead crowning imparted to workpiece gear. 92

Table 6.4: Programmed and measured values of pulse-on time and pulse-off time and used for validations of the developed analytical models. 94

Table 6.5: Model predicted and experimental values of imparted tip relief, root relief, end relief, and lead crowning and their associated volumetric MRR, and variable input parameters for the validation experiments of the developed analytical models. 97

Table 6.6: Average value of profile crowning and MRR for different parametric combinations of the PED process. 100

Table 6.7: Average values of arithmetical average roughness *'Ra'*, maximum height 102

'Ry', and their % reductions *'PRRa' and 'PRRy'* obtained during tip, root, end relieving, and profile, lead crowning of anodic workpiece gear by PED process for different parametric combinations.

Table 6.8: Values of different flank modifications, volumetric MRR, and surface roughness parameters for unhardened and hardened workpiece gears for different parameters of the PED process. 109

Table 6.9: Average values of different flank modifications of the workpiece gears obtained after PED process. 110

Table 6.10: Parameters obtained for unmodified and flank modified workpiece spur gears from graphs of their single flank roll testing [LF: left flank; RF: right flank]. 113

Table 6.11: Parameters obtained for unmodified and flank modified workpiece spur gears from graphs of their double flank roll testing. 118

Table 6.12: Sound pressure level for unmodified and different modified workpiece gears for different rotational speed and applied load. 123

Table 6.13: RMS values of vibrations for the unmodified and different modified workpiece gears for different rotational speed and applied load. 124

Table 6.14: Values of vibrations for unmodified and different modified workpiece gears at gear mesh frequency (GMF) for different rotational speed and applied load. 125

Nomenclature

a_1 Acceleration of anodic workpiece gear during first half of its downward or upward stroke (mm/s^2);

a_2 Deceleration of anodic workpiece gear during second half of its downward or upward stroke (mm/s^2);

A_{er} Area of involute profiles of two consecutive flank surfaces of two adjacent teeth of anodic workpiece gear which will be modified in end relieving (mm^2);

A_{ner} Area of non-involute profiles or roots of two consecutive flank surfaces of two adjacent teeth of anodic workpiece gear which will be modified in end relieving (mm^2);

A_{tler} Area of top land of anodic workpiece gear tooth which will be modified in end relieving (mm^2);

A_{ter} Instantaneous area of anodic workpiece gear tooth which will be modified during end relieving (mm^2). It is equal to $A_{er} + A_{ner} + A_{tler}$;

A_{nrr} Area of non-involute profiles or roots of two consecutive flank surfaces of two adjacent teeth of anodic workpiece gear which will be modified in root relieving (mm^2);

A_{rr} Area of involute profile of anodic workpiece gear flank surface which will be modified in root relieving (mm^2);

A_{trr} Instantaneous area of anodic workpiece gear tooth which will be modified by the conductive portion of the designed cathode gear during root relieving (mm^2). It is equal to $A_{nrr} + A_{rr}$;

A_{lc} Area of involute profile of one flank surface of anodic workpiece gear tooth affected during its lead crowning (mm^2);

A_{nlc} Area of non-involute profile of one flank surface of anodic workpiece gear tooth affected during its lead crowning (mm^2);

A_{tllc} Area of top land of one tooth of anodic workpiece gear tooth affected during its lead crowning (mm^2);

A_{tlc} Instantaneous area of one flank surface of anodic workpiece gear tooth was affected during its lead crowning (mm^2). It is equal to $A_{lc} + A_{nlc} + A_{tllc}$;

A_{tr} Area of involute profiles of two consecutive flank surfaces of two adjacent teeth of anodic workpiece gear which will be modified in tip relieving (mm^2);

A_{tltr} Top land area of anodic workpiece gear tooth which will be modified in tip relieving (mm^2);

A_{ttr} Instantaneous area of anodic workpiece gear tooth which will be modified by the conductive portion of the designed cathode gear during tip relieving (mm^2). It is equal to $A_{tr} + A_{tltr}$;

$b(t)$ Fraction of total face width of anodic workpiece gear meshing with conducting portion of the cathode gear developed for tip or root relieving or lead crowning (mm);

b_t Total face width of anodic workpiece gear (mm);

b_{ccg} Face width of conductive portion of developed cathode gear for tip/root/end relief or lead crowning(mm);

b_{ncg} Face width of non-conductive portion of developed cathode gear for tip/root/end relief or lead crowning(mm);

c_l Area correction factor for involute profile of one flank surface of anodic workpiece gear tooth modified during its lead crowning;

C_{ft} Value of root relief imparted to anodic workpiece gear flank surface (mm);

$C_{\alpha a}$ Value of tip relief imparted to anodic workpiece gear flank surface (mm);

$C_{\alpha t}$ Value of tip relief imparted to anodic workpiece gear tooth along its top land (mm);

$C_{\beta b}$ Value of end relief imparted to bottom/back end of anodic workpiece gear flank surface (mm);

$C_{\beta t}$ Value of End relief imparted to top/front end of anodic workpiece gear flank surface (mm);

C_{β} Value of lead crowning imparted to anodic workpiece gear flank surface (mm);

d_a Addendum circle diameter of cathode gear (mm);

d_b Base circle diameter of cathode gear (mm);

d_p Pitch circle diameter of cathode gear (mm);

d_{pr1} Conductive portion diameter of the cathode gear (greater than pitch circle diameter) designed for profile crowning (mm);

d_{pr2} Conductive portion diameter of the cathode gear (less than pitch circle diameter) designed for profile crowning (mm);

d_{tr} Conductive portion diameter of the cathode gear developed for tip relief (mm);

d_{rr} Electrical insulation tip diameter of cathode gear developed for root relief (mm);

E Electrochemical equivalent of anodic workpiece gear (g);

F Faraday's constant (=96,500 Coulomb);

F_i' Total transmission error (μm);

f_i' Tooth-to-tooth transmission error (μm);

F_l' Total longwave transmission error (μm);

F_i'' Total composite error (μm);

f_i'' Tooth-to-tooth composite error (μm);

F_{rf}'' Radial runout (μm);

i Stroke number of anodic workpiece gear in tip/root relieving;

j Current density (A/mm^2) in the PED process;

L_{erb} Length of end relief imparted to bottom/back end of anodic workpiece gear flank surface (mm);

L_{ert} Length of end relief imparted to top/front end of anodic workpiece gear flank surface (mm);

L_{er} Involute profile arc length of anodic workpiece gear flank surface which will be modified in end relieving (mm);

L_{rr} Involute profile arc length of anodic workpiece gear flank surface which will be modified in root relieving (mm);

L_{tr} Involute profile arc length of anodic workpiece gear flank surface which will be modified in tip relieving (mm);

L_{rf} Arc length of root fillet anodic workpiece gear which will be modified in root/end relieving (mm);

L_{lc} Arc length of involute profile of one flank surface of anodic workpiece gear which will be modified in lead crowning (mm);

L_r Arc length of non-involute profile of one flank surface of anodic workpiece gear which will be modified in lead crowning (mm);

m Module of anodic workpiece gear and cathode gear (mm);

M_{er} Volumetric material removal rate (MRR) during end relieving of anodic workpiece gear teeth (mm^3/s);

M_{rr} Volumetric MRR in root relieving of anodic workpiece gear teeth (mm^3/s);

M_{lc} Volumetric MRR in lead crowning of anodic workpiece gear teeth (mm^3/s);

M_{tr} Volumetric MRR in tip relieving of anodic workpiece gear teeth (mm^3/s);

N Number of reciprocation cycles of anodic workpiece gear;

n Reciprocation stroke number of anodic workpiece gear having its values as 1, 2, 3, .., t_{lc}/t_s in lead crowning;

Q_{er} Volume of material removed from flank surfaces of anodic workpiece gear teeth in end relieving (mm^3);

Q_{ner} Volume of material removed from non-involute profiles or roots of anodic workpiece gear teeth in end relieving (mm^3);

Q_{tler} Volume of material removed from top lands of anodic workpiece gear teeth in end relieving (mm^3);

Q_{ter} Total volume of material removed from anodic workpiece gear teeth in end relieving (mm^3) i.e., $Q_{ter} = Q_{er} + Q_{ner} + Q_{tler}$;

Q_{rr} Volume of material removed from flank surfaces of anodic workpiece gear teeth in root relieving (mm^3);

Q_{nrr} Volume of material removed from non-involute profiles of anodic workpiece gear teeth in root relieving (mm^3);

Q_{lc} Total volume of material removed from flank surfaces of anodic workpiece gear teeth in lead crowning (mm^3);

Q_{nlc} Total volume of material removed from non-involute profiles of anodic workpiece gear teeth in lead crowning (mm^3);

Q_{tllc} Total volume of material removed from top lands of anodic workpiece gear teeth in lead crowning (mm^3);

Q_{tlc} Total volume of material removed in lead crowning of anodic workpiece gear (mm^3) i.e., $Q_{tlc} = Q_{lc} + Q_{nlc} + Q_{tllc}$;

Q_{trr} Total volume of material removed from anodic workpiece gear teeth in root relieving (mm^3) i.e., $Q_{trr} = Q_{rr} + Q_{nrr}$;

Q_{tr} Volume of material removed from flank surfaces of anodic workpiece gear teeth in tip relieving (mm^3);

Q_{tltr} Volume of material removed from top lands of anodic workpiece gear teeth in tip relieving (mm^3);

Q_{ttr} Total volume of material removed from anodic workpiece gear teeth in tip relieving (mm^3) i.e., $Q_{ttr} = Q_{tltr} + Q_{tr}$;

r_a Addendum circle radius of anodic workpiece gear (mm);

r_b Base circle radius of anodic workpiece gear (mm);

r_d Dedendum circle radius of anodic workpiece gear (mm);

r_p Pitch circle radius of anodic workpiece gear (mm);

r_{rf} Root fillet radius of anodic workpiece gear (mm);

r_{rr} Datum circle radius of anodic workpiece gear to impart root relief (mm);

r_{tr} Datum circle radius of anodic workpiece gear to impart tip relief (mm);

Ra Arithmetical average roughness (μm);

Ry Maximum height (μm);

S_l Reciprocating velocity of anodic workpiece gear (mm/s);

t_{fm} Duration of tip/root/end relief or lead crowning of anodic workpiece gear (s);

t_c Cycle time of pulsed direct current (DC) power supply (s);

t_f Time taken by applied voltage to fall from the programmed value to zero (s);

t_r Time taken by applied voltage to reach the programmed value (s);

t_{off} Pulse-off time for pulsed electrical power (s);

t_{onf} Pulse-on time for Faradaic current (s);

t'_{on} Total pulse-on time pulsed electrical power (s);

u_1 Minimum reciprocating velocity of the anodic workpiece gear in lead crowning (mm/s);

u_2 Reciprocating velocity of anodic workpiece gear when its face width is completely engaged or starts disengaging with conductive portion of the cathode gear (mm/s);

u_3 Maximum reciprocating velocity of the anodic workpiece gear in lead crowning (mm/s) ;

V Applied voltage (volts);

V_{er} Volume of material removed from one end of anodic workpiece gear tooth in end relieving (mm^3);

V_{rr} Volume of material removed from one flank surface of anodic workpiece gear tooth in root relieving (mm^3);

V_{tr} Volume of material removed from one flank surface of anodic workpiece gear tooth in tip relieving (mm^3);

w_a Chordal thickness of anodic workpiece gear tooth along its addendum circle (mm);

w_b Chordal thickness of anodic workpiece gear tooth along base circle (mm);

w_p Chordal thickness of anodic workpiece gear tooth along pitch circle (mm);

Y Interelectrode gap (IEG) (mm);

Y_{er} IEG at involute profile of anodic workpiece gear tooth in end relieving (mm);

Y_{ner} IEG at non-involute profile of anodic workpiece gear tooth in end relieving (mm);

Y_{tler} IEG at top land of anodic workpiece gear tooth in end relieving (mm);

Y_{lc} IEG at involute profile of anodic workpiece gear tooth in lead crowning (mm);

Y_{nlc} IEG at non-involute profile of anodic workpiece gear tooth in lead crowning (mm);

Y_{tllc} IEG at top land of anodic workpiece gear tooth in lead crowning (mm);

Y_{nrr} IEG at non-involute profile of anodic workpiece gear tooth in root relieving (mm);

Y_{rr} IEG at involute profile of anodic workpiece gear tooth in root relieving (mm);

Y_{tr} IEG at involute profile of anodic workpiece gear tooth in tip relieving (mm);

Y_{tltr} IEG at top land of anodic workpiece gear tooth in tip relieving (mm);

Z Number of teeth in the anodic workpiece gear;

Δe_1 Minimum circumferential gap between non-conductive and conductive portions in cathode gear designed for imparting end relief (mm);

Δe_2 Maximum circumferential gap between non-conductive and conductive portions in cathode gear designed for imparting end relief (mm);

Δr_1 Circumferential gap between non-conductive and conductive portions at conductive portion diameter of cathode gear designed for imparting tip relief (mm);

Δr_2 Circumferential gap between non-conductive and conductive portions at base circle diameter of cathode gear designed for imparting for tip relief (mm);

Δt Circumferential gap between conductive and non-conductive portions of the cathode gear designed for lead crowning (mm);

Δt_1 Circumferential gap between non-conductive and conductive portions at addendum circle of cathode gear designed for imparting root relief (mm);

Δt_2 Circumferential gap between non-conductive and conductive portions at tip of electrical insulation of cathode gear designed for imparting root relief (mm);

Δt_{pc1} Circumferential gap between non-conductive and conductive portions at the addendum circle of the cathode gear designed for profile crowning (mm);

Δt_{pc2} Circumferential gap between non-conductive and conductive portions at 'd_{pr1}' diameter of the cathode gear designed for profile crowning (mm);

Δt_{pc3} Circumferential gap between non-conductive and conductive portions at 'd_{pr2}' diameter of the cathode gear designed for profile crowning (mm); (mm);

Δt_{pc4} Circumferential gap between non-conductive and conductive portions at the base circle diameter of the cathode gear designed for profile crowning (mm);

ΔV Overvoltage (volts);

δ Duty cycle (%);

η Current efficiency of anodic dissolution (%);

θ Gear roll angle (rad);

θ_a Gear roll angle of point *'A'* on involute profile of anodic workpiece gear flank surface to be root/end relieved (rad);

θ_g Gear roll angle of point *'G'* on involute profile of anodic workpiece gear flank surface to be tip relieved (rad);

θ_h Gear roll angle of point *'H'* on involute profile of anodic workpiece gear flank surface to be tip/end relieved (rad);

θ_q Gear roll angle of point *'Q'* on involute profile of anodic workpiece gear flank surface to be root relieved (rad);

κ_e Electrical conductivity of electrolyte (siemens/mm);

ρ Density of anodic workpiece gear material (g/mm^3);

ψ_g Pressure angle of point 'G' on anodic workpiece gear flank surface to be tip relieved (rad);

ψ_h Pressure angle of point 'H' on anodic workpiece gear flank surface to be tip relieved (rad);

Ψ_p Pressure angle at pitch circle of anodic workpiece gear flank surface to which tip/root/end relief is to be imparted (rad);

Ψ_q Pressure angle of point 'Q' on anodic workpiece gear flank surface to be root relieved (rad);

Ψp Involute pressure angle of point P at involute profile of workpiece spur gear (rad);

Ψq Involute pressure angle of point Q at involute profile of workpiece spur gear (rad);

Abbreviations

CAD	Computer Aided Design
CNC	Computer Numerical Control
DC	Direct Current
ER	End Relief
FEM	Finite Element Method
FFT	Fast Fourier Transform
GMF	Gear Mesh Frequency
IEG	Interelectrode Gap
LC	Lead Crowning
LF	Left Flank
MRR	Material Removal Rate
OFAT	One Factor At a Time
PC	Profile Crowning
PED	Pulsed Electrolytic Dissolution.
PLC	Profile and Lead Crowning
PRRa	Percentage Reduction in Arithmetical Average Roughness
PRRy	Percentage Reduction in Maximum Height
RF	Right Flank
RMS	Root Mean Square
RR	Root Relief
SPL	Sound Pressure Level
TER	Tip and End Relief
TR	Tip Relief
TRER	Tip, Root, and End Relief
TRR	Tip and Root Relief
VFD	Variable Frequency Drive

Chapter 1

Introduction

Gears find wide applications in automobile, aviation, railroad drives, marine transmissions, machine tools, construction equipment, agricultural machines, computer peripherals, helicopter, etc. Different modifications to flank surfaces of a gear are imparted to reduce its running noise and vibrations **(Ghosh and Chakraborty, 2016)** and wear **(Wang et *al.*, 2020)**, to mitigate adverse effects caused by misalignments of shaft of the mating gears **(Neha and Shunmugam, 2017)**, and to improve its functional performance (**Yu and Ting, 2016; Jia et *al.*, 2020)**, transmission efficiency **(Fatourehchi et *al.*, 2018)**, and service life (**Zou et *al.*, 2017; Wang et *al.*, 2021**). Figure 1.1 schematically depicts different benefits of flank modifications of a gear, and the following section Different types of gear flank modifications are discussed in the following section.

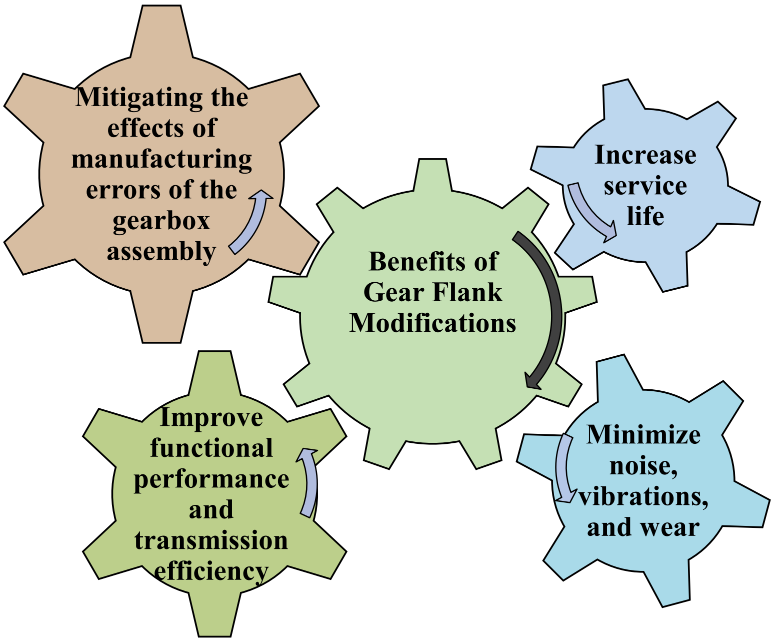

Fig. 1.1: Benefits of flank modifications of a gear.

1.1 Types of Gear Flank Modifications

Figure 1.2 presents different types of flank modifications which are imparted to achieve the desired alterations in flank surfaces of a gear and Fig. 1.3 schematically depicts their concepts. Exact type of the required flank modifications depends on the application and design specifications of a gear. It is crucial to ensure that gear is imparted with those modifications which are appropriate for the intended use and will achieve the desired improvements in its performance.

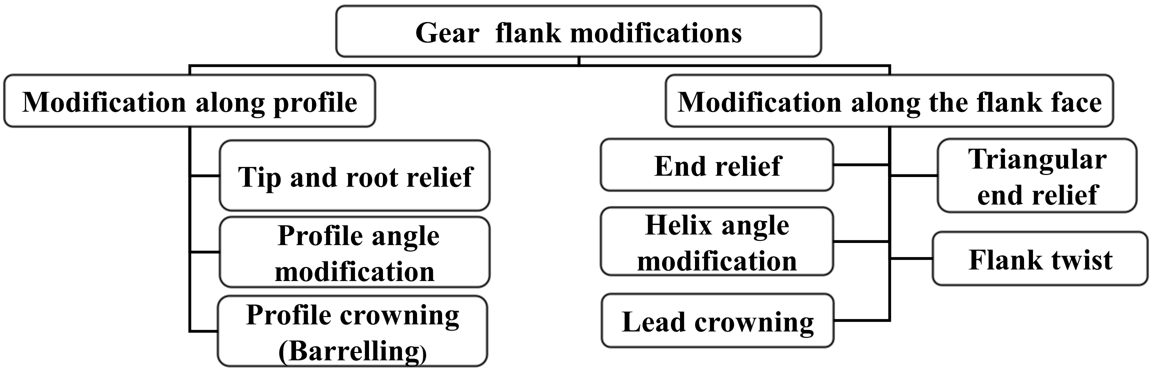

Fig. 1.2: Different types of flank modifications of a gear **(ISO 21771)**.

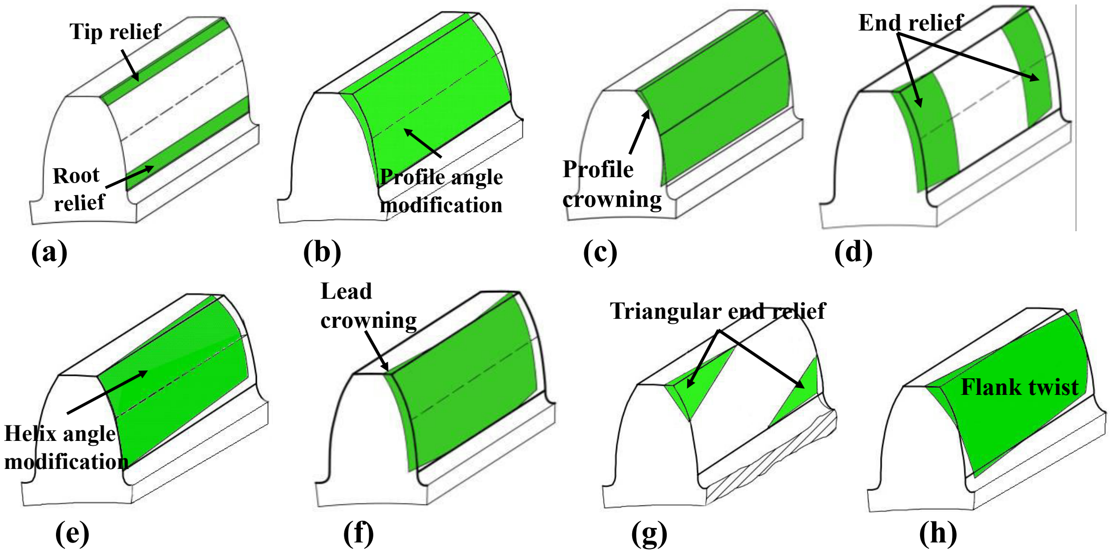

Fig. 1.3: Schematic showing concept of different types of gear flank modifications: (a) Tip and root relief, (b) Profile angle modification, (c) Profile crowning, (d) End relief, (e) Helix angle modification, (f) Lead crowning, (g) Triangular end relief, and (h) Flank twist.

1.2 Flank Modifications Along Gear Profile

1.2.1 Tip and Root Relief

Tip relief '$C_{\alpha a}$' and root relief 'C_{ft}' are provided on some portion of the profile and along entire face width of a gear tooth as shown in Fig. 1.3a. Tip relief is provided by removing material along the entire face width starting from a predefined point above the pitch line and moving towards the tip of a gear tooth. It helps in smooth meshing at the root of the mating gear. Root relief is imparted by removing the material along the entire face width starting from a predefined point below the pitch line and moving towards the root of a gear tooth. It helps in smooth meshing at the tip of the mating gear. Both tip and root relief of a gear ease its loading at the start and end of engagement with its mating gear, reduces transmission error and hence vibrations, and prevents scuffing wear.

1.2.2 Profile Angle Modification

Profile angle modification '$C_{H\alpha}$' is a relief provided to the entire flank surface of gear tooth starting from its base line and towards its tip. It is also known as transverse profile slope modification. It causes the flank surface to curve inwards at only tip of a gear tooth along its profile direction (as shown in Fig. 1.3b) whereas profile crowning causes the flank surface to curve inwards at both tip and root of a gear tooth its profile direction (as depicted in Fig. 1.3c).

1.2.3 Profile Crowning

Profile crowning *'C_α'* is cambering of entire flank surface along profile of gear tooth. It is obtained by removing material along the entire flank surface in such a way that the flank surface is curved inwards at the tip and root of a gear tooth along its profile direction as shown in Fig. 1.3c. It maximizes contact with the mating gear along the pitch line and its adjacent area which reduces the adverse effects of misalignment of shafts of the mating gears. A profile crowned gear has less running noise.

1.3 Flank Modifications Along Gear Flank Surface

1.3.1 End Relief

It is a modification along the entire length of the profile and along some portion of face width of a gear tooth. It is achieved by removing material from both the ends of face width of a gear tooth (denoted as *'$C_{\beta I}$' a*nd *'$C_{\beta II}$'*) along its profile as shown in Fig. 1.3d. It minimizes contact of gear with its mating gear at both ends of its face width which reduces its severe wear.

1.3.2 Helix Angle Modification

Helix angle modification, also known as flank line slope modification, '$C_{H\beta}$' is a continuous end relief from one edge of gear tooth towards another edge along its flank surface causing to curve inwards at one only one edge (as shown in Fig. 1.3e) whereas flank or lead crowing makes the flank surface of gear tooth to curve inwards at its both the ends as illustrated in Fig. 1.3f.

1.3.3 Flank or Lead Crowning

Flank or lead crowning 'C_β' is the cambering of entire flank surface along the face width of a gear tooth. It is achieved by removing material along the entire flank surface in such a manner that the actual profile is curved inwards on both the ends of the face width of a gear tooth as depicted in Fig. 1.3f. It maximizes contact with the mating gear at the middle portion of face width of a gear tooth. It reduces the adverse effects of misalignment of shafts of the mating gears, increases service life and operating performance of the gear.

1.3.4 Triangular End Reliefs

Triangular end reliefs 'C_{Ea}' and *'C_{Ef}'* are provided on diagonally opposite corners on flank surface of gear tooth as shown in Fig. 1.3g.

1.3.5 Flank Twist

A twisted flank surface appears like a surface whose one end is rotated clockwise, and another end is rotated anti-clockwise as shown in Fig. 1.3h. It makes two opposite corners of flank surface curve inward by an amount *'S_α'* and other two opposite corners to curve outward by an amount *'S_β'* as shown in Fig. 1.3h.

1.4 Gear Flank Modifications by Contact Type Processes

Gear grinding, gear shaving, gear honing, gear skiving, and gear hobbing are the conventional type processes which are generally used for flank modifications by different gear manufacturers. All these processes are contact type in which a specially designed tool is used to impart the desired flank modifications to a gear. Table 1.1 summarizes their capabilities and limitations, and the following subsections describe their working principle.

Table 1.1: Capabilities and limitations of conventional contact-type processes for gear flank modifications **(Jain and Petare, 2017).**

Process	Capabilities	Limitations
Gear Grinding	•It is reliable and has good repeatability. •Can impart flank modifications to hard and hardened gears.	•Causes grinding burns, transverse grind lines, fine cracks, thermal distortion, and uneven stress distribution on flank surfaces of the modified gear. •Frequent redressing of grinding wheel. •It is an expensive and complicated process.
Gear Shaving	•It reduces thermal distortions caused by heat treatment. •It is faster and economical.	•It can modify gears up to maximum hardness of 40 HRC only. •Shaved gears have a step mark left on its teeth at the end of the involute profile which causes excessive wear, noise, and vibrations.
Gear Honing	•It generates a crosshatch lay pattern giving tribologically superior surface. •It does not generate internal stress. •It does not alter the microstructure	•Limited life of honing gear tool. •It is a slow process.
Gear Skiving	•It is a multitasking, faster, and reliable process having good repeatability. •Lubricating oil retaining capacity of skived gears is better than that of ground gears.	•It affects surface integrity of flank surfaces of the skived gear (**Ren et al., 2022**). •Skiving cutters are very costly. •Chip removal is a challenging task.
Gear Hobbing	•It is faster, reliable and has good repeatability. •Can be used for spur and helical gears. •It is economical.	•Cannot provide high accuracy. •It affects the surface integrity of flank surfaces of the hobbed gear.

1.4.1 Flank Modifications by Gear Grinding

Though gear grinding is a very costly process, but it can impart flank modifications to those hard and hardened gears which cannot be modified by other conventional process or when the required accuracy cannot be obtained by other conventional process. Ground gears require more inspection to detect presence of grinding burns, transverse grind lines, fine cracks, thermal distortion, and uneven stress distribution. Gear griding is of two types i.e., form or non-generative grinding and generative grinding. **Form Grinding** uses a formed grinding wheel in the space between two consecutive teeth to simultaneously grind the left side of one tooth and the right side of the adjacent tooth. It is used for gears of large module whose grinding is not possible by the generative grinding. Spur and helical gears can be modified by this process. Lead crowing by form grinding process requires relative motion between the grinding wheel and workpiece gear from the following options: (i) approaching motion in the radial direction, (ii) screw motion of the workpiece gear, and (iii) tangential motion of the grinding wheel. Approaching motion in the radial direction is mostly used because it can be used in double flank grinding which is more efficient than the single flank grinding. But this motion generates twist error and profile angle error during lead crowning by the form grinding process. Figure 1.4 shows schematics of 5-axis computer numerical controlled (CNC) machine for form gear grinding. Controlled axes include reciprocating motion along 3 axes and rotary motion along 2 axes. The tangential and axial axes are used for positioning the grinding wheel for its redressing by a dressing wheel which can redress different shapes of gear grinding wheels. The axial axis is coupled with rotation axis of workpiece gear for producing a relative screw motion between the workpiece gear and the grinding wheel.

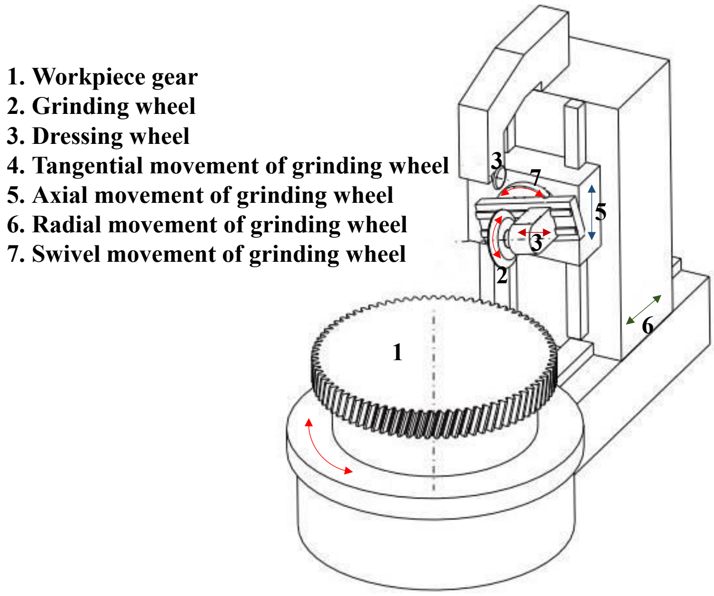

Fig. 1.4: Schematic of helical gear flank modifications by form grinding process using 5-axis CNC machine.

Generative grinding uses following types of grinding wheels: (i) *cup-shaped wheel* which cannot impart tip and root reliefs to a gear, (ii) *dish-shaped wheel*s having 15/20°

included angle between the wheels (Fig. 1.5a) to impart tip and root relief and wheels parallel to each other (Fig. 1.5b) for lead crowning, and *(iii) worm wheel* making the generative gear grinding 6 to 30 times faster than cup-shaped and dish-shaped wheels. It is mainly used for small-to-mid-size gears up to module 7 to 8 mm. Worm wheel can impart all flank modifications to a gear using its machine kinematic provided that the corresponding shape of desired flank modification is provided to it. Profile crowning or lead crowning can be imparted to a gear by adjusting the radial feed with respect to the axial feed of the worm wheel.

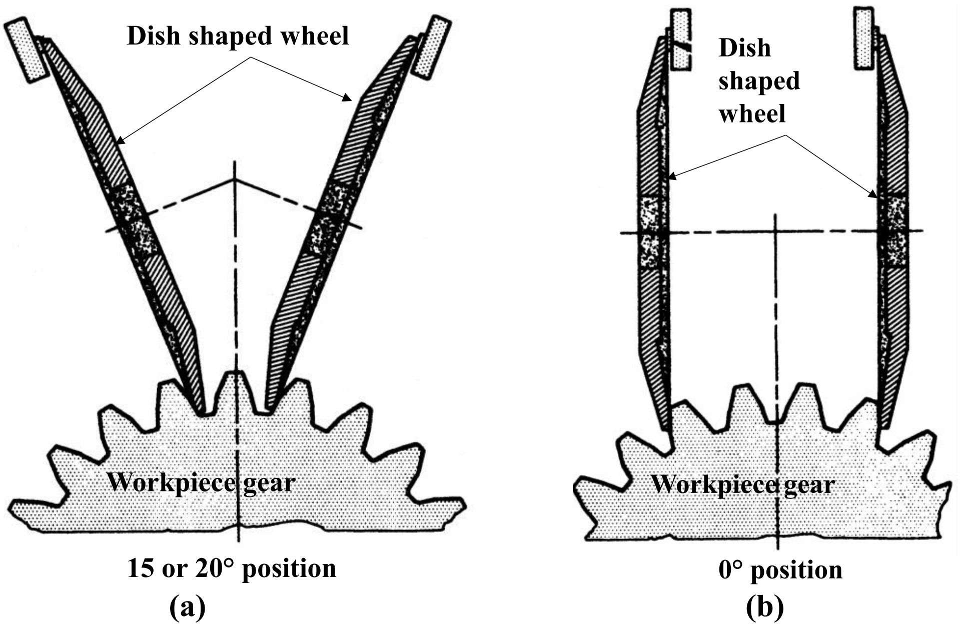

Fig. 1.5: Gear flank modifications by generative gear grinding using dish-shaped wheels: (a) 15/20° position for imparting tip and root relief, and (b) 0° position to impart lead crowning.

1.4.2 Flank Modifications by Gear Shaving

The shaving cutter rotates with the workpiece gear in close mesh in gear shaving process as shown in Fig. 1.6a. The center distance between them is reduced in small and controlled steps to remove material from flank surfaces of the workpiece gear until the required amount of a flank modification is achieved. There are four types of gear shaving processes: diagonal shaving, parallel shaving, underpass shaving, and plunge shaving. Lead crowing can be imparted to the workpiece gear by diagonal shaving, parallel shaving, and underpass shaving processes using an auxiliary mechanism that rocks the workpiece gear with respect to a moving pivot as shown in Fig. 1.6b.

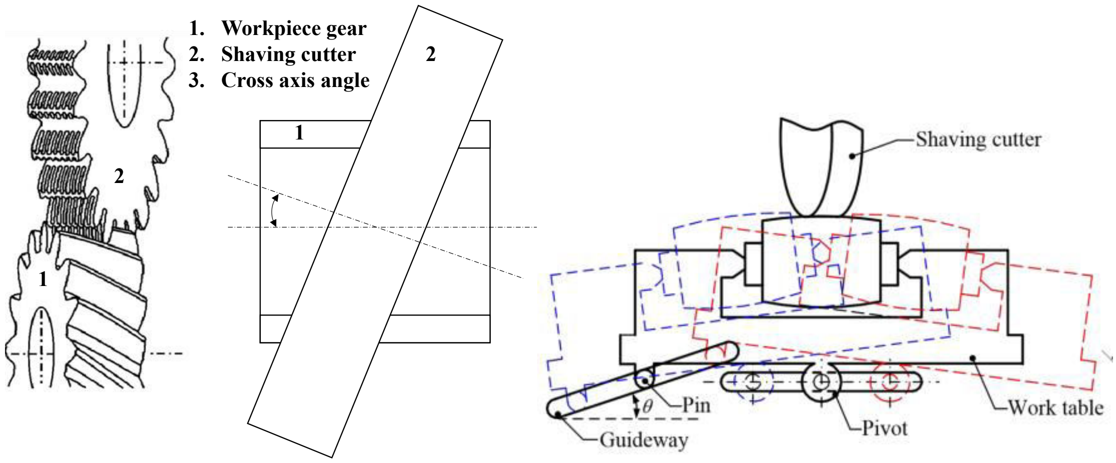

Fig. 1.6: Schematic of helical gear flank modifications by gear shaving process: (a) meshing of shaving cutter and workpiece gear, and (b) auxiliary mechanism to provide lead crowning **(Hsu et *al.*, 2019)**.

1.4.3 Flank Modifications by Gear Honing

Figure 1.7 shows the schematic of external gear honing process. Lead crowning can be imparted to flank surfaces of a workpiece gear by setting proper angle between it and honing tool as a linear function of tangential feed of the honing tool. There are two types of tools used in gear honing process i.e., honing tool made of plastic with abrasive impregnated in it, and metallic tool with renewable bonded abrasive coating. The plastic tool is widely used because it can be discarded at the end of its useful life. The metallic tool is used primarily for fine-pitch gears and applications in which plastic tools is likely to fail early.

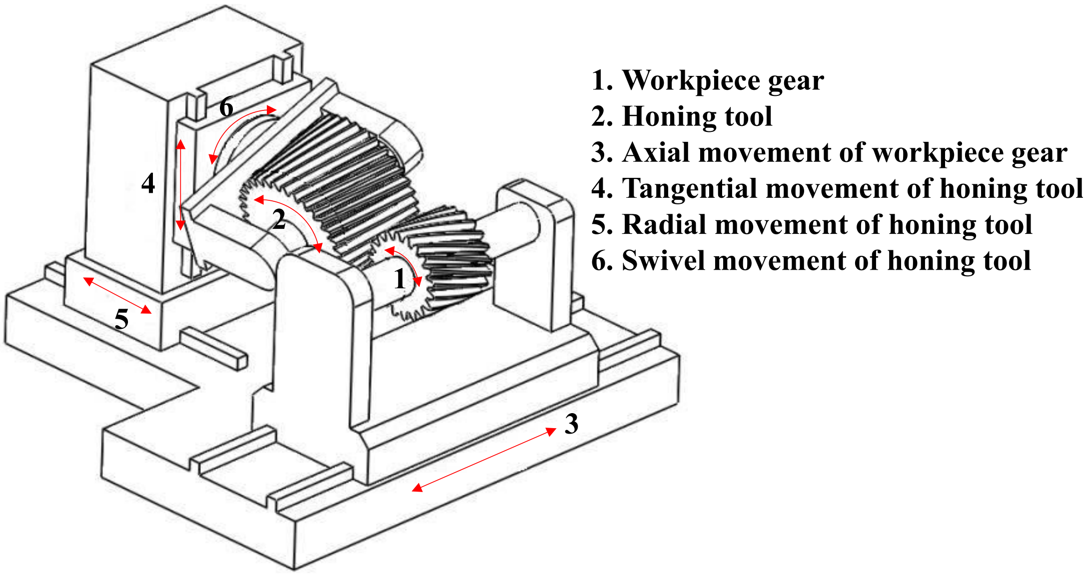

Fig. 1.7: Schematic of helical gear flank modifications by external gear honing process.

1.4.4 Flank Modifications by Gear Skiving

Tooth contact analysis between skiving cutter and workpiece gear, and skiving cutter settings are used for flank modifications by gear skiving process. Axes of skiving cutter and workpiece gear are set at a predefined angle (as shown in Fig. 1.8 for an internal workpiece gear). The skiving cutter and workpiece gear engage with each other and rotate and the skiving cutter reciprocates vertically simultaneously. The interaction of both movements results in a screwing motion that removes material from the gear flank surfaces. Gear skiving corrects all errors introduced in any earlier operation on the flank surfaces of workpiece gear (**Jelaska, 2012**).

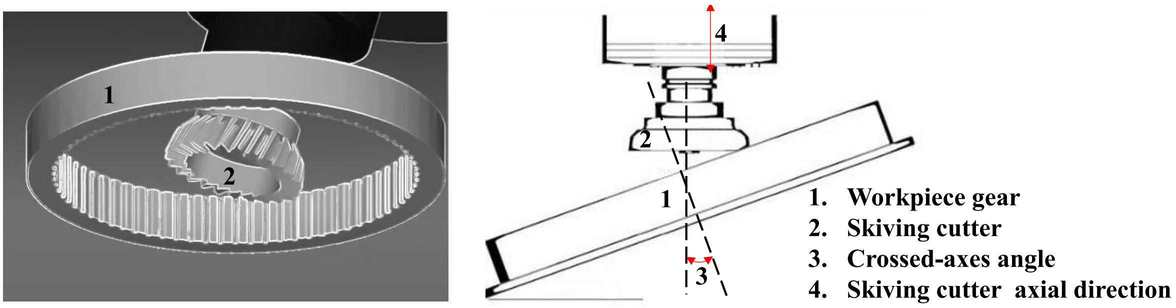

Fig. 1.8: Schematic of flank modifications of an internal gear by gear skiving process.

1.4.5 Flank Modifications by Gear Hobbing

The workpiece gear can be imparted lead crowning by gear hobbing process through varying the center distance between it and the hob cutter as shown in Fig. 1.9. But, variation in center distance produces a twisted flank surface of the workpiece gear.

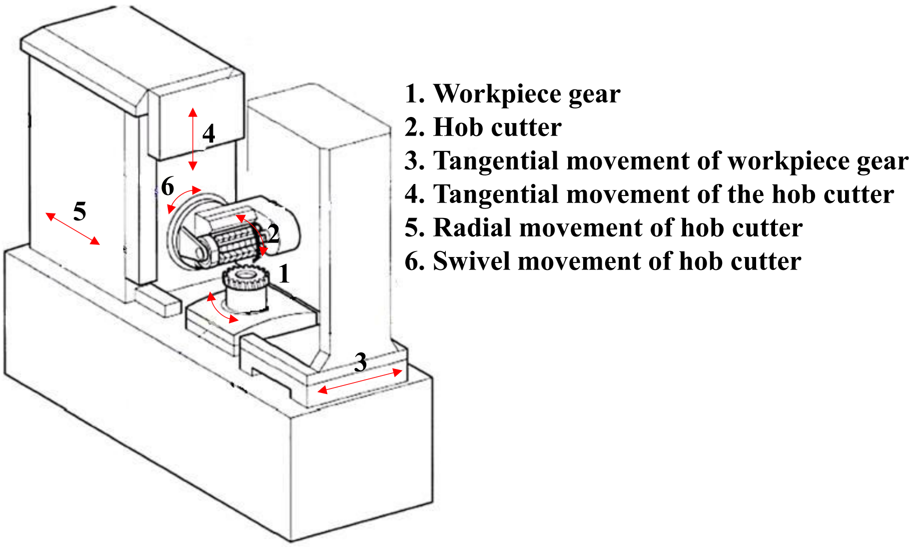

Fig. 1.9: Schematic of spur gear flank modification by hobbing process.

1.5 Gear Flank Modifications by Non-Contact Type Process

The electrolytic dissolution process copies the approximate shape of the cathodic tool to an anodic workpiece through removal of material in a controlled manner at the atomic/molecule level according to Faraday's law of electrolysis. Flank modification by electrolytic dissolution` process does copy the cathode shape but it is designed in such a way that the material is removed from the desired area of flank surfaces of the anodic workpiece gear. This process has capability to modify the flank surfaces of gear in non-contact manner thus resulting in modified flank surfaces to be stress-free and crack-free and without any tool wear. Moreover, its performance is independent of mechanical properties (particularly hardness) of the workpiece gear and being non-contact process, it does not alter mechanical, metallurgical, electrical and magnetic properties of a modified gear.

1.5.1 Advantages of Electrolytic Dissolution Process

The following are the advantages of the electrolytic dissolution process:

- Its performance is independent of hardness of gear material.
- Modified surface is free from thermal and mechanical stresses.
- Redressing of the cathodic tool is not required.
- The cathodic tool has longer life.

1.5.2 Disadvantages of Electrolytic Dissolution Process

- Material should be electrically conductive.
- Electrolyte is of corrosive nature which can corrode the unmodified surfaces.

1.6 Organization of the Thesis

This PhD thesis is organized into the following chapters:

Chapter 2 presents detailed review of the past work done on flank modifications by different contact and non-contact processes, and effects of flank modifications on functional performance, running noise, and vibrations of a gear. It concludes with summary of the past works, identified research gaps, research objectives of the present work, and the methodology used to meet these objectives.

Chapter 3 describes the development of experimental apparatus and cathode gears for non-contact tip relieving, root relieving, end relieving, profile crowning, and lead crowning of spur gears by pulsed electrolytic dissolution (PED) process. It also describes the design and development of a single flank gear roll tester and details of the materials used to develop the apparatus, cathode gears, and workpiece gear.

Chapter 4 describes the development of the analytical models for tip relief, root relief, end relief, and lead crowning of spur gears by the PED process.

Chapter 5 provides the details of planning and design of experiments for confirming the functioning of the developed apparatus and cathode gears, validating the analytical models, and studying effects of parameters of PED process on different flank modifications. It also describes the procedure for measuring the amount of each flank modification, surface roughness, evaluation of surface morphology, noise, vibrations, and functional performance parameters of single and double flank roll testing.

Chapter 6 presents the results and their analyses of different experiments performed to validate the developed apparatus, cathode gears, and analytical models for non-contact flank modifications of spur gears; to study the effects of PED process parameters on different flank modifications; to study the effects of imparting different flank modifications and their combinations to spur gears on their functional performance parameters, running noise, and vibrations; and to study effects of workpiece gear material hardness.

Chapter 7 summarizes the outcomes of the present research work by presenting its significant achievements, conclusions, and some identified avenues for future research work.

Chapter 2

Review of Past Works and Research Objectives

This chapter describes review of the past work done on flank modifications by different contact and non-contact processes, and the effects of flank modifications on functional performance, running noise, and vibrations of a gear. It concludes with a summary of the past works, identified research gaps, research objectives of the present work, and the methodology used to meet these objectives.

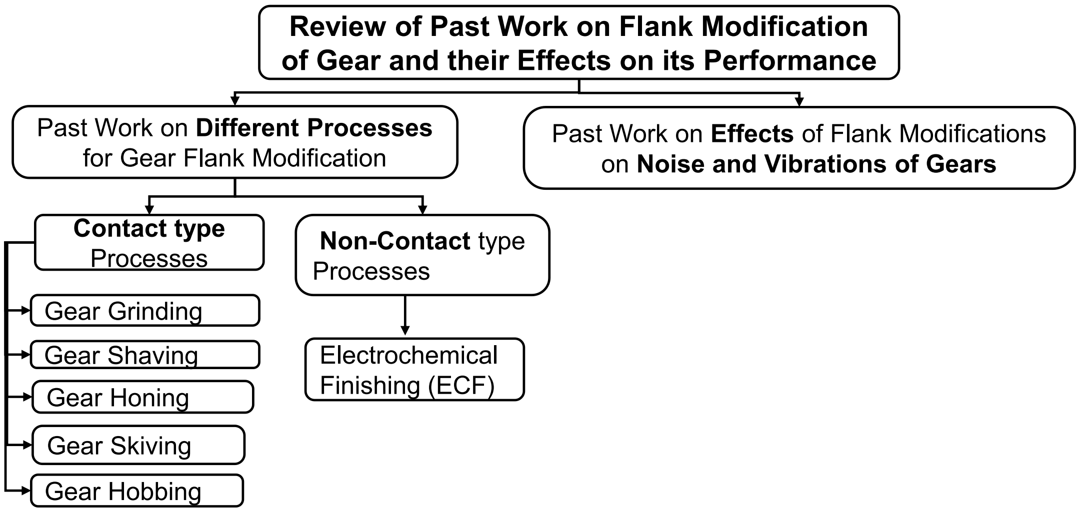

Fig. 2.1: Flow chart for past work on flank modification of gears.

2.1 Past Work on Gear Flank Modifications by Contact Type Processes

The complicated geometry of a gear makes its flank modifications a challenging task. Past works have been reported on using contact type processes such as gear grinding, gear shaving, gear honing, gear skiving, and gear hobbing for different flank modifications of different types of gears. Table 2.1 summarizes them, and the following subsections describe them.

2.1.1 Past Work on Flank Modifications by Gear Grinding

Zhang et *al.* (2014) used a form grinding process for the lead crowning of *helical gears* to minimize twist error. They accomplished this by optimizing the motion of the machine axes using a mathematical model, which allowed them to formulate up to sixth-order polynomials. **Fong and Chen (2016)** used a worm wheel with variable lead to reduce twist error in the lead crowning of *helical gears* by gear grinding. **He et *al.* (2017)** designed the profile of the worm wheel and produced it by ball nose diamond cutter for lead crowning of *helical gears* by generative grinding process. **Yang et *al.* (2018)** proposed a new method to obtain the required profile of the worm wheel for profile crowning of *helical gears* by generative grinding process. This method requires frequent dressing of the worm wheel according to the required modification. **Yu et *al.* (2021)** proposed an approximation model to predict flank twist error in lead crowning of *helical gears* by generative grinding process and validated their proposed model numerically and found that it reduces the flank twist error. They combined gear parameters with their proposed model at the design stage. **Tian et *al.* (2021)** proposed a compensation method to reduce flank twist error to improve the accuracy of generative gear grinding process in lead crowning of *helical gears*. They validated the proposed method through simulation and found that it effectively compensates for the flank twist error. **Tian et *al.* (2022)** used genetic algorithm to evaluate contact traces to solve the problem of flank twist error in the lead crowning of *helical gears* by the generative grinding process without dressing the grinding wheel. **Zhao et *al.* (2022)** proposed a method based on orthogonal polynomials to predict flank twist error in lead crowning of *helical gears* by generative grinding process. They found that flank twist error is directly proportional to lead crowning value and inversely proportional to the face width of the helical gear.

2.1.2 Past Work on Flank Modifications by Gear Shaving

Liu et *al.* (2009) provided *tip relief, root relief,* and l*ead crowning* to *helical gears* by gear shaving process and proposed a methodology to design the shaving cutter. They reported that experimental values of flank modifications closely agree with the designed values. **Hsu and Fong (2010)** imparted lead crowning to *helical gears* by gear shaving process and developed a mathematical model to predict the lead crowning value and to simulate the gear shaving process for a given auxiliary crowning mechanism. **Hsu et *al.* (2019)** used shaving cutter having variable pressure angle for twist-free profile and lead crowning of *helical gears*.

2.1.3 Past Work on Flank Modifications by Gear Honing

Wu and Tran (2015) developed a mathematical model for twist-free lead crowning of *helical gears* by internal gear honing process using a honing tool having variable pressure angle. **Yu et *al.* (2017)** used external gear honing process for *tip relieving, root relieving, and end relieving* of *spur gears* using a worm shaped honing tool for even number of teeth and double-threaded worm shaped honing tool for odd number of teeth. **Han et *al.* (2018)** developed a mathematical model for lead and profile crowning of *helical gears* by internal gear honing process and validated it numerically. They found that when motion is provided along only one axis to the honing tool then there is distortion in the profile direction of gear tooth. **Tran and Wu (2018)** used an internal gear honing process to provide twist-free dual lead crowning to *helical gears* having with large face width by controlling its swivel and rotary movement. **Tran and Wu (2020)** used additional motion in the form of polynomials to radial feed, swivel movement of honing tool, and rotational movement of workpiece *helical gear* for its twist-free lead crowning by internal gear honing process.

Table 2.1: Summary of the past work on gear flank modifications by contact type processes.

Authors and year	**Process name**	**Gear specifications**	**Flank modification and its obtained value**	**Experimental/ theoretical**	**Remarks**
Zhang et *al.*, 2014	Form grinding	**Helical Gear:** Helix angle: 15°; Pressure angle: 20°; Module: 14 mm; Face width: 120 mm; Number of teeth: 35	Lead crowning ≈ 40µm	Theoretical and experimental	Minimized twist error by optimizing motion of the machine axes using a mathematical model.
Fong and Chen, 2016	Generative grinding using worm wheel	**Helical Gear:** Helix angle: 30°; Pressure angle: 22.5°; Module: 5 mm; Face width: 50 mm; Number of teeth: 17, 41	Lead crowning ≈ 30 to 80 µm	Theoretical	Used worm wheel having variable lead to reduce the flank twist error.
He et *al.*, 2017	Generative grinding using worm wheel	**Helical Gear:** Helix angle: 30°; Pressure angle: 20°; Module: 4 mm; Face width: 40 mm; Number of teeth: 48	Lead crowning: ≈ 20 µm, 10 µm	Theoretical and experimental	Obtained the profile of worm wheel to modify the gear flank surface.
Yang et *al.*, 2018	Generative grinding using worm wheel	**Helical Gear:** Helix angle: 20°; Pressure angle: 20°; Module: 4 mm; Number of teeth: 50, 23	Profile crowning ≈10, 15 µm	Experimental	An indirect generative method is proposed to calculate the profile of worm wheel.
Yu et *al.*, 2021	Generative grinding using worm wheel	**Helical Gear:** Helix angle: 15°, 30°; Pressure angle: 20°; Module: 4 mm, 2.5 mm; Face width: 40 mm; Number of teeth: 48	Lead crowning ≈ 20 and 10 µm	Theoretical	Predicted flank twist error and combined it with gear parameters in the design stage to reduce it
Tian et *al.*, 2021	Generative grinding using worm wheel	**Helical Gear:** Helix angle: 30°; Pressure angle: 20°; Module: 4 mm, 2.5 mm; Face width: 40 mm; Number of teeth: 48	Lead crowning	Theoretical	Proposed a compensation method to reduce flank twist error.
Tian et *al.*, 2022	Generative grinding using worm wheel	**Helical Gear**; Helix angle: 30°; Pressure angle: 20°; Module: 4 mm; Face width: 40 mm; Number of teeth: 48	Lead crowning	Theoretical	Proposed a method for lead crowning without dressing the worm wheel.
Zhao et *al.*, 2022	Generative grinding using worm wheel	**Helical Gear:** Helix angle: 30°; Pressure angle: 20°; Module: 4 mm; Face width: 40 mm; Number of teeth: 48	Lead crowning	Experimental	Flank twist error is directly proportional to lead crowning value and inversely proportional to face width of a gear.

Liu et *al.*, 2009	Gear shaving	**Helical Gear:** Helix angle: 15°; Pressure angle: 20°; Module: 3 mm; Face width: 20 mm; Number of teeth: 25	Tip relief ≈ 6.1 µm Root relief ≈ 5.6 µm Lead crowning ≈ 5.6 µm	Experimental	Proposed design methodology for the shaving cutter.
Hsu and Fong, 2010	Parallel gear shaving	**Helical Gear:** Helix angle: 10°,15°,23°; Pressure angle: 20°; Module: 2.65, 3.55, 2.25 mm; Face width: 28.4, 34 mm; Number of teeth: 36, 29, 75	Lead crowning ≈ 2 to 11 µm	Theoretical	A mathematical model developed to determine amount of crowning for the given auxiliary crowning mechanism.
Hsu et *al.*, 2019	Gear shaving	**Helical Gear:** Helix angle: 15°; Pressure angle: 20°; Module: 3 mm; Face width: 20 mm; Number of teeth: 35	Profile crowning ≈ 6 µm Lead crowning ≈ 14 µm	Theoretical	Proposed a shaving cutter having variable pressure angel to minimize the flank twist error.
Wu and Tran, 2015	Internal gear honing	**Helical Gear:** Helix angle: 10°; Pressure angle: 20°; Module: 2.5 mm; Face width: 15 mm; Number of teeth: 25	Lead crowning ≈ 14 to 18 µm	Theoretical	Used honing tool with variable pressure angle for twist-free lead crowing.
Yu et *al.*, 2017	External gear honing	**Spur Gear:** Helix angle: 0°; Pressure angle: 20°; Module: 4 mm; Face width: 40 mm; Number of teeth: 54	Tip relief ≈ 50, 80 µm Root relief ≈ 55, 80 µm End relief ≈ 50, 20 µm	Experimental	Proposed tooth-skipped gear honing and using the same worm-shaped honing wheel for different flank modifications.
Han et *al.*, 2018	Internal gear honing	**Helical Gear:** Helix angle: 33°; Pressure angle: 17.5°; Module: 2.25 mm; Face width: 50 mm; Number of teeth: 73	Lead crowning ≈ 10 to 35 µm	Theoretical	Found distortion in profile direction.
Tran and Wu, 2018	Internal gear honing	**Helical Gear:** Helix angle: 10°; Pressure angle: 30°; Module: 3 mm; Face width: 50 mm; Number of teeth: 7	Lead crowning ≈ 7 to 12 µm; 46 to 57 µm	Theoretical	Twist-free flank modification was done by controlling the swivel angle of honing tool and the rotation angle of workpiece gear.
Tran and Wu, 2020	Internal gear honing	**Helical Gear:** Helix angle: 15°; Pressure angle: 20°; Module: 3 mm; Face width: 20 mm; Number of teeth: 25	Lead Crowning ≈ 17 to 57 µm	Theoretical	Proposed a numerical approach for flank modification of cylindrical gears with twist-free flank surfaces.
Guo et *al.*, 2015	Gear skiving	**Internal spur gear:** Helix angle: 0°; Pressure angle: 20°; Module: 5 mm; Face width: 50 mm; Number of teeth: 41	Lead crowning ≈ 15 µm, 30 µm	Theoretical	Proposed correction method to reduce flank twist error by optimizing the cutter profile.

Zheng et *al.*, 2018	Gear skiving	**Helical gear:** Helix angle: 24°; Pressure angle: 20°; Module: 2.5 mm; Face width: 20 mm; Number of teeth: 27, 42	Lead crowning	Theoretical	Use of cutter offset correction in flank modification resulted in slight flank twist error.
Guo et *al.*, 2023	Gear skiving	**Internal helical gear:** Helix angle: 14°; Pressure angle: 20°; Module: 5 mm; Face width: 20 mm; Number of teeth: 113	Profile crowning ≈ 15 µm Lead crowning ≈ 25 µm	Theoretical	Proposed a new type of skiving cutter with double rake faces. Proposed new algorithm for skiving cutter path to reduce flank twist error.
Wang and Fong, 2008	Gear hobbing	**Spur gear:** Helix angle: 0°; Pressure angle: 20°; Module: 3 mm; Face width: 15 mm; Number of teeth: 17	Lead crowning ≈ 17 µm	Theoretical	Proposed cutting method for lead crowning of spur gear using dual face hobbing cutter whose cutting blades are arranged in cycloidal traces.
Hsu and Fong, 2011	Gear hobbing	**Spur and helical gears:** Helix angle: 10°, 20°; Pressure angle: 20°; Module: 3 mm; Face width: 15 mm; Number of teeth: 50	Lead crowning ≈ 30 to 50 µm	Theoretical	Proposed a mathematical model for a hob cutter having variable tooth thickness to reduce the twist error.
Tran et *al.*, 2014a	Gear hobbing	**Helical gears:** Helix angle: 21°; Pressure angle: 20°; Module: 3 mm; Face width: 14 mm; Number of teeth: 50	Lead crowning ≈ 32 µm	Theoretical	Proposed new dual lead hob cutter with variable pressure angle in its longitudinal direction.
Tran et *al.*, 2014b	Gear hobbing	**Helical gears:** Helix angle: 20°; Pressure angle: 20°; Module: 3 mm; Face width: 15 mm; Number of teeth: 50	Lead crowning ≈ 30 to 60 µm	Theoretical	Proposed an additional rotation angle for the workpiece gear as nonlinear function of swivel and radial movement of hob cutter for twist-free lead crowning.

2.1.4 Past Work on Flank Modifications by Gear Skiving

Guo et *al.* (2015) proposed a correction method to optimize the cutter profile to minimize the twist error in lead crowning of *internal spur gears* by gear skiving. **Zheng et *al.* (2018)** used gear skiving for lead crowing of *helical gears* by the cutter offset correction, cutter tilted correction, and crossed angle correction method. They found that use of cutter offset correction method caused a slight twist error in the lead crowned helical gears. **Guo et *al.* (2023)** proposed a new skiving cutter having double rake faces for each cutting tooth and an algorithm for the skiving cutter path, and designed the side rake angles and customizable cutting edges to reduce flank twist error in profile and lead crowning of *internal helical gears* by gear skiving process.

2.1.5 Past Work on Flank Modifications by Gear Hobbing

Wang and Fong (2008) used gear hobbing to achieve lead crowning on *spur gear* by introducing a new cutting technique that involved a dual face-hobbing cutter whose blades are arranged in cycloidal traces. **Hsu and Fong (2011)** proposed a mathematical model for hob cutter having variable tooth thickness to reduce twist error in lead crowning of helical and spur gears by gear hobbing process and validated it numerically. **Tran et *al.* (2014a)** developed a mathematical model to obtain twist-free lead crowning of *helical gears* by gear hobbing process using dual-lead hob cutter with its pressure angle changing in its longitudinal direction. They set diagonal feed of hob cutter as second order function of its radial movement. **Same authors (2014b)** proposed an additional rotation angle for the workpiece gear as the nonlinear function of the swivel and radial movement of hob cutter to achieve twist-free lead crowning of *helical gears* and validated the proposed concept numerically.

2.2 Past Work on Non-Contact Flank Modifications of Gears

Use of conventional contact-type processes for flank modification of different gears suffers from some major limitations (as mentioned in Table 1.1) despite some of their unique capabilities. Using electrolytic dissolution-based process for non-contact flank modifications of gears offers some unique advantages (as mentioned in Section 1.5.1). But very limited work is available in this direction. **Yi et *al.* (2002)** used electrochemical finishing (ECF) process to modify one tooth of a *spiral bevel gear* at a time by moving a rectangular block shaped cathode tool over it with the help of the developed apparatus. They developed a prediction model for gear flank modification amount by the ECF process using artificial neural networks. **Pang et *al.* (2010)** used pulsed electrochemical finishing (PECF) process on a flat plate and concluded that profile modification of gear could be realized using an variable interelectrode gap (IEG) and lead modification can be realized using the variable velocity of the cathodic tool.

2.3 Past Work on Effects of Flank Modifications on Gear Performance

Some researchers have theoretically and/or experimentally studied the effects of different flank modifications of a gear on its performance characteristics. **Terauchi et *al.* (1982)** studied the effects of imparting tip relief to a *spur gear* on its dynamic load and running noise and found that tip relieving of a spur gear decreased dynamic load on its meshing teeth and reduced its running noise by 5 dB. **Chong et *al.* (2001)** developed a method to calculate optimum amounts of tip relief, end relief and crowning to be imparted to a *helical gear* to reduce its vibration exciting force which is estimated by meshing analysis of the modified helical gear. **Mao (2006)** studied effect of tip relief and crowning on transmission errors of *helical gear and spur gear* by using non-linear finite-element method (FEM) and found that the modified helical gears have lower transmission errors than modified spur gears. **Li (2007)** used FEM to study effects of flank modification, manufacturing errors, and assembly errors on loading capacity and transmission errors of a *spur gear* and reported that manufacturing and assembly errors, and larger amount of flank modification increased its transmission errors. **Tesfahunegn et *al.* (2010)** used non-linear FEM to study influence of shape of profile modifications imparted to a *spur gear* on its transmission errors, and root and contact stresses. They found that shape of profile modifications of a spur gear does not have any significant effects on its contact and root stresses but affects its transmission errors. **Ma et *al.* (2014)** developed a FEM based model to study the effects of tip relief on vibrations of gear and found that they are reduced at lower value of gear mesh frequency**. Ghosh and Chakraborty (2016)** obtained an optimum amount of flank modifications for a *spur gear* using graphical and semi-analytical methods and found that tip relief reduced vibrations of spur gear pair caused by microgeometry errors. **Yang et *al.* (2018)** developed a method to calculate profile of a grinding worm for profile crowning of *helical gears.* They compared vibrations of modified and unmodified helical gears and reported that the modified helical gears have less vibrations at gear mesh frequency and its 2^{nd} and 3^{rd} harmonics.

2.4 Identified Research Gaps

Following research gaps were identified based on the aforementioned review of the relevant past works:

- The majority of flank modifications by contact type processes is focused on lead crowing of helical gears. Very limited work is available on flank modification of spur gears in general and tip, root, and end relieving in particular.

- Spur gear is the most common gear among different types of gears, but no work is available on flank modifications of spur gears by non-contact type process and studying effects of its input parameters on performance characteristics of modified spur gear.
- No work is available on development of theoretical models to predict the amount of flank modification of a spur gear by non-contact type processes.

2.5 Research Objectives

Following research objectives were identified for the present work:

- **RO1:** Development of apparatus for non-contact tip, root and end relieving, and profile and lead crowning (either imparting individually or their combinations) of spur gears by non-contact pulsed electrolytic dissolution (PED) process.
- **RO2:** Design and development of the required cathode gears for non-contact tip, root and end reliving, and profile and lead crowning of spur gears by the PED process along with their explanation of their imparting mechanisms.
- **RO3:** Development of analytical models to predict amount of tip relief, root relief, end relief, and lead crowning imparted to a spur gear by the PED process in a specified modification duration or to compute the required duration for a given value of a flank modification.
- **RO4:** Experimental validation of the developed apparatus, cathode gears, analytical models, and studying effects of PED process parameters on different flank modifications.
- **RO5:** Design and development of *single flank roll tester* for cylindrical gears.
- **RO6:** Comparative study of functional performance characteristics of unmodified and different modified spur gears by imparting four individual flank modifications and four their different combinations by the developed apparatus and cathode gears.

2.6 Research Methodology

Fig. 2.2 presents the flow chart of methodology used to meet objectives of the present research work whereas Table 2.2 presents its detailed version.

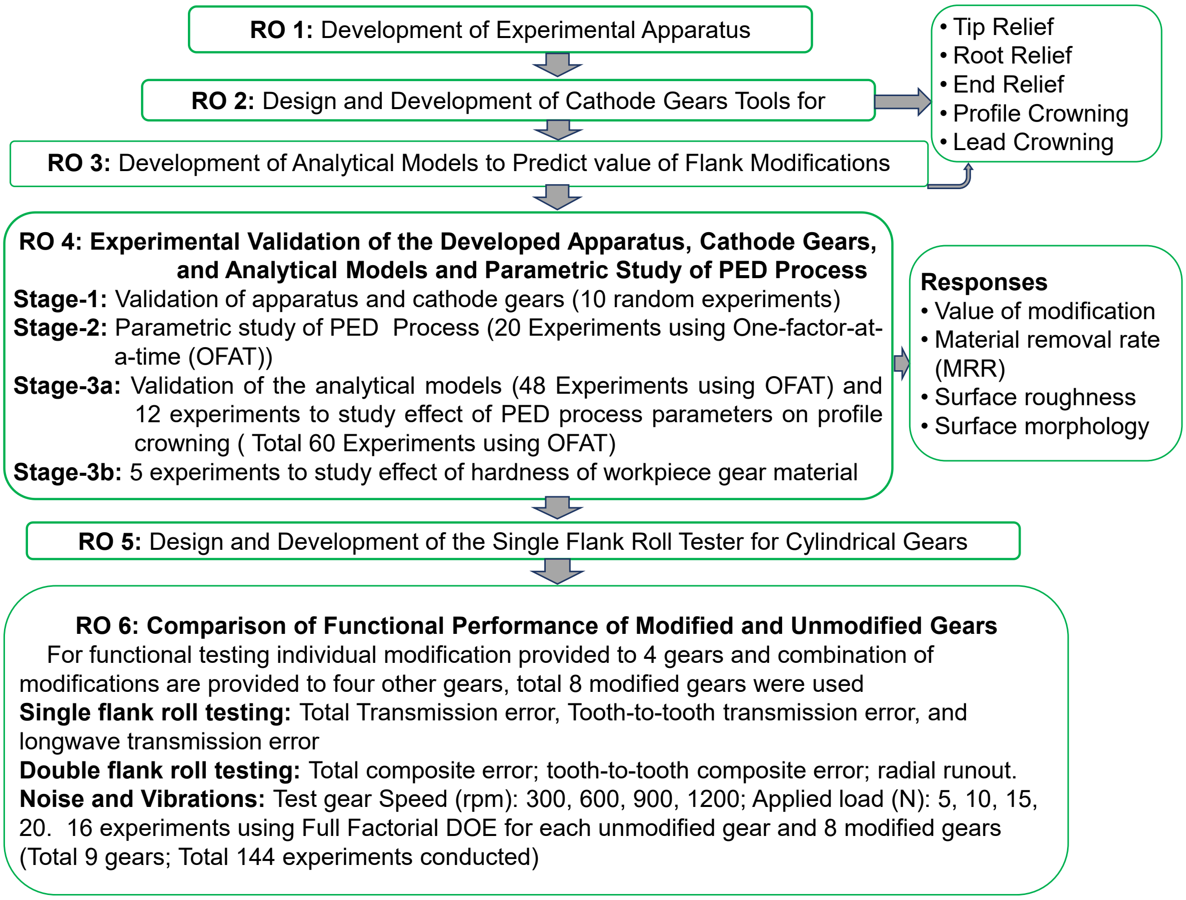

Fig. 2.2: Flow chart of the research methodology used in the present work to achieve the identified research objectives.

The ***next chapter*** describes the development of experimental apparatus and cathode gears for non-contact tip relieving, root relieving, end relieving, profile crowning, and lead crowning of spur gears by pulsed electrolytic dissolution (PED) process. It also describes the design and development of a single flank gear roll tester and details of the materials used to develop the apparatus, cathode gears, and workpiece gear.

Table 2.2: Details of research methodology and experiments used to meet research objectives of the present work.

<table>
<tr><td colspan="3">RO-1: Development of apparatus for non-contact tip, root and end relieving, and profile and lead crowning (imparting individually or their combinations) of spur gear by PED process.</td></tr>
<tr><td colspan="3">RO-2: Design and development of the required cathode gears for non-contact tip, root and end reliving, and profile and lead crowning and explaining their imparting mechanisms.</td></tr>
<tr><td colspan="3">RO-3: Development of analytical models to predict amount of tip relief, root relief, end relief, and lead crowning imparted to a spur gear by PED process in a specified modification duration OR to compute the required modification duration for a given amount of a particular modification.</td></tr>
<tr><td colspan="3">RO-4: Experimental validation of the developed apparatus, cathode gears, analytical models, and study of effects of PED process parameters.</td></tr>
<tr>
<td>Stage-1 experiments: Validation of the developed apparatus and cathode gears through 10 random experiments
Workpiece gear material: 20MnCr5 alloy steel
Variable input parameters:
• Pulse-on time (ms): 1; 3; 5
• Pulse-off time (ms): 2; 4; 5
• Voltage (Volts): 10; 15; 18; 24
• Modification duration (minutes): 8; 12; 16; 20
• Electrolyte concentration: 0.5 Molarity for TR, ER, RR, PC and 1.0 Molarity for LC
• Rotational speed of cathode gear: 8.5 rpm for TR, ER, RR, PC, and 35 rpm for LC
Constant input parameters:
• Electrolyte type: NaCl
• Electrolyte temperature: 30 °C
• Electrolyte flow rate: 20 lpm
• Reciprocating velocity of anodic workpiece gear: 0.96 mm/s for TR, RR, PC, variable reciprocating velocity for LC, and no need of reciprocation of workpiece gear for ER
Responses: Values of the imparted modifications through microgeometry measurement, and material removal rate (MRR)</td>
<td>Stage-2 experiments: Studying effects of parameters related to electrolyte, cathode gear rotational speed, and modification duration in non-contact tip relieving by PED process by conducting 20 experiments using one-factor-at-a-time (OFAT) approach.
Workpiece gear material: 20MnCr5 alloy steel
Variable input parameters:
• Electrolyte temperature (°C): 25; 30; 35; 40
• Electrolyte flow rate (lpm): 10; 20; 30; 40
• Electrolyte concentration (Molarity): 0.5, 1.0; 1.5; 2
• Rotational speed of cathode gear (rpm): 15; 25; 35; 45
• Tip relief duration (minutes): 8; 12; 16; 20
Constant input parameters:
• Electrolyte type: NaCl
• Reciprocating velocity of anodic workpiece gear: 0.96 mm/s
• Responses: Values of the imparted tip relief, % reduction in maximum and average surface roughness, roughness profile, MRR, and morphology of flank surfaces unmodified and modified gears</td>
<td>Stage-3a experiments: Validation of the developed analytical models of TR, RR, ER, and LC by conducting 12 experiments for each (i.e., total 48 experiments) using OFAT approach and 12 experiments to study effects of pulse-on time, pulse-off time, and voltage for PC using OFAT approach
Workpiece gear material: 20MnCr5 alloy steel
Variable input parameters:
• Pulse-on time (ms): 2; 3; 4; 5
• Pulse-off time (ms): 2; 4; 6; 8
• Voltage (Volts): 15; 18; 21; 24 for TR, ER, LC, and PC, and 18; 21; 24; 27 for RR
Constant input parameters:
• Electrolyte type: NaCl; Electrolyte temperature: 30 °C; Electrolyte flow rate: 20 lpm; Electrolyte concentration: 0.5 Molarity for TR, RR, and ER, and 1.0 Molarity for PC and LC; Modification duration: 12 minutes for ER, PC, LC, and 20 minutes for RR; Rotational speed of cathode gear: 15 rpm for TR, RR, and ER, 35 rpm for PC, and LC; Reciprocating velocity of anodic workpiece gear: 0.96 mm/s for TR, RR, PC, and varied from 0.2 to 0.8 mm/s for LC
Responses: Values of the imparted modifications through microgeometry measurement, % reduction in maximum and average surface roughness, roughness profile, and morphology of flank surfaces of unmodified and modified gears
Stage 3b experiments: Five experiments to study effects hardness of workpiece gear material for TR, RR, ER, PC, and LC.
Constant input parameters: pulse-on time: 3 ms for TR, RR, ER, LC and PC; pulse-off time: 2ms for TR and 4 ms for RR, ER, LC and PC; Voltage: 15 Volts for TR, LC, and PC, 18 volts for RR, and 21 volts for ER; Modification duration: 12 minutes for TR, ER, LC, and PC, and 20 minutes for RR.
Responses: Values of the imparted modifications, % reduction in max. and avg. surface roughness values</td>
</tr>
<tr><td colspan="3">RO-5: Design and development of the single flank roll testing equipment for cylindrical gears</td></tr>
<tr><td colspan="3">RO-6: Comparative study of functional performance parameters of unmodified and different flank modified spur gears by imparting four flank modifications individually and their four different combinations by the developed apparatus and cathode gears through Stage 4 experiments
Variable parameters of PED process used in imparting different flank modifications and their combinations to spur gear: Pulse-on time (ms): 3, 5; Pulse-off time (ms): 2, 4; Voltage (Volts): 15, 18; Modification duration (minutes): 12-44; Rotational speed of cathode gear (rpm): 15, 35; Reciprocating velocity of workpiece gear (mm/s): 0.2-0.96; Electrolyte concentration (Molarity): 0.5, 1.0
Variable parameters used in evaluation of running noise and vibrations: Applied load (N): 5; 10; 15; 20; Rotation speed of test or workpiece gear (rpm): 300; 600; 900; 1200;
Constant parameters: Electrolyte type: NaCl; Electrolyte temperature: 30 °C; Electrolyte flow rate (lpm): 20
Responses: Total transmission error, Tooth-to-tooth transmission error, Longwave transmission error, and Total pitch error (Single flank roll testing); Total composite error, Tooth-to-tooth composite errors, and Radial runout (Double flank roll testing); Sound pressure level, and RMS value of vibrations (Vibrations and Noise Testing)</td></tr>
</table>

Chapter 3

Development of Apparatus and Cathode Gears

This chapter describes the development of experimental apparatus and cathode gears for non-contact tip relieving, root relieving, end relieving, profile crowning, and lead crowning of spur gears by pulsed electrolytic dissolution (PED) process. It also describes the design and development of a single flank gear roll tester and details of the materials used to develop the apparatus, cathode gears, and workpiece gear.

3.1 Development of Apparatus for Non-Contact Flank Modification

An innovative apparatus was conceptualized and developed to impart non-contact tip relief, root relief, end relief, profile crowning, and lead crowning either individually or their any combination to spur gear by pulsed electrolytic dissolution (PED) process. It was developed by integrating four subsystems: (i) Flank modification chamber; (ii) Drive system for anodic workpiece and cathode gears; (iii) Power supply system; and (iv) Electrolyte supply and recycling system. Their details are mentioned in the following paragraphs. Figures 3.1a and 3.1b depict a schematic diagram and photograph of the developed apparatus, respectively, and Fig 3.1c shows a photograph of the flank modification chamber. Table 3.1 shows the photographs of different components of apparatus and their specifications, and Table 3.2 presents the details of materials selected for different components of the apparatus, anodic workpiece gear and cathode gears, and their selection criteria.

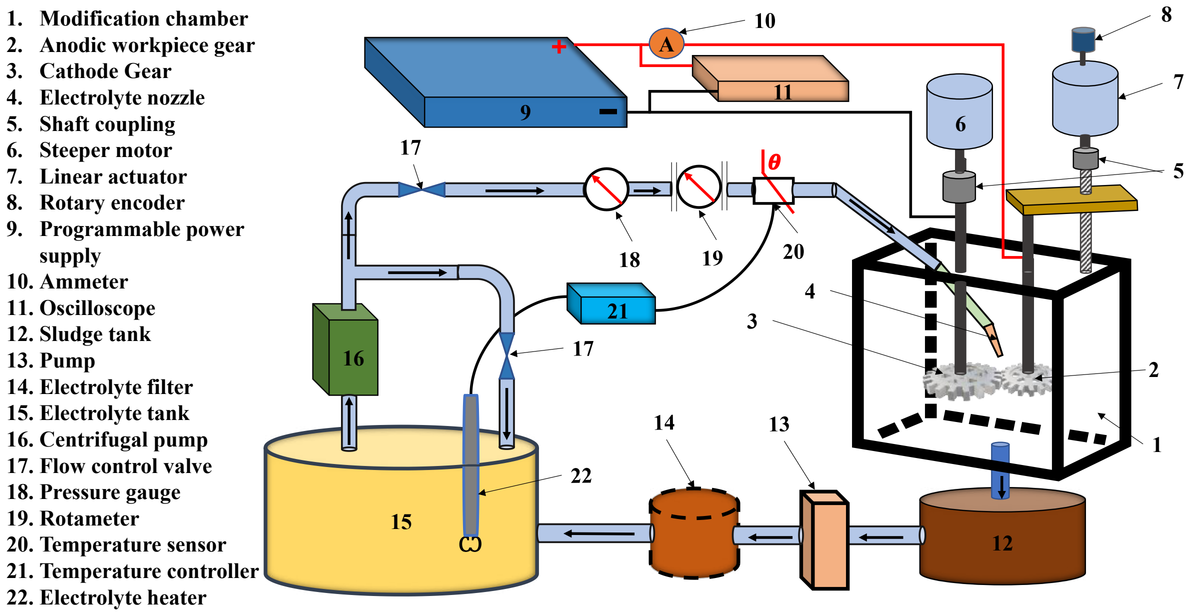

(a)

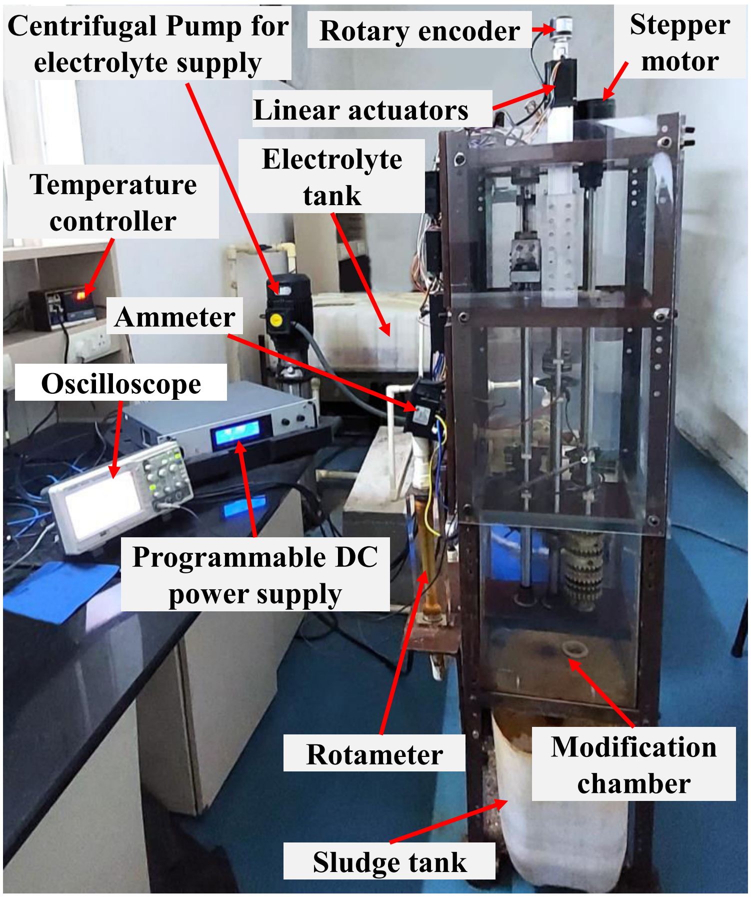

(b)

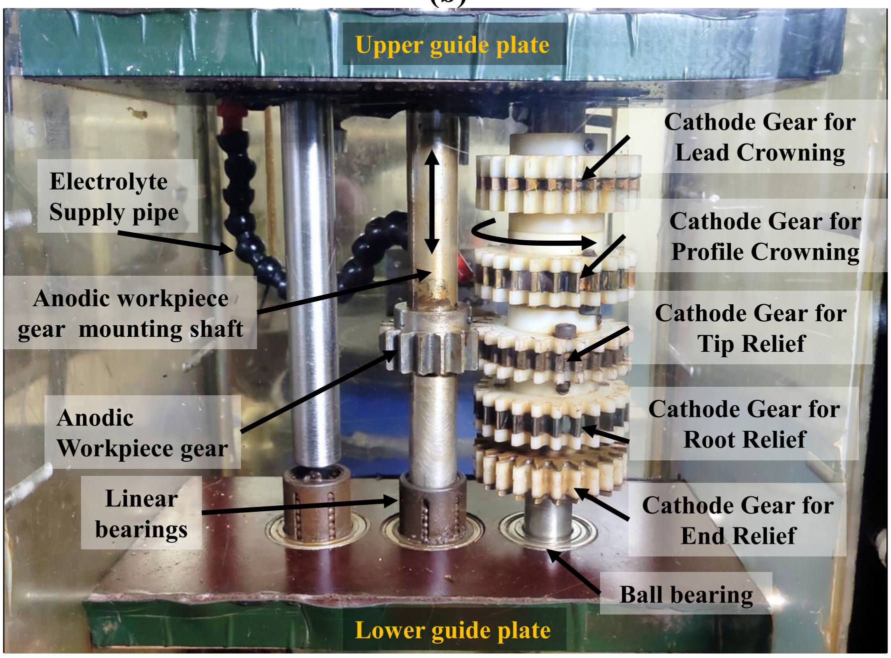

(c)

Fig. 3.1: Apparatus developed for flank modification of a workpiece gear by pulsed electrolytic dissolution process: (a) schematic, (b) photograph of apparatus, and (c) photograph of flank modification chamber showing relative positioning of the developed cathode gears and workpiece gear.

Table 3.1: Functions and specifications of different components used in the apparatus.

Programmable Power Supply
Model: SM-100-AR-75
Make: Delta Elektronika, Netherlands
Specifications: Current: 0-75 A; Voltage: 0-100 volts; Maximum Power: 3300 W

Linear actuator: to control reciprocating motion of anodic workpiece gear.
Model: 57HB76L4-30DB-B
Make: 3D Printronics, India
Specifications: Max. Torque: 1.6 N-m; Step angle: 1.8°; Pitch of ball screw: 5 mm

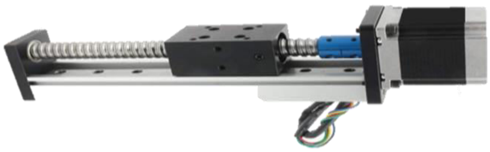

Stepper motor: to provide rotary motion to cathode gear.
Model: 103H8222-5141
Make: Sanyo Denki Co. Ltd. Japan
Specifications: Max. Torque: 5.09 Nm; Step angle: 1.8°

Stepper motor driver: to control the input current to stepper motor and its steps/rev
Model: DM542
Make: Leadshine Technology Co. Ltd. China
Specifications: Output current; 1-4.2 A, max. Micro step: 25000 Steps/rev.

Arduino-UNO control board: to control or program motion of stepper motor and linear actuator.
Model: Arduino UNO
Make: Arduino, Italy
Specifications: Clock speed: 16MHz

Rotary encoder:
Model: RMCS-5105
Make: Rhino Motion Controls
Specifications: Pulse per revolution (PPR): 600

Oscilloscope: to monitor pulse-on time, pulse-off time, and voltage.
Model: SMO 1002;
Make: Scientific Mes-Technik Pvt. Ltd. India
Specifications: Signal bandwidth: 100 MHz
Max real time sampling: 1 GSa/s

Ammeter: to monitor the current utilized in flank modification by PED process
Model:
Make: Shanti Instruments Pvt. Ltd. India
Specifications: Measuring range: 0-50 A

Temperature sensor: to measure electrolyte temperature.
Specifications: J-type thermocouple

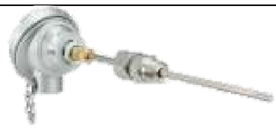

Stainless steel centrifugal pump: to pressurize the electrolyte.
Model: SRN-5-22
Make: Shakti Pumps India Ltd.
Specifications: Power: 5 HP

Temperature controller: to maintain constant temperature of electrolyte by controlling the power supply to electrolyte heater.
Model: *i-therm* AI-5941
Make: Innovative Instruments & Controls Ltd. India
Specifications: Sensor Input T/C: J, K, R, S; RTD: Pt-100

Rotameter
Make: AAR Industrial Products (India)
Specifications: Measuring range: 10-100 lpm

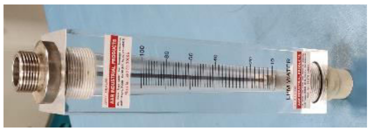

Pressure gauge: to measure pressure of electrolyte.
Make: Micro Process Controls Ltd. India
Specifications: Max pressure: 14 kg/cm^2 (13.73bar)

Stainless steel electrolyte filter

3.1.1 Flank Modification Chamber

It consists of a novel arrangement of five developed cathode gears in such a manner that the anodic workpiece gear can be provided tip relief, root relief, end relief, profile crowning, and lead crowning either individually or their selected combination. Figure 3.1c shows its photograph. It comprises lower and upper guide plates made of Bakelite. Linear bearings are attached to both guide plates to provide smooth reciprocating movement to the shaft on which anodic workpiece gear is mounted. Ball bearings are attached to both guide plates to provide rotary motion to the shaft on which five developed cathode gears are mounted.

3.1.2 Drive System for Anodic Workpiece Gear and Cathode Gear

The drive system consists of a linear actuator connected to the shaft on which the anodic workpiece gear is mounted, and one stepper motor connected to the shaft on which five cathode gears are mounted. Its functions are: (i) to engage the anodic workpiece gear with a particular cathode gear to impart the intended flank modification, (ii) to provide reciprocating motion to the anodic workpiece gear by a linear actuator, (iii) to provide rotatory motion to the cathode gear by a stepper motor, and (iv) disengage the anodic workpiece gear after providing the intended flank modification. The stepper motor and linear actuator are controlled by Arduino Uno board programmed using Arduino Software. A rotary encoder is connected to a linear actuator to measure reciprocating velocity of the anodic workpiece gear, whereas a non-contact tachometer was used to measure the rotary speed of the stepper motor.

3.1.3 Power Supply System

Pulsed direct current (DC) power supply unit SM-100-AR-75 from *Delta Elektronika* having the capacity to supply voltage up to 100 V and current up to 75A was used to supply the required electrical power for providing the flank modifications. Carbon brushes were used to connect the positive and negative terminals of the power supply to the shafts of the anodic workpiece gear and cathode gear respectively as shown in Fig. 3.2. They have been used due to their ability to slip over the shafts and maintain an uninterrupted power supply. An oscilloscope is used to monitor the DC power supplied to the modification chamber and an ammeter is used to measure the supplied current.

3.1.4 Electrolyte Supply and Recycling System

The prepared electrolyte solution is supplied using a stainless steel multistage centrifugal pump through flexible pipes to the modification chamber from the electrolyte tank. The flow rate of electrolyte is regulated by a flow control valve and measured by a rotameter, its pressure is measured by a pressure gauge, and its temperature is measured by a thermocouple. The used electrolyte is collected in a sludge tank kept below the modification chamber. It is then filtered and sent back to the electrolyte tank by a pump for its recirculation.

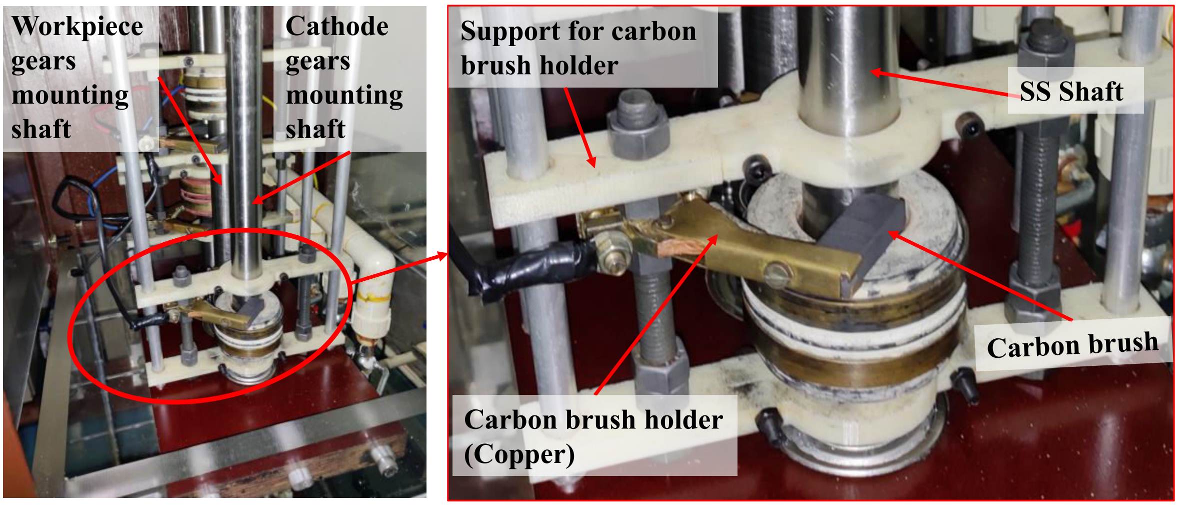

Fig. 3.2 Electrical connection between power supply and shafts mounting workpiece and cathode gears through carbon brush.

Table 3.2: Details of the materials selected for different components of the apparatus along with their selection criteria.

Component	Selected material	Selection criteria
Anodic workpiece gear	20MnCr5 alloy steel	Commercially used for manufacturing spur gears and electrically conductivity
Cathode gears sandwiching of non-conductive and conductive portions	Conductive portion: copper Non-conductive portion: Metalon	Copper: High electrical conductivity Metalon: Corrosion resistance, electrical insulation
Holding system for workpiece gear in the modification chamber	Perspex	Corrosion resistance, electrical insulation, excellent dimensional stability
Positioning system for workpiece and cathode gears	Guide plates: Bakelite	Corrosion resistance, electrical insulation,
	Stainless steel for the shafts and bearings for mounting the workpiece and cathode gears	Corrosion resistance, good strength, electrically conductive
Electrical connection between power supply and shafts mounting workpiece and cathode gears	Carbon brushes	Ability to slip over the rotating shaft and good electrical conductor

3.2 Development of Cathode Gears and their Flank Modification Mechanisms

Innovative designs of five cathode gears were conceptualized to impart non-contact tip relief, root relief, end relief, profile crowning, and lead crowning to anodic spur gear by the PED process using the developed apparatus. Table 3.3 presents specifications for these five cathode gears.

Table 3.3 Specifications of the developed five cathode gears for non-contact flank modifications of anodic spur gear.

Flank modification name	Thickness of conductive (i.e., copper) portion	Thickness of non-conductive (i.e., Metalon) portion	Dimensions	Common dimensions
Tip relief	10 mm	5 mm of top and bottom portions	d_{tr}: 69.7 mm Δr_1: 1.0 mm Δr_2: 0.5 mm	Module: 3 mm Number of teeth: 24 Pressure angle: 20°
Root relief	10 mm	5 mm of top and bottom portions	d_{rr}: 76.5 mm Δt_1: 0.7mm Δt_2: 0.8 mm	d_p: 72 mm d_a: 78 mm d_b: 67.7 mm
End relief	t: 3 mm of top and bottom portions	14 mm	Δe_1: 0.5 mm Δe_2: 1.0 mm	Face width 'b': 20 mm Bore diameter: 25 mm
Profile crowning	10 mm	5 mm of top and bottom portions	d_{pr1}: 73 mm d_{pr2}: 71 mm Δt_{pc1}: 0.5 mm Δt_{pc2}: 1.0 mm Δt_{pc3}: 1.0 mm Δt_{pc4}: 0.5 mm	Hub height: 10 mm Hub thickness: 10 mm
Lead crowning	5 mm	7.5 mm of top and bottom portions	Δt: 0.5 mm	

The designed cathode gears for tip relief, root relief, profile crowing, and lead crowning have a conductive portion sandwiched between two non-conductive portions, whereas the cathode gear for end relief has a non-conductive portion sandwiched between two conductive portions. Copper for conductive portion and Metalon for non-conductive portion was used to manufacture each cathode gear. Figure 3.3 shows the manufacturing and assembling of the different portions of cathode gear for tip relief. A concentric bore of 25 mm diameter (45 mm diameter for the top portion of the cathode gear for end relief) was trepanned by the computer numerically controlled (CNC) wire spark erosion machine *SprintCut Win* (from Electronica Ltd. Pune) in each conductive portion of all the five cathode gears. Then the designed teeth were machined in the same setup in each conductive portion of all the five cathode gears. The designed teeth in each non-conductive portion of the cathode gears for tip relief, root relief, and profile crowning were machined on the CNC milling machine *EMCO Mill E350* (from EMCO Inc. Austria). The designed teeth in each non-conductive portion of the cathode gear for end relief and lead crowning were machined by the gear hobbing machine. Before machining their teeth, a concentric bore of 25 mm diameter was drilled in each non-conductive portion of all the five cathode gears, followed by making a hub of 45 mm outside diameter and 10 mm height in upper non-conductive portion (middle portion for the end relief cathode gear) of each cathode gear. Two diametrically opposite holes (depicted in Fig. 3.3) were made in the hub to enable tight mounting of the cathode gear on their shaft. Sandwiching of conductive and non-conductive portions of a cathode gear was done with the help of an adhesive. Subsequently, two holes were drilled on all three portions of a cathode gear (can be seen in Fig. 3.3) by the CNC milling machine for their tight fastening by means of two grub screws made of stainless steel. Design and development of each cathode gear are described in the following subsections along with corresponding flank modification mechanism.

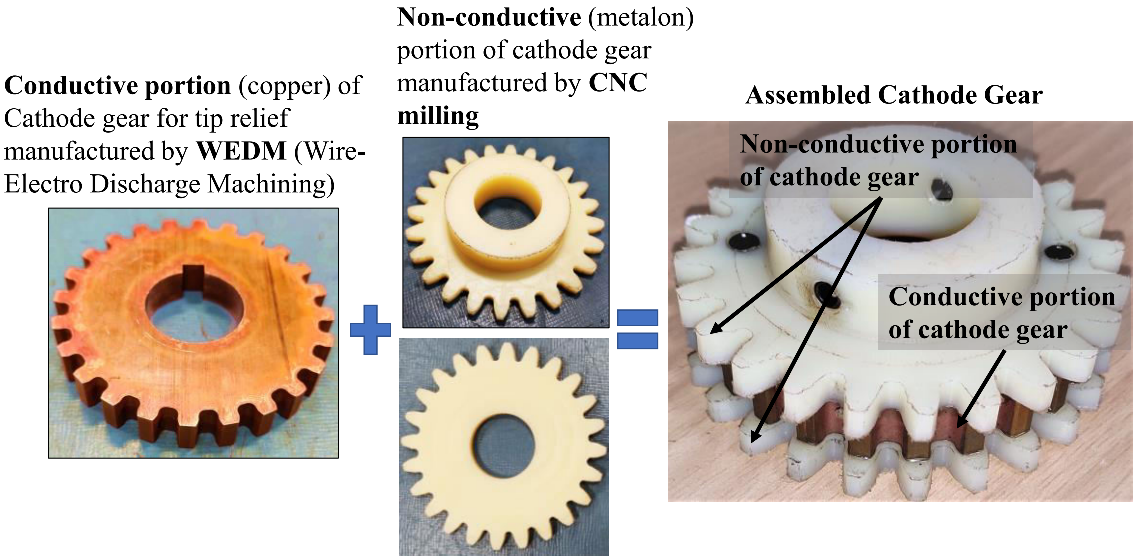

Fig. 3.3: Manufacturing processes used for different portions of cathode gear for tip relief.

3.2.1 Cathode Gear for Tip Relief

Figure 3.4a shows schematic of developed cathode gear for non-contact tip relieving of anodic workpiece gear, Fig. 3.4b depicts its photograph and Fig. 3.4c schematically shows design of its single tooth. It is designed in such a way that (i) material is removed only from the tip of the teeth of anodic workpiece gear, thus providing it the desired amount of tip relief. It is ensured by truncating the teeth of the conductive portion of the cathode gear, and (ii) variable interelectrode gap (IEG) is provided between its conductive portion and the anodic workpiece gear during their meshing. It is achieved by varying circumferential gap between non-conductive and conductive portions of the cathode gear. Its value is maximum (i.e., Δr_1 = 1 mm) at conductive portion diameter 'd_{tr}' and is minimum (i.e., Δr_2 = 0.5 mm) at base circle diameter 'd_b' as shown in Fig. 3.4c Variable IEG provides flexibility to limit electrolyte action above the pitch circle diameter of the cathode gear and helps to remove material only from the tip of anodic workpiece gear teeth. Figures 3.d to 3.4f illustrate the mechanism of non-contact tip relieving of an anodic workpiece gear by the designed cathode gear with red color circles showing the region of discussion. Though Figs 3.4d to 3.4f; (and Figs. 3.5d to 3.5f; and 3.7d to 3.7f) may seem to be repetitive but each figure shows different points of contact between the anodic workpiece gear tooth and corresponding cathode gear tooth during their meshing (shown by the red circle marked in the respective figure) and consequently the new location of the IEG along the line of action. Figure 3.4d depicts the start of meshing of left-flank tip of anodic workpiece gear with the non-conductive portion of the cathode gear with minimum IEG occurring along the line of action. According to Faraday's laws of electrolysis, the amount of the material removed in the PED process is more where IEG is smaller therefore more material will be removed from the left-flank tip of the anodic workpiece gear. The design of the cathode gear makes the IEG vary along the line of action as the gears slightly rotate further to their new position (as shown in Fig. 3.4e) and consequently the amount of material removal from the tip of anodic workpiece gear also decreases. Further rotation of the anodic workpiece gear starts disengagement of its left-flank tip with the non-conductive portion of the cathode gear thus stopping material removal from it and the same action shifts to its right-flank tip as shown in Fig. 3.4f. This sequence of events continues for all the teeth of the anodic workpiece gear for a given duration of tip relief by the PED process.

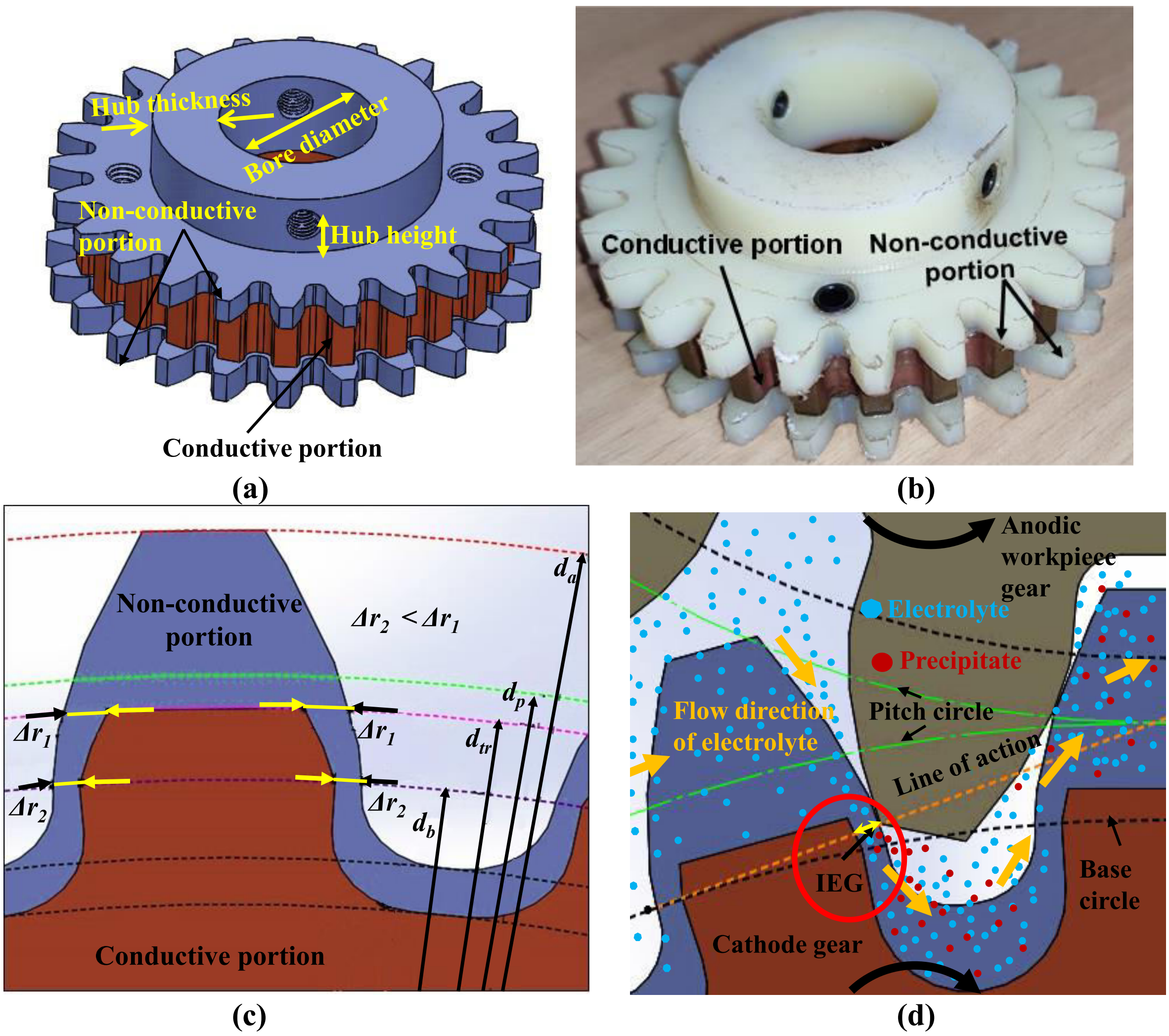

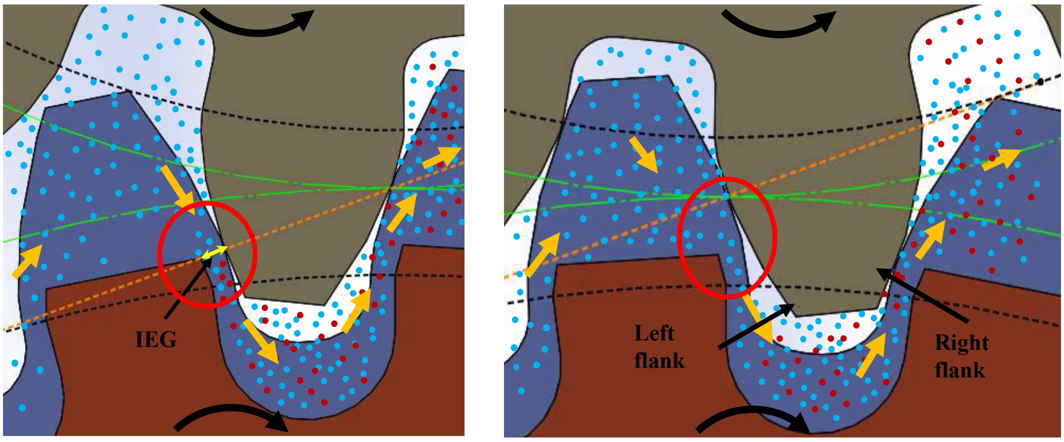

(e) (f)

Fig. 3.4: Developed cathode gear *for non-contact tip relieving* of an anodic workpiece gear and its imparting mechanism: (a) schematic diagram, (b) photograph, (c) design details of its single tooth, (d) minimum IEG at start of meshing of left-flank tip of anodic workpiece gear tooth with non-conductive portion of cathode gear tooth, (e) new position of IEG after slight rotation of gears, (f) left-flank tip of anodic workpiece gear tooth disengaging with the non-conductive portion of the cathode gear.

3.2.2 Cathode Gear for Root Relief

Figures 3.5a depicts schematic of developed cathode gear for non-contact root relieving of anodic workpiece gear and Fig. 3.5b shows its photograph. It has spikes on its conductive portion, which are electrically insulated with the help of insulation tape, except for their tips. The exposed tips of these spikes are responsible for providing the desired amount of root relief to the anodic workpiece gear. Figure 3.5c presents design details of single tooth of the developed cathode gear for non-contact root relieving. It has circumferential gap between non-conductive and conductive portions at the addendum circle 'Δt_1' as 0.7 mm and its value at the tip of electrical insulation 'Δt_2' as 0.8 mm. and, respectively. Figures 3.5d to 3.5f illustrate the mechanism of non-contact root relieving an anodic workpiece gear by the designed cathode gear with the marked red color circles highlighting the regions for discussion. Figure 3.5d shows the start of meshing of the right-flank of the anodic workpiece gear with tip of non-conductive portion of cathode gear and the occurrence of minimum IEG outside the base circle. According to the electrolysis laws of Faraday, it will give maximum removal of material from the root of the involute profile on the right-flank of the anodic workpiece gear tooth. Continuous rotation of the gears to the new positions shifts the conducting portion of spikes inside the base circle thus increasing the IEG (as shown in Fig. 3.5e) which reduces the amount of material removal. Further rotation of gears causes disengagement of the right-flank of the anodic workpiece gear tooth from the tip of non-conductive portion of the cathode gear tooth (as shown in Fig. 3.5f). Subsequently, same action shifts to left flank of the anodic workpiece gear tooth. This sequence of events continues for all the teeth of the anodic workpiece gear for the entire duration of root relief by the PED process.

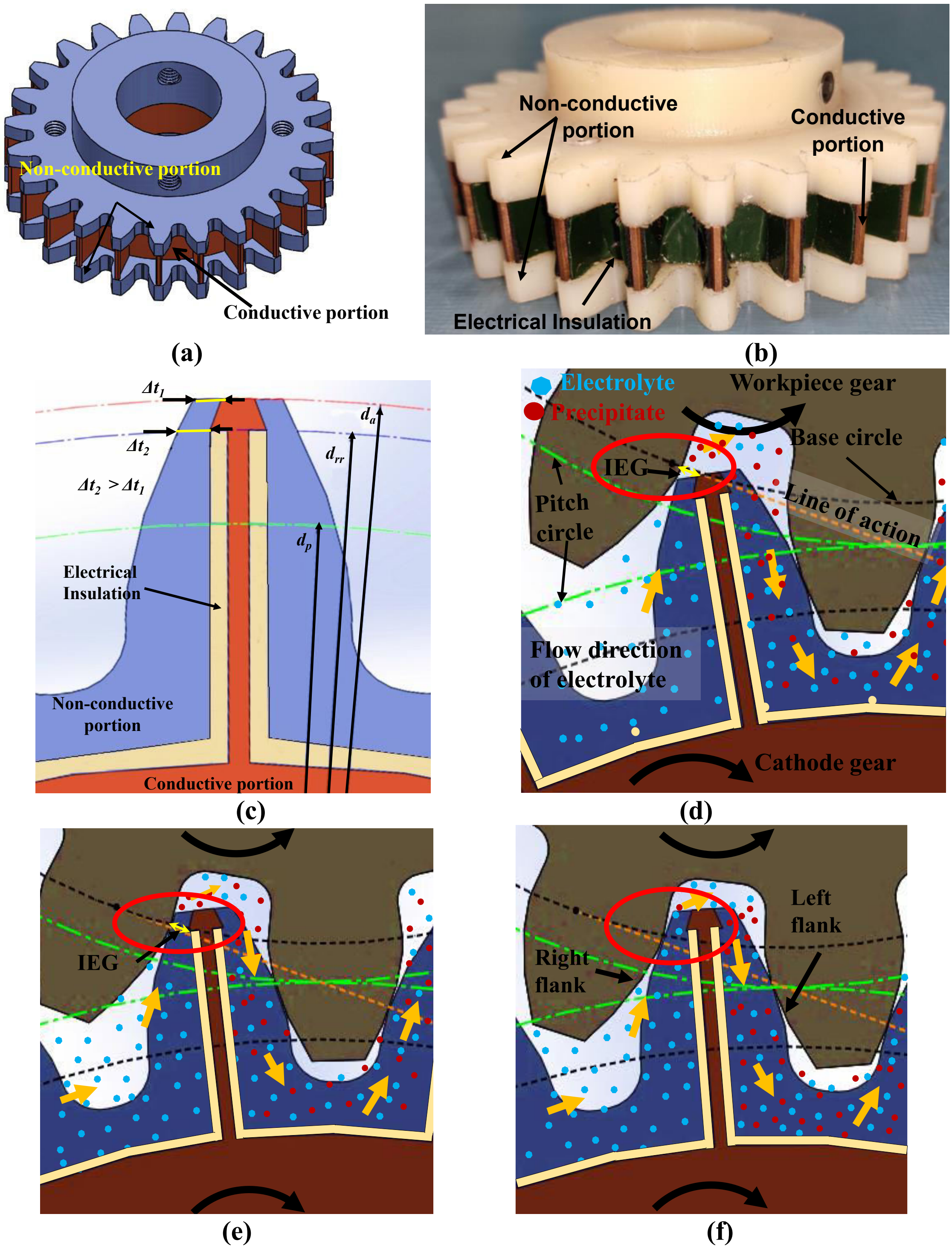

Fig. 3.5: Developed cathode gear for *non-contact root relieving* of a anodic workpiece gear and its mechanism: (a) schematic diagram, (b) photograph, (c) design details of its single tooth, (d) occurrence of minimum IEG outside the base circle at the start of meshing of right-flank of the workpiece gear with tip of non-conductive portion of the cathode gear, (e) new position of IEG after slight rotation of gears, (f) disengagement of right-flank of workpiece gear tooth from tip of non-conductive portion of the cathode gear tooth.

3.2.3 Cathode Gear for End Relief

Figure 3.6a presents schematic of meshing of anodic workpiece gear with the developed cathode gear for its non-contact end relieving by PED process along with its two enlarged views. Figures 3.6b and 3.6c respectively depict schematic and photograph of the developed cathode gear for end relieving. It is designed in such a manner that it removes the material only from the top and bottom ends of anodic workpiece gear teeth along their profile. It is achieved through the following measures: (i) Sandwiching 14 mm thick non-conductive portion between the two conductive portions of 3 mm thickness each as shown in Figs. 3.6a and 3.6b. When the designed cathode gear meshes with the anodic workpiece gear, then electrochemical dissolution takes place at the top and bottom ends of the anodic workpiece gear teeth by the top and bottom conductive portions of the cathode gear. Thickness of the conductive portion determines length of the end relief, (ii) Providing taper to the conducting portion teeth along their face width such that their flank surfaces are tapered towards the non-conducting portion. It will cause the circumferential gap between the non-conductive and conductive portion to vary from minimum value (i.e., Δe_1) of 0.5 mm to maximum value (i.e., Δe_2) of 1 mm as shown in the enlarged view in Fig. 3.6a. It will lead IEG varying in a range from 0.5 to 1.0 mm will result in removal of maximum material from the anodic workpiece gear at minimum IEG and vice-versa. This will yield continuous relieving of ends of anodic workpiece gear teeth without the formation of any step, and (iii) Not providing reciprocating velocity to anodic workpiece gear because end relief does not occur on entire face width of its gear teeth therefore, the rotary motion of cathode gear is sufficient to impart end relief to all teeth of anodic workpiece gear. The bore diameters in bottom and top conductive portions of the cathode gear are 25 mm and 45 mm respectively for mounting of the top conductive portion on the hub of non-conductive portion as shown in Fig. 3.6b. It results in the bottom conductive portion being in direct contact with its mounting shaft, but the top conductive portion is not. To ensure that electrochemical dissolution takes places at top and bottom conductive portions of the cathode gear, two holes were drilled on all three portions of a cathode gear (shown in Fig. 3.6b) to connect the bottom conductive portion with the top conductive portion by two grub screws made of stainless steel thus electrically connecting top conductive portion with the mounting shaft.

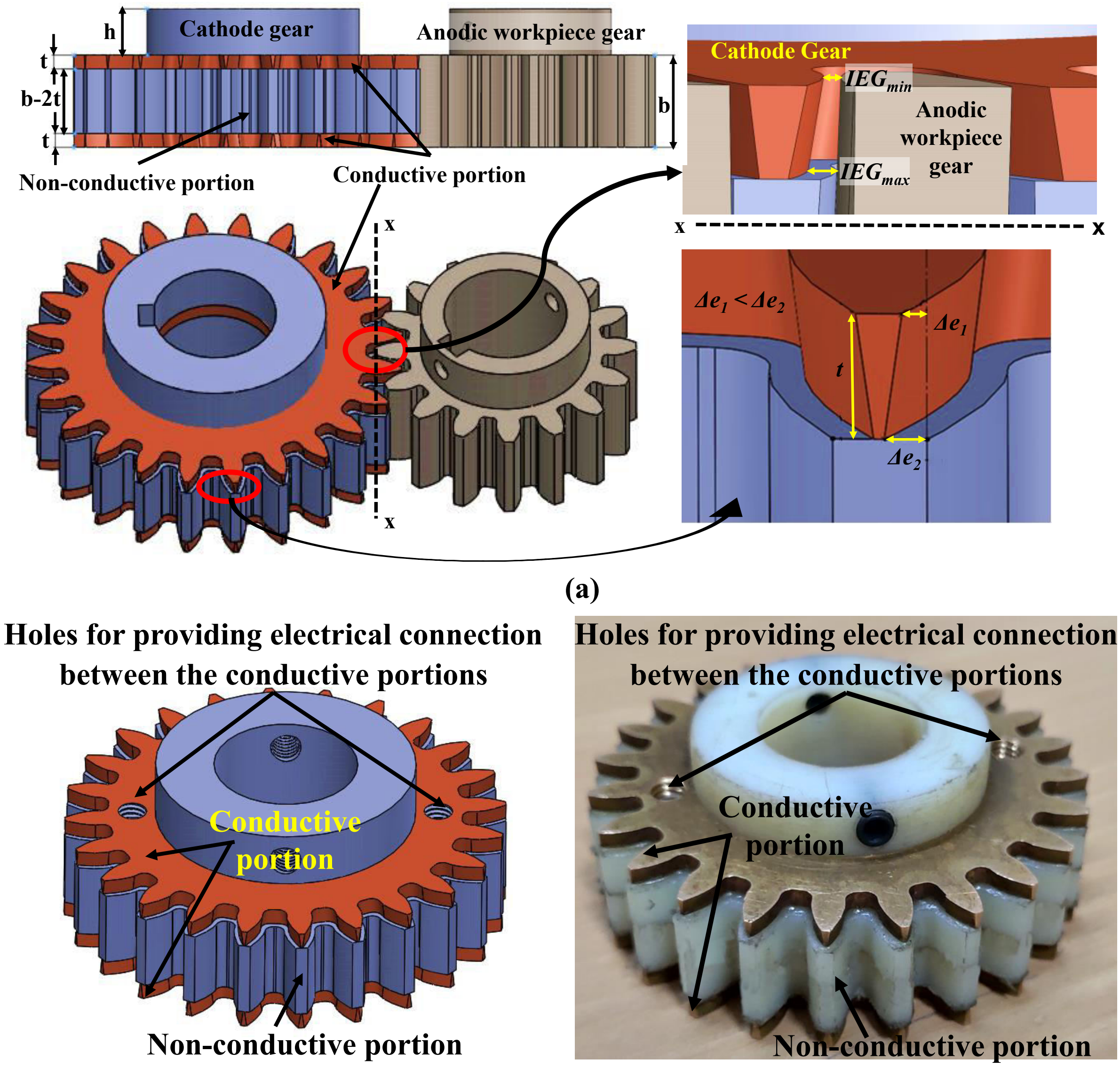

(b) (c)

Fig. 3.6: Developed cathode gear for *non-contact end relieving* of an anodic workpiece gear by PED process: (a) schematic of engagement of cathode and anode gears along with enlarged view of their teeth meshing, (b) schematic of cathode gear, (c) photograph of developed cathode gear.

3.2.4 Cathode Gear for Profile Crowning

Figures 3.7a depicts schematic of the developed cathode gear for non-contact profile crowning of anodic workpiece gear, Fig. 3.7b shows its photograph, and Fig. 3.7c shows design details of its single tooth. It is designed in such a manner that more material is removed from the tip and root of the anodic workpiece gear, and it gradually decreases towards its pitch line, forming a convex flank surface which cambers along the profile of anodic workpiece gear teeth. It is achieved by (i) varying the circumferential gap between non-conductive and conductive portions from a minimum value of 0.5 mm which is occurs as 'Δt_{pc1}' and 'Δt_{pc4}' respectively at addendum and base circle diameters of the cathode gear to a maximum value of 1.0 mm which occur as 'Δt_{pc2}' and 'Δt_{pc3}' at diameters 'd_{pr1}' and 'd_{pr2}'

respectively as shown in Fig. 3.7c, and (ii) by providing electrical insulation to the conductive portion teeth at their pitch line and below their base circle as shown in Figs. 3.7c. Cathode gear's conductive portion teeth profiles between addendum circle and pitch circle removes the material from dedendum region of flank surfaces of the anodic workpiece gear whereas conductive portion teeth profiles between their pitch circle and base circle remove the material from addendum region of flank surface of anodic workpiece gear. Figures 3.7d to 3.7g show the mechanism of non-contact profile crowning of anodic workpiece gear by the designed cathode gear with the red color circles highlighting the regions of discussion. When root of right-flank the anodic workpiece gear tooth meshes with tip of non-conductive portion of the cathode gear then minimum IEG occurs between it and conductive portion of cathode gear (as depicted in Fig. 3.7d) causing removal of more material from it. Slight rotation of both the gears gradually increases the IEG from addendum circle to pitch circle of the cathode gear (as depicted in Fig. 3.7e) thereby causing decrease in material removal. Further slight rotation of both the gears again gradually decreases the IEG from pitch circle to base circle diameter of cathode gear (as shown in Fig. 3.7f). It again increases the amount of material removed from pitch circle to right-flank tip of anodic workpiece gear tooth. Further gear rotation causes disengagement of the right-flank tip of anodic workpiece gear tooth as depicted in Fig. 3.7g and sequence of events shifts to left-flank tip of the anodic workpiece gear. This cycle of events continues for all the teeth of anodic workpiece gear in entire profile crowning duration by PED process in which variable IEG removes more materials from tip and root of anodic workpiece gear teeth and very less material around its pitch line giving profile crowned anodic workpiece gear.

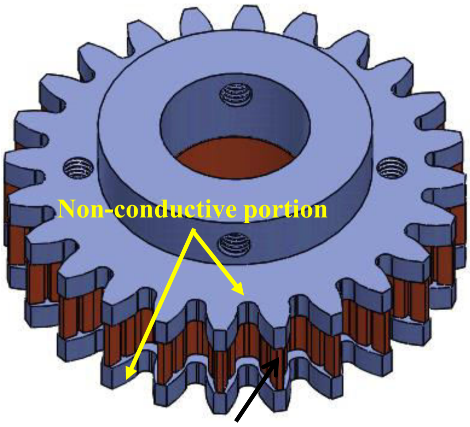

(a)

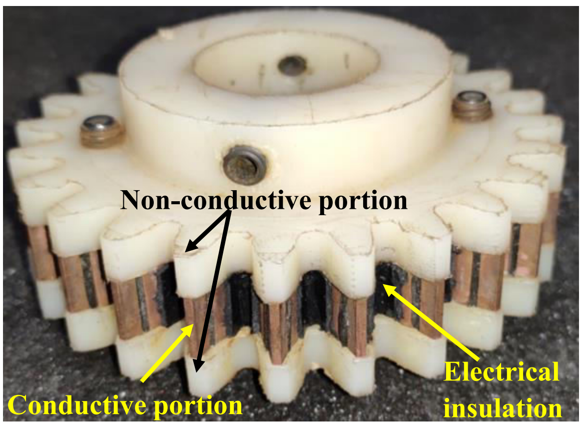

(b)

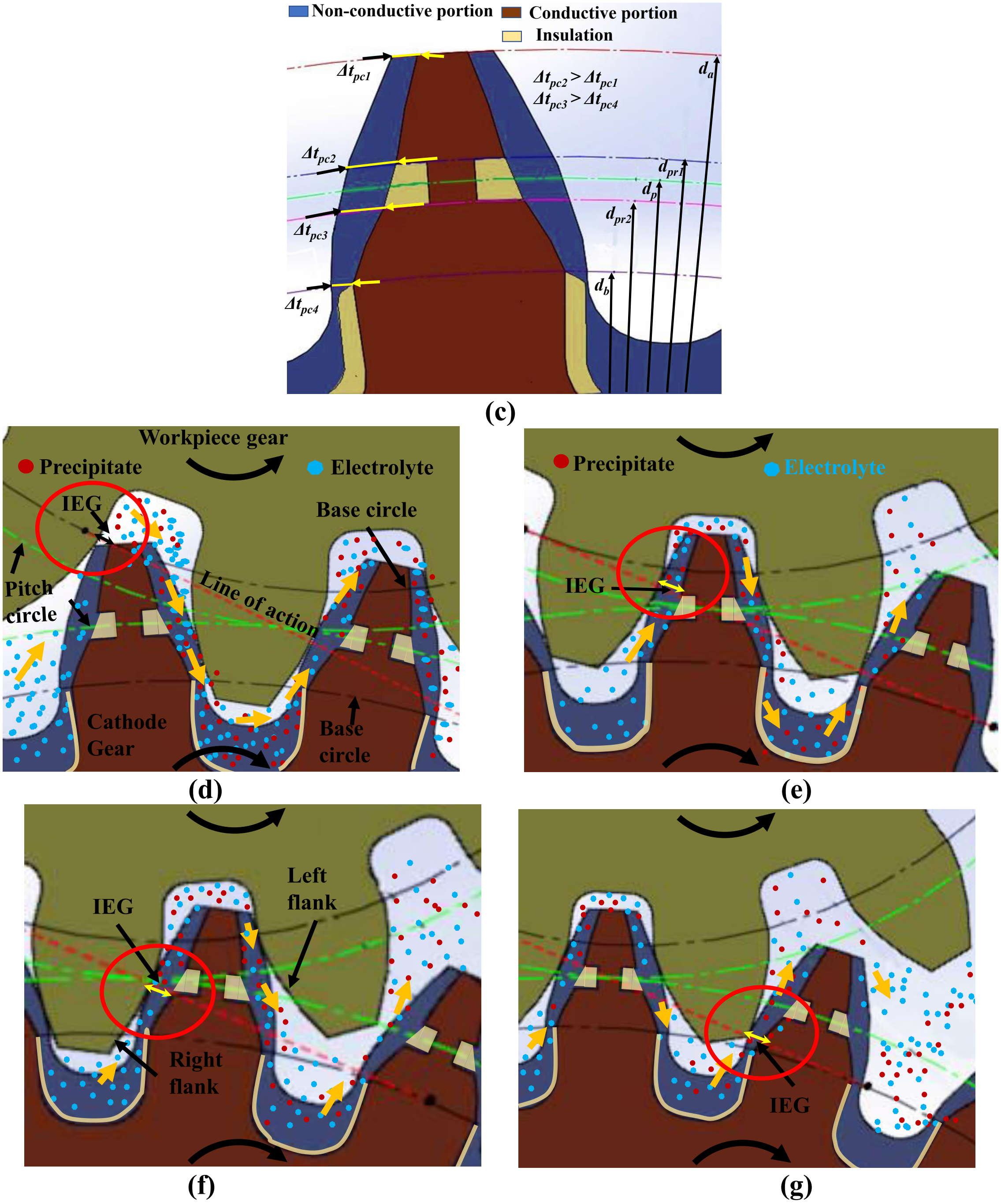

Fig. 3.7: Developed cathode gear for *non-contact profile crowning* of a anodic workpiece gear and its mechanism: (a) schematic diagram, (b) photograph, (c) design of its single tooth, (d) minimum IEG at start of meshing of right-flank root of anodic workpiece gear tooth with tip of non-conductive portion of cathode gear, (e) increase in IEG from addendum circle to pitch circle of the cathode gear, (f) decrease in IEG from pitch circle to base circle diameter of cathode gear, (g) right-flank tip of anodic workpiece gear disengaging with non-conductive portion of cathode gear.

3.2.5 Cathode Gear for Lead Crowning

Figures 3.8a depicts schematic of developed cathode gear for non-contact lead crowning of anodic workpiece gear, Fig. 3.8b shows its photograph, and Fig. 3.8c shows details of its single tooth. Lead crowning of an anodic spur gear requires that material removal should be varied along its face width so that convex flank surface cambering along the face width is generated on its teeth. Therefore, cathode gear for lead crowning is designed to have a uniform gap of 0.5 mm between non-conductive and conductive portions of the cathode gear along its profile (shown in Fig. 3.8c) which is responsible for an IEG between the conductive portion of cathode gear and anodic workpiece gear. Lead crowning of anodic workpiece gear is achieved by varying its reciprocating velocity and using the mechanism explained in Figs. 3.8d to 3.8f. Movement of the anodic workpiece gear is started downward when bottom end of anodic workpiece gear is above the conductive portion of the cathode gear as shown in Fig. 3.8d. Its reciprocating velocity is increased continuously from this point till midpoint of face width of anodic workpiece gear meshes with midpoint of conductive portion of the cathode gear as shown in Fig. 3.8e. Then it is decreased till the top end of face width of anodic workpiece gear reaches below conductive portion of the cathode gear as depicted in Fig. 3.8f. Subsequently, anodic workpiece gear is moved upward with same acceleration and deceleration. Figure 3.8g depicts variation in reciprocating velocity of anodic workpiece gear with the distance travelled by it. Such variation in reciprocating velocity of anodic workpiece gear changes time available for material removal along its face width, thus changing amount of the material removed. Since reciprocating velocity is maximum when anodic workpiece gear is meshing with conductive portion of cathode gear at midpoint of their face widths therefore, very less material is removed from middle region of face width of anodic workpiece gear teeth. Whereas reciprocating velocity is minimum towards the face width ends of anodic workpiece gear teeth thus removing more material from them. This variation in the material removal along face width of anodic workpiece gear teeth and simultaneous rotation of cathode gear enables the PED process to impart non-contact lead crowning to it.

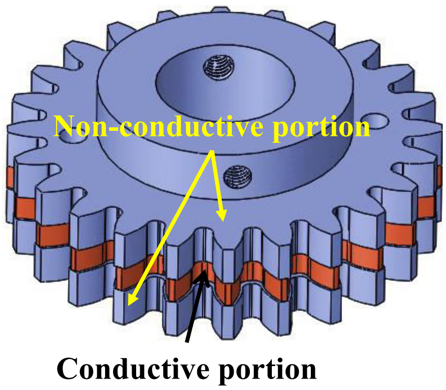

(a)

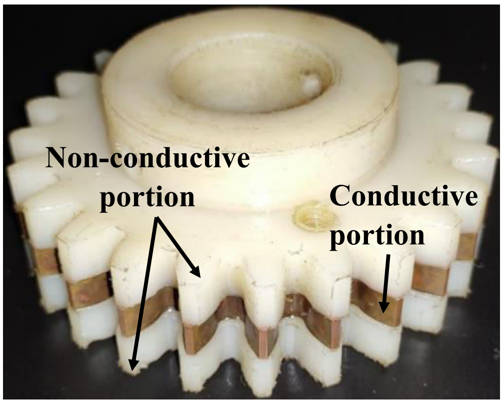

(b)

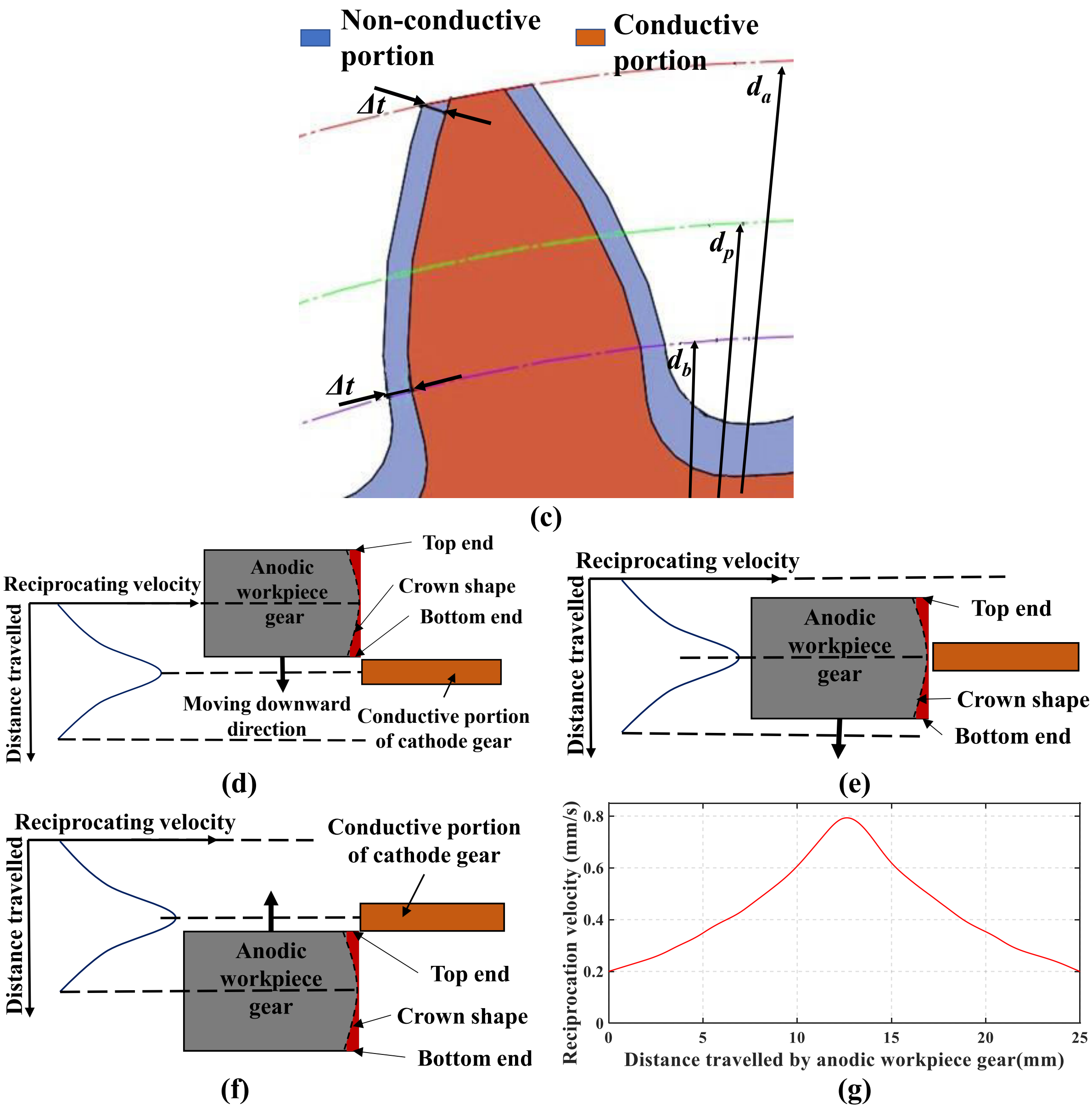

Fig. 3.8: Developed cathode gear for non-contact *lead crowning* of an anodic workpiece gear and its mechanism: (a) schematic diagram, (b) photograph, (c) design details of its single tooth, (d) anodic workpiece gear starts moving downward when the bottom end of face width of anodic workpiece gear is above conductive portion of the cathode gear, (e) anodic workpiece gear meshing conductive portion of the cathode gear at midpoints of their face widths, (f) top end of face width of anodic workpiece gear reaches below conductive portion of the cathode gear, (g) variation in reciprocating velocity of anodic workpiece gear with distance travelled.

3.3 Development of Single Flank Roll Tester

Single flank roll testing is also known as tangential composite testing. Figure 3.9 shows schematically working principle of the single flank roll testing in which workpiece gear and master gear are rotated at a specified center distance. Master gear is rotated by a motor which in turn drives the workpiece gear, and their angular positions are recorded by rotary encoders.

Single flank roll testing is carried out at low speed so that its results are not affected due to vibrations and tooth deformations occurring at high speed. Table 3.4 presents specifications of the components used to develop the single flank roll tester.

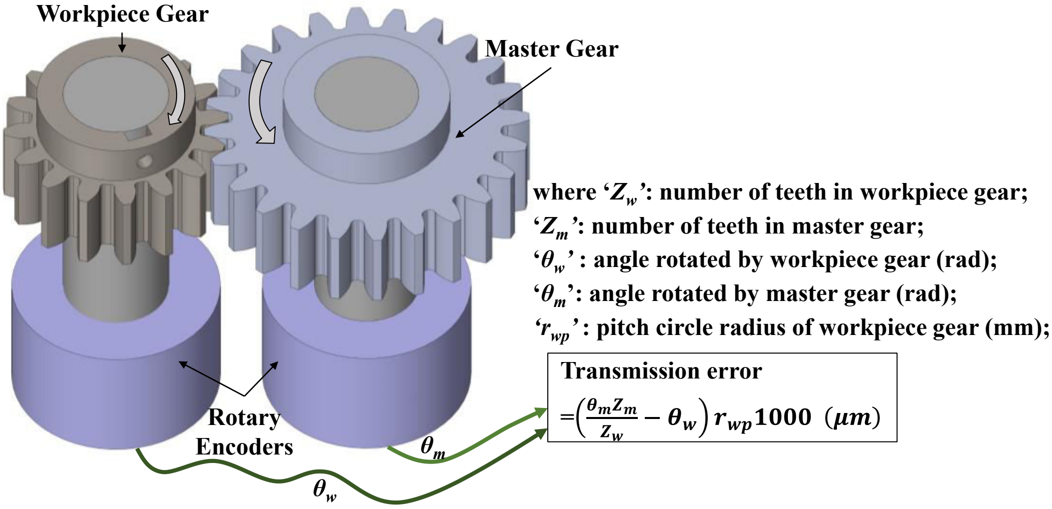

Fig. 3.9: Schematic of working principle of single flank roll testing.

Table 3.4: Specifications of the components used in development of single flank roll tester.

Rotary Encoder **Model:** E60H20-8192-6-L-5 **Make:** Autonics, South Korea **Specifications:** Pulse per revolution (PPR): 8192; Count per revolution (CPR): 32768	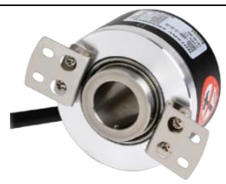
Arduino Due board used to transfer the data from encoders to the system. **Model:** Arduino Due **Make:** Arduino, Italy **Specifications:** Clock Speed: 84 MHz 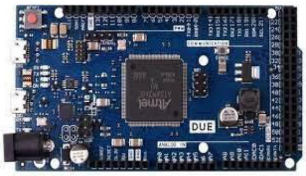	**Stepper motor** **Model:** 86HS78-5504 NEMA34 **Specifications:** Max. Torque: 4.5 Nm Step angle: 1.8° 
DC Power supply **Model:** LRS-100-24 **Make:** Mean Well Enterprises Co. Ltd., Taiwan **Specifications:** Max. output voltage: 24 volts Max. output current: 4.5 A; Power: 100 W	

Fig. 3.10 shows photograph of the developed single flank roll tester. It gives data about differences in theoretical and actual angular positions of the workpiece (or test) gear. The master gear is provided backlash of 0.25 mm on its one flank surface so that it has single-flank contact with the test gear which can be unmodified or modified spur gear during their meshing. The master gear is provided rotary motion by a stepper motor whose driver is controlled by the Arduino controller board. Optical rotary encoders have been fixed to both master and test gears to obtain signals of their angular positions in one complete revolution of the master gear. Clockwise and anti-clockwise rotatory motion is used to get data for both

flank surfaces of the test gear. The acquired data are further processed in MATLAB to determine transmission error of the test gear which is given by the following relation:

$$Tranmission\ error = \left(\frac{\theta_m Z_m}{Z_w} - \theta_w\right) r_{wp} 1000 \ \ (\mu m) \qquad (3.1)$$

The results obtained are normally expressed as a sinusoidal graph in which the abscissa is the angle of rotation, and the ordinate is the transmission error of the test as shown in Fig. 3.10b. Following parameters of single flank roll testing are evaluated on the basis of the measurements: (i) Total transmission errors 'F_i'' which is the difference between the maximum and minimum angular deviation in one revolution of the test gear, (ii) Tooth-to-tooth transmission errors 'f_i'' which is the maximum difference in angular deviations that occur during meshing of one tooth of test gear and master gear, and (iii) Longwave transmission error 'F_l'' is the difference between the maximum and minimum values of mean sinusoidal curve fitted to actual angular deviations curve.

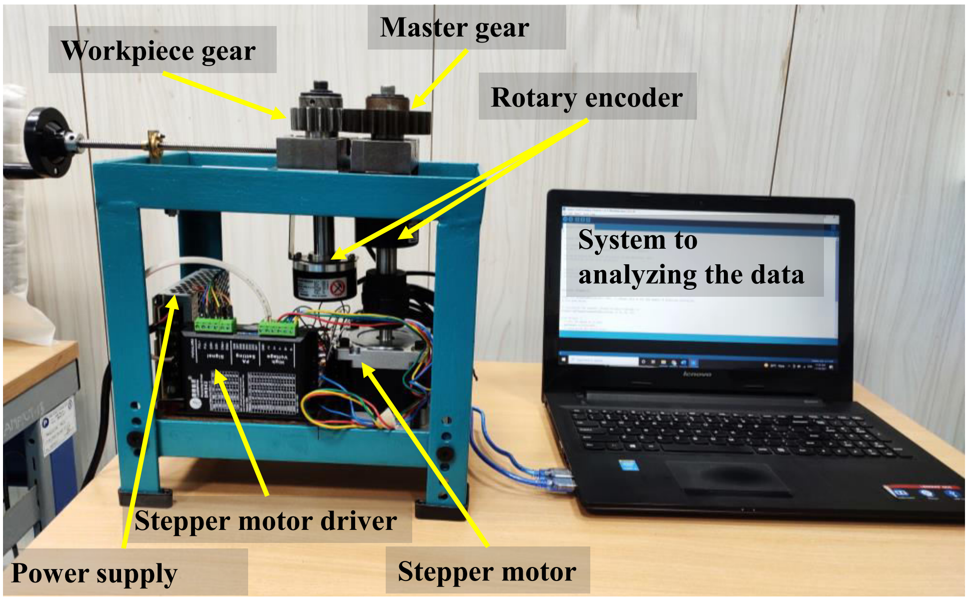

(a)

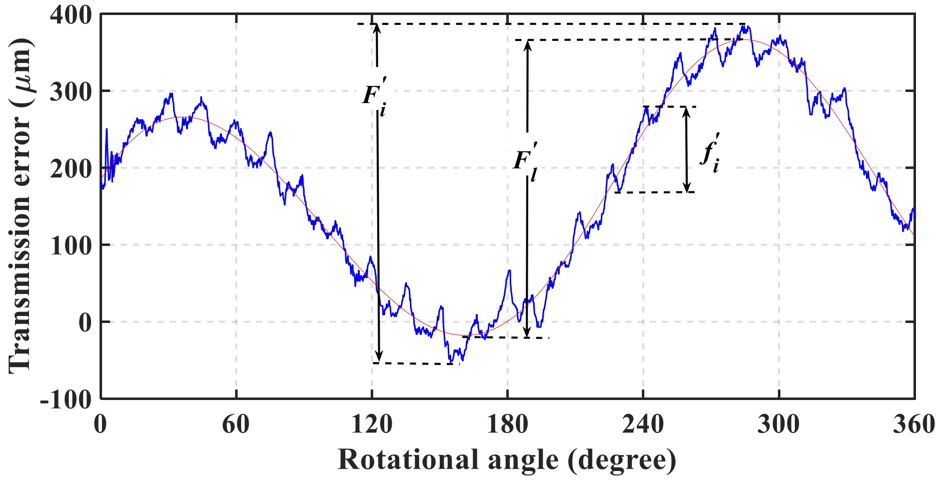

(b)

Fig. 3.10: Developed single flank roll tester: (a) Photograph, and (b) its sample results.

3.4 Specifications and Material of Workpiece Gear

Figure 3.11 shows the CAD drawing of the workpiece gear with its specifications. Alloy steel 20MnCr5 was chosen as workpiece gear material due to its commercial use in the manufacturing of spur gears. Composition of 20MnCr5 alloy steel is C 0.17-0.22%, Si 0.4%, Mn 1.1-1.4%, P 0.025%, S 0.035%, and Cr 1.0-1.3%. Vickers microhardness of the used 20MnCr5 alloy steel is 312 HV which is equivalent to 30 HRC. Some gears are carburized to increase their microhardness to 58-60 HRC.

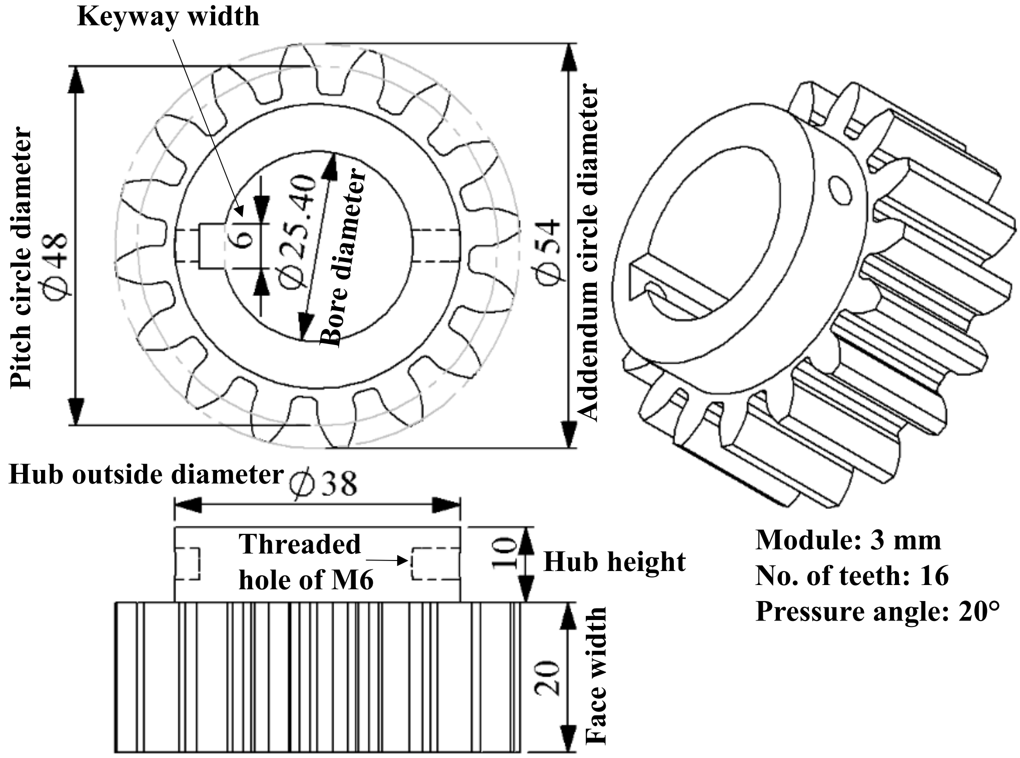

Fig. 3.11: CAD drawing of workpiece gear and its specifications.

Next Chapter describes the development of the analytical models for tip relief, root relief, end relief, and lead crowning of spur gears by the PED process.

Chapter 4

Development of Analytical Models for Flank Modifications

This chapter describes the development of the analytical models for non-contact tip relief, root relief, end relief, and lead crowning of anodic spur gear by the PED process. Analytical models are developed using two different approaches to calculate volume of material removal during flank modification by PED process i.e., first approach is using Faraday's law of electrolysis and second approach is using spur gear tooth geometry. The final expression for value of flank modification is obtained by equating the expressions of volumes of material removed obtained from both the approaches. The following common assumptions were made in the development of these analytical models.

4.1 Assumptions

1. Electrical conductivities of materials of anodic workpiece gear and cathode gear are much larger than electrolyte conductivity therefore they are considered as equipotential surfaces.
2. Effective voltage applied across anodic workpiece gear and cathode gear is $(V\text{-}\Delta V)$, where ΔV is total overpotential for both the electrodes, and it is assumed to be constant during entire process of tip/root/end relieving or lead crowning of anodic workpiece gear by the PED process.
3. Electrolyte temperature has been maintained constant therefore electrical conductivity of electrolyte has been assumed to remain constant during tip/root/end relieving or lead crowning by the PED process.
4. Interelectrode gap (IEG) between anodic workpiece gear and cathode gear remains constant at a particular location during the entire process of tip/end/root relieving or lead crowning by PED process but it may change with respect to location.
5. Evolutions of hydrogen gas at cathode gear and oxygen gas at anodic workpiece gear are neglected.
6. The shape of the tip or root or end relieved portion of anodic workpiece gear is assumed to be linear and shape of lead crowning is assumed to be a parabolic curve.
7. All the teeth of anodic workpiece gear and cathode gear are identical, and same value of tip/root/end relief or lead crowning is provided to right and left flanks of all the teeth of anodic workpiece gear.

4.2 Development of Model for Tip Relief

Figure 4.1a presents schematic of meshing of anodic workpiece gear with the cathode gear developed for its tip relieving by the PED process. The developed cathode gear has a conductive portion copper sandwiched between two non-conductive portions of Metalon. Therefore, reciprocating motion is provided to the anodic workpiece gear to impart tip relief along its entire face width, and simultaneously rotary motion is provided to the developed cathode gear to impart same amount of tip relief to its all teeth. Development of an analytical model for the amount of tip relief imparted to anodic workpiece gear flank surface '$C_{\alpha a}$' (mm) requires development of the following equations: (i) instantaneous area of anodic workpiece gear tooth which will be modified by the conductive portion of the developed cathode gear 'A_{ttr}' shown as hatched portion in Fig. 4.1b. It is equal to summation of top land area 'A_{tltr}' and area of involute profile of two consecutive flank surfaces of two adjacent teeth 'A_{tr}' i.e., $A_{ttr} = A_{tltr} + A_{tr}$, and (ii) involute profile arc length of anodic workpiece gear flank surface 'L_{tr}' which will be modified in tip relieving as depicted in Fig. 4.1b, (iii) chordal thickness 'w_a' of anodic workpiece gear tooth along its addendum circle as shown in Fig. 4.1b, and (iv) total volume of material removed from anodic workpiece gear teeth in tip relieving 'Q_{ttr}' using Faraday's law of electrolysis. In addition to the common assumptions mentioned in section 4.1 it is assumed that material is removed from top land and involute profile from addendum to datum circle (shown in Fig. 4.3a) of the anodic workpiece gear.

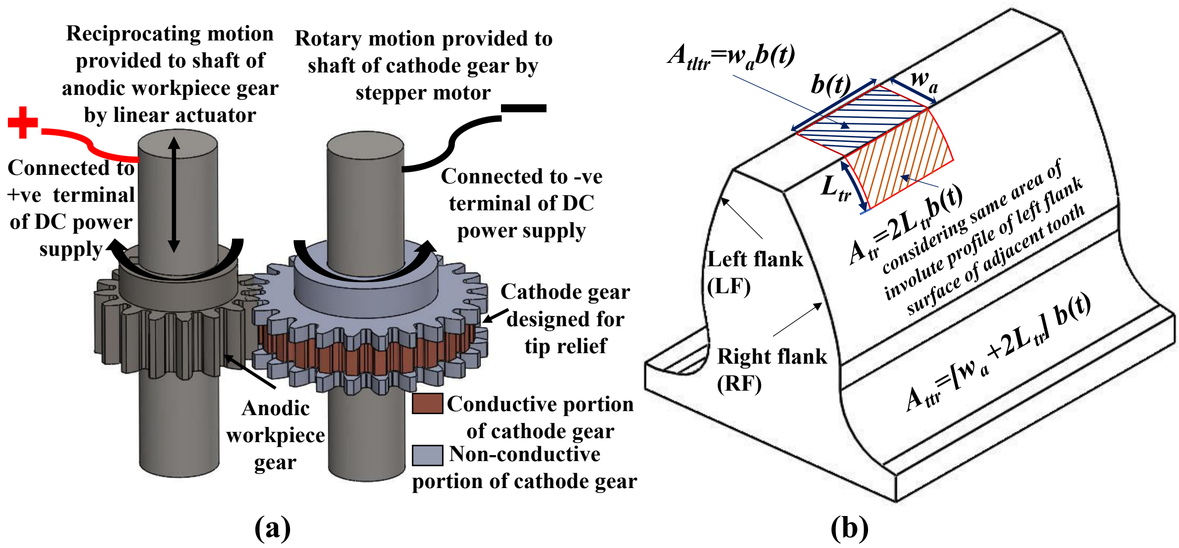

Fig. 4.1: Non-contact *tip relieving* of anodic workpiece gear by PED process: (a) schematic of meshing with the developed cathode gear, and (b) instantaneous area of anodic workpiece gear tooth 'A_{ttr}' that will be modified by conductive portion of the developed cathode gear.

4.2.1 Volumetric MRR during Tip Relieving

The following relation based on Faraday's law of electrolysis **(Jain 2009)** can be used for the total volume of material removed from the teeth of anodic workpiece gear 'Q_{ttr}' (mm^3) in non-contact tip relieving by the PED process:

$$Q_{ttr} = \int_0^{t_{fm}} dQ_{ttr} = \frac{\eta E}{\rho F}\int_0^{t_{fm}} jA_{ttr}\,dt \qquad (4.1a)$$

where 'η' is current efficiency of anodic dissolution (%); 'E' and 'ρ' are electrochemical equivalent (g) and density of anodic workpiece gear material (g/mm^3); 'F' is Faraday's constant; 'j' is current density (A/mm^2) and is given by $j = \kappa_e (V - \Delta V)/Y$ [in which 'κ_e' is electrical conductivity of the electrolyte (S/mm); 'Y' is IEG (mm); 'V' is applied voltage (volt); and 'ΔV' is overvoltage (volt)]; 't_{fm}' is tip relieving duration of the anodic workpiece gear (seconds); and 'A_{ttr}' is instantaneous area of anodic workpiece gear tooth modified by the conductive portion of the developed cathode gear (shown as the hatched area in Fig. 4.1b). Substituting its expression '$A_{ttr} = A_{tltr} + A_{tr} = w_a b(t) + 2L_{tr} b(t)$' in Eq. 4.1a gives the following expression:

$$Q_{ttr} = Q_{tltr} + Q_{tr} = \frac{\eta E}{\rho F} \int_0^{t_{fm}} j [w_a + 2L_{tr}] b(t)\ dt \qquad (4.1b)$$

where, 'Q_{tltr}' is volume of material removed from top lands of anodic workpiece gear teeth; 'Q_{tr}' is volume of material removed from involute profiles of anodic workpiece gear teeth in its non-contact tip relieving (mm^3), '$b(t)$' is fraction of total face width of anodic workpiece gear which varies with time during its meshing with conducting portion of the developed cathode gear for tip relieving (mm); 'w_a' is chordal thickness of anodic workpiece gear tooth along its addendum circle (mm); and 'L_{tr}' is involute profile arc length of anodic workpiece gear flank surface modified in its tip relieving (mm). Since the overvoltage 'ΔV' and electrical conductivity of electrolyte 'κ_e' have been assumed to remain constant during non-contact tip relieving by the PED process by maintaining electrolyte temperature constant and using higher flow rate of the electrolyte, therefore, numerator in expression of current density 'j' (i.e., $\kappa_e (V - \Delta V)/Y$) can be taken out of integration. Using location-specific expression for the IEG i.e., 'Y_{tltr}' as IEG at top land, and 'Y_{tr}' as IEG at involute profile of the anodic workpiece gear tooth (mm) in Eq. 4.1b leads to the following equation using the assumption that IEG at a particular location does not change during tip relieving:

$$Q_{ttr} = \frac{\eta E}{\rho F} \kappa_e (V - \Delta V) \left[\frac{w_a}{Y_{tltr}} + \frac{2L_{tr}}{Y_{tr}} \right] \int_0^{t_{fm}} b(t)\, dt \qquad (4.1c)$$

Volumetric MRR during non-contact tip relieving of anodic workpiece gear teeth 'M_{tr}' (mm^3/s) is computed by dividing the total material removed 'Q_{ttr}' (mm^3) by the duration of tip relieving 't_{fm}' (s) and representing integral part of Eq. 4.1c [i.e., $\int_0^{t_{fm}} b(t)\, dt$] as '$I$' in it gives the following relation:

$$M_{tr} = \frac{Q_{ttr}}{t_{fm}} = \frac{\eta E}{\rho F} \frac{\kappa_e (V - \Delta V)}{t_{fm}} \left[\frac{w_a}{Y_{tltr}} + \frac{2L_{tr}}{Y_{tr}} \right] I \qquad (4.2)$$

Equation 4.2 requires computations of 'L_{tr}' and 'w_a', which are described by Equations A2 and A4 in Appendix-A, the development of expression for 'I' considering continuous reciprocating motion of the anodic workpiece gear and use of pulsed DC power which is described in the next subsubsection. The values of IEG for the anodic workpiece gear tooth at its at top land 'Y_{tltr}' (mm), and at its involute profile 'Y_{tr}' (mm) depend on the design of the cathode gear developed for its tip relief.

4.2.2 Effects of Continuous Reciprocation of Workpiece Gear and Pulsed DC Power Supply

Anodic workpiece gear is continuously reciprocating during its tip or root relieving by the PED process. It causes continuous change in fraction of total face width *'b(t)'* of anodic workpiece gear during its meshing with conductive portion *'b_{ccg}'* of the cathode gear as depicted in Fig. 4.2a. When anodic workpiece gear starts its downward stroke with the reciprocating velocity *'S_l'* (mm/s) depicted as position 1 in Fig. 4.2a, it is in contact with non-conductive portion *'b_{ncg}'* of the cathode gear hence value of *'b(t)'* is zero at position 1. Value of *'b(t)'* increases up to face width of conductive portion of the cathode gear when anodic workpiece gear moves to position 2, it remains constant from position 2 to position 3 and decreases from position 3 to position 4 of anodic workpiece gear. The same sequence of these events occurs during upward stroke of the anodic workpiece gear from position 4 to position 7 as depicted in Fig. 4.2a and the same cycle is repeated. Since the conductive portion face width of developed cathode gear *'b_{ccg}'* is 10 mm (5 mm face width of each non-conducting portion giving total face width as 20 mm). Therefore, the maximum value of *'b(t)'* will be 10 mm. Figure 4.2b shows trapezium shaped variation of *'b(t)'* at different time instants during non-contact tip/root relieving of anodic workpiece gear, Figure 4.2c shows concept of pulsed DC power superimposed with trapezium shaped variation of '*b(t)*', and Table 4.1 presents expressions for different time instants in downward and upward stroke of anodic workpiece gear.

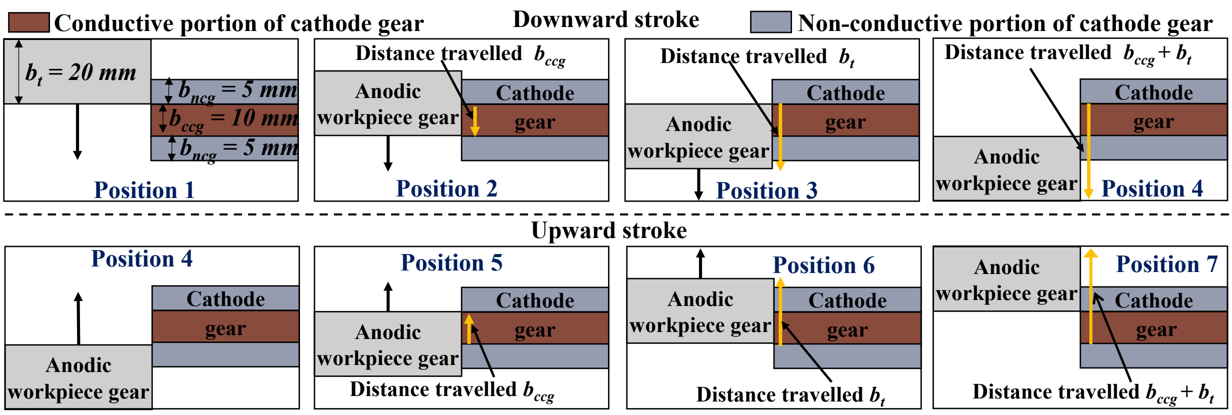

(a)

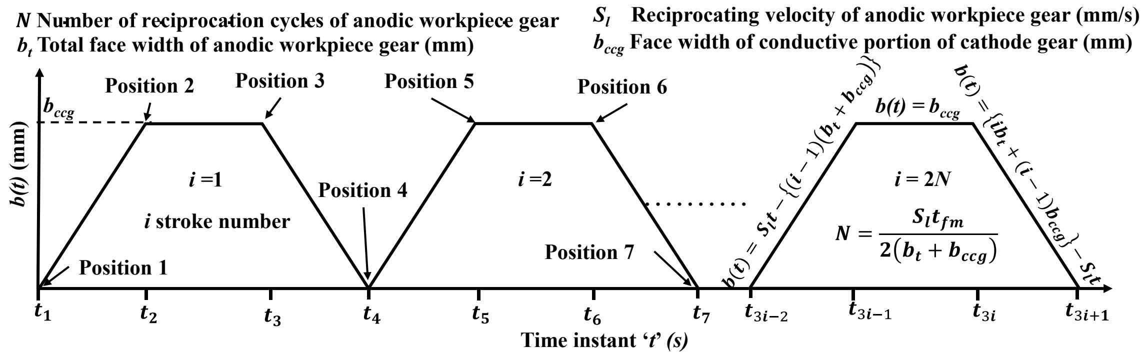

(b)

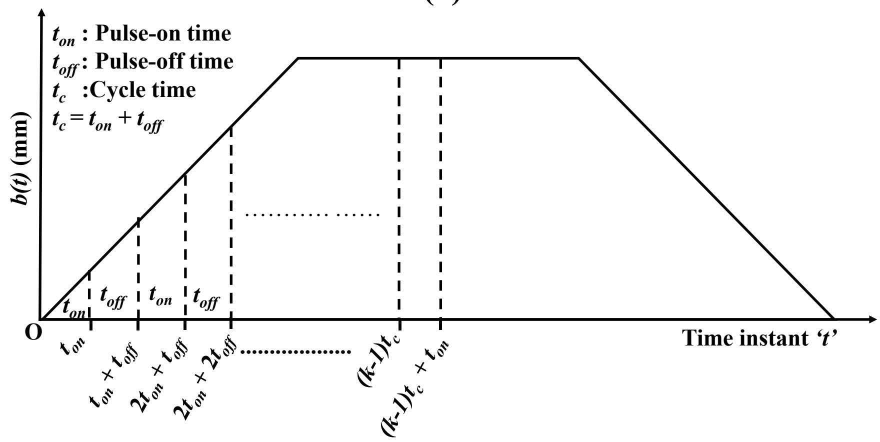

(c)

Fig. 4.2: Variation of fraction of total face width *'b(t)'* of anodic workpiece gear tooth while meshing with conductive portion of the cathode gear during its reciprocating motion: (a) different meshing positions, and (b) trapezium shaped variation of *'b(t)'* with time, and (c) concept of pulsed DC power superimposed with trapezium shaped variation of '*b(t)'*.

Table 4.1: Expressions for different time instants in downward and upward stroke of anodic workpiece gear in its non-contact tip or root relieving by PED process.

Stroke number	Time instant in tip/root relieving at the start of downward or upward stroke	Time instant in tip/root relieving at position 2 in downward or position 5 in upward stroke	Time instant in tip/root relieving at position 3 in downward or position 6 in upward stroke	Time instant in tip/root relieving at the end of a stroke
1st (i=1)	$t_1 = 0$	$t_2 = \frac{b_{ccg}}{S_l}$	$t_3 = \frac{b_t}{S_l}$	$t_4 = \frac{(b_t+b_{ccg})}{S_l}$
2nd (i=2)	$t_4 = \frac{(b_t+b_{ccg})}{S_l}$	$t_5 = \frac{b_t+2b_{ccg}}{S_l}$	$t_6 = \frac{2b_t+b_{ccg}}{S_l}$	$t_7 = \frac{2(b_t+b_{ccg})}{S_l}$
3rd (i=3)	$t_7 = \frac{2(b_t+b_{ccg})}{S_l}$	$t_8 = \frac{2b_t+3b_{ccg}}{S_l}$	$t_9 = \frac{3b_t+2b_{ccg}}{S_l}$	$t_{10} = \frac{3(b_t+b_{ccg})}{S_l}$
ith	$t_{3i-2} = \frac{(i-1)(b_t+b_{ccg})}{S_l}$	$t_{3i-1} = \frac{(i-1)b_t+ib_{ccg}}{S_l}$	$t_{3i} = \frac{ib_t+(i-1)b_{ccg}}{S_l}$	$t_{3i+1} = \frac{i(b_t+b_{ccg})}{S_l}$

The following relation is obtained for fraction of total face width of anodic workpiece gear *'b(t)'* by combining its equations in the trapezium corresponding to its i^{th} stroke during its tip or root relieving (as shown in Fig. 4.2b):

$$b(t) = \begin{cases} s_l t - \{(i-1)(b_t + b_{ccg})\} & t_{3i-2} < t \le t_{3i-1} \\ b_{ccg} & t_{3i-1} < t \le t_{3i} \\ \{ib_t + (i-1)b_{ccg}\} - S_l t & t_{3i} < t \le t_{3i+1} \end{cases} \quad (4.3)$$

where, *'b_t'* is the total face width of anodic workpiece gear (i.e., 20 mm); 'b_{ccg}' is conductive portion face width of developed cathode gear for tip relief (i.e., 10 mm); *'S_l'* is reciprocating velocity of anodic workpiece gear (mm/s); 'i' is stroke number of anodic workpiece gear having its values as 1, 2, ..., *2N;* in which '*N'* is its number of reciprocation cycles given by the ratio of total distance travelled by it to the distance travelled by it in its one reciprocation cycle i.e., $N = \frac{S_l t_{fm}}{2(b_t + b_{ccg})}$. Since pulsed DC power is used in the PED process therefore, tip/root/end relieving or lead crowning occurs during the pulse-on time 't_{on}' only, whereas pulse-off time *'t_{off}'* is used for effective flushing of the material removed from the anodic workpiece gear. Figure 4.2c shows concept of pulsed DC power superimposed with the trapezium shaped variation of '*b(t)',* which necessitates the following modification in integration limits of integral part *'I'* of Eq. 4.2.

$$I = \int_0^{t_{fm}} b(t)dt = \sum_{k=1}^{k=X} \int_{(k-1)t_c}^{(k-1)t_c + t_{on}} b(t)dt \quad (4.4)$$

where, 't_c' is cycle time of pulsed DC power; 't_{on}' is its pulse-on time; *'k'* is an index for the cycle of DC pulse with $k = 1, 2, ..., X$ in which $X = t_{fm}/t_c$. Following equation 4.5 is obtained for integral part *'I'* after combining the effect of continuous reciprocation of anodic workpiece gear (given by Eq. 4.3) with effect of using pulsed DC power (given by Eq. 4.4):

$$I = \sum_{k=1}^{k=X} \begin{cases} \int_{(k-1)t_c}^{(k-1)t_c + t_{on}} [S_l t - \{(i-1)(b_t + b_{ccg})\}]\, dt & t_{3i-2} < t \le t_{3i-1} \\ \int_{(k-1)t_c}^{(k-1)t_c + t_{on}} b_{ccg} dt & t_{3i-1} < t \le t_{3i} \\ \int_{(k-1)t_c}^{(k-1)t_c + t_{on}} [\{ib_t + (i-1)b_{ccg}\} - S_l t]\, dt & t_{3i} < t \le t_{3i+1} \end{cases} \quad (4.5)$$

4.2.3 Analytical Model for Tip Relief

Non-contact tip relieving of one flank surface of anodic workpiece gear by the PED process changes its involute profile from arc *GH* to line *GE* as shown in Figs. 4.3a and 4.3b and removes 'V_{tr}' volume of material from its one flank surface (as depicted in Fig. 4.3c) which is given by $Q_{tr}/2Z$ (here *'Z'* is no. of teeth in anodic workpiece gear). Dividing it by total face width of anodic workpiece gear *'b_t'* (mm) gives expression for area of *GEHG* given by Eq. 4.6:

$$V_{tr} = b_t\{Area\ of\ GEHG\} \Rightarrow Area\ of\ GEHG = \frac{Q_{tr}}{2Zb_t} \quad (4.6)$$

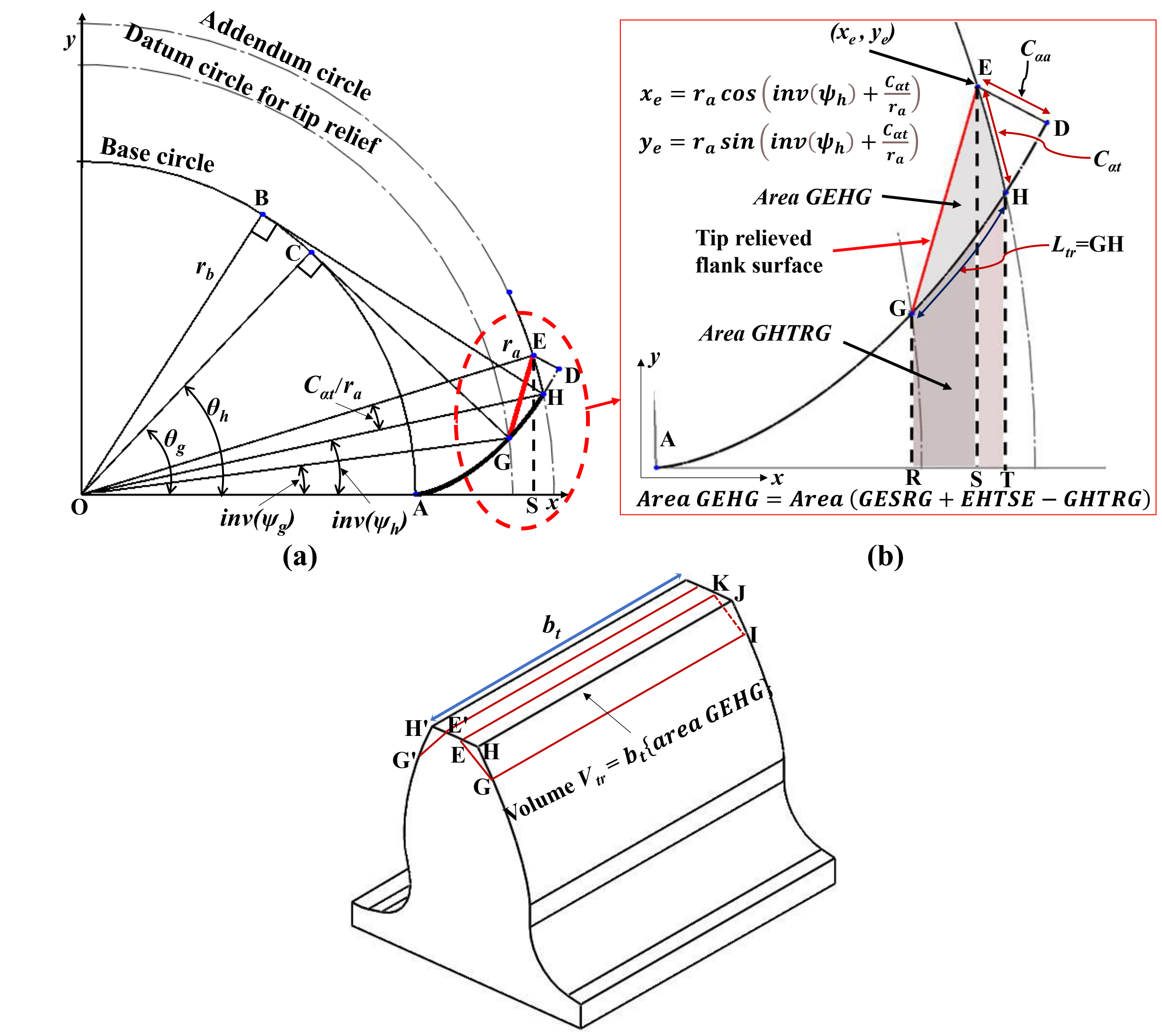

(c)

Fig. 4.3: Effect of non-contact *tip relieving* by the PED process on flank surface of anodic workpiece gear tooth: (a) change in its involute profile, (b) enlarged view used to compute area of *GEHG,* and (c) volume of material removed.

The *area of GEHG* can also be computed using the geometry shown in Fig. 4.3b. *'EH'* can be considered as a straight line on addendum circle for ease of computation of *area of EHTSE*. It can be observed in Fig. 4.3b that *area of GESRG* and *area of EHTSE* are trapezium shaped therefore, expression for *area of GEHG* can be expressed by Eq. 4.7a:

$$Area\ GEHG = \frac{1}{2}(y_g + y_e)(x_e - x_g) + \frac{1}{2}(y_e + y_e)(x_h - x_e) - Area\ GHTRG \quad (4.7a)$$

Equating Eq. 4.7a and Eq.4.6 for the *Area GEHG* gives the following Eq.

$$\Rightarrow \frac{Q_{tr}}{2Zb_t} = \frac{1}{2}\left[y_e(x_h - x_g) - x_e(y_h - y_g) + x_h y_h - x_g y_g\right] - Area\ GHTRG \quad (4.7b)$$

where, (x_g, y_g,) and (x_h, y_h) are cartesian coordinates of points '*G*' and '*H*', which can be computed using the parametric equations (i.e., Eq. A1b in Appendix-A) for involute profile and (x_e, y_e) are cartesian coordinates of point '*E*' which are mentioned in Fig. 4.3b.

Substituting expression for Area of GHTRG from Eq. A3b (from Appendix-A) in Eq. 4.7b; using expressions for 'x_e' and 'y_e'; and rearranging the terms gives the following expression for '$C_{\alpha t}$' (For details please refer to Eqs. A5 to A9b in Appendix-A):

$$C_{\alpha t} = r_a \left[sin^{-1} \left\{ \frac{\frac{Q_{tr}}{Zb_t} + D_{t1}}{D_{t2}} \right\} + D_{t3} \right] \tag{4.8}$$

where, 'D_{t1}', 'D_{t2}', and 'D_{t3}' are given by the following expressions:

$$D_{t1} = r_b{}^2 \left[\frac{sin2\theta_h - sin2\theta_g + \theta_g{}^2 sin2\theta_g - \theta_h{}^2 sin2\theta_h}{2} + \frac{\theta_g{}^3 - \theta_h{}^3}{3} + \theta_g cos2\theta_g - \theta_h cos2\theta_h \right] + y_g x_g - y_h x_h$$

$$D_{t2} = r_a \sqrt{\left(x_h - x_g\right)^2 + \left(y_h - y_g\right)^2}\ ; \qquad D_{t3} = tan^{-1}\left(\frac{y_h - y_g}{x_h - x_g}\right) - inv(\psi_h)$$

where, '$C_{\alpha t}$' is amount of tip relief imparted to anodic workpiece gear tooth along its top land (mm). Using the relation $C_{\alpha a} = \frac{r_b}{r_a} C_{\alpha t}$ **(Jelaska, 2012)** and substituting $Q_{tr} = \frac{\eta E}{\rho F} \kappa_e (V - \Delta V) \frac{2L_{tr}}{Y_{tr}} I$ in Eq. 4.8 gives the following equation for the amount of non-contact tip relief imparted to anodic workpiece gear flank surface '$C_{\alpha a}$' (mm) by the PED process:

$$\boldsymbol{C_{\alpha a} = r_b \left[\sin^{-1} \left\{ \frac{\frac{\eta E}{\rho F} \frac{\kappa_e (V - \Delta V)}{Zb_t} \frac{2L_{tr}}{Y_{tr}} I + D_{t1}}{D_{t2}} \right\} + D_{t3} \right]} \tag{4.9}$$

4.3 Development of Model for Root relief

Figure 4.4a presents schematic of meshing of anodic workpiece gear with the cathode gear developed for its non-contact root relieving by the PED process. The developed cathode gear has a conductive portion of copper sandwiched between two non-conductive portions of Metalon. It necessitates simultaneously providing reciprocating motion to anodic workpiece gear by linear actuator to impart non-contact root relief along its entire face width, and rotary motion to cathode gear by stepper motor for root relieving of all the teeth of anodic workpiece gear. Development of analytical model for amount of root relief imparted to anodic workpiece gear flank surface 'C_{ft}' (mm) requires development of the following equations: (i) instantaneous area of anodic workpiece gear tooth which will be modified by the conductive portion of the developed cathode gear 'A_{trr}' shown as hatched portion in Fig. 4.4b. It is equal to summation of area of involute profiles and area of non-involute profiles of two consecutive flank surfaces of two adjacent teeth of anodic workpiece gear which will be modified in root relieving (mm^2) i.e., $A_{trr} = A_{nrr} + A_{rr}$, (ii) involute profile arc length of anodic workpiece gear flank surface which will be modified 'L_{rr}' as depicted in Fig. 4.4b, (iii) arc length of root fillet of anodic workpiece gear which will be modified 'L_{rf}' as shown in Fig. 4.4b, and (iv) total volume of material removed from anodic workpiece gear teeth in its non-contact root relieving 'Q_{trr}' using Faraday's law of electrolysis. In addition to the common assumptions mentioned in section 4.1, it is assumed that material is removed from involute profile from the datum circle to base circle and from non-involute root of anodic workpiece gear flank surfaces.

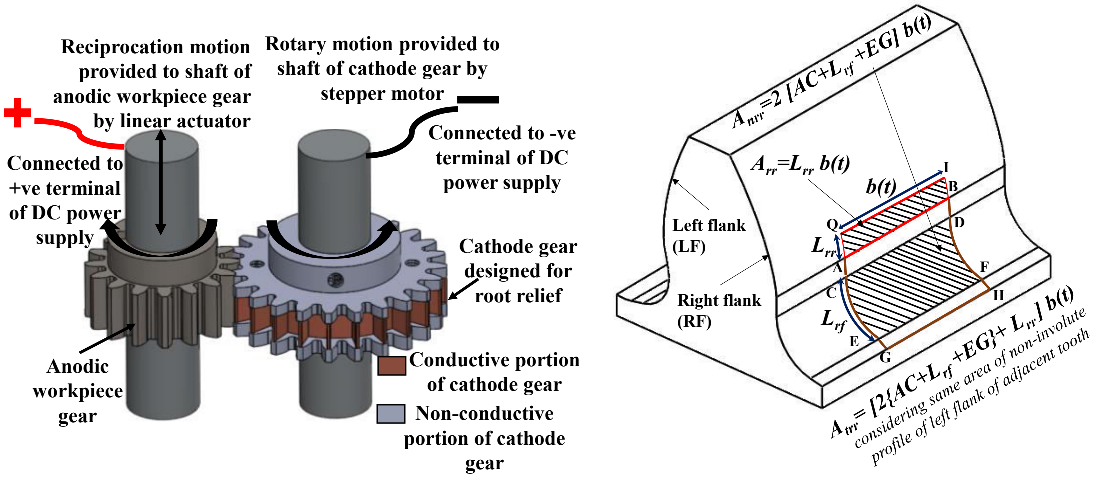

Fig. 4.4: *Non-contact root relieving* of anodic workpiece gear by PED process: (a) schematic of meshing with the developed cathode gear, and (b) instantaneous area of anodic workpiece gear tooth *'A_{trr}'* that will be modified by conductive portion of the developed cathode gear.

4.3.1 Volumetric MRR during Root Relieving

Total volume of material removed from anodic workpiece gear teeth in its non-contact root relieving (mm^3) by the PED process 'Q_{trr}' is given by the following equation based on Faraday's law of electrolysis:

$$Q_{trr} = \int_0^{t_{fm}} dQ_{trr} = \frac{\eta E}{\rho F}\int_0^{t_{fm}} jA_{trr}dt \qquad (4.10a)$$

where *'η'* is current efficiency of anodic dissolution (%); *'E'* and *'ρ'* are electrochemical equivalent (g) and density of anodic workpiece gear material (g/mm^3); *'F'* is Faraday's constant; *'t_{fm}'* is duration of root relieving of anodic workpiece gear by PED process (seconds); *'A_{trr}'* is instantaneous area of anodic workpiece gear tooth which will be modified by the conductive portion of the developed cathode gear in root relieving (shown as the hatched area in Fig. 4.4b); and 'j' is current density (A/mm^2) and is given by $j= \kappa_e (V-\Delta V)/Y$. Taking numerator of current density expression out of integration in Eq. 4.10a (because overvoltage and electrolyte conductivity have been assumed to be constant in root relieving of anodic workpiece gear by the PED process), using location-specific expression for the IEG i.e., *'Y_{nrr}'* as IEG at non-involute profile (mm), and *'Y_{rr}'* as IEG at involute profile (mm) of anodic workpiece gear tooth in root relieving, and substituting the relation for *'$A_{trr} = A_{nrr} + A_{rr} = [2\{AC + L_{rf} + EG\} + L_{rr}]b(t)$'* gives the following expression for 'Q_{trr}':

$$Q_{trr} = Q_{nrr} + Q_{rr}$$

$$= \frac{\eta E \kappa_e (V - \Delta V)}{\rho F} \left\{ \frac{2\left(AC + L_{rf} + EG\right)}{Y_{nrr}} + \frac{L_{rr}}{Y_{rr}} \right\} \int_0^{t_{fm}} b(t)\, dt \qquad (4.10b)$$

where, 'Q_{nrr}' and *'Q_{rr}'* are volumes of material removed from non-involute and involute profiles of anodic workpiece gear teeth in its non-contact root relieving (mm^3); *'AC'* is an arc length between involute profile and root fillet (mm); *'EG'* is length of an arc from dedendum circle of anodic workpiece gear (mm); *'L_{rr}'* is involute profile arc length of anodic workpiece gear flank surface which will be modified in its root relieving (mm); and *'L_{rf}'* is root fillet arc length of anodic workpiece gear which will be modified in its root relieving (mm). The fillet at the root of anodic workpiece gear tooth can be considered as an arc of circle having radius as $r_{rf} = 0.4m$; in which *'m'* is its module **(Gupta et *al.*, 2017).** Volumetric MRR *'M_{rr}'* during non-contact root relieving of anodic workpiece gear can be computed dividing the total material removed *'Q_{trr}'* by the root relieving duration 't_{fm}' and representing integral part of Eq. 10b [i.e., $\int_0^{t_{fm}} b(t)dt$] as *'I'* gives the following relation:

$$M_{rr} = \frac{Q_{trr}}{t_{fm}} = \left\{ \frac{\eta E \kappa_e (V - \Delta V)}{\rho F t_{fm}} \right\} \left\{ \frac{2\left(AC + L_{rf} + EG\right)}{Y_r} + \frac{L_{rr}}{Y_{rr}} \right\} I \qquad (4.11)$$

Equation 4.11 requires computations of lengths of arcs '*AC*', '*EG*', 'L_{rf}', and *'L_{rr}'* which are described by the Eqs. A10; A12, A13, and A14 respectively in Appendix-A. Values of IEG for the anodic workpiece gear tooth at its non-involute profile 'Y_{nrr}' (mm), and at its involute profile 'Y_{rr}' (mm) depend on the design of the cathode gear developed for its root relief. Combined effects of the following (represented by Eq. 4.5) is also used for non-contact root relieving of anodic workpiece gear by the PED process: (i) continuous reciprocation of anodic workpiece gear which causes continuous change in its fraction of total face width *'b(t)'* meshing with the conductive portion of the developed cathode gear as represented by Eq. 4.3, and (ii) use of pulsed DC power which requires changing the integration limits of integral part of Eq. 4.10b i.e., $I = \int_0^{t_{fm}} b(t)dt$; which is represented by Eq. 4.4.

4.3.2 Analytical Model for Root Relief

Volume of material removed from involute profiles of anodic workpiece gear teeth in its non-contact root relieving by the PED process *'Q_{rr}'* (mm^3) is given by the following equation:

$$Q_{rr} = \frac{\eta E \kappa_e (V - \Delta V)}{\rho F} \frac{L_{rr}}{Y_{rr}} I \qquad (4.12)$$

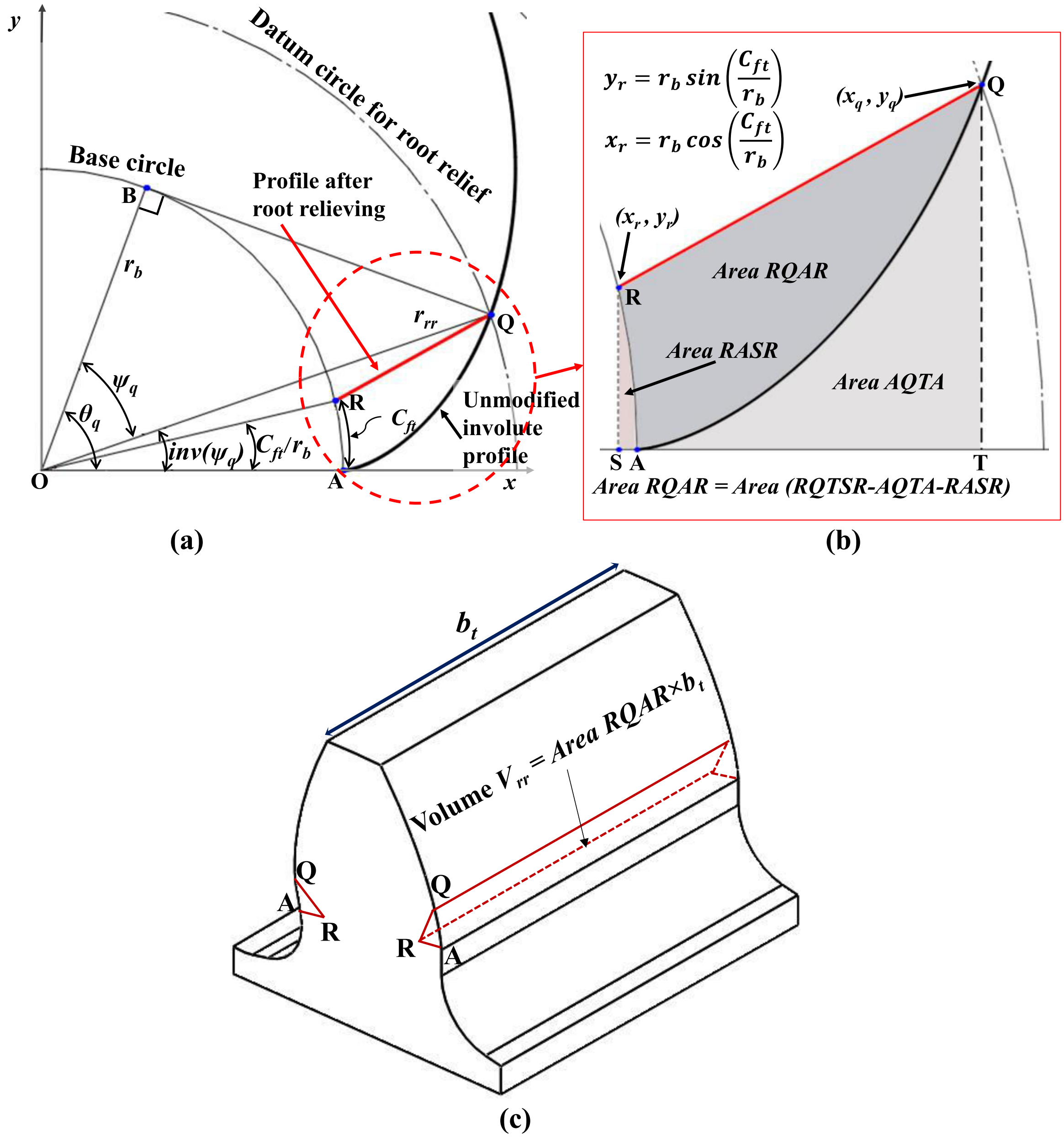

Fig. 4.5: Effect of non-contact *root relieving* by the PED process on flank surface of anodic workpiece gear tooth: (a) change in its involute profile, (b) enlarged view used to compute area of *RQAR,* and (c) volume of material removed.

Non-contact root relieving of anodic workpiece gear changes its involute profile from arc *'AQ'* to line *'RQ'* as depicted in Figs. 4.5a and 4.5b and removes 'V_{rr}' volume of material removed from its one flank surface (shown in Fig. 4.5c), which is given by $Q_{rr}/2Z$ (here *'Z'* is no. of teeth in anodic workpiece gear). Dividing it by total face width of anodic workpiece gear *'b_t'* gives *area of RQAR* as expressed by Eq. 13:

$$V_{rr} = b_t\{Area\ RQAR\} \Rightarrow Area\ RQAR = \frac{Q_{rr}}{2Zb_t} \tag{4.13}$$

Geometry of *area RQAR* shown in Fig. 4.5b is used to develop the following equation:

Area RQAR= Area of trapezium RQTSR - Area of AQTA - Area of RASR (4.14a)

Equating Eqs. 4.13 and 4.14a for *area of RQAR* gives the following equation:

$$\frac{Q_{rr}}{2Zb_t} = Area\ of\ trapezium\ RQTSR - Area\ of\ AQTA - Area\ of\ RASR \qquad (4.14b)$$

Using the Eq. A15 for *Area of AQTA;* Eq. A16 for *Area of RQTSR;* and Eq. A17 for *Area of RASR* (from Appendix-A) in Eq. 4.14b gives the following equation:

$$\frac{Q_{rr}}{2Zb_t} = \frac{1}{2}\left\{y_q + r_b \sin\left(\frac{C_{ft}}{r_b}\right)\right\}\left\{x_q - r_b \cos\left(\frac{C_{ft}}{r_b}\right)\right\} - \frac{r_b^2}{2}\left(\frac{\sin 2\theta_q - \theta_q^2 \sin 2\theta_q}{2} - \frac{\theta_q^3}{3} - \theta_q \cos 2\theta_q\right) - \frac{1}{2}\left\{r_b - r_b \cos\left(\frac{C_{ft}}{r_b}\right)\right\} r_b \sin\left(\frac{C_{ft}}{r_b}\right) \qquad (4.14c)$$

where, (x_q, y_q) are the cartesian coordinates of point *'Q'*; 'C_{ft}' is amount of non-contact root relief imparted to a flank surface of anodic workpiece gear by PED process (mm); 'r_b' is the base circle radius of the anodic workpiece gear. Substituting 'Q_{rr}' form Eq. 4.12 in Eq. 4.14c and rearranging the terms gives the following expression for 'C_{ft}' (For details please refer to Eqs. A18 to A22 in Appendix-A):

$$\boldsymbol{C_{ft} = r_b\left[\sin^{-1}\left\{\frac{\frac{\eta E}{\rho F}\frac{\kappa_e(V-\Delta V)}{Zb_t}\frac{L_{rr}}{Y_{rr}} I + D_{r1}}{D_{r2}}\right\} + D_{r3}\right]} \qquad \textbf{(4.15)}$$

where, 'D_{r1}', 'D_{r2}', and 'D_{r3}' are given by the following expressions:

$$D_{r1} = r_b^2\left(\frac{\sin 2\theta_q - \theta_q^2 \sin 2\theta_q}{2} - \frac{\theta_q^3}{3} - \theta_q \cos 2\theta_q\right) - x_q y_q$$

$$D_{r2} = \sqrt{\left(x_q r_b - r_b^2\right)^2 + \left(y_q r_b\right)^2} \qquad D_{r3} = \tan^{-1}\left(\frac{y_q r_b}{x_q r_b - r_b^2}\right)$$

4.4 Development of Model for End Relief

Figure 4.6a presents a schematic of the engagement of anodic workpiece gear with the cathode gear developed for its non-contact end relieving by the PED process. The developed cathode gear has a non-conductive portion of Metalon sandwiched between two conductive portions of copper. The rotary motion is provided to cathode gear by a stepper motor to impart end relief to all teeth of the anodic workpiece gear, but the reciprocating motion is not needed for non-contact end relieving of anodic workpiece gear by the PED process, unlike its tip and root relieving. Development of analytical model for amount of end relief imparted to bottom/back and top/front end of anodic workpiece gear flank surface '$C_{\beta b}$' or '$C_{\beta t}$' needs development of equations for (i) instantaneous area of anodic workpiece gear tooth that will be modified during end relieving 'A_{ter}' as shown hatched portion in Fig. 4.6b. It is equal to the summation of top land area of anodic workpiece gear tooth 'A_{tler}', area of involute profile 'A_{er}', and area of non-involute profile of anodic workpiece gear flank surface 'A_{ner}' i.e., $A_{ter} = A_{tler} + A_{er} + A_{ner}$, (ii) involute profile arc length of anodic workpiece gear flank surface that will be modified 'L_{er}' as depicted in Fig. 4.6b, (iii) chordal thickness of anodic workpiece gear tooth along its addendum circle *'w_a'* as shown in Fig. 4.6b, (iv) arc length of root fillet of anodic workpiece gear that will be modified in end relieving *'L_{rf}'* as shown in Fig. 4.6b, and (v) total volume of material removed from anodic workpiece gear teeth in non-contact end relieving 'Q_{ter}' by the PED process using Faraday's law of electrolysis. In addition to the common assumptions mentioned in section 4.1, it is assumed that (i) material is removed from the top land, involute profile from addendum to base circle, and from the non-involute portion of anodic workpiece gear flank surfaces; (ii) equal amount of end relief is provided to top/front and bottom/back ends of each flank surface, i.e., $C_{\beta b} = C_{\beta t}$; (iii) thickness of both the conductive portions of the developed cathode gear 'b_{ccg}' is same which will result in $L_{ert} = L_{erb} = b_{ccg}$

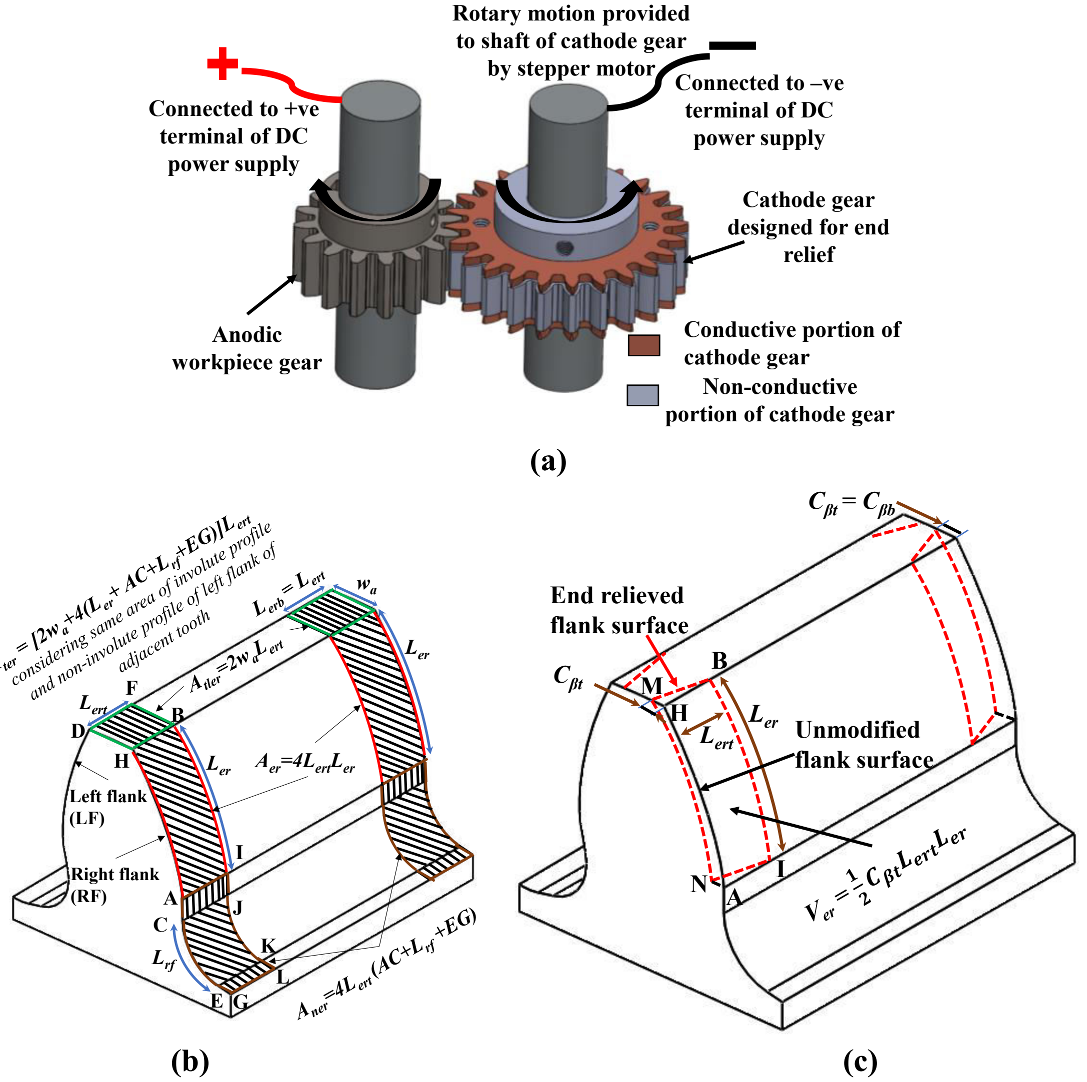

Fig. 4.6: Non-contact *end relieving* of anodic workpiece gear by PED process: (a) schematic of meshing with the developed cathode gear, (b) instantaneous area of anodic workpiece gear tooth which will be modified *'A_{ter}'*, and (c) volume of material removed from one end of anodic workpiece gear tooth.

4.4.1 Volumetric MRR during End Relieving

The total volume of material removed from anodic workpiece gear teeth in its non-contact end relieving by the PED process 'Q_{ter}' (mm^3) is given by the following equation based on Faraday's law of electrolysis:

$$Q_{ter} = \int_0^{t_{fm}} dQ_{ter} = \frac{\eta E}{\rho F}\int_0^{t_{fm}} jA_{ter}\,dt \qquad (4.16a)$$

where 'η' is current efficiency of anodic dissolution (%); 'E' and 'ρ' are electrochemical equivalent (g) and density of anodic workpiece gear material (g/mm^3); 'F' is Faraday's constant; 't_{fm}' is duration of end relieving of anodic workpiece gear (seconds); 'A_{ter}' is instantaneous area of anodic workpiece gear tooth that will be modified during end relieving. Using the expression for current density $j= \kappa_e (V-\Delta V)/Y$ and taking its numerator out of integration in Eq. 4.16a (because overvoltage and electrolyte conductivity have been assumed to be constant in non-contact end relieving of anodic workpiece gear by the PED process), using location-specific expression for the IEG, i.e., 'Y_{tler}' as IEG at top land (mm), 'Y_{er}' as IEG at involute profile (mm), and 'Y_{ner}' as IEG at non-involute profile (mm) of anodic workpiece gear tooth in its end relieving, and using relations for '$A_{ter}=A_{tler} + A_{er} + A_{ner}=[2w_a + 4L_{er} + 4AC+ 4L_{rf}+ 4EG]L_{ert}$' gives the following expression for 'Q_{ter}':

$$Q_{ter} = Q_{tler} + Q_{er} + Q_{ner} = \frac{\eta E \kappa_e (V-\Delta V)}{\rho F}\left\{\frac{2w_a}{Y_{tler}} + \frac{4L_{er}}{Y_{er}} + \frac{4(AC + L_{rf} + EG)}{Y_{ner}}\right\} L_{ert}\int_0^{t_{fm}} dt \quad (4.16b)$$

where, 'Q_{tler}', 'Q_{er}', and 'Q_{ner}' are respectively, volumes of material removed (mm^3) from top lands, involute profiles, non-involute profiles or roots of anodic workpiece gear teeth in its non-contact end relieving; 'L_{ert}' is the length of end relief imparted to top/front end of anodic workpiece gear flank surface (mm) which is assumed to be equal to the length of end relief imparted to bottom/back end of anodic workpiece gear flank surface 'L_{erb}' and both are equal to the face width of the conductive portion of developed cathode gear 'b_{ccg}' for end relieving (mm); 'AC' is an arc length between involute profile and root fillet (mm); 'EG' is the length of an arc from dedendum circle of anodic workpiece gear (mm); 'L_{er}' is the involute profile arc length of anodic workpiece gear flank surface that will be modified in end relieving. Computation of 'AC', 'EG', 'L_{rf}', and 'L_{er}' are described by Eqs. A10; A12; A13; and A23, respectively in Appendix-A. Pulsed DC power supply in the PED process causes end relieving of anodic workpiece gear flank surface to occur during pulse-on time 't_{on}' only, and no electrolytic dissolution takes place during the pulse-off time 't_{off}' therefore, integration limits of an integral part of Eq. 4.16b ought to be changed by splitting duration of end relieving 't_{fm}' into repetitive pulses of cycle time 't_c' in the following manner:

$$I = \int_0^{t_{fm}} dt = \frac{t_{fm}}{t_c}\left[\int_0^{t_{on}} dt + \int_{t_{on}}^{t_{off}} dt\right] = \frac{t_{fm}}{t_c} t_{on} \Rightarrow I = t_{fm}\delta \qquad (4.17)$$

where, 'δ' is duty cycle (%) given by $\delta = \frac{t_{on}}{t_c} = \frac{t_{on}}{t_{on}+t_{off}}$. The following expression is obtained for 'Q_{ter}' after using Eq. 4.17 in Eq. 4.16b:

$$Q_{ter} = \frac{\eta E \kappa_e (V - \Delta V)}{\rho F}\left\{\frac{2w_a}{Y_{tler}} + \frac{4L_{er}}{Y_{er}} + \frac{4\left(AC + L_{rf} + EG\right)}{Y_{ner}}\right\} L_{ert} t_{fm} \delta \qquad (4.18)$$

Volumetric MRR *'M_{er}'* (mm^3/s) during non-contact end relieving of anodic workpiece gear by the PED process can be computed by dividing the 'Q_{ter}' by the duration of end relieving 't_{fm}' which gives the following relation:

$$M_{er} = \frac{Q_{ter}}{t_{fm}} = \frac{\eta E \kappa_e (V - \Delta V)}{\rho F}\left\{\frac{2w_a}{Y_{tler}} + \frac{4L_{er}}{Y_{er}} + \frac{4\left(AC + L_{rf} + EG\right)}{Y_{ner}}\right\} L_{ert} \delta \qquad (4.19)$$

Values of IEG for the anodic workpiece gear at its top land *'Y_{tler}' (mm),* at its involute profile *'Y_{er}' (mm),* and at its non-involute profile (mm) *'Y_{ner}'* (used in Eqs. 4.18 and Eq. 4.19) depends on the design of the cathode gear developed for its end relief.

4.4.2 Analytical Model for End Relief

Volume of material removed from flank surfaces of anodic workpiece gear teeth in its non-contact end relieving by the PED process *'Q_{er}'* (mm^3) is given by the following equation:

$$Q_{er} = \frac{\eta E \kappa_e (V - \Delta V)}{\rho F}\frac{4L_{er}L_{ert}}{Y_{er}}\int_0^{t_{fm}} dt \Rightarrow Q_{er} = \frac{\eta E \kappa_e (V - \Delta V)}{\rho F}\frac{4L_{er}L_{ert}}{Y_{er}} t_{fm}\delta \qquad (4.20)$$

It can be observed from Fig. 4.6c that the volume of material 'V_{er}' was removed from one end of the anodic workpiece gear tooth. One tooth of anodic workpiece gear consists of four ends to be relieved by an equal amount by the PED process. Therefore, it can be expressed by the following relation:

$$V_{er} = \frac{Q_{er}}{4Z} = \frac{1}{2} C_{\beta t} L_{ert} L_{er} \Rightarrow C_{\beta t} = \frac{Q_{er}}{2Z L_{ert} L_{er}} \qquad (4.21)$$

Substituting the relation for *'Q_{er}'* from Eq. 4.20 in Eq. 4.21 and rearranging the terms gives the following equation for '$C_{\beta t}$' *or '$C_{\beta b}$'* (mm):

$$\boldsymbol{C_{\beta t} = C_{\beta b} = \frac{\eta E\, \kappa_e (V - \Delta V)}{\rho F}\frac{2t_{fm}\delta}{Z}\frac{}{Y_{er}}} \qquad (\mathbf{4.22})$$

4.5 Development of Model for Lead Crowning

Figure 4.7a presents schematic of meshing of anodic workpiece gear with the cathode gear developed for its non-contact lead crowning by the PED process. The developed cathode gear has a conductive portion of copper sandwiched between two non-conductive portions of Metalon. Therefore, variable reciprocating velocity is provided to anodic workpiece gear to impart lead crowning to its entire flank surface, and simultaneously rotary motion is provided to cathode gear to impart same amount of lead crowning to all teeth of anodic workpiece gear. Development of an analytical model for the amount of lead crowning 'C_β' (mm) of anodic workpiece gear flank surface by the PED process requires development of the following equations: (i) instantaneous area of anodic workpiece gear tooth that will be modified by the conductive portion of the developed cathode gear 'A_{tlc}' shown as the hatched portion in Fig. 4.7b. It is equal to summation of top land area 'A_{tllc}' and area of involute profile 'A_{lc}', area of non-involute profile of anodic workpiece gear flank surface 'A_{nlc}' i.e., $A_{tlc} = A_{tllc} + A_{lc} + A_{nlc}$, and (ii) involute profile arc length of anodic workpiece gear flank surface 'L_{lc}' that will be modified in its lead crowning as depicted in Fig. 4.7b, (iii) chordal thickness 'w_a' of anodic workpiece gear tooth along its addendum circle as shown in Fig. 4.7b, and (iv) arc length of non-involute profile of anodic workpiece gear that will be modified in lead crowning '$L_r = AC + EG + L_{rf}$' as shown in Fig. 4.7b, (v) total volume of material removed from anodic workpiece gear teeth in its non-contact lead crowning 'Q_{tlc}' using Faraday's law of electrolysis. In addition to the common assumptions mentioned in section 4.1, it is assumed that reciprocating velocity provided to anodic workpiece gear varies linearly.

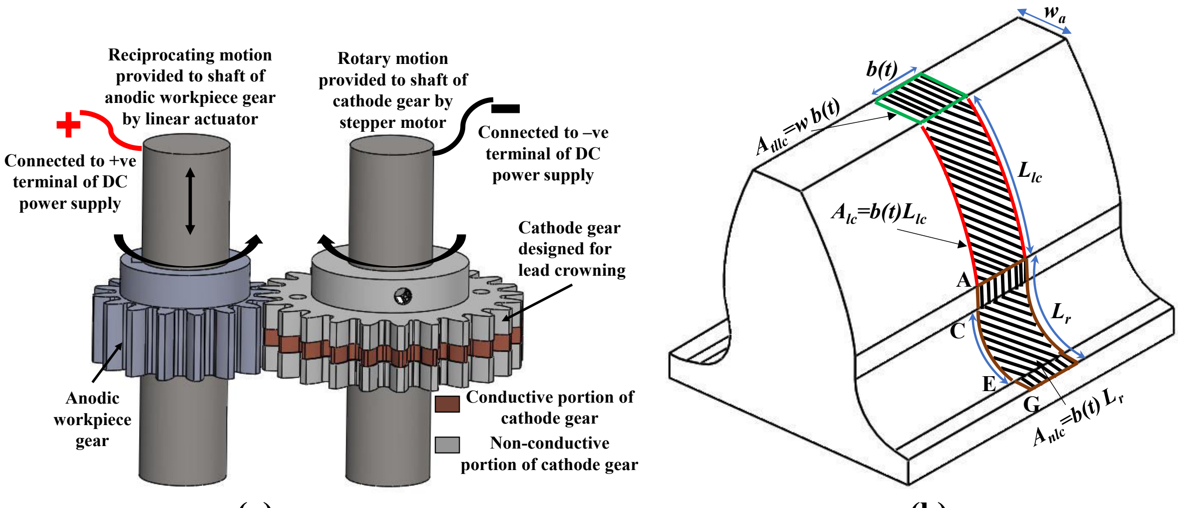

Fig. 4.7: Non-contact *lead crowning* of anodic workpiece gear by PED process: (a) schematic of meshing with the developed cathode gear, (b) instantaneous area of anodic workpiece gear tooth which will be modified 'A_{tlc}'.

4.5.1 Volumetric MRR During Lead Crowning

The total volume of material removed from anodic workpiece gear teeth in non-contact lead crowning by the PED process 'Q_{tlc}' (mm^3) is given by the following equation based on Faraday's law of electrolysis:

$$Q_{tlc} = \int_0^{t_{fm}} \frac{\eta E}{\rho F} j A_{tlc} dt = \frac{\eta E}{\rho F} \int_0^{t_{lc}} j A_{tlc} dt \qquad (4.23)$$

where, 'E' and 'ρ' are electrochemical equivalent (g) and density (g/mm^3) of the anodic workpiece gear material; 'η' is current efficiency of anodic dissolution (%); 'j' is current density (A/mm^2); 'F' is Faraday's constant (i.e., 96,500 Coulomb); 't_{fm}' is the duration of lead crowning (s); and 'A_{tlc}' is instantaneous area of one flank surface of workpiece gear tooth affected by its lead crowning (mm^2) which is the hatched area as depicted in Fig. 4.7b. Using the expression for current density $j= \kappa_e (V-\Delta V)/Y$ and taking its numerator out of integration in Eq. 4.23 (because overvoltage and electrolyte conductivity have been assumed to be constant in non-contact lead crowning of anodic workpiece gear by the PED process), using location-specific expression for the IEG, i.e., 'Y_{tllc}' as IEG at top land, 'Y_{lc}' as IEG at involute profile, and 'Y_{nlc}' as IEG at non-involute profile of anodic workpiece gear tooth in non-contact lead crowning, and using relations for '$A_{tlc} = A_{tllc} + A_{lc} + A_{nlc}=[w_a + c_l L_{lc} + L_r]b(t)$' gives the following expression for 'Q_{tlc}':

$$Q_{tlc} = Q_{tllc} + Q_{lc} + Q_{nlc} = \frac{\eta E \kappa_e (V - \Delta V)}{\rho F}\left(\frac{w_a}{Y_{tllc}} + c_l \frac{L_{lc}}{Y_{lc}} + \frac{L_r}{Y_{nlc}}\right)\int_0^{t_{fm}} b(t)dt \qquad (4.24)$$

where 'Q_{tllc}' is total volume of material removed from top lands of anodic workpiece gear teeth during its lead crowning (mm^3); 'Q_{lc}' and 'Q_{nlc}' are respective total volumes of material removed (mm^3) from involute profiles and non-involute profiles of anodic workpiece gear during its lead crowning; 'c_l' is area correction factor for involute profile of one flank surface of anodic workpiece gear tooth affected during its lead crowning. Volumetric MRR during tip relieving of anodic workpiece gear teeth 'M_{lc}' (mm^3/s) is computed by dividing the total material removed 'Q_{tlc}' (mm^3) by duration of lead crowning 't_{fm}' (s) and representing integral part of Eq. 4.24 [i.e., $\int_0^{t_{fm}} b(t)\, dt$] as '$I_l$' in it gives the following relation:

$$M_{lc} = \frac{Q_{tlc}}{t_{fm}} = \frac{\eta E}{\rho F}\frac{\kappa_e (V - \Delta V)}{t_{fm}}\left[\frac{w_a}{Y_{tllc}} + c_l \frac{L_{lc}}{Y_{lc}} + \frac{L_r}{Y_{nlc}}\right] I_1 \qquad (4.25)$$

where '$L_r = AC + EG + L_{rf}$'. Equation 4.25 requires computations of 'w_a', 'AC', 'EG', 'L_{rf}', 'L_{lc}' which are described by Eqs., A4, A10, A12, A13, A23 in Appendix-A. Values of IEG for the anodic workpiece gear at its top land 'Y_{tllc}' (mm), at its involute profile 'Y_{lc}' (mm), and at its non-involute profile (mm) 'Y_{nlc}' (used in Eqs. 4.25) depend on the design of cathode gear developed for its lead crowning. Development of expression for 'I_l' taking into account the effects of variable reciprocating velocity of the anodic workpiece gear and use of pulsed DC power is described in the next subsubsection.

4.5.2 Effects of Variable Reciprocation of Workpiece Gear and Pulsed DC Power Supply

Non-contact lead crowning of flank surfaces of anodic workpiece gear requires providing it variable reciprocating velocity programmed through Arduino controller. Fig. 4.8a shows relative position of anodic workpiece gear face width 'b_t' with respect to width of conducting portion of the cathode gear 'b_{ccg}'. Fig. 4.8b depicts change in reciprocating velocity of the anodic workpiece gear (measured by the rotary encoder) with the distance travelled by it. Figure 4.8c illustrates change in fraction of total face width of workpiece gear *'b(t)'* (engaging with conductive portion of the cathode gear) with lead crowning time *'t'*. Figure 4.8d shows combined effect of change *b(t)'* and use of pulsed DC power.

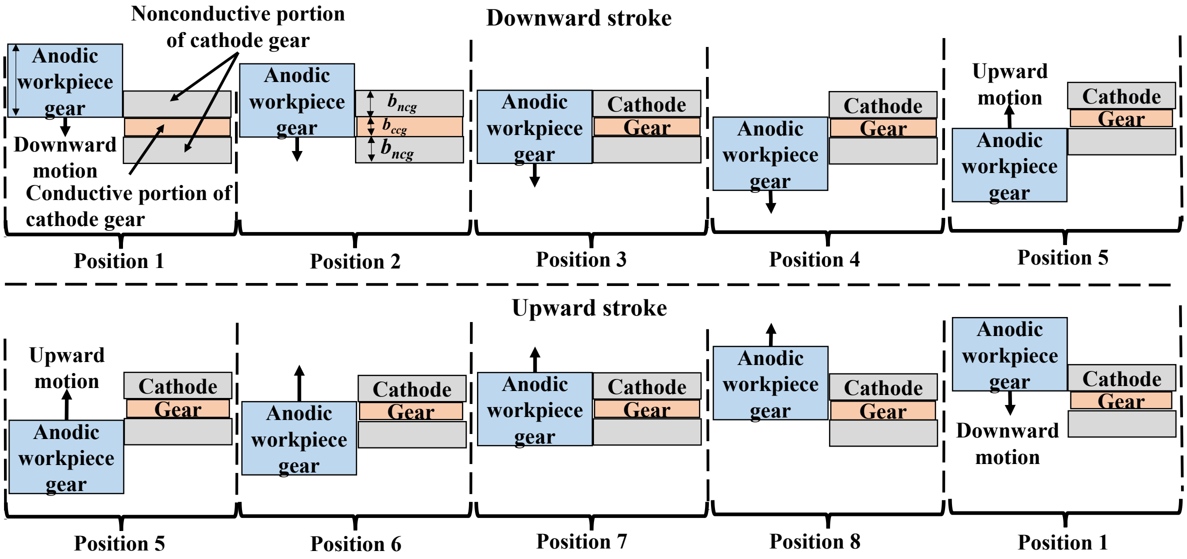

(a)

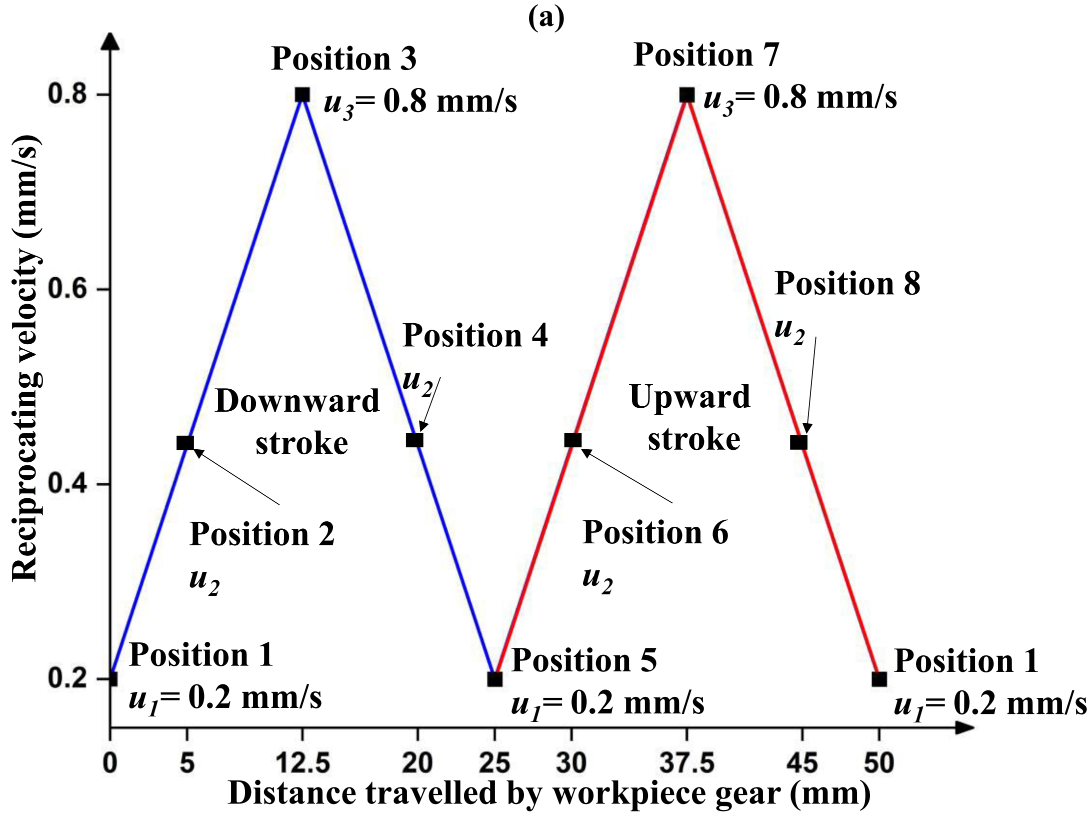

(b)

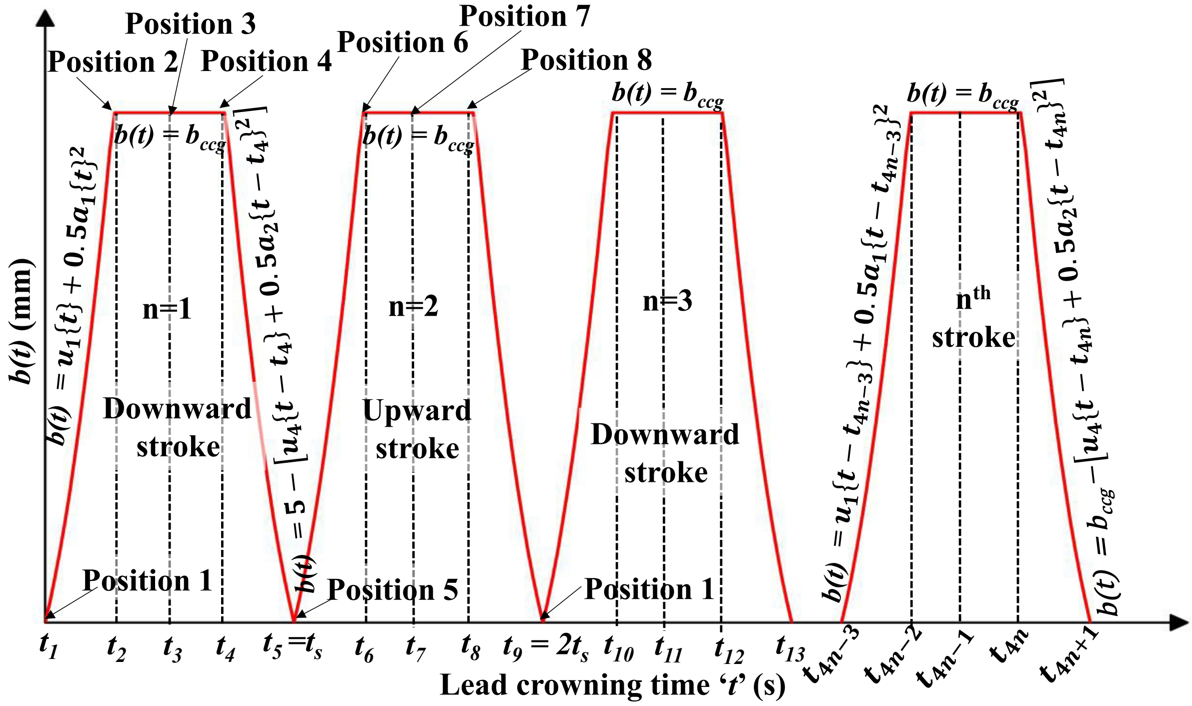

(c)

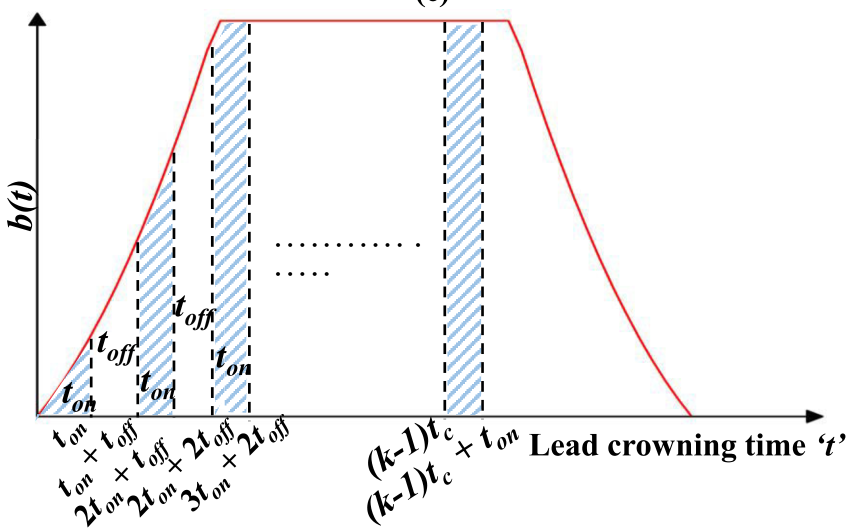

(d)

Fig. 4.8: Sequence of events in non-contact *lead crowning* of anodic workpiece gear by PED process: (a) relative position of workpiece gear face width with respect to conducting portion of the cathode gear, (b) change in reciprocating velocity of workpiece gear with the distance travelled by it, (c) change in fraction of total face width of workpiece gear *'b(t)'* with lead crowing time *'t'*, (d) combined effect of change *b(t)'* and use of pulsed DC power.

Minimum value of reciprocating velocity of the anodic workpiece gear 'u_1' (mm/s) occurs (Fig. 4.8b) when workpiece gear starts engaging with conducting portion of the cathode gear i.e., position 1 at the start of downward stroke and position 5 at the start of upward stroke as shown in Fig. 4.8a. Its value increases as anodic workpiece gear continues its downward movement and attains 'u_2' when anodic workpiece gear face width is completely engaged with the face width of conductive portion of cathode gear at position 2 in downward stroke and position 6 in upward stroke. Its value further increases as anodic workpiece gear continue its downward movement and attains its maximum value 'u_3' (mm/s) (Fig. 4.8b) at midpoint of engagement between face widths of anodic workpiece gear and conductive portion of cathode gear i.e., position 3 during the downward stroke and position 7 during the upward stroke (Fig. 4.8a). Then it starts decreasing and attains value 'u_2' (mm/s) again when anodic workpiece gear face width starts its disengagement with the conductive portion of the cathode gear i.e., position 4 in the downward stroke and position 8 in the upward stroke as shown in Fig. 4.8a. It again attains its minimum value 'u_1' at position 5 in upward stroke and position 1 in downward stroke. After completion of downward stroke, the workpiece gear starts upward stroke following same sequence of the events i.e., position 5 to position 1 (Fig. 4.8a). Such variation in reciprocating velocity imparts acceleration 'a_1' (mm/s^2) to anodic workpiece gear during first half of its downward/upward stroke and deceleration 'a_2' during second half of its downward/upward stroke. Values of 'u_4', 'a_1', and 'a_2' can be computed using reciprocating velocity variation graph from Fig. 4.8b. Total reciprocation distance travelled by the anodic workpiece gear either in its downward or upward stroke is equal to summation of face width of conductive portion of the cathode gear and total face width of anodic workpiece gear i.e., $b_{ccg} + b_t$. Time for completion of first half of a stroke 't_3' (from position 1 to position 3 in downward stroke or from position 5 to position 7 in upward stroke) can be computed from Newton's first equation of motion using change in reciprocating velocity of the anodic workpiece gear (from Fig. 4.8b). Time for completion of one upward/downward stroke of workpiece gear 't_s' is twice of 't_3'. Table 4.2 presents expressions of lead crowning times at different positions of workpiece gear during its downward/upward reciprocating stroke using Newton's equation of motions (described in section A4, Appendix-A). Using the generalized equations for the n^{th} stroke of workpiece gear from Fig. 4.8c, the following relation is obtained for '$b(t)$':

$$b(t) = \begin{cases} u_1\{t - t_{4n-3}\} + 0.5a_1\{t - t_{4n-3}\}^2 & for\ \ t_{4n-3} \le t < t_{4n-2} \\ b_{ccg} & for\ \ t_{4n-2} \le t < t_{4n} \\ b_{ccg} - [u_2(t - t_{4n}) + 0.5a_2(t - t_{4n})^2] & for\ \ t_{4n} \le t < t_{4n+1} \end{cases} \quad (4.26)$$

where, 'n' is a number indicating reciprocation stroke of anodic workpiece gear and has its values as 1, 2, 3,..., t_{fm}/t_s.

Table 4.2: Expressions for lead crowning time at different positions of the anodic workpiece gear during its downward/upward reciprocating motion in its non-contact lead crowning by PED process.

Stroke number	Lead crowning time at the stroke start	Lead crowning time at position 2 in downward or position 6 in upward stroke	Lead crowning time at position 3 in downward or position 7 in upward stroke	Lead crowning time at position-4 in downward or position 8 in upward stroke	Lead crowning time at the end of a stroke
1st *(n = 1)*	$t_1 = 0$	$t_2 = \frac{-u_1+\sqrt{u_1^2+2a_1b_{ccg}}}{a_1}$	$t_3 = \frac{u_3-u_1}{a_1}$	$t_4 = t_3 + \left(-\frac{u_3}{a_2} + \frac{\sqrt{u_3^2+a_2(b_t-b_{ccg})}}{a_2}\right)$ $t_4 = \frac{u_3-u_1}{a_1} + \left(-\frac{u_3}{a_2} + \frac{\sqrt{u_3^2+a_2(b_t-b_{ccg})}}{a_2}\right)$	$t_5 = t_s = 2t_3$ $t_5 = 2\left(\frac{u_3-u_1}{a_1}\right)$
2nd *(n = 2)*	$t_5 = t_s$	$t_6 = t_5 + t_2$ $t_6 = 2t_s + \frac{-u_1+\sqrt{u_1^2+2a_1b_{ccg}}}{a_1}$	$t_7 = t_s + t_3 = 3t_3$ $t_7 = 3\left(\frac{u_3-u_1}{a_1}\right)$	$t_8 = t_7 + \left(-\frac{u_3}{a_2} + \frac{\sqrt{u_3^2+a_2(b_t-b_{ccg})}}{a_2}\right)$ $t_8 = 3\left(\frac{u_3-u_1}{a_1}\right) + \left(-\frac{u_3}{a_2} + \frac{\sqrt{u_3^2+a_2(b_t-b_{ccg})}}{a_2}\right)$	$t_9 = 2t_s$
3rd *(n = 3)*	$t_9 = 2t_s$	$t_{10} = t_9 + t_2$ $t_{10} = 2t_s + \frac{-u_1+\sqrt{u_1^2+2a_1b_{ccg}}}{a_1}$	$t_{11} = 2t_s + t_3 = 5t_3$ $t_{11} = 5\left(\frac{u_3-u_1}{a_1}\right)$	$t_{12} = t_{11} + \left(-\frac{u_3}{a_2} + \frac{\sqrt{u_3^2+a_2(b_t-b_{ccg})}}{a_2}\right)$ $t_{12} = 5\left(\frac{u_3-u_1}{a_1}\right) + \left(-\frac{u_3}{a_2} + \frac{\sqrt{u_3^2+a_2(b_t-b_{ccg})}}{a_2}\right)$	$t_{13} = 3t_s$
nth	$t_{4n-3} = (n-1)t_s$	$t_{4n-2} = (n-1)t_s + \frac{-u_1+\sqrt{u_1^2+2a_1b_{ccg}}}{a_1}$	$t_{4n-1} = (2n-1)\left(\frac{u_3-u_1}{a_1}\right)$	$t_{4n} = (2n-1)\left(\frac{u_3-u_1}{a_1}\right) + \left(\frac{-u_3+\sqrt{u_3^2+a_2(b_t-b_{ccg})}}{a_2}\right)$	$t_{4n+1} = nt_s$

Use of pulsed DC power in non-contact lead crowing removes the material removal from flank surfaces of the anodic workpiece gear during the pulse-on time 't_{on}' only and flushing of the removed material from the lead crowning zone during the pulse-off time 't_{off}'. Concepts of pulse-on time 't_{on}', and pulse-off time 't_{off}', and cycle time 't_c' (where $t_c = t_{on} + t_{off}$) can used to divide the plot of '*b(t)*' as shown in Fig. 4.8d thus combining the effects of change *b(t)*' and use of pulsed DC power. It is used to modify limits of integration of '*b(t)*' (mentioned in Eq. 4.24) in the following manner.

$$I_1 = \int_0^{t_{fm}} b(t)\, dt = \sum_{k=1}^{X} \int_{(k-1)t_c}^{(k-1)t_c+t_{on}} b(t)\, dt \qquad (4.27)$$

where, 'X' is total number of DC power pulses which is given by the ratio of lead crowning duration and cycle time i.e., $X= t_{fm}/t_c$; and 'k' is index for DC power pulses with k = 1, 2, 3……, X. Eq. 4.28 is obtained for integral of '*b(t)*' (i.e., 'I_1' in Eq. 4.25) after combining the modified integration limits (Eq. 4.27) with the relation for '*b(t)*' (Eq. 4.26):

$$I_1 = \sum_{k=11}^{N_e} \begin{cases} \int_{(k-1)t_c}^{(k-1)t_c+t_{on}} [u_1\{t - t_{4n-3}\} + 0.5a_1\{t - t_{4n-3}\}^2]dt & t_{4n-3} \le t < t_{4n-2} \\ \int_{(k-1)t_c}^{(k-1)t_c+t_{on}} b_{ccg}\, dt & t_{4n-2} \le t < t_{4n} \\ \int_{(k-1)t_c}^{(k-1)t_c+t_{on}} \left[b_{ccg} - \{u_2(t - t_{4n}) + 0.5a_2(t - t_{4n})^2\}\right]dt & t_{4n} \le t < t_{4n+1} \end{cases} \qquad (4.28)$$

4.5.3 Analytical Model for Lead Crowning

Providing non-contact lead crowning to one flank surface of anodic workpiece gear tooth by 'C_β' amount changes its shape from *NPSU* to *MQRV* as depicted in Fig. 4.9a. It results in changing the straight edge of rectangular shaped top land from *NOP* to the parabolic curve *MOQ* as shown in Fig. 4.9b. Lead crowning of another flank surface of the same anodic workpiece gear tooth by 'C_β' amount changes shape of other straight edge of top land from *GHI* to a parabolic curve *JHK* as shown in Fig. 4.9b. Equation for the parabolic curve *MOQ* or *JHK* shown in Fig. 4.9c is given by $x = ay^2$; where 'x' and 'y' are the coordinates and 'a' is a constant whose expression can be found using x, y coordinate of the point M as 'C_β' and '$b_t/2$' respectively in $x = ay^2$ i.e., $a = 4\, C_\beta / (b_t)^2$. Using it in $x = ay^2$ gives Eq. 4.29 for the parabolic curve *MOQ* or *JHK*.

$$x = \frac{4C_\beta}{b_t^{\,2}}\, y^2 \qquad (4.29)$$

Area *MNOM* (shown as hatched area in Fig. 4.9c) can be calculated by Eq. 4.30 using its geometry.

$$Area\ of\ MNOM = \int_0^{b_t/2} xdy = \int_0^{b_t/2} \frac{4C_\beta}{{b_t}^2} y^2\, dy \Rightarrow \frac{4C_\beta}{{b_t}^2} \int_0^{\frac{b_t}{2}} y^2 dy = \frac{C_\beta b_t}{6} \quad (4.30)$$

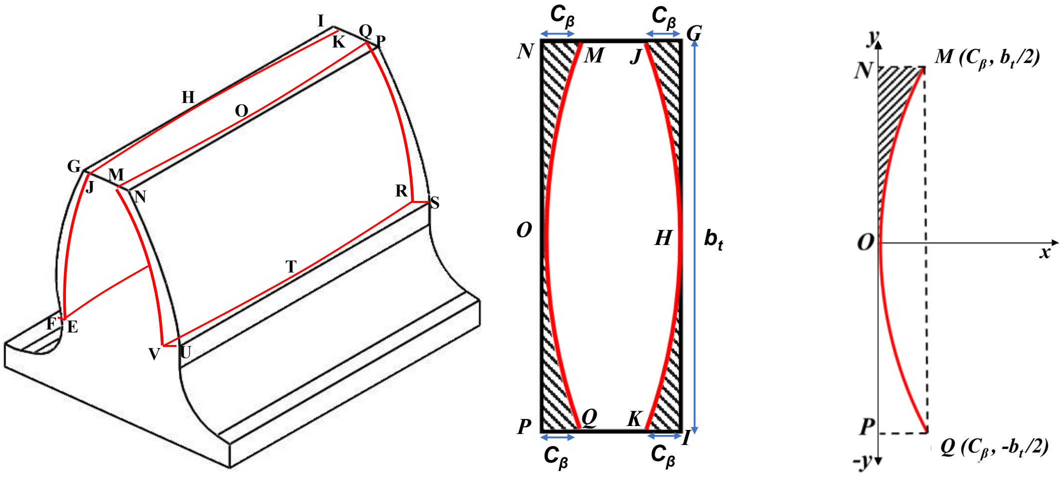

(a) **(b)** **(c)**

Fig. 4.9: Volume of material removed in lead crowning of anodic workpiece gear by PED process: (a) single tooth, (b) top land geometry of lead crown gear, and (c) shape of lead crowning.

Total volume of material removed from involute profiles of anodic workpiece gear teeth 'Q_{lc}' can be obtained by Eq. 4.31.

$$Q_{lc} = 4(\text{Area of MNOM})L_{lc}Z \Rightarrow Q_{lc} = \frac{4C_\beta b_t L_{lc} Z}{6} \Rightarrow C_\beta = \frac{3Q_{lc}}{2b_t L_{lc} Z} \quad (4.31)$$

where, 'L_{lc}' is arc length of involute profile of one flank surface of anodic workpiece gear tooth during its lead crowning (mm); and 'Z' is number of teeth in the anodic workpiece gear. Substituting $Q_{lc} = \frac{\eta E \kappa_e (V - \Delta V)}{\rho F} c_l \frac{L_{lc}}{Y_{lc}} I_1$ in Eq. 4.31 and rearranging the terms gives the following expression for amount of non-contact lead crowning *'C_β'* imparted by PED to the anodic workpiece gear.

$$\boldsymbol{C_\beta = \frac{3\eta E \kappa_e (V - \Delta V) c_l}{2 b_t Z \rho F Y_l} I_1} \quad (\mathbf{4.32})$$

where, 'I_1' is integral of '$b(t)$' which is the portion of total face width of anodic workpiece gear which engages with conducting portion of the developed cathode gear at *'t'* instant of time during its reciprocating motion and it is given by Eq. 4.28.

The ***next chapter*** provides the details of planning and design of experiments for confirming the functioning of the developed apparatus and cathode gears, validating the developed analytical models, and studying effects of parameters of PED process on different flank modifications. It also describes the evaluation procedure for amount of each flank modification, surface roughness, surface morphology, noise, vibrations, and functional performance parameters from the single and double flank roll testing.

Chapter 5

Experimentation

This chapter presents the details of planning and design of experiments for confirming the functioning of the developed apparatus and cathode gears, validating the developed analytical models, and studying the effects of parameters of the PED process on different flank modifications. It also describes the evaluation procedure for amount of each flank modification, surface roughness, surface morphology, noise, vibrations, and functional performance parameters from the single and double flank roll testing.

5.1 Planning and Design of Experiments

Important parameters of the PED process that considerably influence the non-contact flank modification of the workpiece gear can be categorized into the following three groups:

- **Parameters related to DC power:** It includes voltage, pulse-on time, pulse-off time, and duty cycle.
- **Parameters related to electrolyte:** Type, composition, concentration, temperature, flow rate, and conductivity of the electrolyte belong to this group.
- **Other parameters:** Flank modification duration, rotational speed of the cathode gear, and reciprocating velocity of the workpiece gear belong to this category.

A detailed study was performed by planning and conducting the experiments in three stages to understand (details presented in Table 2.2) and analyze effects of above-mentioned PED parameters on the considered response in the present work. The following subsections present details of different experiments. Selection of appropriate electrolyte is a very important first step in conducting the experimental study of non-contact flank modification by the PED process. An aqueous solution of sodium chloride (NaCl) was selected as an electrolyte in the present research work due to its sludging and non-passivating nature. It allows it to be filtered and reused in non-contact flank modifications of spur gear flank surfaces. It is easy to handle, readily available, and economical also.

5.2.1 Stage-1 Experiments: Confirm Functioning of the Developed Cathode Gears and Apparatus

Total 10 experiments were performed by choosing random values of voltage, pulse-on time, pulse-off time, electrolyte concentration, flank modification duration, and rotational speed of cathode gear, as per the details presented in Table 2.2, to confirm the functioning of the developed apparatus and cathode gears. Of these, 4 experiments were performed for non-contact tip relieving, 3 experiments for non-contact root relieving, and one experiment each for non-contact end reliving, profile crowning, and lead crowning of spur gears by the PED process. Other PED process parameters such as electrolyte temperature, electrolyte flow rate, and reciprocating velocity of workpiece gear were kept constant in these experiments. The values of the imparted flank modifications measured through microgeometry, and material removal rate (MRR) were used as the responses.

5.2.2 Stage-2 Experiments: Effects of PED Process Parameters on Tip Relief

Total 20 experiments were conducted in Stage-2 to study effects of electrolyte temperature, electrolyte flow rate, electrolyte concentration, rotational speed of cathode gear, and modification duration on non-contact tip relieving of spur gears by the PED process. These parameters were varied at four levels each using one-factor-at-a-time (OFAT) experimental design approach. Values of DC voltage, pulse-on time, pulse-off time, and reciprocating velocity of workpiece gear were kept constant during these experiments. Table 5.1 presents values of fixed and variable parameters used in conducting the stage-2 experiments. These experiments identified feasible ranges of concentration, temperature and flow rate of electrolyte, rotational speed of cathode gear, and modification duration for further experiments using the values of imparted tip relief, % reduction in maximum and average surface roughness, roughness profile, MRR, and morphology of flank surfaces of spur gears before and after their tip relieving as the responses.

Table 5.1: Values of fixed and variable parameters used in studying the effects of PED process parameters on non-contact tip relieving of the workpiece spur gear.

Variable parameters	Values	Fixed parameters	Value
Electrolyte concentration (Molarity)	0.5; 1.0; 1.5; 2.0	Electrolyte type	NaCl
Electrolyte temperature (°C)	25; 30; 35; 40	Voltage (Volt)	18
Electrolyte flow rate (lpm)	10; 20; 30; 40	Pulse-on time (ms)	3
Modification duration (minutes)	8; 12; 16; 20	Pulse-off time (ms)	4
Rotational speed of cathode gear (rpm)	15; 25; 35; 45	Reciprocating velocity of workpiece gear (mm/s)	0.96
Value of variable parameters when they were not varying			
Electrolyte concentration (Molarity)	0.5		
Electrolyte temperature (°C)	30		
Electrolyte flow rate (lpm)	20		
Modification duration (minutes)	12		
Rotational speed of cathode gear (rpm)	15		

5.2.3 Stage-3a Experiments: Validation of the Developed Analytical Models and Effects of PED Process Parameters on Profile Crowning

The developed analytical models for non-contact tip relieving (TR), root relieving (RR), end relieving (ER), and lead crowning (LC) were validated by conducting 12 experiments for each developed model (i.e., total of 48 experiments) in Stage-3a experiments. Voltage, pulse-on time, and pulse-off times were varied at four levels each using OFAT approach of experiment design in these experiments. Other parameters of the PED process were kept constant. Total of 12 experiments were conducted to study effects of voltage, pulse-on time, and pulse-off time on non-contact *profile crowning* (PC) of spur gears by the PED process by varying them at four levels each according to OFAT experimental design approach. These experiments identified a range of profile crowning that can be achieved by varying the PED process parameters and give an idea of change in value of profile crowning with them. Table 5.2 presents values of the fixed and variable parameters used in Stage-3a experiments. Values of the imparted flank modifications, % reduction in maximum and average surface roughness, roughness profile, and morphology of workpiece gear flank surfaces before and after its flank modification were used as the responses. These experiments identified ranges of flank modifications that can be achieved by for the considered ranges of the PED process parameters and give an idea of change in value of flank modification with them.

Table 5.2: Values of fixed and variable parameters used in validation of the developed analytical models.

Variable parameter	**Values**	**Fixed parameter**	**Value**
Voltage	15; 18; 21; 24 volts for TR, ER, PC, and LC 18; 21; 24; 27 volts for RR	Electrolyte type	Aqueous solution of NaCl
Pulse-on time	2; 3; 4; 5 ms	Electrolyte concentration	0.5 Molarity for TR, RR, and ER, and 1.0 Molarity for LC and PC
Pulse-off time	2; 4; 6; 8 ms	Electrolyte temperature	30°C
		Electrolyte flow rate	20 lpm
		Modification duration	12 minutes for TR, ER, LC, and PC; 20 minutes for RR
		Rotational speed of cathode gear	15 rpm for TR, RR, ER, and 35 rpm for LC and PC
		Reciprocating velocity of workpiece gear	0.96 mm/s for TR, RR and PC; From 0.2 to 0.8 mm/s for LC; Not required in ER
Value of variable parameters when they were not varying			
Voltage	18 volts for TR, ER, PC, and LC, 27 for volts for RR		
Pulse-on time	3 ms		
Pulse-off time	4 ms		

5.2.4 Stage-3b Experiments: Effects of Workpiece Gear Material Hardness

Five experiments were conducted to study the effects of hardness of workpiece gear material on different flank modifications of spur gear using values of the PED process parameters as presented in Table 5.3. Values of the imparted modifications, % reduction in max. and avg. surface roughness, and roughness profile were used as the responses.

Table 5.3: Values of PED process parameters used in studying the effects of hardness of workpiece gear material.

Exp. No.	Name of flank modification	Modification duration (minutes)	Voltage (volts)	Pulse-on time (ms)	Pulse-off time (ms)	Electrolyte concentration (Molarity)	Rotational speed of cathode gear (rpm)
1	Tip relief (TR)	12	15	3	2	0.5	8.5
2	Root relief (RR)	20	18	3	4	0.5	8.5
3	End relief (ER)	12	21	3	4	0.5	15
4	Lead crowning (LC)	12	15	3	4	1.0	35
5	Profile crowning (PC)	12	15	3	4	1.0	35

Constant parameters: Electrolyte type: Aqueous solution of NaCl; Electrolyte temperature: 30°C; Electrolyte flow rate: 20 lpm; Reciprocating velocity of workpiece gear: 0.96 mm/s for TR, RR, and PC, and varying from 0.2 to 0.8 mm/s for LC.

5.3 Evaluation of the Responses

Following subsections describe details of procedure and equipment used in the evaluation of the following responses used in different stages of experiments in the present work: value of each flank modification, volumetric material removal rate (MRR), avg. and max. surface roughness values, surface roughness profile, surface morphology, total and tooth-to-tooth, and longwave transmission errors through single flank roll testing, total and tooth-to-tooth composite errors, and radial runout through double flank roll testing, and running noise and vibrations through the test rig.

5.3.1 Measurement of Flank Modification Value

Value of each flank modification was found through microgeometry measurement on the computer numerical controlled (CNC) gear metrology machine *Smart Gear 500* from *Wenzel GearTech Germany* using a 3 mm diameter ruby probe as shown in Fig. 5.1. This machine has resolution of 0.1 μm. The probe was traced along the profile on the middle of workpiece gear flank surface for measuring the value of tip relief or root relief or profile crowning. And it was traced along the face width on the pitch line of workpiece gear flank surface (i.e., along the lead direction) for measuring the value of end relief or lead crowning. Total 8 measurements were taken on both left and right flank surfaces of four randomly chosen teeth of workpiece gear for each flank modification (i.e., 8 measurement each for tip relief, root relief, end relief, lead crowing, and profile crowning) and arithmetic average of the measured values was used for the analysis of the corresponding flank modification. The microgeometry of workpiece gear along its profile and lead was also measured before imparting any flank modification.

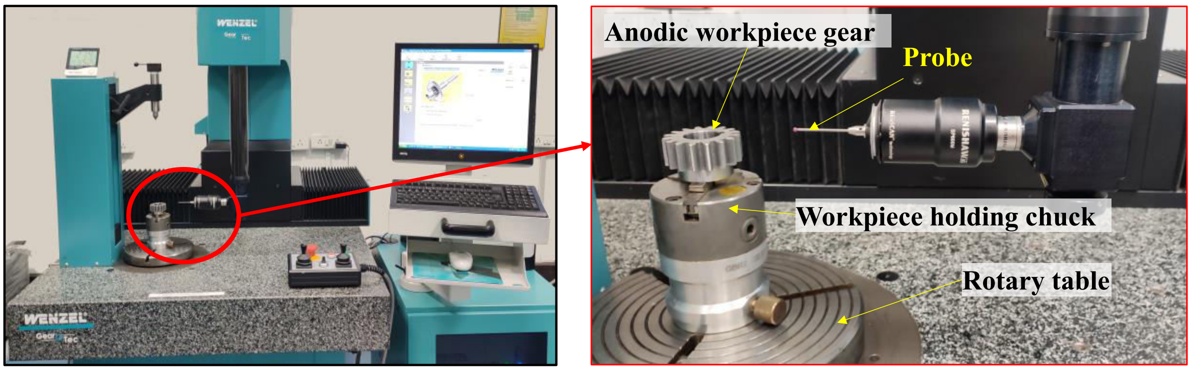

Fig. 5.1: Measurement of value of flank modification on CNC gear metrology machine.

5.3.2 Measurement of Volumetric MRR

The volumetric MRR from workpiece gear in imparting a flank modification to it was computed using Eq. 5.1 through measurement of its weights before and after its flank modification on a precision weighing balance (model: *DS 852G*, from *Essae-Teraoka Ltd*) having 10 mg least count. The measured weight difference was divided by the product of duration of flank modification and density of workpiece gear material.

$$MRR = \frac{Weight\ of\ workpiece\ gear\ before\ flank\ modification\ (g) - Weight\ of\ workpiece\ gear\ after\ its\ flank\ modification\ (g)}{Duration\ of\ flank\ modification\ (s) \times Density\ of\ workpiece\ gear\ material\ (g/mm^3)} \quad (5.1)$$

5.3.3 Measurement of Roughness of Workpiece Gear Flank Surfaces

Maximum and average surface roughness (now referred to as the maximum height '*Ry*' and arithmetical average roughness '*Ra*' as per Standard ISO 21920-2021) of a workpiece gear were measured by 3D surface roughness measuring and contour tracing equipment *MarSurf LD-130* (from *Mahr Metrology, Germany*) by tracing 2 µm diameter probe along the profile direction (Fig. 5.2) for a section length of 2 mm on left and right flank surfaces of two randomly chosen workpiece gear teeth before and after imparting it a flank modification *(FM)* by PED process i.e., total 4 values of *Ry* and 4 values of *Ra* were measured before and after flank modification. The arithmetic mean of the four measured values of *Ry* was used for computing percentage reduction in maximum height (*PRRy*) by Eq. 5.2, and similarly, percentage reduction in arithmetical average roughness (*PRRa*) was computed. The Gaussian filter was used to distinguish between roughness and waviness parameters.

$$PRRy = \frac{Avg.value\ of\ Ry\ before\ FM\ - Avg.value\ of\ Ry\ after\ FM}{Avg.value\ of\ Ry\ before\ FM} 100 \quad (5.2)$$

5.3.4 Evaluation of Morphology of Workpiece Gear Flank Surfaces

Morphology of flank surface a workpiece gear before and after imparting it a flank modification were studied by using field emission scanning electron microscope (*FE-SEM) SUPRA 55* from *Carl Zeiss, Germany* (refer Appendix-C for more details). Flank modified workpiece gear having a higher percentage reduction in maximum surface roughness was chosen for this and its random tooth flank surface was used to capture the surface morphology.

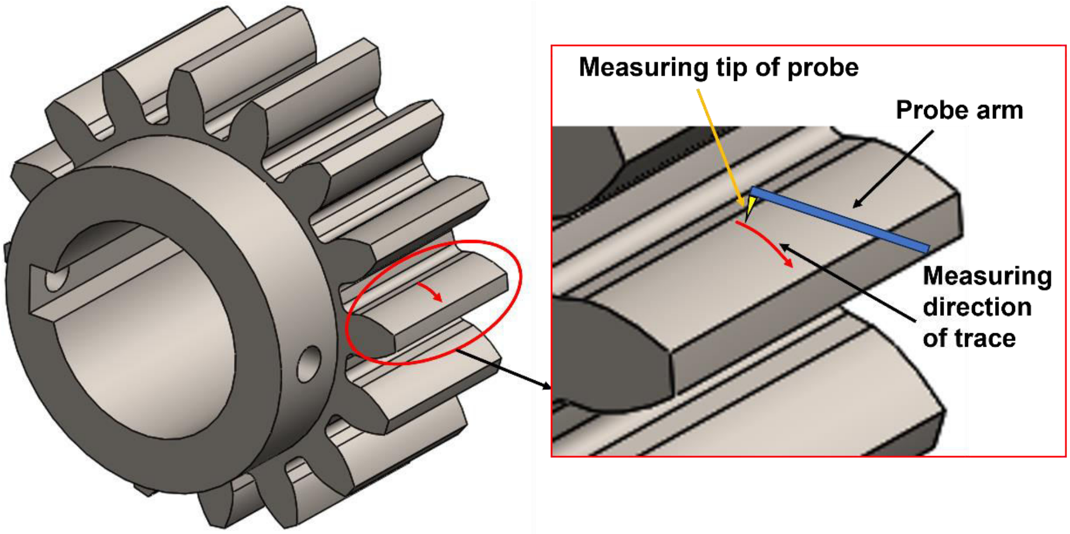

Fig. 5.2: Direction of trace for measurement of surface roughness parameters.

5.4 Stage 4 Experiments: Comparative Study of Functional Performance Parameters of Flank Modified and Unmodified Workpiece Gears

Functional testing of a gear simulates its actual working conditions, and it involves meshing of workpiece gear with a master gear, rotating them together and recording the functional performance parameters during their rolling action. Therefore, it is also known as roll testing. Functional testing is a qualitative form of inspection to determine whether a gear will work as intended or not. There are two types of functional or roll testing of a gear: (i) single flank roll testing or tangential composite testing and (ii) double flank roll testing or radial composite testing.

These tests are considered as 'composite' since their results are not individual parameters rather, they represent simultaneous influence of different parameters. The primary advantage of functional testing of a gear is the ability to predict its operational performance **(Pueo et *al.*, 2017)**. Effects of different flank modifications of workpiece spur gear on its functional testing parameters and running noise and vibrations were studied by imparting 4 flank modifications individually (i.e., tip relief, end relief, lead crowning, and profile crowning) and 4 combinations of flank modifications (i.e., tip and root relief; tip and end relief; tip, root, and end relief; and profile and lead crowning). Table 5.4 presents values of PED process parameters used in imparting these eight modifications to workpiece spur gears. An aqueous solution of NaCl was used as the electrolyte in these experiments. It was supplied at 20 liter per minute and its temperature was maintained at 30°C. Evaluation details of functional performance parameters are described in the following subsections.

Table 5.4: Values of variable parameters of PED process used in imparting different flank modifications and their combinations to workpiece spur gear.

Name of PED process parameter	**Gear-1** Tip relief (TR)	**Gear-4** End relief (ER)	**Gear-7** Lead crowning (LC)	**Gear-6** Profile crowning (PC)	**Gear-2** Combined tip and root relief (TRR)	**Gear-3** Combined tip and end relief (TER)	**Gear-5** Combined tip, root, and end relief (TRER)	**Gear-8** Profile and lead crowning (PLC)
Modification duration (minutes)	16	12	12	12	16+20	16+12	12+20+12	12+12
Voltage '*V*' (volt)	18	15	18	18	18	18	18	18, 15
Pulse-on time 't_{on}' (ms)	3	5	3	5	3	3	5	3
Pulse-off time 't_{off}' (ms)	4	4	2	4	4	4	4	4
Electrolyte concentration (M)	0.5	0.5	1	1	0.5	0.5	0.5	1
Rotational speed of cathode gear (rpm)	15	8.5	35	35	8.5	15	15	35
Reciprocating velocity of workpiece gear (mm/s)	0.96	Not needed	0.2-0.8	0.96	0.96	0.96	0.96	0.96 for PC and 0.2 to 0.8 for LC

5.4.1 Evaluation of Parameters from Single Flank Roll Testing

In house developed single flank roll tester (described in section 3.3 of Chapter 3) was used to measure the following parameters of a workpiece spur or test gear by allowing only its one flank surface (i.e., either left flank or right flank) to contact with a flank surface of master gear at any point of time during their rolling action:

- **Total transmission error 'F_i''** or *total tangential composite error* is the difference between the actual position of an output or driven gear (i.e., workpiece gear) and the position it would occupy if the mating gears were perfectly conjugate. It is a measure of profile conjugacy of two mating gears. It is measured as the difference between maximum and minimum angular deviations in one complete revolution of the test gear as explained in Fig. 3.10b.
- **Tooth-to-tooth transmission error 'f_i''** or *tooth-to-tooth tangential composite error* is a consequence of profile errors and single pitch errors. It is measured as the maximum difference in angular deviations that occur during meshing of one tooth of test gear and master gear (i.e., 360^0/number of teeth in the test gear) as depicted in Fig. 3.10b.
- **Longwave transmission error 'F_l''** or *longwave tangential composite error* is the difference between the maximum and minimum values of mean sinusoidal curve fitted to actual angular deviations curve as illustrated in Fig. 3.10b.

5.4.2 Evaluation of Parameters from Double Flank Roll Testing

Double flank roll testing, also known as radial composite testing, measures the variation in center distance when the test gear is rolled in tight mesh with the master gear. It reveals any errors in tooth form, pitch, runout and concentricity of pitch line. When two gears are in mesh with each other, then any of the above errors will cause the variation of their center distance. Figure 5.3a depicts photograph of in-house developed double flank roll tester for cylindrical gears which has been used to determine double flank roll testing parameters of unmodified and flank modified workpiece gears. The test gear (i.e. unmodified or flank modified spur gear) and the master gear are run in tight mesh ensuring double-flank contact between them. The test gear is constrained from all motions except rotatory motion which is provided by a stepper motor whose driver is controlled by the Arduino controller board. The master gear is mounted on a movable plate so that its position is changed when there is variation in the center-to-center distance. A laser displacement sensor records variation in center-to-center distance between the test gear and the master gear by observing the movement of the plate on which the master gear is mounted.

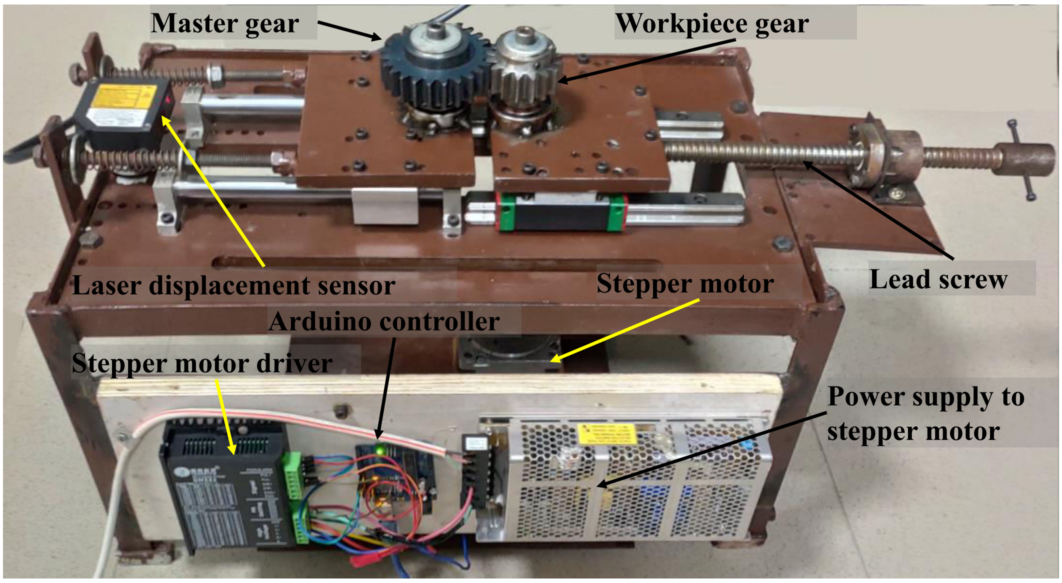

(a)

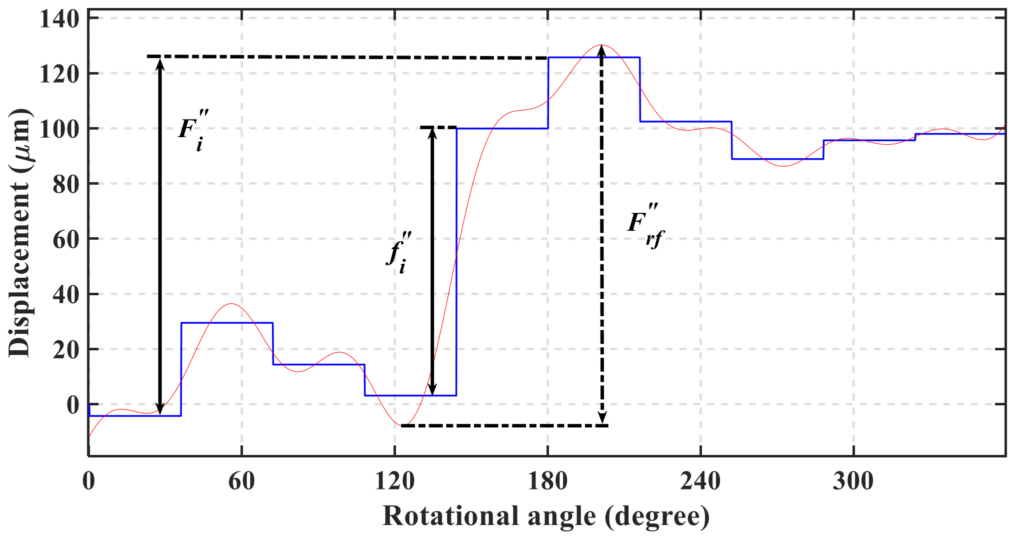

(b)

Fig. 5.3: Double flank roll testing of cylindrical gears: (a) photograph of in-house developed apparatus; and (b) its sample results.

The acquired data are used in MATLAB to plot graphs for center-to-center variation for workpiece gear from which following parameters are determined during their rolling action of test and master gears for further analysis:

- **Tooth-to-tooth composite error '$f_i^{''}$'** is a variation in the center-to-center distance per revolution per tooth of the test gear (i.e., 360^0/number of teeth). It is the maximum difference of the center distance occurring within an angle of rotation corresponding to the pitch as shown in Fig. 5.3b. It includes the effects of errors in profile, pitch, tooth thickness, and tooth alignment in both the test and master gears.
- **Total composite error '$F_i^{''}$'** is the total change in the center-to-center distance in one complete revolution of the test gear. It is the difference between the maximum and minimum center distance within one revolution of the test gear as depicted in Fig. 5.3b. It is the combination of runout with tooth-to-tooth composite error.
- **Radial runout '$F_{rf}^{''}$'** is the difference between the maximum and minimum radial distance from the gear axis after removing the short-term or undulation pitch deviations and analyzing the long-term sinusoidal waveform. It is the long-wave component of '$F_i^{''}$' and it is obtained by the difference between the maximum and minimum value of the long-wave component as illustrated in Fig. 5.3b **(Arteta et al., 2013)**.

5.4.3 Measurement of Running Noise and Vibrations

Sixteen full factorial experiments were performed each for the unmodified workpiece gear (i.e., before imparting any flank modification) and the eight modified workpiece gears by varying speed of test gear (i.e., workpiece spur gear) at 300; 600; 900; and 1200 rpm and applying a load of 5; 10; 15; and 20 N i.e., total 144 experiments were performed to analyze their running noise and vibrations. An in-house developed experimental test rig (depicted in Fig. 5.4) was used to measure running noise and vibrations of the unmodified and different modified workpiece spur gears. It has a motor-driven separate gearbox for testing the workpiece gear while meshing with a master gear mounted on a parallel shaft supported by pedestal bearings on the other end. The test rig has a variable frequency drive (VFD) to control the speed of the driver gear (i.e., workpiece gear) through its motor. The motor of a gearbox is run at the desired speed and the desired value of the load is applied manually on the driven master gear. A microphone (placed at standard distance of 1 meter distance from the gearbox) was used to acquire the signals of noise in terms of sound pressure and a tri-axial accelerometer (mounted over the gearbox) was used to get signal of vibrations in terms of acceleration. These signals are recorded in time-domain by four-channel noise and vibration data acquisition system *OR 35* (from OROS, France) and its associated software NV Gate 9.0

is used to convert them in frequency domain and analyze them. Change in noise level and change in vibrations for i^{th} modified workpiece gear with respect to unmodified gear 'ΔN_{G_i}' and 'ΔV_{G_i}' are computed using the following equations:

$$\Delta N_{G_i}\ (dBA) = \textit{Noise of unmodified gear} - \textit{Noise of } i^{th} \textit{ modified gear} \tag{5.3}$$

$$\Delta V_{G_i}(m/s^2) = \textit{Vibrations of unmodified gear} - \textit{Vibrations of } i^{th} \textit{modified gear} \tag{5.4}$$

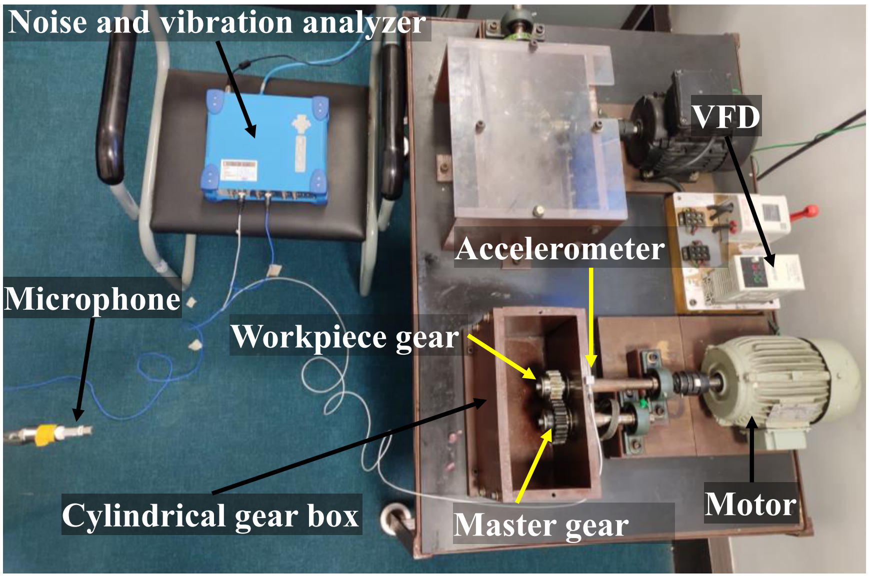

Fig. 5.4: Photograph of the test-rig used for measurement of noise and vibrations of unmodified and flank modified workpiece gears.

The ***next chapter*** presents the results and their analyses for different experiments performed to (i) to confirm functioning of the developed apparatus and cathode gears for non-contact flank modifications of spur gears, (ii) to validate the developed analytical models, (iii) to study the effects of PED process parameters on different flank modifications, (iv) to study the effects of imparting different flank modifications and their combinations to spur gears on their functional performance parameters, running noise, and vibrations, and (v) to study effects of workpiece gear material hardness.

Chapter 6

Results and Analysis

This chapter describes the results and their analyses for different experiments performed (i) to confirm functioning of the developed apparatus and cathode gears for non-contact flank modifications of spur gears, (ii) validate the developed analytical models, (iii) to study the effects of PED process parameters on different flank modifications, (iv) to study the effects of imparting different flank modifications and their combinations to spur gears on their functional performance parameters, running noise, and vibrations, and (v) to study effects of workpiece gear material hardness.

6.1 Functioning Confirmation of Developed Cathode Gears and Apparatus

Table 6.1 presents the results of the 10 experiments performed in Stage-1 to confirm the functioning of the developed cathode gears and apparatus for imparting non-contact flank modifications to spur gears. It mentions average values of tip relief, root relief, end relief, lead crowning, and profile crowning imparted to left and right flanks of the anodic workpiece gear, and corresponding volumetric MRR. Average imparted value of a flank modification was computed by taking difference between its value on hobbed spur gear and corresponding flank modified spur gear.

Table 6.1: Results of experiments performed to confirm functioning of the developed cathode gears and apparatus for non-contact flank modifications of spur gears by the PED process.

Exp. No.	Name of flank modification	Voltage 'V' (volts)	Pulse-on time 't_{on}' (ms)	Pulse-off time 't_{off}' (ms)	Duty Cycle	Modification duration 't_{fm}' (minutes)	MRR (mm^3/s)	Imparted average value of flank modification (µm)		
									Left flank	Right flank
1	Tip relief (TR)	10	1	2	0.33	8	0.05		103	22.7
2		15	3	5	0.37	8	0.10		26.5	22.7
3		15	3	2	0.60	12	0.14		13.1	85.9
4		15	3	2	0.60	16	0.18		109	95.2
5	Root relief (RR)	15	3	2	0.60	12	0.05		3.5	34.3
6		15	3	2	0.60	16	0.03		9.1	14.7
7		18	3	4	0.43	20	0.08		*28.4*	*28.8*
8	End relief (ER)	15	5	4	0.55	12	0.17	C_{top}	109.1	144.6
								C_{bottom}	94.6	93.4
9	Lead crowning (LC)	15	3	4	0.43	12	0.14		16.8	35.6
10	Profile crowning (PC)	24	3	4	0.43	12	0.19		25.3	17.9

Constant parameters for *tip relief, root relief, end relief,* and *profile crowning:* Electrolyte concentration: 0.5 M (2.84% concentration by weight); Electrolyte flow rate: 20 lpm; Electrolyte temperature: 20°C; Rotational speed of cathode gear: 8.5 rpm; Reciprocating velocity of workpiece gear: 0.96 mm/s.

Constant parameters for *lead crowning:* Electrolyte concentration: 1 M (5.52% concentration by weight); Electrolyte flow rate: 20 lpm; Electrolyte temperature: 20°C; Rotational speed of cathode gear: 35 rpm; Reciprocating velocity of workpiece gear: varied in range 0.2-0.8 mm/s.

Figure 6.1 illustrates photographs of anodic workpiece gear before any flank modification or in unmodified condition (Fig. 6.1a), after imparting tip relieving to it (Fig. 6.1b), after its root relieving (Fig. 6.1c), after its end relieving (Fig. 6.1d), after its lead crowning (Fig. 6.1e), and after its profile crowning (Fig. 6.1f) by the PED process. Figure 6.2 presents the charts for anodic workpiece gear showing its microgeometry along profile direction (i) before and after its tip relieving (Figs. 6.2a_1 and 6.2a_2); (ii) before and after its root relieving (Figs. 6.2b_1 and 6.2b_2); (iii) before and after profile crowning (Figs. 6.2c_1 and 6.2c_2); and anodic workpiece gear microgeometry charts along lead direction (i) before and after its end relieving (Figs. 6.2d_1 and 6.2d_2); and (ii) before and after its lead crowning (Figs. 6.2e_1 and 6.2e_2).

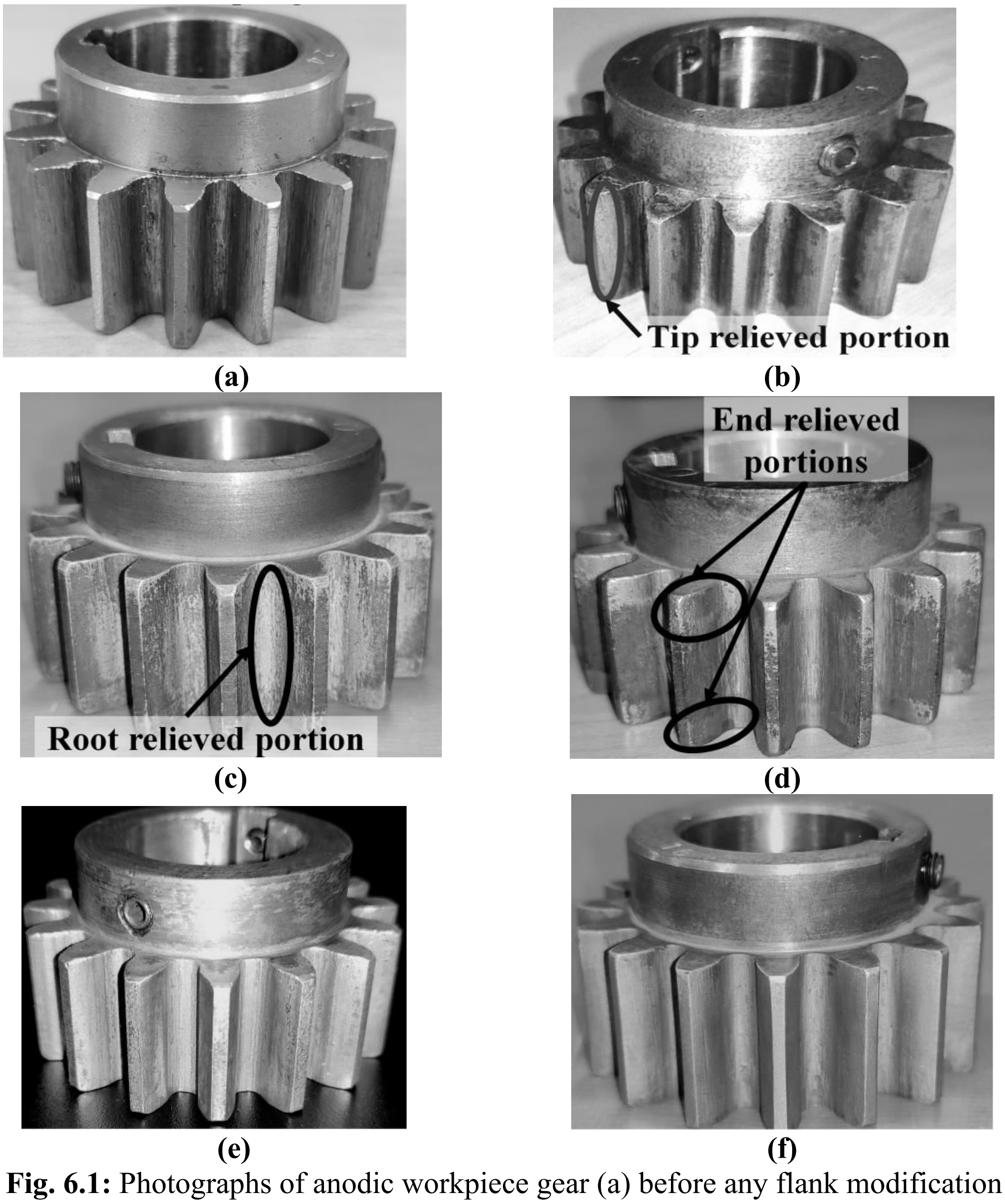

Fig. 6.1: Photographs of anodic workpiece gear (a) before any flank modification i.e., unmodified, (b) after tip relieving, (c) after root relieving, (d) after end relieving, (e) after lead crowning, and (f) after profile crowning.

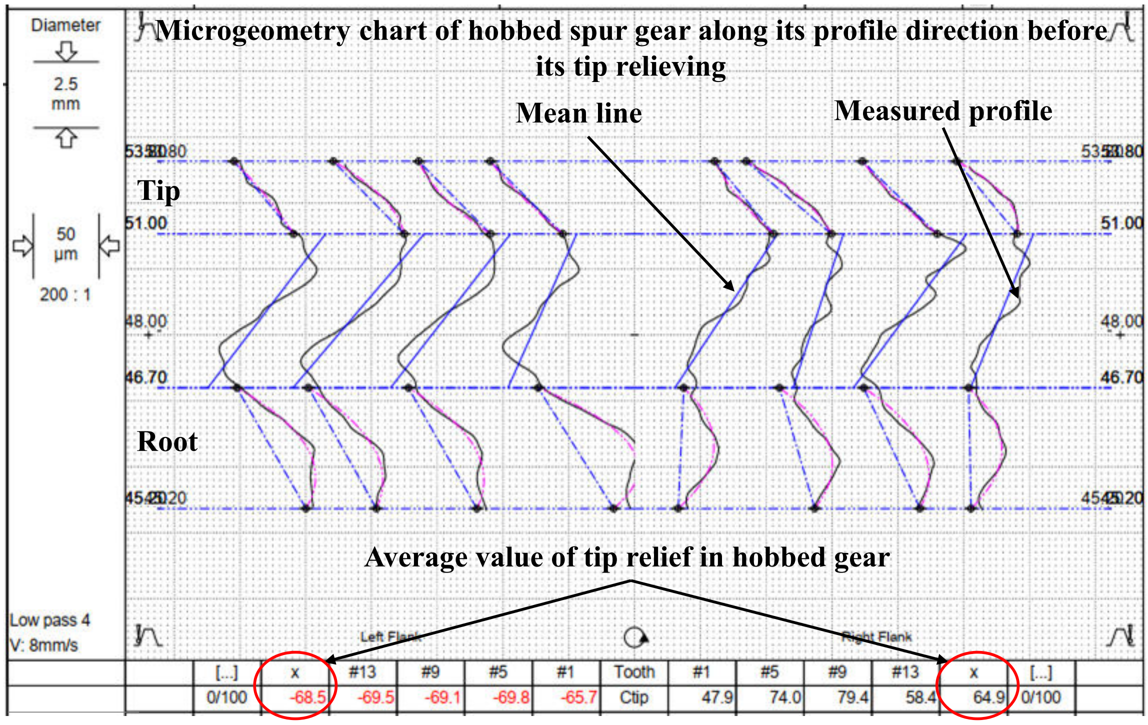
Microgeometry chart of hobbed spur gear along its profile direction before its tip relieving
Mean line
Measured profile
Tip
Root
Diameter
2.5 mm
50 µm
200 : 1
Average value of tip relief in hobbed gear
Low pass 4
V: 8mm/s
Left Flank
Right Flank
[...] x #13 #9 #5 #1 Tooth #1 #5 #9 #13 x [...]
0/100 -68.5 -69.5 -69.1 -69.8 -65.7 Ctip 47.9 74.0 79.4 58.4 64.9 0/100

(a1)

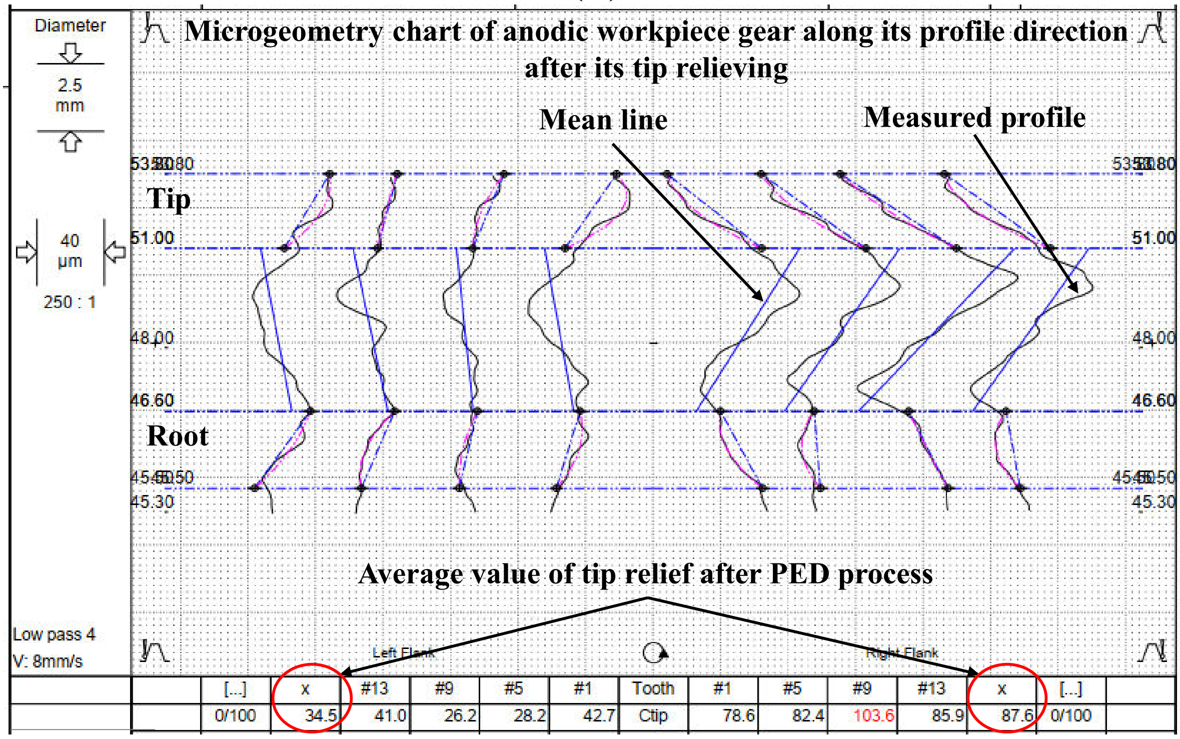
Microgeometry chart of anodic workpiece gear along its profile direction after its tip relieving
Mean line
Measured profile
Tip
Root
Diameter
2.5 mm
40 µm
250 : 1
Average value of tip relief after PED process
Low pass 4
V: 8mm/s
Left Flank
Right Flank
[...] x #13 #9 #5 #1 Tooth #1 #5 #9 #13 x [...]
0/100 34.5 41.0 26.2 28.2 42.7 Ctip 78.6 82.4 103.6 85.9 87.6 0/100

(a2)

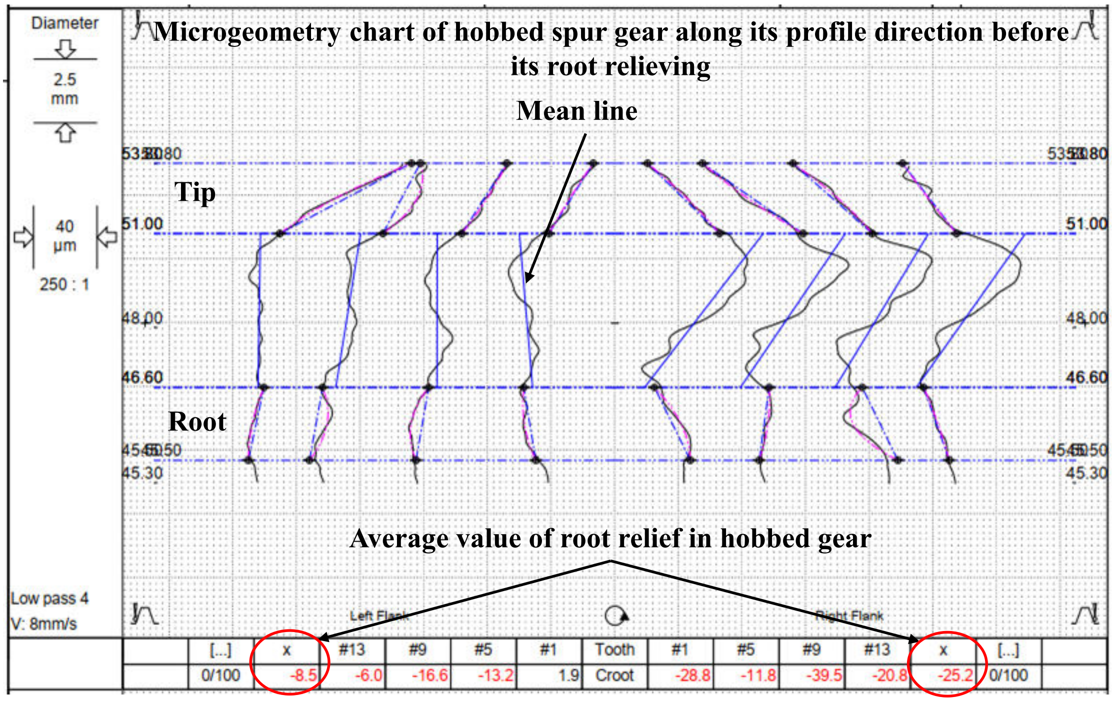

Diameter
2.5 mm
40 µm
250 : 1
Microgeometry chart of hobbed spur gear along its profile direction before its root relieving
Mean line
Tip
Root
53.80
51.00
48.00
46.60
45.50
45.30
Average value of root relief in hobbed gear
Low pass 4
V: 8mm/s
Left Flank
Right Flank
[...] x #13 #9 #5 #1 Tooth #1 #5 #9 #13 x [...]
0/100 -8.5 -6.0 -16.6 -13.2 1.9 Croot -28.8 -11.8 -39.5 -20.8 -25.2 0/100

(b1)

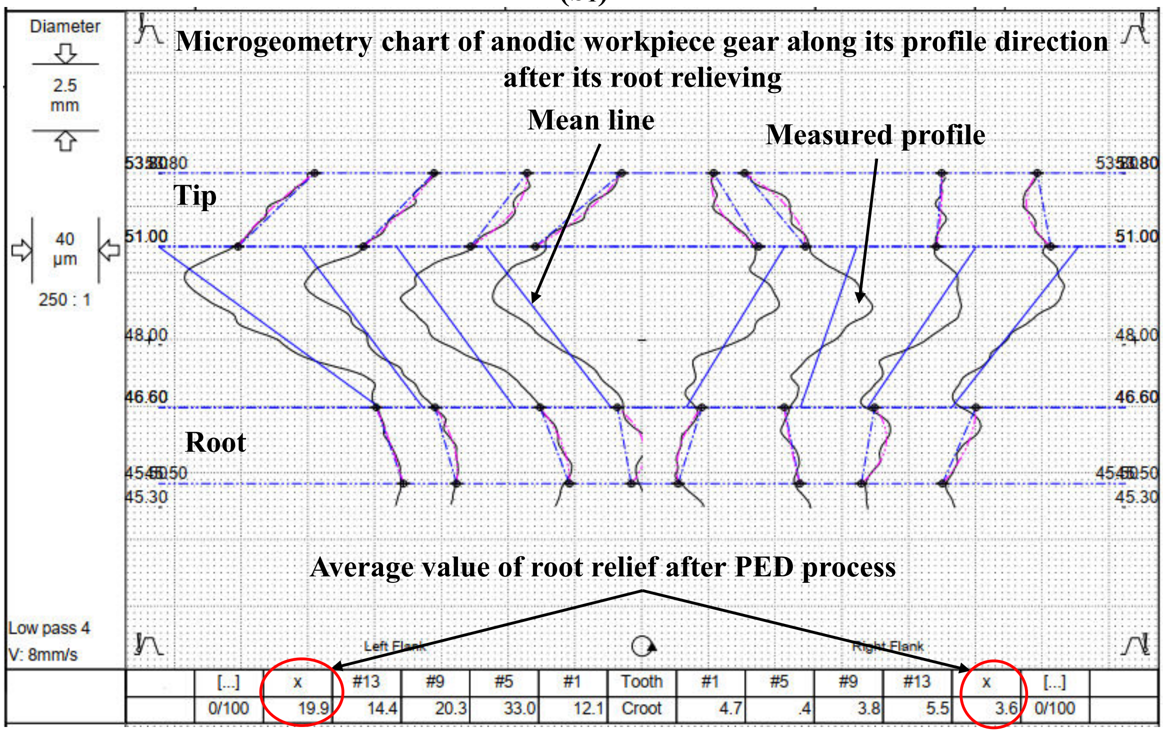

Diameter
2.5 mm
40 µm
250 : 1
Microgeometry chart of anodic workpiece gear along its profile direction after its root relieving
Mean line
Measured profile
Tip
Root
53.80
51.00
48.00
46.60
45.50
45.30
Average value of root relief after PED process
Low pass 4
V: 8mm/s
Left Flank
Right Flank
[...] x #13 #9 #5 #1 Tooth #1 #5 #9 #13 x [...]
0/100 19.9 14.4 20.3 33.0 12.1 Croot 4.7 .4 3.8 5.5 3.6 0/100

(b2)

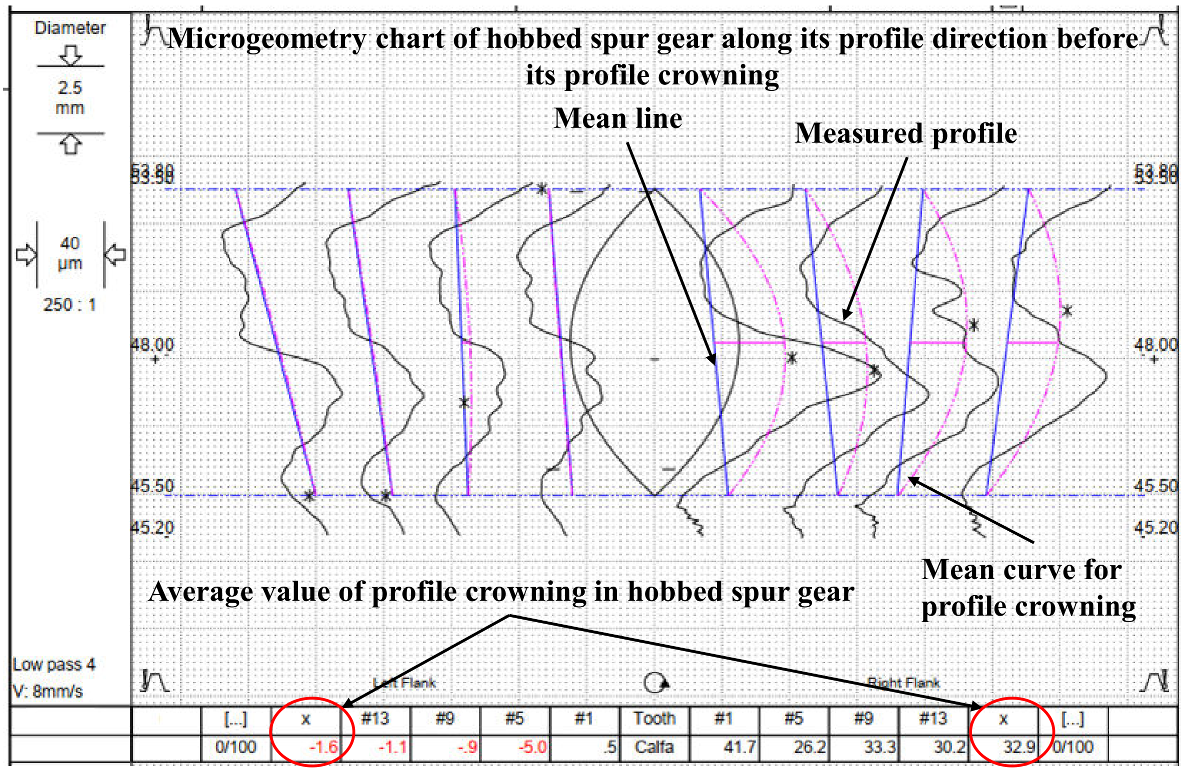

Diameter
2.5 mm
40 µm
250 : 1
Microgeometry chart of hobbed spur gear along its profile direction before its profile crowning
Mean line
Measured profile
53.80
53.50
48.00
45.50
45.20
Mean curve for profile crowning
Average value of profile crowning in hobbed spur gear
Low pass 4
V: 8mm/s
Left Flank
Right Flank
[...] x #13 #9 #5 #1 Tooth #1 #5 #9 #13 x [...]
0/100 -1.6 -1.1 -.9 -5.0 .5 Calfa 41.7 26.2 33.3 30.2 32.9 0/100

(c1)

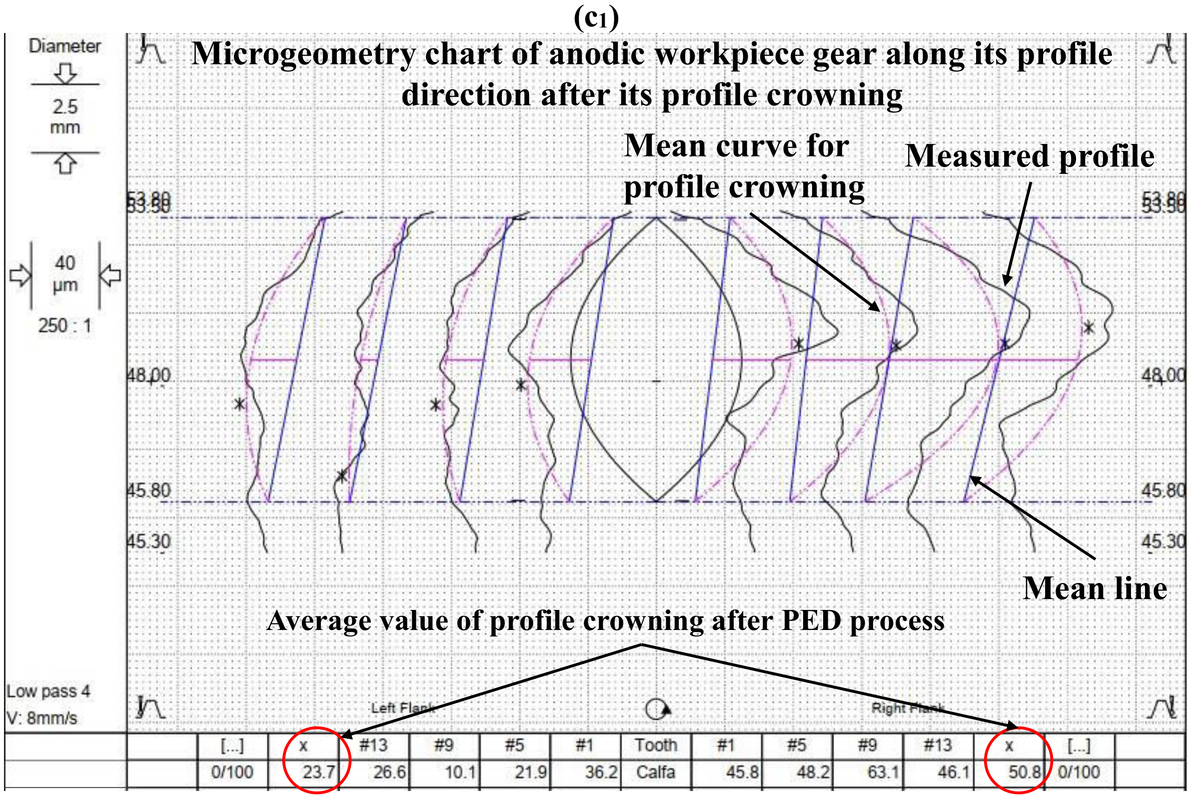

Diameter
2.5 mm
40 µm
250 : 1
Microgeometry chart of anodic workpiece gear along its profile direction after its profile crowning
Mean curve for profile crowning
Measured profile
53.80
53.50
48.00
45.80
45.30
Mean line
Average value of profile crowning after PED process
Low pass 4
V: 8mm/s
Left Flank
Right Flank
[...] x #13 #9 #5 #1 Tooth #1 #5 #9 #13 x [...]
0/100 23.7 26.6 10.1 21.9 36.2 Calfa 45.8 48.2 63.1 46.1 50.8 0/100

(c2)

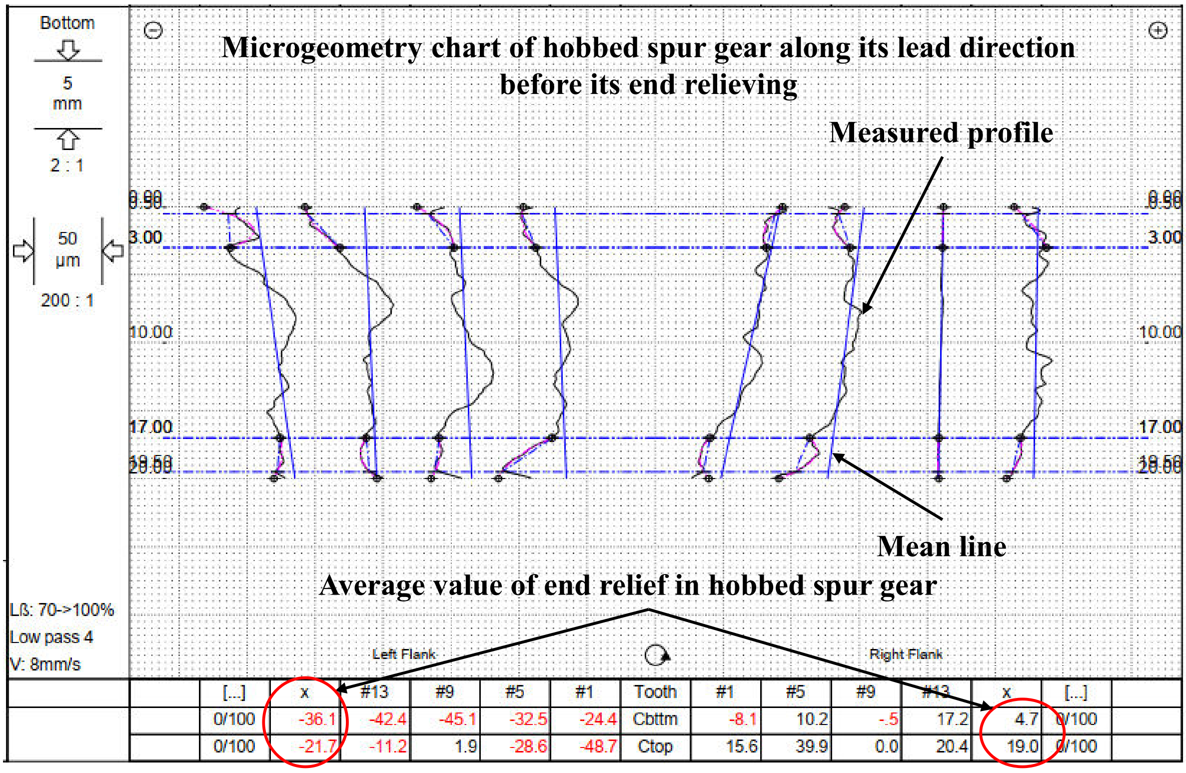

Microgeometry chart of hobbed spur gear along its lead direction before its end relieving
Bottom
5 mm
2 : 1
50 µm
200 : 1
Measured profile
Mean line
Average value of end relief in hobbed spur gear
LB: 70->100%
Low pass 4
V: 8mm/s
Left Flank
Right Flank
[...] x #13 #9 #5 #1 Tooth #1 #5 #9 #13 x [...]
0/100 -36.1 -42.4 -45.1 -32.5 -24.4 Cbttm -8.1 10.2 -.5 17.2 4.7 0/100
0/100 -21.7 -11.2 1.9 -28.6 -48.7 Ctop 15.6 39.9 0.0 20.4 19.0 0/100

(d1)

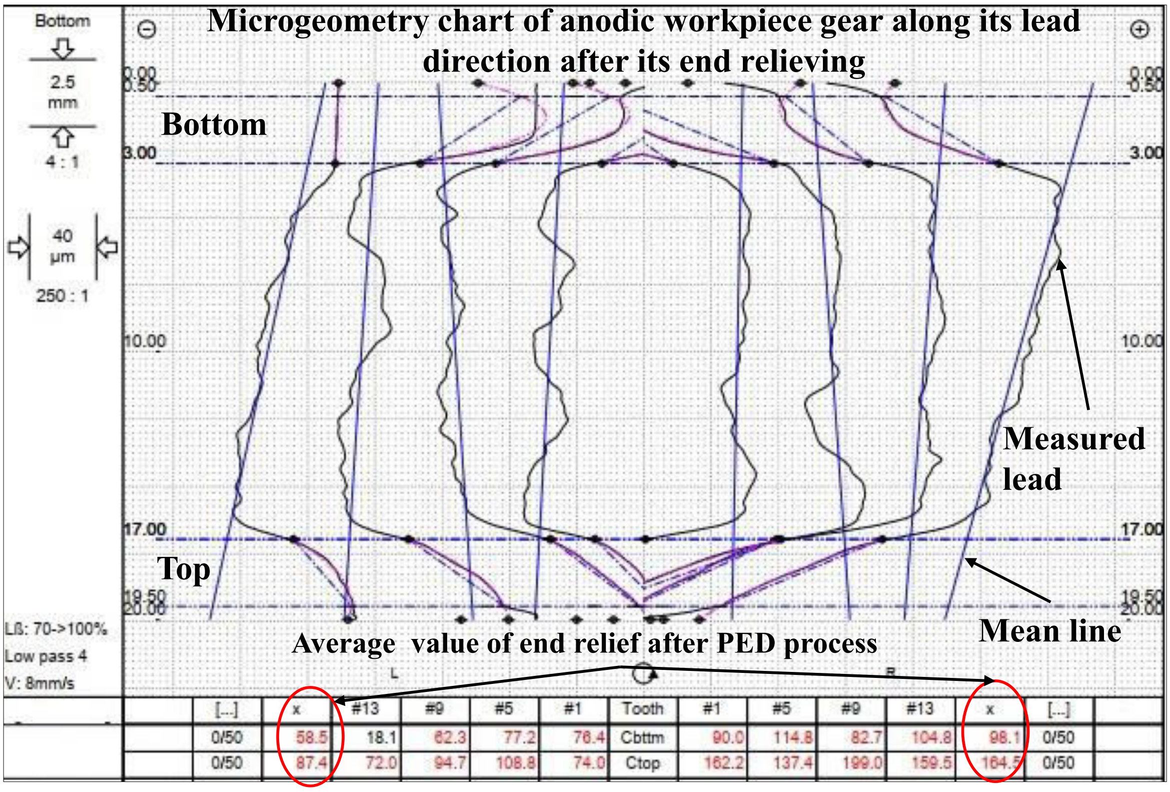

Microgeometry chart of anodic workpiece gear along its lead direction after its end relieving
Bottom
2.5 mm
4 : 1
40 µm
250 : 1
Bottom
Top
Measured lead
Mean line
Average value of end relief after PED process
LB: 70->100%
Low pass 4
V: 8mm/s
[...] x #13 #9 #5 #1 Tooth #1 #5 #9 #13 x [...]
0/50 58.5 18.1 62.3 77.2 76.4 Cbttm 90.0 114.8 82.7 104.8 98.1 0/50
0/50 87.4 72.0 94.7 108.8 74.0 Ctop 162.2 137.4 199.0 159.5 164.5 0/50

(d2)

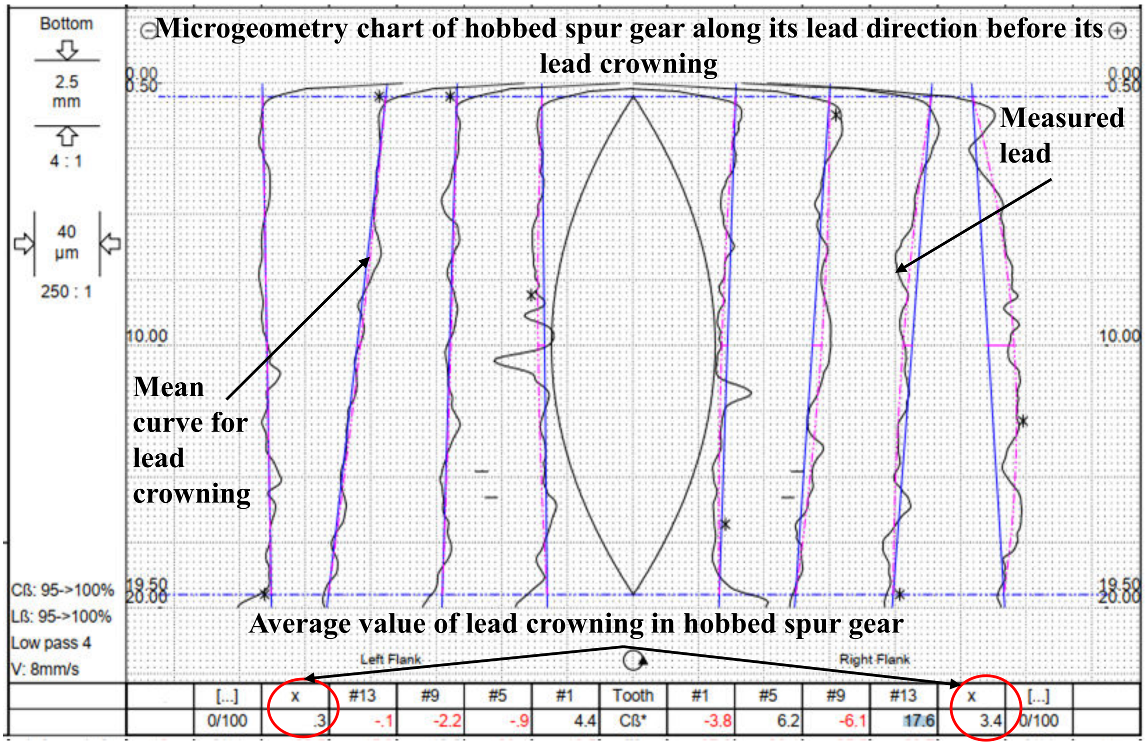

(e1)

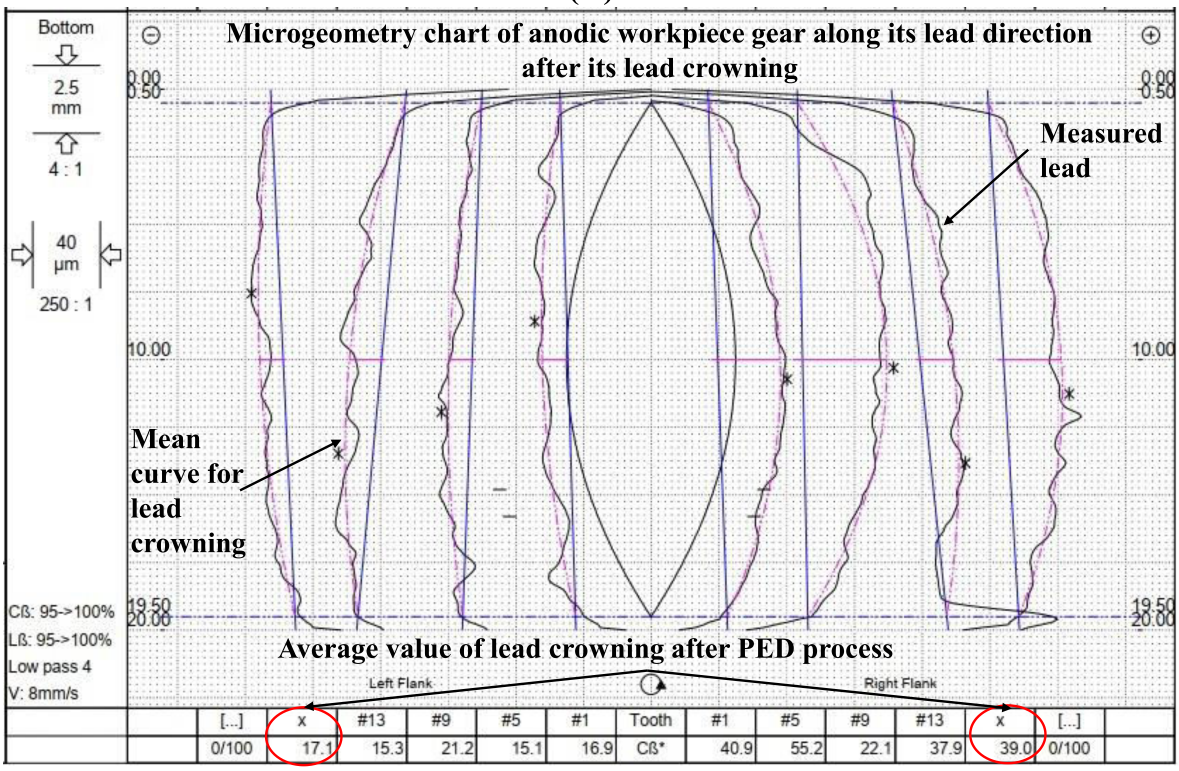

(e2)

Fig. 6.2: Charts for anodic workpiece gear showing its microgeometry along profile direction: (**a1** and **a2**) before and after its tip relieving, (**b1** and **b2**) before and after its root relieving, and (**c1** and **c2**) before and after profile crowning; and microgeometry charts for anodic workpiece along its lead direction (**d1** and **d2**) before and after its end relieving, and (**e1** and **e2**) before and after its lead crowning.

Following are observations from Fig. 6.1, Table 6.1, and Fig. 6.2 and their explanations:

- It is evident from the comparison of photograph of workpiece spur gear before any flank modification (Fig. 6.1a) with photographs of the workpiece gear after flank modification (Figs. 6.1b to Fig. 6.1f) that the developed cathode gears and apparatus through the PED process have successfully imparted tip relief (Fig. 6.1b), root relief (Fig. 6.1c), end relief (Fig. 6.1d), lead crowning (Fig. 6.1e), and profile crowning (Fig. 6.1f) to workpiece spur gear in non-contact manner. It is confirmed by the respective microgeometry charts presented in Figs. 6.2 and the values mentioned in Table 6.1.
- It can be observed from Table 6.1 that the developed cathode gears and apparatus imparted slightly different average values of tip relief (except Exp. No. 1 and 3), root relief (except Exp. No. 5), end relief, lead crowning, and profile crowning to the left and right flanks of workpiece spur gear. This is confirmed by Figs. 6.2b_1 and 6.2b_2 for root relief, Figs. 6.2c_1 and 6.2c_2 for profile crowning, Figs. 6.2d_1 and 6.2d_2 for end relief, and Figs. 6.2e_1 and 6.2e_2 for lead crowning. Slight difference in average values of profile crowning imparted to left and right flanks of workpiece spur gear can be explained with the help of Fig. 6.3g which shows the deviations between theoretical and measured mean profile of spur gear tooth that led to different values of the IEG along tooth profile thus affecting the electrolyte flow during profile crowning by the developed cathode gear and the apparatus. Similar explanations can be given for the slight difference between imparted average values of end relief and lead crowning to the left and right flanks of workpiece spur gear.
- Considerable difference between the average values of tip relief (for Exp. No. 1 as shown in Fig. 6.2a_2 and for Exp. No. 3) and root relief (for Exp. No. 5) imparted to left and right flanks of workpiece spur gear are due to uncertainty in the presence of type of tip or root, among the following types, on the workpiece spur gear before its tip or root relieving by the PED process **(Gimpert, 2007)**: (i) *negative tip* or *root* in which the actual involute profile is inside the theoretical profile at the tooth tip or root as shown in Figs. 6.3a and 6.3d respectively, (ii) *positive tip* or *root* as depicted in Figs. 6.3b and 6.3e, which has the actual involute profile outside the theoretical profile at tooth tip or root respectively, and (iii) positive tip or root on right flank and negative tip or root on left flank or vice versa as shown in Figs. 6.3c and 6.3f. Such uncertainty causes the IEG to be different at different locations along the profile of the workpiece gear. Wherever the IEG is less, more material will be removed and vice versa. It results in a change of the negative value of tip/root either to its less negative or small positive value and positive value of tip/root to its more positive value.

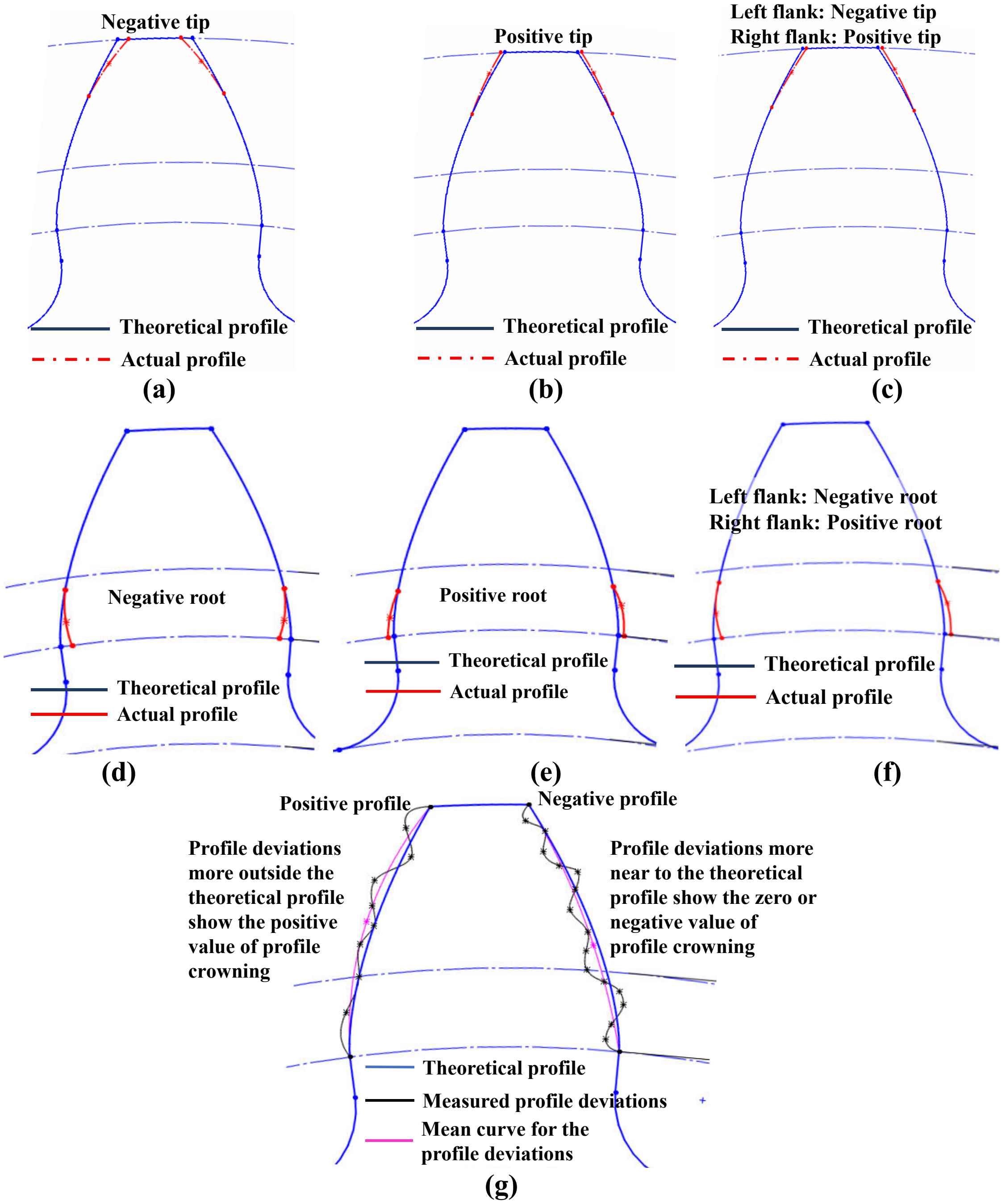

Fig. 6.3: Concept for different types of tips, roots, and profile of a hobbed spur gear: (a) negative tip, (b) positive tip, (c) both negative and positive tip, (d) negative root, (e) positive root, (f) both negative and positive root, and (g) negative and positive involute profile.

Figure 6.4 shows the effect of flank modification duration on average values of tip and root relief and their associated volumetric MRR. It can be observed from Fig. 6.4 that (i) the imparted average values of tip relief to the workpiece spur gear and their associated volumetric MRR continuously increase with modification duration and their maximum values occur at modification duration of 16 minutes corresponding to Exp. No. 4 having applied voltage of 15 volts; 3 ms pulse-on time; and 2 ms pulse-off time, and (ii) minimum values of imparted average root relief and its associated MRR are observed in Exp. 6 having modification duration of 16 minutes and applied voltage as 15 volts whereas their maximum value occurs for modification duration of 20 minutes corresponding to Exp. No. 7 having applied voltage of 18 volts; 3 ms pulse-on time; and 2 ms pulse-off time. It implies that modification duration for root relieving should be at least 20 minutes. Above-mentioned observations can be explained by Faraday's law of electrolysis which implies that the value of material removed is directly proportional to current density and electrolysis duration. Larger value of modification duration increases the amount of the material removed during tip or root relieving which increases their imparted average values. An increase in the applied voltage increases current density, which also leads to more material removal, thus increasing the value of imparted flank modification. Therefore, 20 minutes has been used as root relieving duration for further experiments of Stages 3a and 3b.

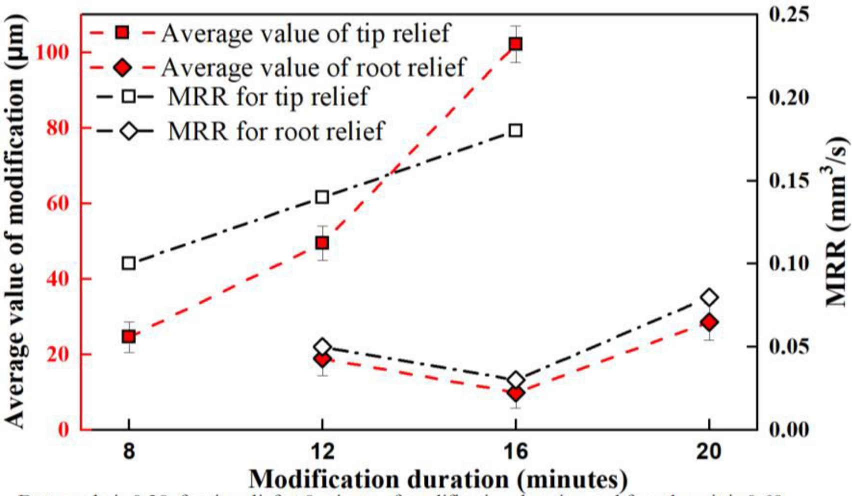

Duty cycle is 0.38 for tip relief at 8 minute of modification duration and for others it is 0.60
Applied oltage is 18 V for root relief at 20 minute of modification duration and for others it is 15 V

Fig. 6.4: Change in the imparted average values of tip and root relief and their associated volumetric material removal rate (MRR) with the modification duration.

6.2 Effects of PED Process Parameters on Tip Relief

Table 6.2 presents average values of tip relief imparted to workpiece spur gear by PED process, associated volumetric MRR, arithmetical average roughness *'Ra'*, maximum height '*Ry*', percentage reduction in *'Ra'* (i.e., *PRRa)*, and percentage reduction in *'Ry* (i.e., *PRRy*) for the 20 experiments conducted in Stage-2 [using one-factor-at-a-time (OFAT) approach] to study the effects of concentration, temperature and flow rate of the electrolyte, modification (or tip relieving) duration, and rotational speed of cathode gear. It also mentions values of the constant parameters used in these experiments. Figure 6.5 depicts the variation of average values of tip relief and associated volumetric MRR, and Fig. 6.6 shows variation in '*PRRa'* and '*PRRy*' with concentration, temperature, and flow rate of the electrolyte, tip relieving duration, and rotational speed of cathode gear.

Table 6.2: Average value of tip relief, material removal rate, and surface roughness parameters for different parametric combinations of the PED process.

Exp. no.	Tip relieving duration (minutes)	Electrolyte concentration (Molarity)	Electrolyte temperature (°C)	Electrolyte flow rate (lpm)	Rotational speed of cathode gear (rpm)	Avg. value of imparted tip relief (µm)	MRR (mm^3/s)	Arithmetical average roughness '*Ra*' (µm)			Maximum height '*Ry*' (µm)		
								Before tip relieving	After tip relieving	'*PRRa*' (%)	Before tip relieving	After tip relieving	'*PRRy*' (%)
1	8					38.4	0.101	2.12	1.71	19.3	20.34	13.49	33.7
2	12					62.2	0.108	2.21	1.23	44.3	19.23	8.51	55.7
3	16	0.5	30	20	15	80.7	0.107	2.42	1.91	21.1	17.98	12.85	28.5
4	20					92.6	0.111	2.38	1.47	38.3	13.79	11.15	19.1
5		0.5				52.3	0.108	1.89	1.34	29.1	11.35	9.45	16.8
6		1.0				59.9	0.242	1.34	1.21	9.7	8.66	8.21	5.1
7		1.5				73.1	0.287	1.34	0.68	49.1	8.82	4.32	51.1
8		2.0				80.9	0.317	1.61	0.80	50.2	14.60	6.86	53.0
9			25			54.3	0.096	2.21	0.97	56.3	13.05	7.41	43.2
10			30			51.2	0.105	1.57	1.20	24.0	11.32	10.93	3.4
11			35			62.5	0.113	2.11	1.51	28.2	13.25	11.02	16.9
12			40			63.4	0.117	2.98	1.44	51.7	18.50	10.39	43.8
13				10		63.0	0.104	2.15	1.45	32.6	13.95	10.22	26.7
14				20		64.3	0.106	2.67	1.14	57.4	16.88	9.86	41.6
16				30		69.3	0.111	1.45	1.09	25.3	9.64	7.39	23.4
16				40		65.7	0.115	1.67	1.34	19.9	14.07	9.45	32.9
17					15	60.0	0.110	3.76	2.12	43.8	23.44	13.49	42.4
18	12	0.5	30	20	25	55.8	0.119	1.45	1.01	30.4	10.18	6.44	36.7
19					35	53.9	0.103	2.36	1.84	21.8	14.09	13.40	4.9
20					45	78.2	0.131	2.12	1.45	31.5	12.78	12.57	1.6

Constant parameters: Electrolyte type: Aqueous NaCl; *V*oltage (*V*): 18 volts; Pulse-on time (t_{on}): 3 ms; Pulse-off time (t_{off}): 4 ms; Duty cycle (δ): 0.43; Reciprocating velocity of anodic workpiece gear: 0.96 mm/s

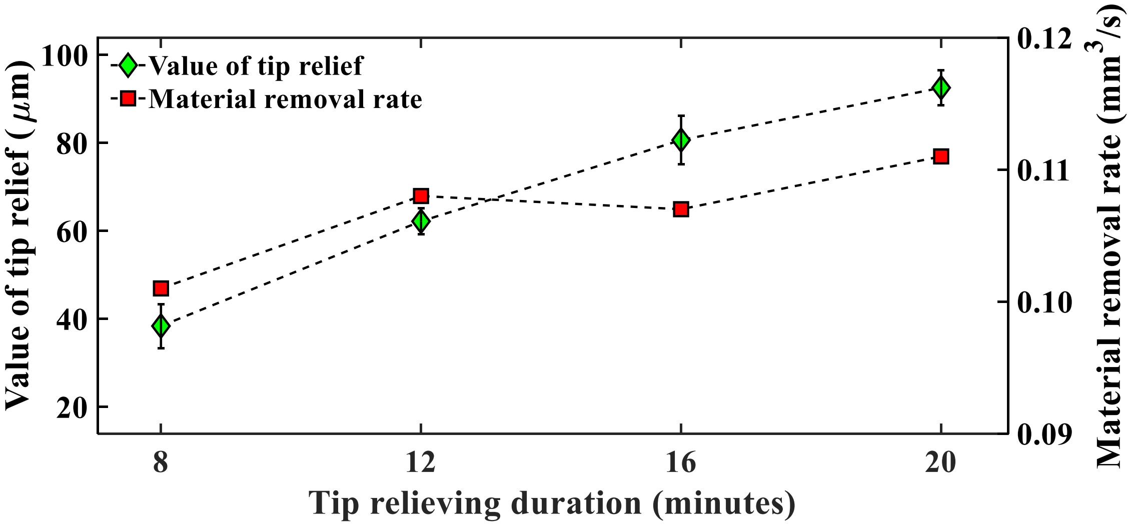
Value of tip relief
Material removal rate
Value of tip relief (μm)
Material removal rate (mm^3/s)
Tip relieving duration (minutes)
100
80
60
40
20
0.12
0.11
0.10
0.09
8
12
16
20

(a)

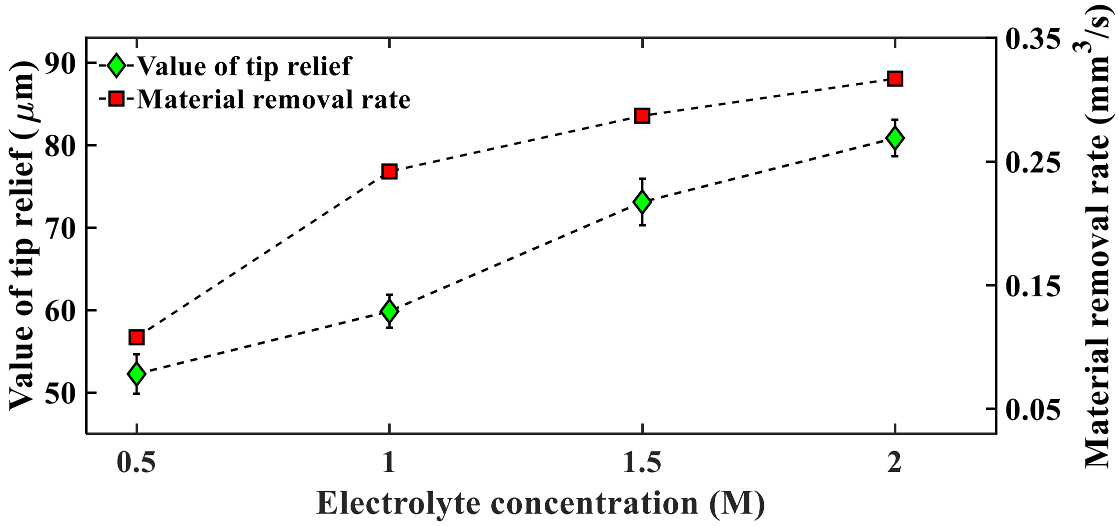
Value of tip relief
Material removal rate
Value of tip relief (μm)
Material removal rate (mm^3/s)
Electrolyte concentration (M)
90
80
70
60
50
0.35
0.25
0.15
0.05
0.5
1
1.5
2

(b)

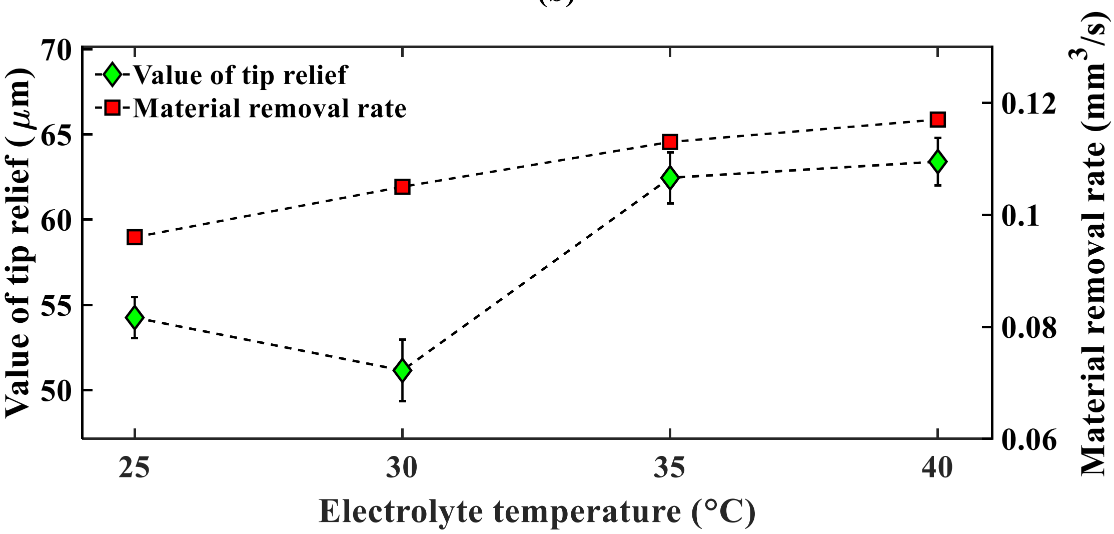
Value of tip relief
Material removal rate
Value of tip relief (μm)
Material removal rate (mm^3/s)
Electrolyte temperature (°C)
70
65
60
55
50
0.12
0.1
0.08
0.06
25
30
35
40

(c)

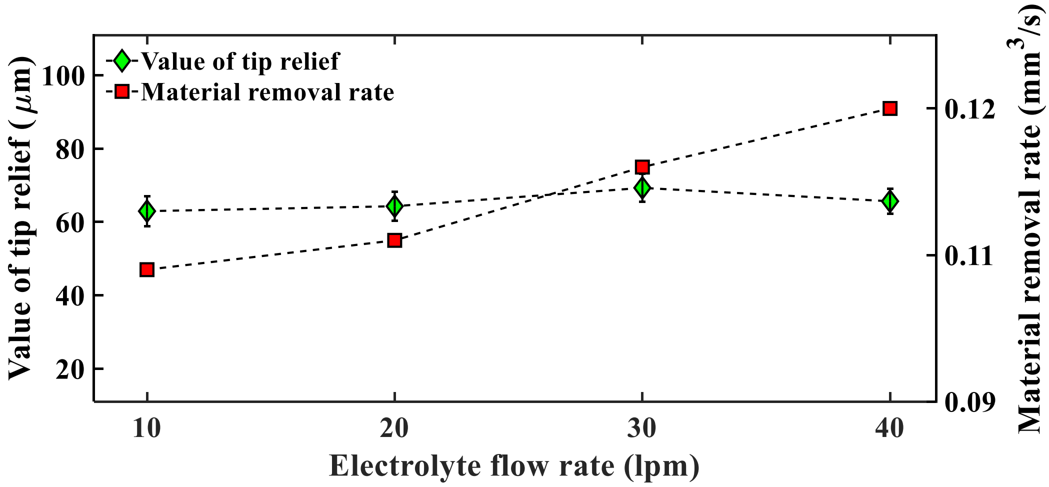

(d)

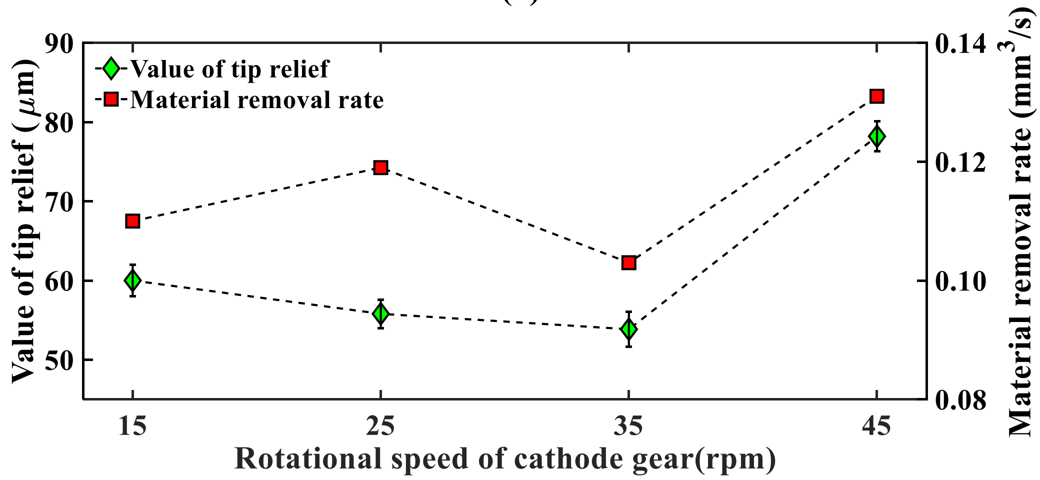

(e)

Fig. 6.5: Change in value of tip relief provided to workpiece spur gear and associated volumetric material removal rate with (a) tip relieving duration, (b) electrolyte concentration, (c) electrolyte temperature, (d) electrolyte flow rate, and (e) rotational speed of cathode gear.

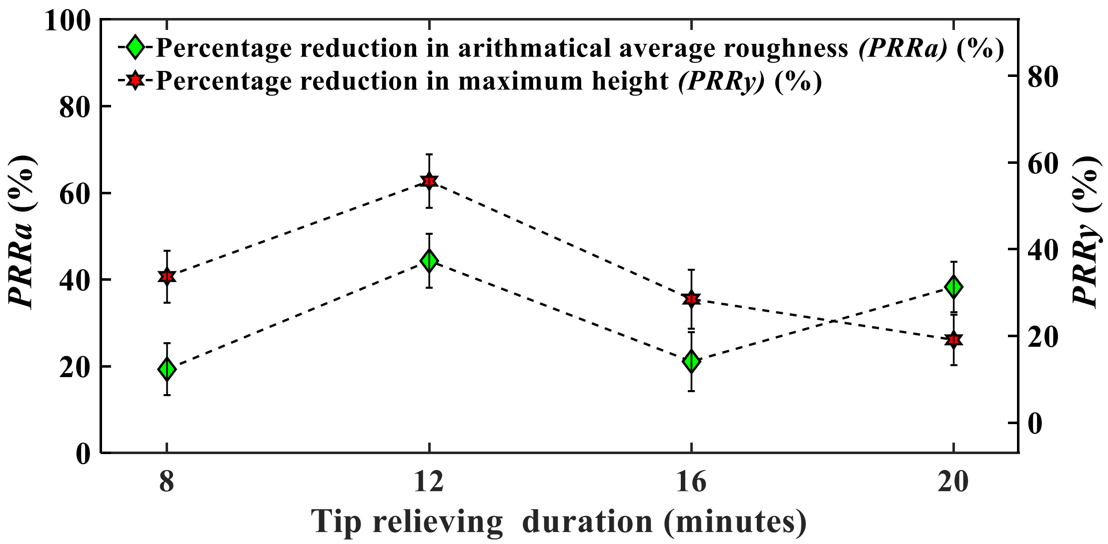

(a)

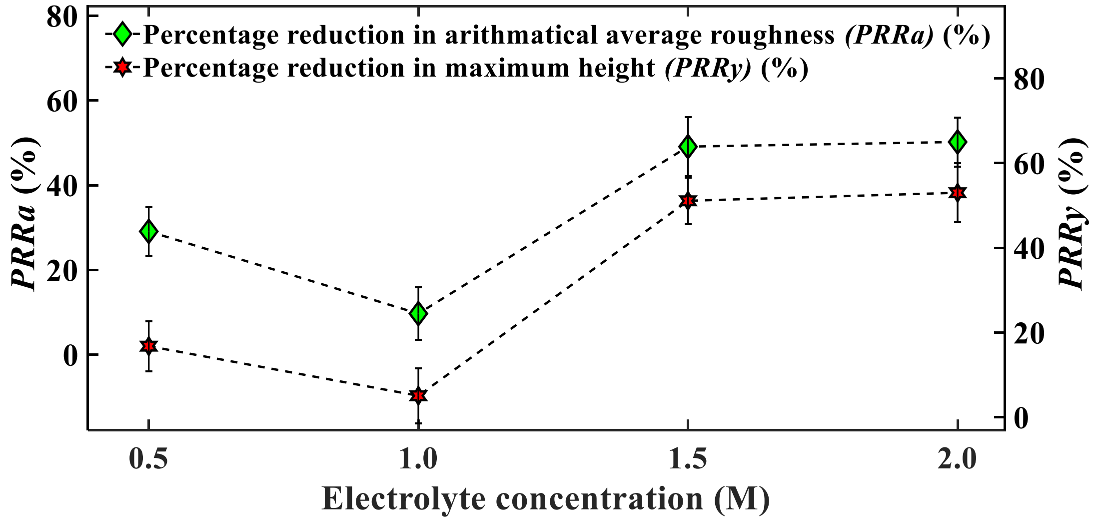
Percentage reduction in arithmatical average roughness *(PRRa)* (%)
Percentage reduction in maximum height *(PRRy)* (%)
PRRa (%)
PRRy (%)
Electrolyte concentration (M)

(b)

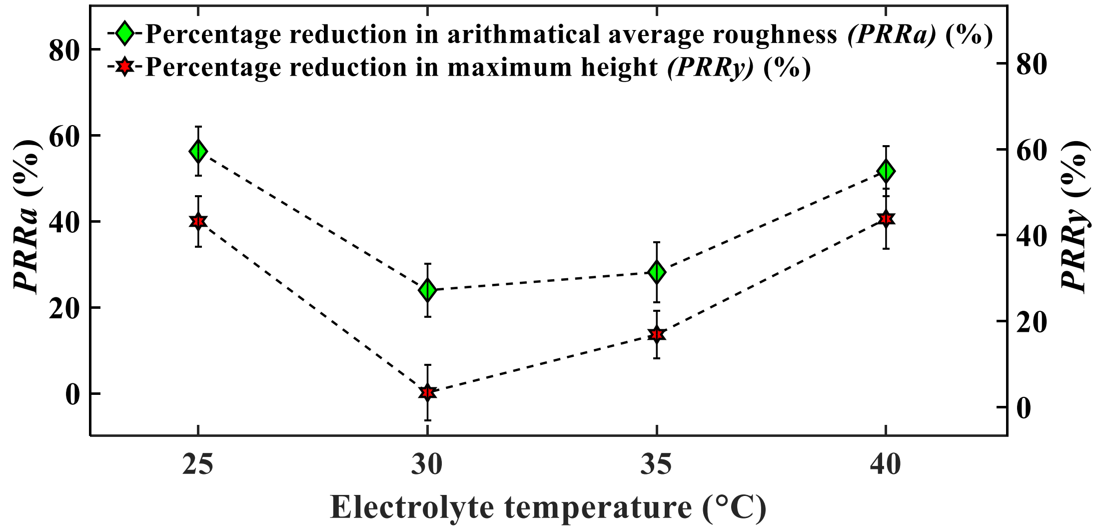
Percentage reduction in arithmatical average roughness *(PRRa)* (%)
Percentage reduction in maximum height *(PRRy)* (%)
PRRa (%)
PRRy (%)
Electrolyte temperature (°C)

(c)

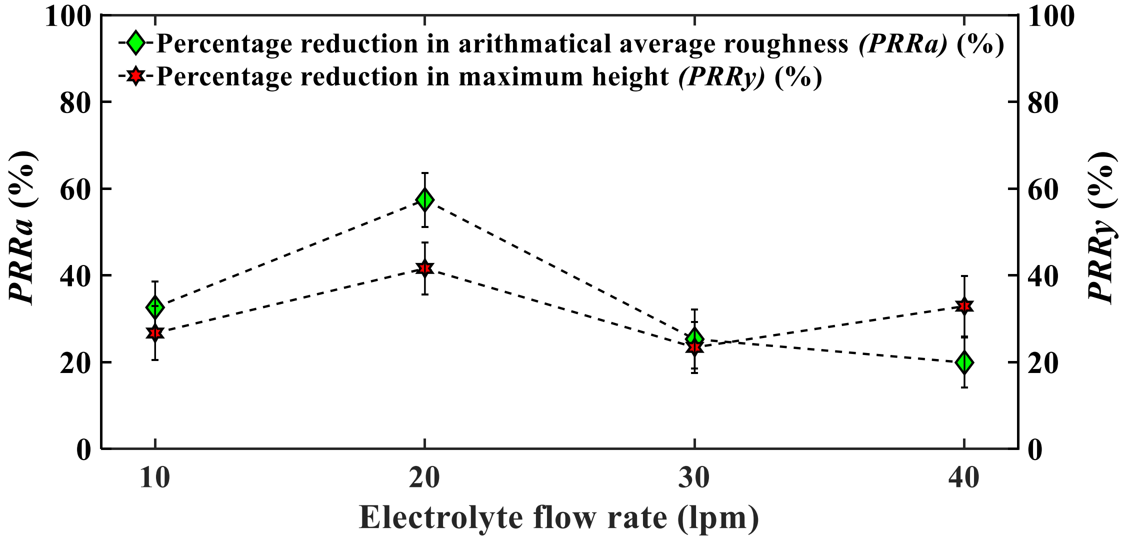
Percentage reduction in arithmatical average roughness *(PRRa)* (%)
Percentage reduction in maximum height *(PRRy)* (%)
PRRa (%)
PRRy (%)
Electrolyte flow rate (lpm)

(d)

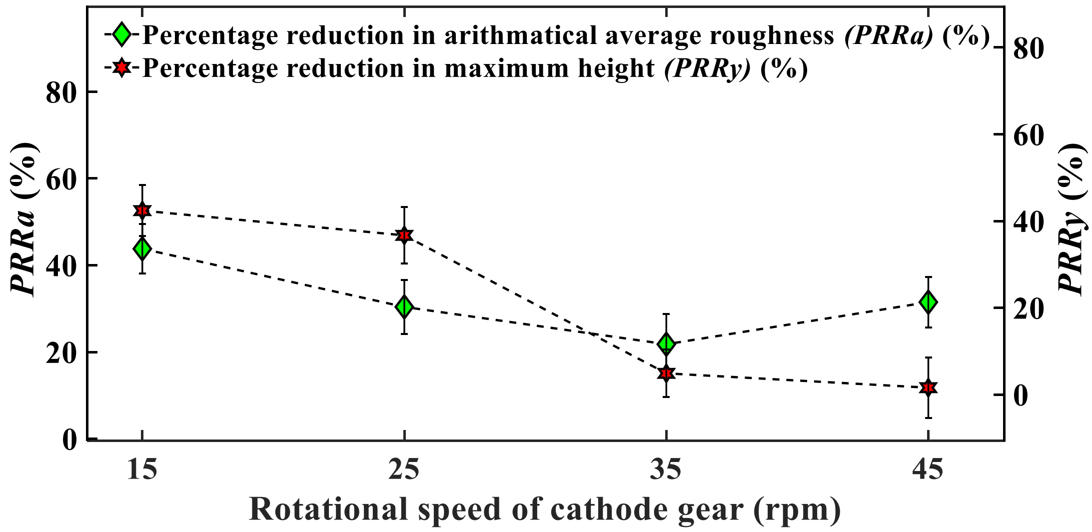

(e)

Fig. 6.6: Change in percentage reduction in surface roughness parameters with (a) modification duration, (b) electrolyte concentration, (c) electrolyte temperature, (d) electrolyte flow rate, and (e) rotational speed of cathode gear.

Following are the observations from Figs. 6.5 and 6.6 along with their explanations:

- Increase in tip relieving duration increases average value of tip relief and associated volumetric MRR (Fig. 6.5a). Average value of tip relief increases at a relatively faster rate for tip relieving duration from 8 to 16 minutes but increases at a slower rate from 16 to 20 minutes. It is due to an increase in IEG between the conductive portion of the developed cathode gear and anodic workpiece gear caused by an increase in volumetric MRR. It decreases current density and consequently reduces the rate of increase in tip relief. Figure 6.6a depicts that percentage reduction in arithmetical average roughness *'PRRa'* and maximum height *'PRRy'* attain their maximum values at 12 minutes of tip relieving duration. It is due to removal of more material at the start of tip relieving by the PED process from those locations on flank surfaces of anodic workpiece spur gear which have less value of IEG (i.e., where surface peaks are present) as per Faraday's laws of electrolysis. This continues till *'PRRa'* and *'PRRy'* attain their maximum values. However, this follows law of diminishing returns because as the tip relieving continues the flank surfaces of the anodic workpiece spur gear becomes more and more smoother which leads to smaller values of *'PRRa',* and *'PRRy'*. Therefore, 12 minutes has been selected as duration of tip relieving, end relieving, profile crowning, and lead crowning in the experiments of Stages 3a and 3b.
- The average value of tip relief and the associated volumetric MRR continuously increase with an increase in electrolyte concentration from 0.5 to 2 Molarity (Fig. 6.5b). Whereas values of '*PRRa'* and '*PRRy'* attain their maximum values for a narrow range

of electrolyte concentration from 1.5 to 2 Molarity (Fig. 6.6b). These can be explained by the fact that electrolyte conductivity increases with its concentration which results in the removal of more material from flank surfaces of workpiece spur gear and, subsequently more smoothening of them. But more material removal by the PED generates more products from electrolytic dissolution of anodic workpiece gear, necessitating their effective flushing from the flank modification zone to avoid any short-circuiting between the cathode gear and anodic workpiece gear. Failure to do so gives undesired results. Based upon these results, 0.5 and 1.0 Molarity were chosen for further experiments on tip, root and end relieving, and lead and profile crowning respectively.

- Average value of tip relief decreases as electrolyte temperature increase from 25 to 30°C and attains its minimum value at 30°C, followed by rapid increase from 30°C to 35°C, and becomes almost constant during 35 to 40°C whereas associated volumetric MRR increase continuously with electrolyte temperature (Fig. 6.5c) implying that 35°C is optimum electrolyte temperature to impart maximum value of tip relief to spur gears by the PED process. But, values of '*PRRa*' and '*PRRy*' are maximum at 25ºC and are minimum at 30°C electrolyte temperature (Fig. 6.6c). Such contradictory effects are due to complicated dependence of electrolyte conductivity, evolution of gases, and valency of dissolution of anodic material on electrolyte temperature. Increase in electrolyte temperature increases its conductivity which helps to remove more material from flank surfaces of anodic workpiece gear thus smoothening their surface roughness peaks. But it increases evolution of oxygen at anodic workpiece gear and hydrogen at cathode gear, and causes electrolytic dissolution of anodic workpiece gear material at its higher valency (in case of multi-valent material) which tend to reduce material removal and less smoothening their surface roughness. Whereas, material removal is slower but uniform at less electrolyte temperature. The net results of these complicated dependence determine the value of electrolyte temperature at which maximum and minimum values of tip relief, associated volumetric MRR, '*PRRa*' and '*PRRy*' occur. Consequently, 30°C was selected as electrolyte temperature for further experiments of Stages 3a and 3b to avoid above-described complications.
- Electrolyte flow rate has an insignificant effect on average values of tip relief but it slightly increases its associated volumetric MRR (Fig. 6.5d) whereas maximum values of '*PRRa*' and '*PRRy*' occur at electrolyte flow rate of 20 lpm (Fig. 6.6d). This is again due to complicated interrelation between flow rate and conductivity of electrolyte along the flow direction and flushing away of the removed material from the modification

zone. Higher flow rate of electrolyte aids in flushing away of the removed material from the modification zone, filling it with the fresh electrolyte, and taking away the heat generated during flank modification by PED process which helps to increase volumetric MRR. Smaller flow rate of electrolyte increases the electrolyte temperature along its flow direction thus increasing its electrical conductivity resulting higher values of '*PRRa*', and '*PRRy*'. Though it results in improper flushing away of the removed material which restricts further removal of material from the anodic workpiece gear. Consequently, 20 lpm has been used as electrolyte flow rate for experiments of Stage 3a and 3b.

- Average value of tip relief decreases for rotational speed of cathode gear range from 15 to 35 rpm, attains its minimum value at 35 rpm along with its associated volumetric MRR, and followed by rapid increase in both from 35 to 45 rpm. Its maximum value occurs at 45 rpm and 2^{nd} maximum value occurs at 15 rpm. But, values of '*PRRa*' and '*PRRy*' are maximum at 15 rpm and minimum at 45 rpm (Fig. 6.6e). Occurrence of maximum average value of tip relief at 45 rpm due to rapid engagement and disengagement between the teeth of the cathode and anodic workpiece gear, which helps to fill the IEG with fresh electrolyte. It facilitates rapid flushing of the removed material and the oxygen evolved at the anodic workpiece gear and hydrogen at the cathode gear from the modification zone. However, it results in abrupt removal of material from surface roughness peaks from flank surfaces of anodic workpiece gear leading to minimum values of '*PRRa*' and '*PRRy*'. Therefore, 15 rpm has been used rotational speed of cathode gear for tip, root, and end reliving of anodic workpiece gear in experiments of Stages 3a and 3b.

6.3 Validation of the Developed Analytical Models

The analytical models developed to predict values of tip relief, root relief, end relief, and lead crowning imparted to spur gear by the PED process were validated by conducting 12 experiments for each model (i.e., total 48 experiments) by varying the voltage, pulse-on time, and pulse-off time at four levels each using one-factor-at-a-time (OFAT) design of experiment approach in Stage-3a Experimentation. Table 6.3 presents values of different constant parameters used in validation of these models.

Table 6.3: Values of different constant parameters used in the developed analytical models to predict the values of tip, root, end relief, and lead crowning imparted to workpiece gear.

Parameter	Notation	Value
Number of teeth in workpiece gear	Z	16
Total face width of the workpiece gear tooth (mm)	b_t	20
Addendum circle radius of workpiece gear (mm)	r_a	27
Pitch circle radius of workpiece gear (mm)	r_p	24
Base circle radius of workpiece gear (mm)	r_b	22.55
Dedendum circle radius of workpiece gear (mm)	r_d	20.25
Datum circle radius of imparting root relief (mm)	r_{rr}	23.3
Datum circle radius of imparting tip relief (mm)	r_{tr}	25.5
Root fillet radius (mm)	r_{rf}	1.2
Arc length of root fillet of workpiece gear (mm)	L_{rf}	1.82
Chordal thickness of workpiece gear tooth along addendum circle (mm)	w_a	2.0
Chordal thickness of workpiece gear tooth along base circle (mm)	w_b	5.1
Chordal thickness of workpiece gear tooth along pitch circle (mm)	w_p	4.71
Involute profile arc length of workpiece gear flank surface modified in TR (mm)	L_{tr}	1.75
Involute profile arc length of workpiece gear flank surface modified in RR (mm)	L_{rr}	0.76
Involute profile arc length of workpiece gear flank surface modified in ER (mm)	L_{er}	4.89
Involute profile arc length of workpiece gear flank surface modified in LC (mm)	L_{lc}	4.89
Length of end relief imparted on top end of workpiece gear flank surface (mm)	L_{ert}	3
Pressure angle of point *'G'* on workpiece gear tooth before tip relieving (rad)	ψ_g	0.49
Pressure angle of point *'H'* on workpiece gear tooth before tip relieving (rad)	ψ_h	0.58
Pressure angle of the involute profile of workpiece and cathode gear (rad)	ψ_p	0.35
Area correction factor for involute profile of workpiece gear flank surface in LC	c_l	0.8
Minimum reciprocating velocity of workpiece gear in its lead crowning (mm/s)	u_1	0.2
Reciprocating velocity of workpiece gear when its face width is completely engaged or starts disengaging with conductive part of the cathode gear in its lead crowning (mm/s)	u_2	$(\sqrt{7})/5$
Maximum reciprocating velocity of workpiece gear in its lead crowning (mm/s)	u_3	0.8
Acceleration of workpiece gear during first half of its downward or upward stroke in its lead crowning (mm/s^2)	a_1	3/125
Acceleration of workpiece gear during second half of gear during first half of its downward or upward stroke in its lead crowning (mm/s^2)	a_2	-3/125
Workpiece gear reciprocating velocity in tip and root relieving (mm/s)	S_l	0.96
Avg. value of IEG at involute profile of workpiece gear flank surface in ER (mm)	Y_{er}	1.5
Avg. value of IEG at involute profile of workpiece gear flank surface in RR (mm)	Y_{rr}	0.75
Avg. value of IEG at involute profile of workpiece gear flank surface in TR (mm)	Y_{tr}	0.75
Avg. value of IEG at involute profile of workpiece gear flank surface in LC (mm)	Y_{lc}	0.5
Avg. value of IEG at non-involute profile of workpiece gear flank surface in ER (mm)	Y_{ner}	0.75
Avg. value of IEG at non-involute profile of workpiece gear flank surface in RR (mm)	Y_{nrr}	0.75
Avg. value of IEG at non-involute profile of workpiece gear flank surface in LC (mm)	Y_{nlc}	0.75
Avg. value of IEG at top land of workpiece gear flank surface in ER (mm)	Y_{tler}	1.25
Avg. value of IEG at top land of workpiece gear flank surface in TR (mm)	Y_{tltr}	1.25
Avg. value of IEG at top land of workpiece gear flank surface in LC (mm)	Y_{tllc}	1.25
Density of workpiece gear material (g/mm^3)	ρ	7.85×10^{-4}
Electrochemical equivalent weight of the workpiece gear material (Computed using percentage by weight method)	E	27.76
Current efficiency of electrolytic dissolution *(%)* **(Lin et *al.*, 2021** and **Mayank et *al.*, 2018)**	η	100%
Electrical conductivity of electrolyte for NaCl concentration of 0.5 M (S/mm)	κ_e	0.0049
Electrical conductivity of electrolyte for NaCl concentration of 1 M (S/mm)	κ_e	0.0079
Faraday's constant (Coulomb)	F	96,500
Overvoltage for NaCl concentration of 0.5 Molarity (volts)	$\Delta V_{0.5}$	0.63
Overvoltage for NaCl concentration of 1 Molarity (volts)	$\Delta V_{1.0}$	0.56

Validation of the developed analytical models for tip relief, root relief, end relief, and lead crowning also required measurement of values of overvoltage, electrolyte conductivity, and actual values of pulse-on time and pulse-off time provided by the DC power supply unit. Their measurement procedure is described in the following paragraphs.

Overvoltage was measured by linear swept voltammetry using platinum wire as an auxiliary or counter electrode (cathode), silver/silver-chloride as the reference electrode, and an electrode made of workpiece gear material as the working electrode (or anode) as shown in Fig 6.7a. Measured values of DC current and voltage at scan rate of 0.002 V/s were used to plot the Tafel curve as shown in Fig. 6.7b from which value of overvoltage 'ΔV' is obtained.

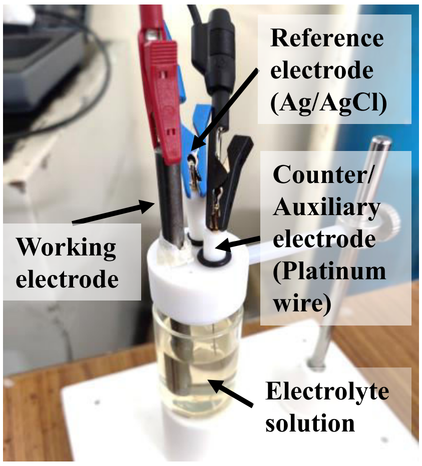

(a)

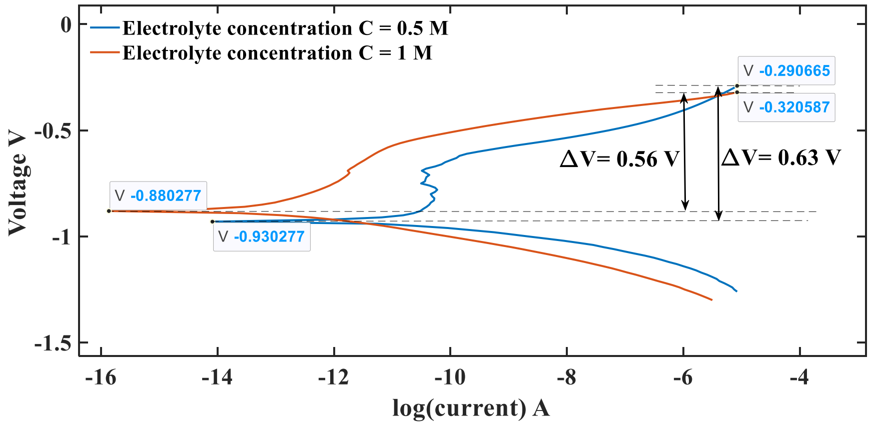

(b)

Fig. 6.7: Measurement of overvoltage: (a) Photograph of electrochemical cell with the working, reference, and counter/auxiliary electrodes dip in the electrolyte solution, and (b) Tafel curve used to obtain the value of overvoltage.

Electrical conductivity of the chosen electrolyte was measured by a conductivity meter having a cell constant of 0.98/cm. Three readings were taken for each concentration of the electrolyte and their average value was used in the validation of the developed analytical models. The average value of electrical conductivity for electrolyte solution of concentration 0.5 M and 1M are presented in Table 6.3.

The supplied pulsed DC power was monitored by an oscilloscope (from Scientific, model: SMO 1002) by measuring the actual values of pulse-off time 't'_{off}', and pulse-on time 't'_{on}'. Table 6.4 summarizes the programmed and measured values of pulse-on and pulse-off times for their all combinations used in experimental validation of the developed analytical models. Figure 6.8 depicts an illustration of the measurement corresponding to Exp. No. 6 in Table 6.4. It can be observed from Table 6.4 that measured values of pulse-on time 't'_{on}' are greater than their corresponding programmed values 't_{on}', whereas measured values of pulse-off time 't'_{off}' are less than their corresponding programmed values 't_{off}'. It is due to (i) the time which is used to reach the programmed value of the applied voltage from its zero value is considered part of actual pulse-on time as depicted in Fig. 6.8. This time is known as rise time 't_r', and (ii) the time which is used by voltage to fall from its programmed value to zero is also considered a part of pulse-on time as shown in Fig. 6.8. It is known as fall time 't_f' but material removal occurs during the pulse-on time corresponding to Faradaic current 't_{onf}' i.e., excluding the rise and fall time **(Mithu et *al.*, 2011).**

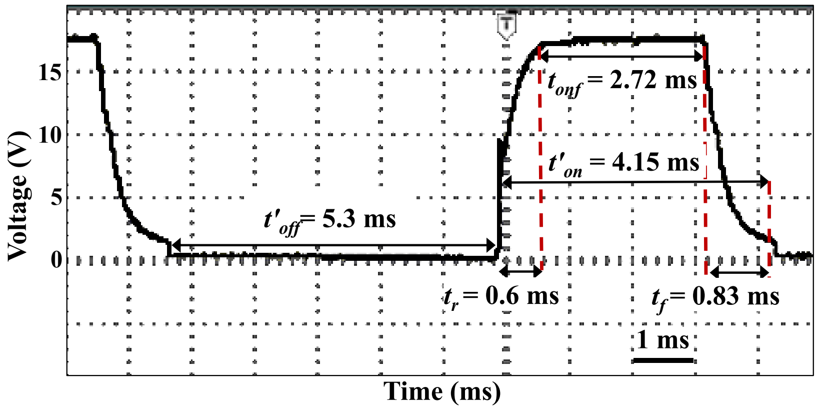

Fig. 6.8: An illustration of measurement of pulse form and actual values of pulse-on and pulse-off times supplied to the PED process during tip, root, end relieving, and lead crowning of anodic workpiece gear.

Table 6.4: Programmed and measured values of pulse-on time and pulse-off time and used for validations of the developed analytical models.

S. No.	**Programmed values**		**Measured values**				
	Pulse-on time 't_{on}' (ms)	**Pulse-off time 't_{off}' (ms)**	**Pulse-on time for Faradaic current 't_{onf}' (ms)**	**Time to reach the programmed voltage 't_r' (ms)**	**Time to fall from the programmed voltage 't_f' (ms)**	**Actual pulse-on time (ms) $t'_{on} = t_{onf} + t_r + t_f$**	**Actual pulse-off time 't'_{off}' (ms)**
1.	2	4	1.72	0.60	0.66	2.98	3.63
2.	3	4	2.74	0.51	0.57	3.82	3.64
3.	4	4	3.74	0.58	0.65	4.97	3.51
4.	5	4	4.74	0.63	0.95	6.32	3.18
5.	3	2	2.75	0.50	0.91	4.15	1.35
6.	3	6	2.72	0.60	0.83	4.15	5.30
7.	3	8	2.76	0.48	1.03	4.27	7.18

Table 6.5 presents the model predicted and experimental values of tip relief, root relief, end relief, and lead crowning, corresponding prediction error (computed by Eq. 6.1), the associated volumetric MRR, and variable and constant input parameters used in the validation experiments of the developed analytical models.

$$Prediction\ Error = \frac{Value\ predicted\ by\ the\ developed\ model - Experimental\ value}{Experimental\ value} 100(\%) \quad (6.1)$$

It can be observed from Table 6.5 that the values of tip, root, end relief, and lead crowning predicted by their developed analytical models have an overall close agreement with their experimental values and that the following are the minimum and maximum values of prediction errors of developed analytical models:

- **For tip relief:** -20.8% in Exp. No. 1 (experimental and predicted values 45.2 μm and 35.8 μm) and 25.1% in Exp No. 12 (experimental and predicted values 16.7 μm and 20.9 μm).
- **For root relief:** -17.3% Exp. No. 5 (experimental and predicted values 17.7 μm and 14.6 μm) and 21.0% in Exp. No. 8 (experimental and predicted values 43.3 μm and 52.4 μm)
- **For end relief:** -21.9% in Exp. No. 8 (experimental and predicted values 118.5 μm and 92.6 μm) and 14.1% in Exp. No. 3 (experimental and predicted values 70.0 μm and 79.9 μm)
- **For lead crowning:** -14.0% in Exp. No. 11 (experimental and predicted values 31.2 μm and 26.8 μm) and 21.6% in Exp. No. 2 (experimental and predicted values 28.3 μm and 34.4 μm).

It implies that the developed analytical models overpredict values of tip, root, end relief, and lead crowning by 25.1%; 21.0%; 14.1%; and 21.6% respectively and underpredict their values by 20.8%; 17.3%; 21.9%; and 14.1% respectively. These observations can be attributed to the consequences of the following assumptions made during development of these models:

- Electrical conductivity of the electrolyte is assumed to be constant during tip/root/end relieving or lead crowning by the PED process. However, flow of electric current causes electrolyte temperature to increase slightly along electrolyte flow direction, which increases electrolyte conductivity and consequently current density along the direction of electrolyte flow. It increases the amount of material removed and consequently the value of the imparted tip/root/end relief or lead crowning.
- Location specific IEG assumed constant during the tip/root/end relieving or lead crowning by the PED process. But IEG at a particular location may vary with time, and it is not uniform due to varying circumferential gap between the conductive and non-conductive portions of a cathode gear (except for lead crowning). An increase in IEG decreases the

current density, decreases material removal, and consequently value of the imparted tip/root/end relief or lead crowning.

- Evolution of hydrogen gas at cathode gear and oxygen gas at anodic workpiece gear are not considered. Their concentrations increase along the electrolyte flow direction, thus decreasing electrolyte conductivity and consequently current density. It decreases material removal and, consequently the value of tip/root/end relief or lead crowning. Generation of oxygen at anodic workpiece gear creates a protective passivating layer on its flank surfaces reducing further material removal from them which reduces tip/root/end relief or lead crowning values.
- All teeth of anodic workpiece gear are assumed identical and equal values of tip/root/end relief or lead crowning are provided to its left and right flanks of a tooth. However, all teeth of a manufactured gear may have different microgeometry deviations therefore value of tip/root/end relief or lead crowning provided to all teeth may not be the same.

Figure 6.9 shows effects of applied voltage (Fig. 6.9a), pulse-on time (Fig. 6.9b), and pulse-off time (Fig. 6.9c) on the model predicted and experimental values of tip relief, root relief, end relief, and lead crowning. These values increase with the applied voltage (Fig. 6.9a). Higher applied voltage increases input energy to the flank modification zone, which increases current density as well as temperature of the electrolyte, thus increasing electrical conductivity of electrolyte. It results in removal of more material from the anodic workpiece gear flank surfaces yielding higher values of tip, root, end relief, and lead crowning imparted to the workpiece gear. Model predicted and experimental values of root/tip/end relief or lead crowning show a continuously increasing trend with pulse-on time (Fig. 6.9b) due to the availability of more time for electrolytic dissolution of material from anodic workpiece gear flank surfaces as well as less time to take away the heat generated at the flank modification zone. It increases the electrolyte temperature along the flow direction which aids in removing more material. The model predicted values for end relief show slightly higher disagreement with its experimental values than tip relief, root relief, and lead crowning. Both model predicted and experimental values of root/tip/end relief or lead crowning show a monotonically decreasing trend with an increase in pulse-off time (Fig.6.9c). It is due to a decrease in the time duration available for imparting tip/root/end relief or lead crowning to the anodic workpiece gear flank surfaces that reduces their values. It can be summarized from the model predicted values of tip relief, root relief, end relief, and lead crowning closely agree with their respective experimental values for the considered ranges of applied voltage, pulse-on time, and pulse-off time.

Table 6.5: Model predicted and experimental values of imparted tip relief, root relief, end relief, and lead crowning and their associated volumetric MRR, and variable input parameters for the validation experiments of the developed analytical models.

Exp no	Applied voltage (volts)	*Pulse-on time* (ms)	*Pulse-off time* (ms)	Duty cycle (δ)	Avg. value of *tip relief* '$C_{\alpha a}$' (µm)			Volumetric MRR in *tip relieving* (mm³/s)			Avg. value *of root relief* 'C_{ft}' (µm)			Volumetric MRR in *root relieving* (mm³/s)			Avg value of *end relief* '$C_{\beta t}$' (µm)			Volumetric MRR in *end relieving* (mm³/s)		
					Experi-mental	Pred-icted	Prediction error (%)	Experi-mental	Pred-icted	Prediction error (%)	Experi-mental	Pred-icted	Prediction error (%)	Experi-mental	Pred-icted	Prediction error (%)	Experi-mental	Pred-icted	Prediction error (%)	Experi-mental	Pred-icted	Prediction error (%)
1	15				45.2	35.8	-20.8	0.087	0.078	-10.3	--	--	--	--	--	--	58.9	56.4	-4.3	0.120	0.098	-18.3
2	18	3	4	0.43	52.3	50.9	-2.6	0.108	0.095	-12.0	13.6	11.5	-15.1	0.076	0.078	2.6	59.8	68.2	14.0	0.175	0.119	-32.0
3	21				68.7	66.0	-3.9	0.131	0.111	-15.3	19.3	18.2	-5.5	0.089	0.092	3.4	70.0	79.9	14.1	0.196	0.14	-28.6
4	24				75.7	81.0	7.0	0.149	0.127	-14.8	29.2	24.8	-15.1	0.094	0.105	11.7	98.6	91.7	-7.0	0.244	0.16	-34.4
4a	27				--	--	--	--	--	--	29.1	31.4	8.1	0.099	0.119	20.2	--	--	--	--	--	--
5		2		0.33	20.5	25.4	23.9	0.074	0.067	-9.5	17.7	14.6	-17.3	0.083	0.084	1.2	45.2	48.3	6.8	0.111	0.084	-24.3
6	18 (for tip and end relief)	3		0.43	55.6	50.9	-8.4	0.113	0.095	-15.9	34.5	31.4	-8.9	0.105	0.119	13.3	70.9	68.2	-3.8	0.176	0.119	-32.4
7		4		0.50	65.9	68.4	3.8	0.127	0.114	-10.2	39.1	43.3	10.9	0.144	0.143	-0.7	72.9	81.9	12.4	0.186	0.143	-23.1
8		5		0.55	72.3	82.1	13.6	0.147	0.128	-12.9	43.3	52.4	21.0	0.166	0.162	-2.4	118.5	92.6	-21.9	0.230	0.162	-29.6
9			2	0.60	81.5	82.2	0.9	0.154	0.129	-16.2	51.9	52.5	1.2	0.163	0.162	-0.6	93.9	92.6	-1.4	0.214	0.162	-24.3
10	27 (for root relief)	3	4	0.43	51.5	50.9	-1.1	0.102	0.095	-6.9	36.4	31.4	-13.6	0.102	0.119	16.7	66.5	68.2	2.6	0.132	0.119	-9.8
11			6	0.33	28.6	32.0	12.1	0.087	0.074	-14.9	18.6	18.9	1.6	0.090	0.093	3.3	58.0	53.4	-7.9	0.129	0.093	-27.9
12			8	0.27	16.7	20.9	25.1	0.070	0.062	-11.4	13.5	11.5	-14.5	0.081	0.078	-3.7	56.0	44.7	-20.1	0.102	0.078	-23.5

Exp no	Applied voltage (volts)	*Pulse-on time* (ms)	*Pulse-off time* (ms)	Duty cycle (δ)	Avg. value of *lead crowning* 'C_β' (µm)			Vol. MRR in *lead crowning* (mm³/s)		
					Exper-imental	Pred-icted	Prediction error (%)	Experi-mental	Pred-icted	Prediction error (%)
1	15				26.2	28.5	8.8	0.137	0.099	-27.8
2	18	3			28.3	34.4	21.6	0.145	0.119	-18.1
3	21		4	0.43	33.7	40.2	19.5	0.175	0.140	-19.9
4	24				46.4	46.1	-0.5	0.230	0.160	-30.4
5		2		0.33	22.4	24.3	8.7	0.109	0.084	-23.2
6		3		0.43	29.0	34.4	18.8	0.158	0.119	-24.9
7		4		0.50	34.8	41.8	20.1	0.189	0.143	-24.5
8		5		0.55	43.1	47.2	9.6	0.211	0.162	-23.1
9			2	0.60	46.1	47.0	2.1	0.223	0.162	-27.3
10	18	3	4	0.43	30.1	34.4	14.3	0.158	0.119	-24.9
11			6	0.33	31.2	26.8	-14.1	0.133	0.093	-29.9
12			8	0.27	21.5	22.6	5.1	0.111	0.078	-30.0

Constant parameters in lead crowning:
Electrolyte concentration: 1 M (5.52 wt%);
Electrolyte flow rate: 20 lpm;
Electrolyte temperature: 30 °C;
Lead crowning duration: 12 minutes;
Rotational speed of cathode gear: 35 rpm.
Variable reciprocating velocity of workpiece gear: 0.2 to 0.8 mm/s

Constant parameters in tip, root and end relief:
Electrolyte concentration: 0.5 M (2.84 wt%);
Electrolyte flow rate: 20 lpm;
Electrolyte temperature: 30 °C;
Modification duration: 12 minutes for TR, and ER, 20 minutes for RR;
Rotational speed of cathode gear: 15 rpm;
Reciprocating velocity of workpiece gear: 0.96mm/s

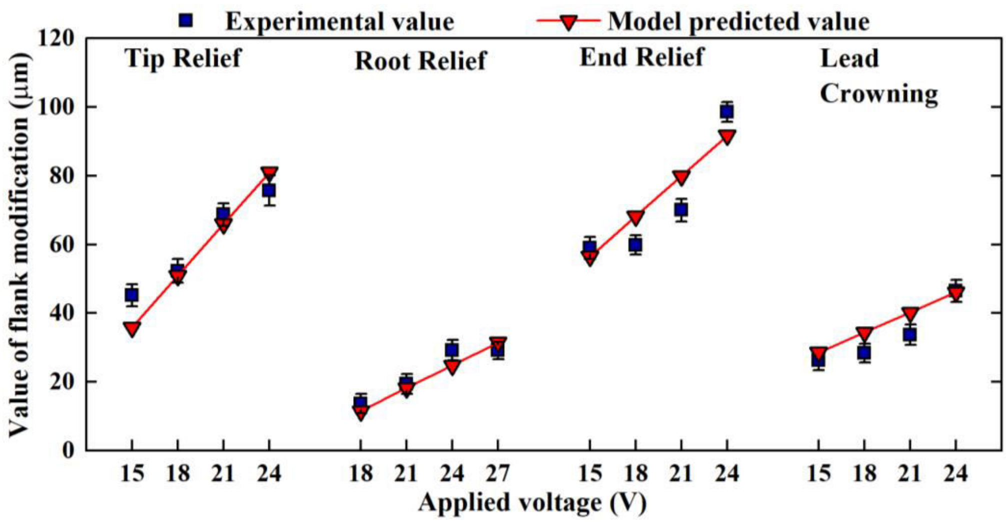

(a)

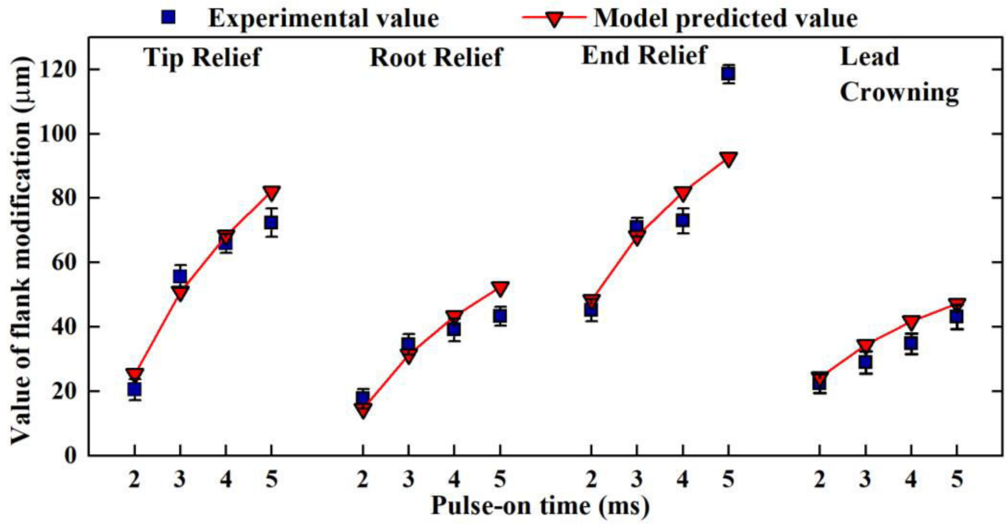

(b)

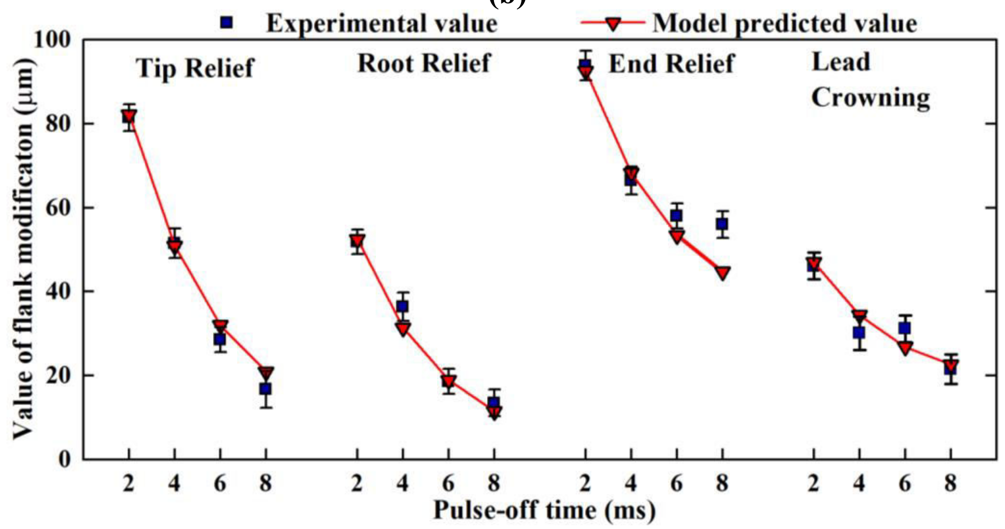

(c)

Fig. 6.9: Change in analytical model predicted and experimental values of tip relief, root relief, end relief, and lead crowning with (a) applied voltage, (b) pulse-on time, and (c) pulse-off time.

Figure 6.10 presents flank surface topography of anodic workpiece gear (corresponding to Exp No. 3 in Table 6.5) before its lead crowning (Fig. 6.10a) and after its *twist-free non-contact lead crowning* (Fig. 6.10b) by the developed cathode gear and apparatus through the PED process. The grid of blue color lines in Fig. 6.10 represents the theoretical shape of the anodic workpiece gear flank surface and grid of black color lines represents its actual shape. Comparison of topography of tooth of anodic workpiece gear corresponding to Exp. No. 3 before lead crowning (Fig. 6.10a) and after its lead crowning (Fig. 6.10b) reveals more deviation between the blue color grid (theoretical shape) and black color grid (actual shape) at the central portion of the anodic workpiece gear flank surface along its lead direction thus confirming that the developed cathode gear and apparatus through the PED process have imparted *twist-free non-contact* lead crowning to anodic workpiece gear flank surfaces.

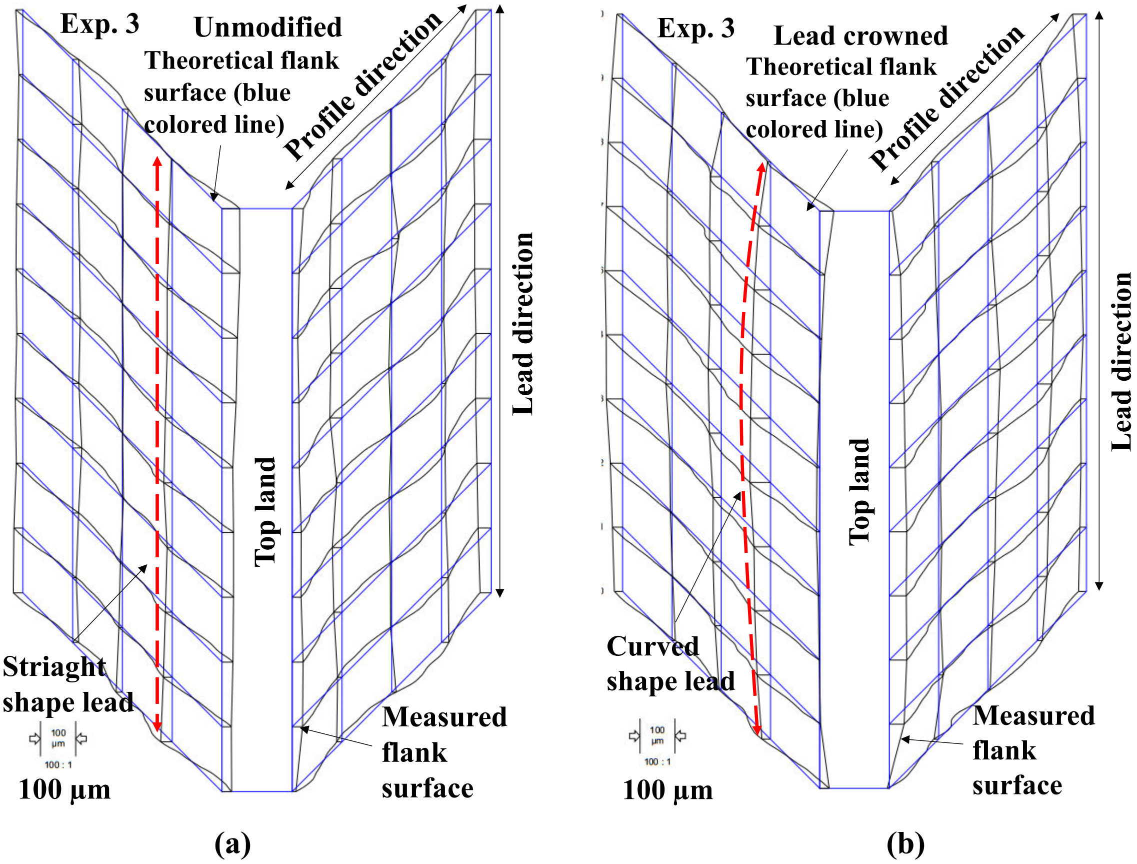

Fig. 6.10: Topography of flank surface of anodic workpiece gear corresponding to Exp No. 3 in Table 6.5: (a) before its lead crowning i.e., unmodified or hobbed condition, (b) after its twist-free lead crowning by the developed cathode gear and apparatus through PED process.

6.4 Effects of PED Parameters on Profile Crowning

Table 6.6 presents the average values of profile crowning 'C_β' and its associated volumetric MRR corresponding to the 12 experiments that were conducted to study the effects of the applied voltage, pulse-on time, and pulse-off time on the profile crowning imparted to workpiece spur gear by the developed cathode gear and apparatus through PED process by varying them at four levels each in Stage-3a experiments. Other parameters of the PED process were kept constant in these experiments. Figure 6.11 graphically depicts these effects. The value of profile crowning decreases from 15 to 18 volts of the applied voltage and then increases continuously, while its associated MRR continuously increases with the applied voltage. It is due to the higher voltage causing higher current density and hence removal of more material from flank surface of the workpiece gear, thus imparting higher value of profile crowning. The value of profile crowning decreases from 2 to 3 ms of pulse-on time and attains its minimum value and then increases continuously with pulse-on time, however its associated MRR increases continuously. It is because more time is available for the electrolytic dissolution of workpiece gear material from its flank surfaces with an increase in pulse-on time. The values of profile crowning show a zig-zag trend of variation with pulse-off time i.e., it decreases then increases and again decreases. Its associated MRR continuously decreases with an increase in pulse-off time. It is due to reduction in the time available for electrolytic dissolution of the anodic workpiece gear. But, increase in pulse-off time increases the time available for flushing out the removed material from the flank modification zone. It allows supply of more amount of fresh electrolyte to the flank modification zone, which increases the electrolytic dissolution of more material from flank surfaces of workpiece gear. Net effect of these contradictory phenomena determines value of the imparted profile crowning, and this may be the reason for its zig-zag variation with pulse-off time.

Table 6.6: Average value of profile crowning and MRR for different parametric combinations of the PED process.

Exp. No.	**Voltage (volts)**	**Pulse-on time (ms)**	**Pulse-off time (ms)**	**Duty cycle (δ)**	**Avg. value of imparted profile crowning 'C_β' (μm)**	**Volumetric MRR (mm^3/s)**
1	15			0.43	9.6	0.142
2	18			0.43	6.7	0.198
3	21	3	4	0.43	12.9	0.211
4	24			0.43	16.4	0.242
5		2		0.33	16.0	0.157
6		3		0.43	12.4	0.178
7		4		0.50	18.8	0.241
8		5		0.55	21.1	0.242
9			2	0.60	22.3	0.226
10	18	3	4	0.43	15.6	0.188
11			6	0.33	23.4	0.159
12			8	0.27	13.0	0.142

Constant parameters: Electrolyte type: Aqueous solution of NaCl; Electrolyte concentration: 1 M (5.52% concentration by weight); Electrolyte temperature: 30°C; Electrolyte flow rate: 20 lpm; Profile crowning duration: 12 minutes; Rotational speed of cathode gear: 35 rpm; Reciprocating velocity of workpiece gear: 0.96 mm/s.

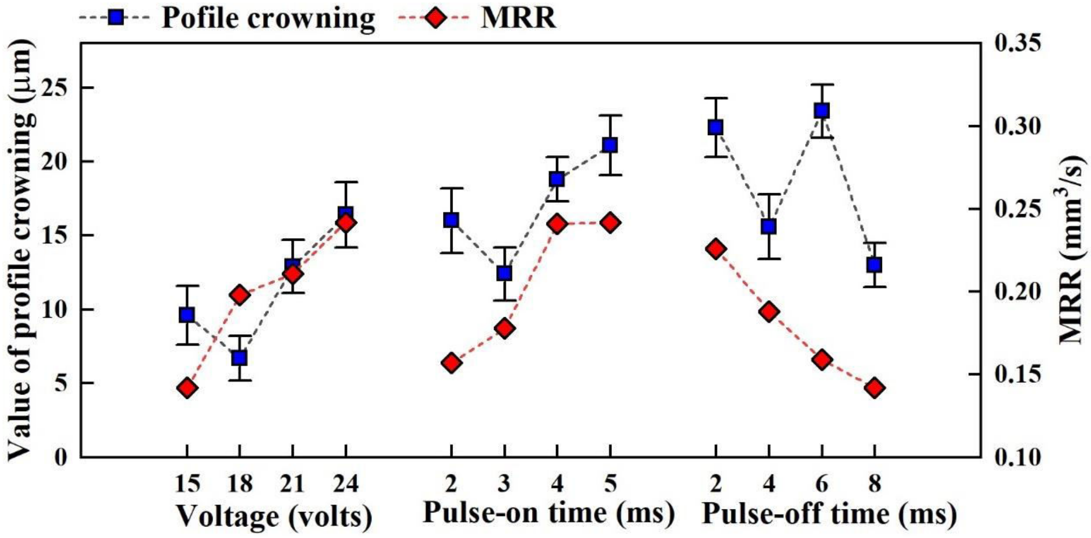

Fig. 6.11: Change in values of profile crowning of workpiece spur gear and associated volumetric MRR with the applied voltage, pulse-on time, and pulse-off time.

6.5 Analysis of Surface Roughness and Morphology

Table 6.7 presents average values of arithmetical average roughness *'Ra'*, maximum height *'Ry'*, % reductions in them i.e., *'PRRa'* and *'PRRy'* corresponding to different combinations of applied voltage, pulse-on time, and pulse-off time used in non-contact tip relieving, root relieving, end relieving, profile crowning, and lead crowning of workpiece spur gear by PED process using the developed cathode gears and the apparatus in Stage-3a experiments. Figure 6.12 depicts surface roughness profile, arithmetical average roughness '*Ra*', and maximum height '*Ry*' of left and right flanks of randomly chosen tooth no.1 (Fig. 12a), and tooth no. 2 (Fig. 12b) of workpiece spur gear before and after its lead crowning corresponding to Exp. No. 4 in Table 6.7 (having applied voltage as 24 volts and 12 minutes as the modification duration). Figure 6.13 graphically depicts the effects of applied voltage (Fig. 6.13a), pulse-on time (Fig. 6.13b), and pulse-off time (Fig. 6.13c) on *'PRRy'* and *'PRRa'* of tip relieved, root relieved, end relieved, profile crowned, and lead crowned workpiece spur gear.

Table 6.7: Average values of arithmetical average roughness *'Ra'*, maximum height *'Ry'*, and their % reductions *'PRRa' and 'PRRy'* obtained during tip, root, end relieving, and profile, lead crowning of anodic workpiece gear by PED process for different parametric combinations.

Exp no	Voltage (volts)	Pulse-on time (ms)	Pulse-off time (ms)	Duty cycle (δ)	Avg. value of arithmetical average roughness *'Ra'* (μm)			Avg. value of maximum height 'Ry' (μm)			Avg. value of arithmetical average roughness *'Ra'* (μm)			Avg. value of maximum height 'Ry' (μm)			Avg. value of arithmetical average roughness *'Ra'* (μm)			Avg. value of maximum height 'Ry' (μm)		
					Before TR	After TR	*'PRRa'* (%)	Before TR	After TR	*'PRRy'* (%)	Before RR	After RR	*'PRRa'* (%)	Before RR	After RR	*'PRRy'* (%)	Before ER	After ER	*'PRRa'* (%)	Before ER	After ER	*'PRRy'* (%)
1	*15*	*3*	*4*	0.43	1.87	1.53	18.6	14.34	10.65	25.7	--	--	--	--	--	--	2.54	2.13	16.1	15.43	14.95	3.1
2	18				1.69	1.50	11.6	12.31	9.50	22.8	1.49	1.05	29.4	11.77	9.37	20.4	1.85	1.50	19.0	13.44	9.50	29.3
3	21				2.38	1.19	50.3	15.27	8.81	42.3	2.60	1.48	43.2	19.49	11.01	43.5	2.38	2.34	2.0	17.73	15.27	13.9
4	24				2.43	1.30	46.6	15.77	9.13	42.1	1.33	0.85	36.6	9.32	6.61	29.0	2.61	2.43	7.0	19.82	15.77	20.5
4a	27				--	--	--	--	--	--	2.11	0.68	*67.7*	13.25	5.44	59.0	--	--	--	--	--	--
5	18 (for tip and end relief)	2		0.33	1.71	1.36	20.9	13.78	10.63	22.8	1.25	0.81	35.6	9.79	5.21	46.8	3.17	2.39	24.5	22.18	13.91	37.3
6		3		0.43	1.71	0.70	59.1	13.49	5.07	*62.5*	2.38	0.94	60.7	13.79	7.54	45.3	2.21	1.11	49.6	13.05	7.29	44.2
7		4		0.50	1.86	1.72	7.1	14.14	12.58	11.0	1.61	0.90	44.0	10.51	7.60	27.7	4.49	1.69	62.4	27.35	10.90	60.1
8		*5*		*0.55*	1.72	1.49	13.4	12.11	11.48	5.2	1.23	0.51	58.5	7.63	4.18	45.2	1.60	0.94	41.2	12.75	10.90	14.5
9	27 (for root relief)	3	2	0.60	2.07	1.49	28.1	13.57	10.48	22.7	1.62	0.54	66.6	11.25	4.15	63.1	2.54	2.01	20.8	16.91	15.94	5.8
10			4	0.43	2.67	1.04	*61.1*	16.88	7.15	57.7	2.21	0.83	62.4	19.23	6.19	*67.8*	1.67	0.60	*63.8*	14.07	4.70	*66.6*
11			6	0.33	2.55	1.83	28.3	17.50	12.81	26.8	1.38	0.59	57.3	10.15	4.85	52.2	2.75	2.12	23.1	20.38	13.49	33.8
12			8	0.27	2.13	1.47	31.1	13.33	10.64	20.2	2.15	0.71	67.1	13.95	6.00	57.0	2.66	1.97	25.9	20.84	12.79	38.6

Exp no	Voltage (volts)	Pulse-on time (ms)	Pulse-off time (ms)	Duty cycle (δ)	Before LC	After LC	*'PRRa'* (%)	Before LC	After LC	*'PRRy'* (%)	Before PC	After PC	*'PRRa'* (%)	Before PC	After PC	*'PRRy'* (%)
1	15	3	4	0.43	1.29	1.25	3.1	8.61	8.56	0.6	1.26	1.04	17.5	11.84	8.57	27.6
2	18			0.43	1.35	1.09	19.3	10.33	7.09	31.4	1.29	1.08	16.9	9.12	8.56	6.0
3	21			0.43	1.35	1.04	23.0	11.48	8.57	25.3	1.61	1.38	14.2	11.08	8.86	20.0
4	24			0.43	1.29	0.88	31.8	8.55	6.20	27.5	1.15	1.12	2.0	11.01	8.44	23.4
5	18	2		0.33	1.50	1.38	8.0	12.22	8.86	27.5	1.45	1.15	20.9	11.68	8.70	25.5
6		3		0.43	1.49	1.10	26.2	14.42	10.08	30.1	1.88	1.32	*29.9*	13.94	7.95	*43.0*
7		4		0.50	1.75	1.15	*34.3*	12.71	8.44	*33.6*	1.71	1.23	28.2	11.94	8.81	26.2
8		5		0.55	1.52	1.12	26.3	11.50	8.70	24.3	1.72	1.32	23.4	12.40	9.24	25.5
9		3	2	0.60	1.58	1.43	9.50	10.82	10.41	3.8	1.78	1.46	18.1	11.90	9.52	20.0
10			4	0.43	1.64	1.27	22.6	14.23	9.87	30.6	1.74	1.48	14.9	11.44	8.93	21.9
11			6	0.33	1.81	1.66	8.3	13.64	10.81	20.7	1.75	1.41	19.2	13.39	10.00	25.3
12			8	0.27	1.71	1.47	14.0	11.94	9.57	19.8	1.54	1.49	3.1	11.57	10.47	9.5

Constant parameters in lead and profile crowning: Electrolyte concentration: 1 M; Electrolyte flow rate: 20 lpm; Electrolyte temperature: 30 °C; LC duration: 12 minutes; Rotational speed of cathode gear: 35 rpm; Reciprocating velocity of workpiece gear: 0.96mm/s for PC, and 0.2 to 0.8 mm/s for LC

Constant parameters in tip, root, and end relieving: Electrolyte concentration: 0.5 M; Electrolyte flow rate: 20 lpm; Electrolyte temperature: 30 °C; Modification duration: 12 minutes for TR, ER, 20 minutes for RR; Rotational speed of cathode gear: 15 rpm; Reciprocating velocity of workpiece gear: 0.96mm/s

It can be observed from Table 6.7 that *'PRRa'* and *'PRRy'* have positive values for the 12 experiments conducted each for tip relief, root relief, end relief, profile crowning, lead crowning. Following are the maximum values of *'PRRa'* and *'PRRy'* for different flank modifications:

- **After tip relieving**: 61.1% and 62.5% respectively (corresponding to Exp. No. 10 and Exp. No. 6) having combination of applied voltage as 18 volts; 3 ms pulse-on time; and 4 ms pulse-off time (i.e., 0.43 % duty cycle).
- **After root relieving:** 67.7% and 67.8% respectively (corresponding to Exp. No. 4a and Exp. No. 10) for parametric combination of applied voltage as 27 volts; 3 ms pulse-on time; and 4 ms pulse-off time (i.e., 0.43 % duty cycle).
- **For end relieving:** 63.8% and 66.6% respectively (corresponding to Exp. No. 10) having combination of applied voltage as 18 volts; 3 ms pulse-on time; and 4 ms pulse-off time (i.e., 0.43 % duty cycle).
- **For lead crowning:** 34.3% and 33.6% respectively (corresponding to Exp. No. 7) having combination of applied voltage as 18 volts; 4 ms pulse-on time; and 4 ms pulse-off time (i.e., 0.50 % duty cycle).
- **For profile crowning:** 29.9% and 43.0%, respectively (corresponding to Exp. No. 6) having combination of applied voltage as 18 volts; 3 ms pulse-on time; and 4 ms pulse-off time (i.e., 0.43 % duty cycle);

It can be observed from roughness profile of flank surfaces of workpiece gear before and after its lead crowning (corresponding to Exp. No. 4 Table 6.7) shown in Fig. 6.12 that the value of *'Ra'* is reduced for randomly chosen tooth no. 1 (from 1.47 μm to 0.85 μm for left flank and from 1.41 μm to 0.97 μm for right flank) and tooth no. 2 (from 1.24 μm to 0.8 μm for left flank and from 1.03 μm to 0.87 μm for right flank). Similarly, values of *'Ry'* are reduced significantly for tooth no. 1 (from 9.92 μm to 5.54 μm for left flank and from 10.14 μm to 5.77 μm for right flank) and slightly for left flank of tooth no. 2 (from 6.71 μm to 6.17 μm) but slightly increased for its right flank (from 7.43 μm to 7.47 μm).

Randomly chosen **tooth no. 1** of workpiece gear

Left flank before lead crowning

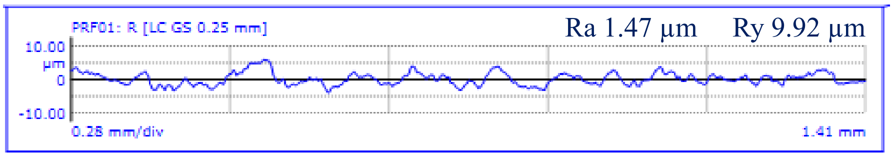

Left flank after lead crowning

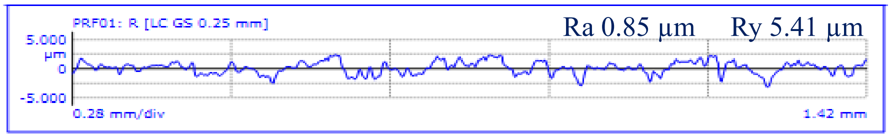

Right flank before lead crowning

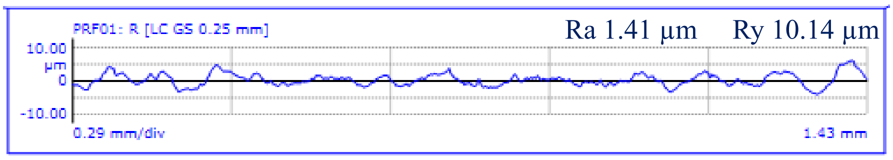

Right flank after lead crowning

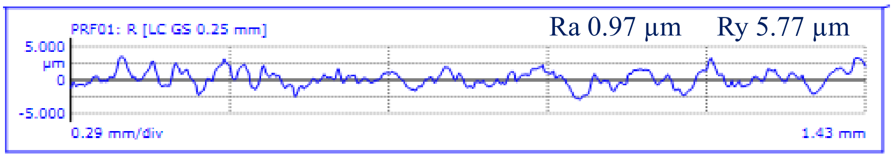

(a)

Randomly chosen **tooth no. 2** of workpiece gear

Left flank before lead crowning

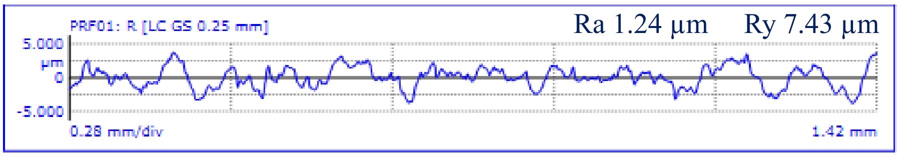

Left flank after lead crowning

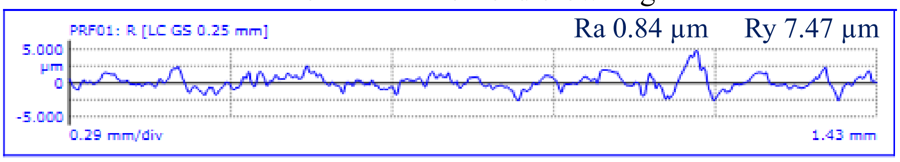

Right flank before lead crowning

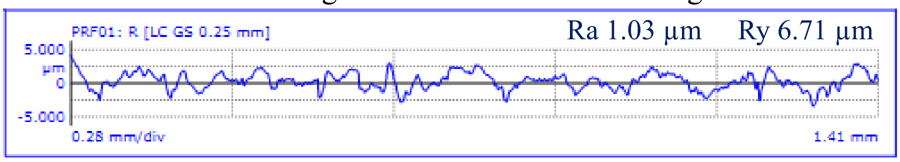

Right flank after lead crowning

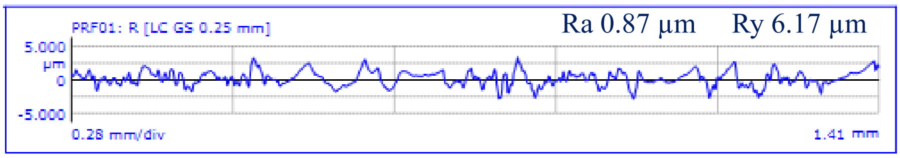

(b)

Fig. 6.12: Surface roughness profiles of left and right flanks of anodic workpiece gear before and after lead crowning by the PED process (Exp. No. 4 in Table 6.7) for randomly chosen (a) tooth no.1, and (b) tooth no. 2.

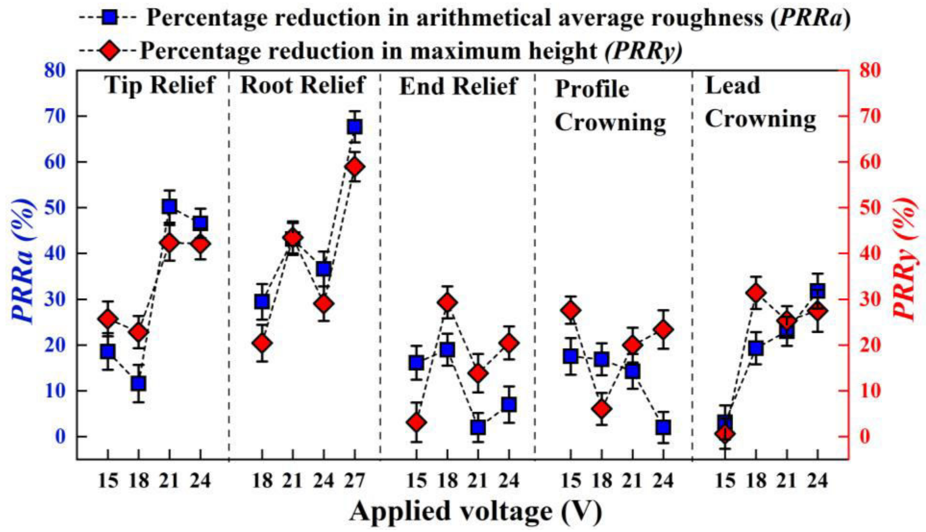

(a)

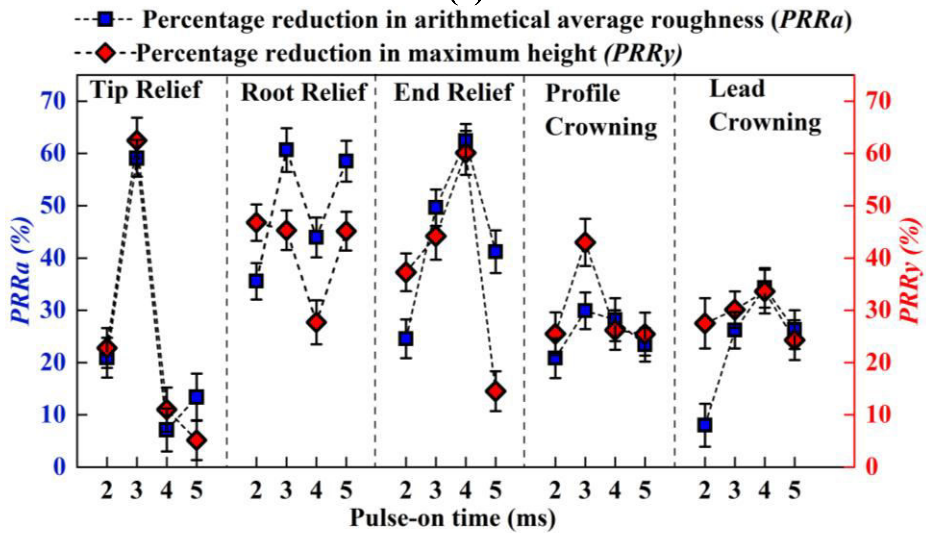

(b)

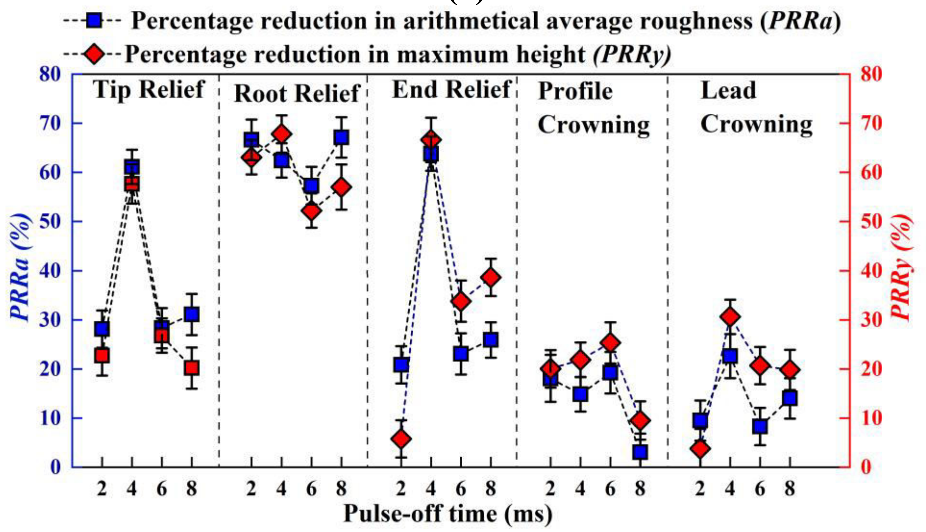

(c)

Fig. 6.13: Change in experimental values of percentage reductions in maximum height *'PRRy'* and in arithmetical average roughness *'PRRa'* of tip relieved, root relieved, end relieved, profile crowned, and lead crowned anodic workpiece gear by the PED process with (a) applied voltage, (b) pulse-on time, and (c) pulse-off time.

It can be observed from the graphs presented in Fig. 6.13a that (a) values of *'PRRa'* and *'PRRy'* vary in a zigzag manner with applied voltage for tip, root, and end relieving of the anodic workpiece gear and attain their maximum values at 21 volts, 27 volts, and 18 volts respectively, (b) values of *'PRRa'* and *'PRRy'* for profile crowning attain their maximum value at 15 volts with *'PRRa'* decreasing continuously and *'PRRy'* decreasing up to 18 volts and then increasing, and (c) values of *'PRRa'* continuously increase with the applied voltage for lead crowning and attains its maximum value at 24 volts, whereas '*PRRy*' increases and attains its maximum value at 18 volts and then decreases. These observations can be explained by the fact that an increase in applied voltage increases current density which removes more material from the roughness peaks on flank surfaces of workpiece spur gear thus smoothening them. Figure 6.13b shows values of *'PRRa'* and *'PRRy'* increase with the pulse-on time for tip and end relieving, and profile and lead crowning, attain their maximum values at 3 ms for tip relieving and profile crowning, and at 4 ms for end relieving and lead crowning, and then decrease. However, *'PRRa'* for root relieving varies in a zigzag manner with pulse-on time attaining its maximum value at 3 ms whereas *'PRRy'* attains maximum value at 2 ms pulse-on time. An increase in pulse-on time increases the time available for smoothening of the flank surfaces of workpiece spur gear but after a particular value of pulse-on time the material is removed abruptly which adversely affects flank surface finish. It can be seen from Fig. 6.13c that maximum values of *'PRRy'* and *'PRRa'* occur at 4 ms pulse-off time for tip relief, end relief, and lead crowning and at 6 ms for profile crowning of the workpiece spur gear whereas they attain their maximum value at 4 ms and 2 ms respectively for root relieving of the workpiece spur gear. Though an increase in pulse-off time decreases the time available for flank modification but it increases the time available for flushing out the removed material from flank modification zone and filling it with the fresh electrolyte for the subsequent process. Hence increase in pulse-off time increases the *'PRRa'*, and *'PRRy'* initially and after a certain value they decrease.

Figure 6.14 presents SEM images showing the surface morphology of flank surfaces of the workpiece spur gear before flank modification (Fig. 6.14a), and after its tip relieving (Fig. 6.14b), root relieving (Fig. 6.14c), end relieving (Fig. 6.14d), profile crowning (Fig. 6.14e), and lead crowning (Fig. 6.14f). It can be seen from these SEM images that the PED process completely removed the hob cutter mark and cracks from the flank surfaces of the modified workpiece gear but exposed some micro-pits present on them.

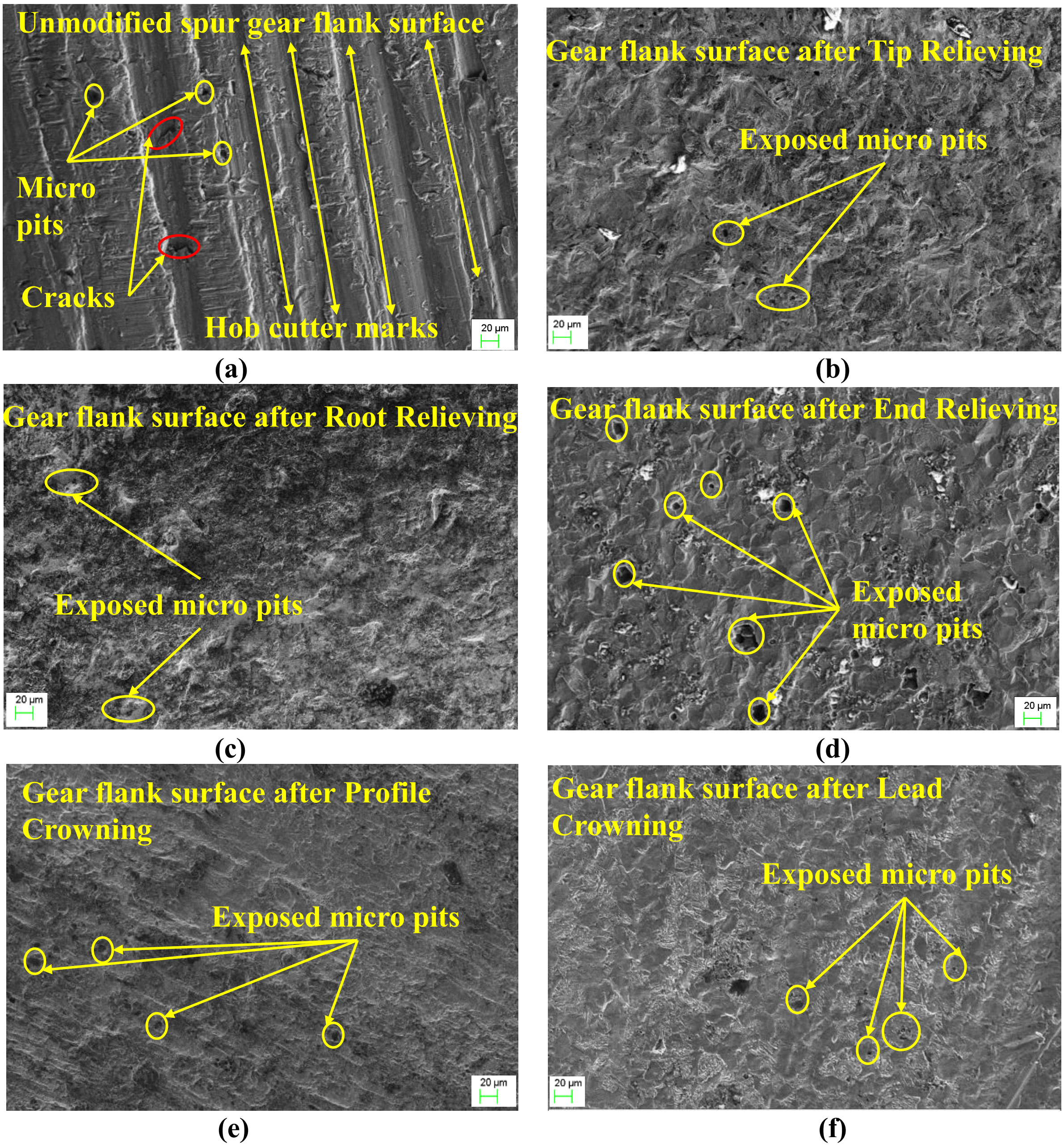

Fig. 6.14: Surface morphology of a workpiece gear flank surfaces: (a) before any flank modification, and after its (b) tip relieving (corresponding to Exp. No. 6 in Table 6.7), (c) root relieving (corresponding to Exp. No. 10 in Table 6.7), (d) end relieving (corresponding to Exp. No. 10 in Table 6.7), (e) profile crowning (corresponding to Exp. No. 6 in Table 6.7), and (f) lead crowning (corresponding to Exp. No. 7 in Table 6.7).

It can be concluded from Table 6.7, and Figs. 6.12, 6.13 and 6.14 that (i) the designed cathode gears and the apparatus through the PED process have significantly reduced arithmetical average roughness *'Ra'*, maximum height *'Ry'* of flank surfaces of workpiece spur gear and completely removed the hob cutter marks and cracks from them but exposed some micro-pits present on them, and (ii) values of pulse-on time and pulse-off time in a range from 2 to 4 ms yielded maximum values of *'PRRa'* and *'PRRy'* for all five types of flank modifications of the workpiece spur gear.

6.6 Effects of Workpiece Gear Material Hardness

Effect of hardness of workpiece gear material on its non-contact flank modification was studied by imparting tip relief, root relief, end relief, profile crowning, and lead crowning each to a case-hardened spur gear (having 58-60 HRC as Rockwell hardness on scale-C) spur gear by the PED process and comparing their results with the experimental results for unhardened workpiece spur gears (having 28-30 HRC as Rockwell hardness on scale-C). These results included the Stage-1 experimental results for tip relief (TR) and root relief (RR) [i.e., Exp. No. 3 and 7 in Table 6.1] and Stage-3a experimental results for end relief (ER), profile crowning (PC), and lead crowning (LC) [i.e., Exp. Nos. 3 and 1 in Table 6.5, and Table 6.6].

Table 6.8 presents values of volumetric MRR, average values of the imparted flank modification, arithmetical average roughness *'Ra'* and maximum height *'Ry'* before and after flank modification, corresponding *'PRRa'* and *'PRRy'* for both 5 unhardened and 5 case-hardened workpiece spur gears along with used variable and constant parameters of the PED process. The microgeometry charts of the case-hardened gears are presented in section B6 of Appendix-B.

It can be concluded from the results presented in Table 6.8 that the developed cathode gears and apparatus through PED process:

- Gave similar values of volumetric MRR for case-hardened and unhardened workpiece spur gears while imparting all 5 flank modifications implying that it is independent of workpiece gear material hardness.
- Imparted higher values of tip relief, profile crowning, and lead crowning to the case-hardened workpiece spur gears than the corresponding unhardened spur gears but imparted slightly smaller values of root relief and end relief to case-hardened workpiece spur gear than the corresponding unhardened workpiece spur gears.
- Yielded significantly higher values of percentage reductions in *Ra* and *Ry* values i.e., *'PRRa'* and *'PRRy'* for case-hardened workpiece spur gear than the corresponding unhardened workpiece spur gear during their tip relieving, end relieving, profile crowning, and lead crowning.
- Resulted in slightly smaller values of *'PRRa'* and *'PRRy'* for case-hardened workpiece spur gear than the corresponding unhardened workpiece spur gear during their root relieving.
- Overall, it implies that the developed cathode gears and apparatus gave better performance for case-hardened spur gears in terms of imparting a flank modification and in surface finish and improvement.

Table 6.8: Values of different flank modifications, volumetric MRR, and surface roughness parameters for unhardened and hardened workpiece gears for different parameters of the PED process.

Exp. No.	**Name of flank modification**	**Modification duration (minutes)**	**Applied voltage (volts)**	**Pulse-off time (ms)**	**Duty cycle**	**Volumetric MRR (mm^3/s)**		**Avg. value of imparted flank modification (μm)**		**Percentage reduction in arithmetical average roughness *'PRRa'* (%)**		**Percentage reduction in maximum height *'PRRy'* (%)**	
						Unhardened gear	Case-hardened gear	Unhardened gear	Case-hardened gear	Unhardened gear	Case-hardened gear	Unhardened gear	Case-hardened gear
1	TR	12	15	2	0.60	0.14	0.15	49.5	59.7	0.7	25.6	13.7	26.5
2	RR	20	18	4	0.43	0.08	0.09	28.6	20.4	31.1	29.8	24.4	23.4
3	ER	12	21	4	0.43	0.20	0.18	70.0	67.1	2.0	51.6	13.9	52.8
4	PC	12	15	4	0.43	0.14	0.15	9.6	17.1	17.5	37.4	3.0	43.5
5	LC	12	15	4	0.43	0.14	0.13	26.2	31.1	3.1	50.4	0.6	54.0

Common parameters for all: Electrolyte type: Aqueous solution of NaCl; Electrolyte temperature: 30°C; Electrolyte flow rate: 20 lpm; pulse-on time: 3 ms
PED process parameters for *tip, root, and end relief* of case-hardened and unhardened workpiece spur gears: Electrolyte concentration: 0.5 M (2.84% concentration by weight); Rotational speed of cathode gear: 8.5 rpm for TR, RR, and 15 rpm for ER; Reciprocating velocity of anodic workpiece gear: 0.96 mm/s.
PED process parameters for *profile and lead crowning* of case-hardened and unhardened workpiece spur gears: Electrolyte concentration: 1.0 M (5.52% concentration by weight); Rotational speed of cathode gear: 35 rpm; Reciprocating velocity of anodic workpiece gear: 0.96 mm/s for profile crowning and varying from 0.2 to 0.8 mm/s for lead crowning.

6.7 Comparative Study of Functional Performance Parameters of Flank Modified and Unmodified Workpiece Gears

Eight workpiece spur gears were imparted 4 individual flank modifications and four combinations of different flank modifications in Stage 4 experiments by the PED process using the developed cathode gears and the apparatus to study their effects on functional performance parameters, running noise and vibrations of the modified spur gears and compare them with unmodified spur gear. Table 6.9 presents average values of different flank modifications and their combinations imparted to workpiece spur gears and the following subsections describe their effects on functional performance parameters of such flank modified workpiece spur gears.

Table 6.9: Average values of different flank modifications of the workpiece gears obtained after PED process.

Workpiece gear	Individual/Combination of Flank modification(s)	Name of flank modification	Avg. value of imparted flank modification (µm)
Gear-1	Tip relief (TR)		62.2
Gear-2	End relief (ER)		102.1
Gear-3	Lead crowning (LC)		44.8
Gear-4	Profile crowning (PC)		28.8
Gear-5	Tip and root relief (TRR)	Tip relief	61.1
		Root relief	11.8
Gear-6	Tip and end relief (TER)	Tip relief	68.5
		End relief	62.1
Gear-7	Tip, root, and end relief (TRER)	Tip relief	70.9
		Root relief	39.9
		End relief	116.7
Gear-8	Profile and lead crowning (PLC)	Profile crowning	15.0
		Lead crowning	28.1

6.7.1 Analysis of Single Flank Roll Testing Results

Figure 6.15 present results of single flank roll testing graphically showing variation in transmission error (determined from Eq. 3.1) for left flank (LF) and right flank (RF) of of workpiece spur gear before imparting any flank modification i.e. unmodified or simply hobbed spur gear (Figs. 6.15a$_1$, 6.15a$_2$), tip relieved gear (Figs. 6.15b$_1$, 6.15b$_2$), end relieved gear (Figs. 6.15c$_1$, 6.15c$_2$), lead crowned gear (Figs. 6.15d$_1$, 6.15d$_2$), profile crowned gear (Figs. 6.15e$_1$, 6.15e$_2$), tip and root relieved gear (Figs. 6.15f$_1$, 6.15f$_2$), tip and end relieved gear (Figs. 6.15g$_1$, 6.15g$_2$), combined tip, root and end relieved gear (Figs. 6.15h$_1$, 6.15h$_2$), and profile and lead crowned gear (Figs. 6.15i$_1$, 6.15i$_2$) by the PED process. Computed values of functional performance parameters from single flank roll testing (i.e., total transmission error 'F_i'', tooth-to-tooth transmission error 'f_i'', and total longwave transmission error 'F_l'') are shown on these graphs and they are summarized in Table 6.10.

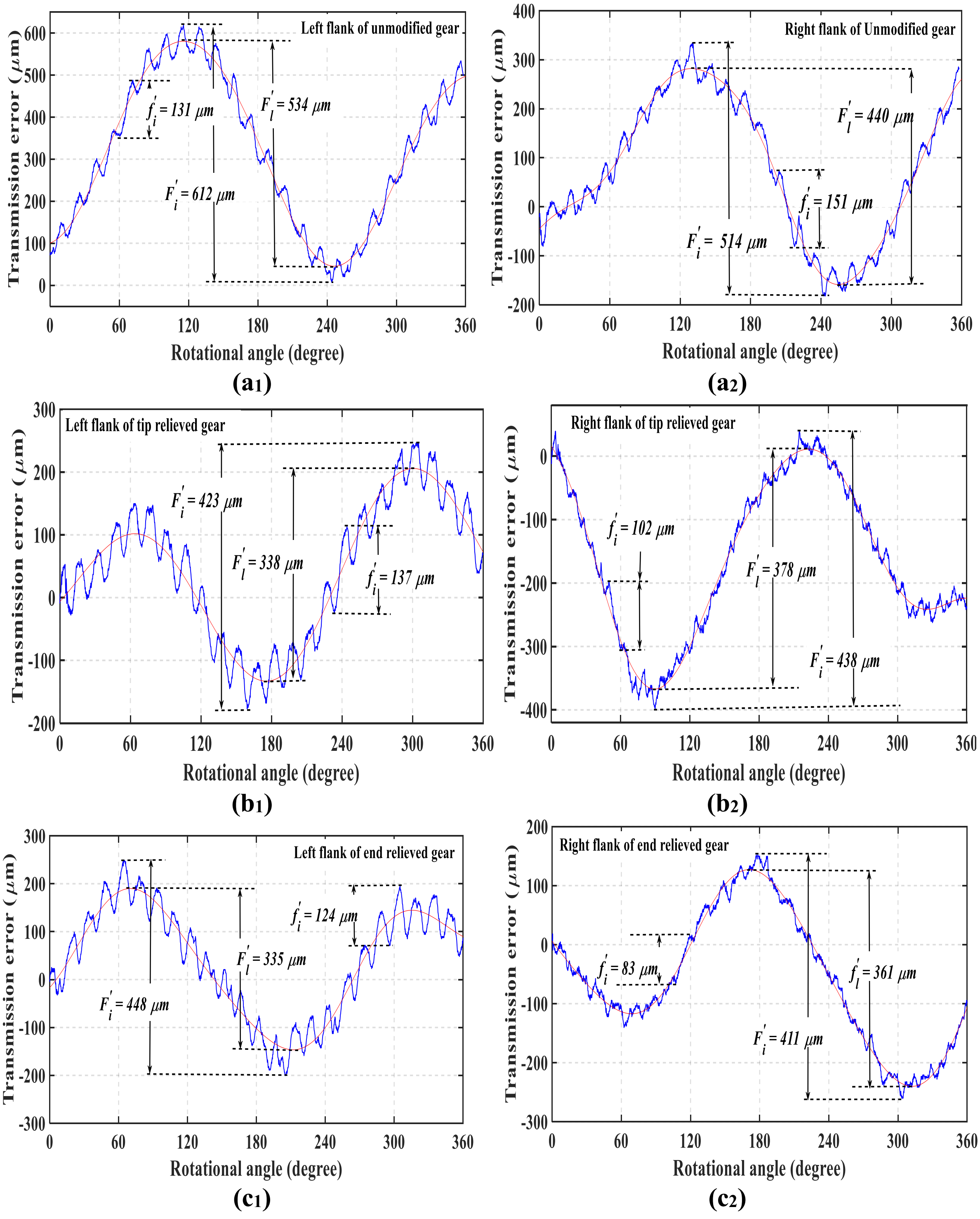

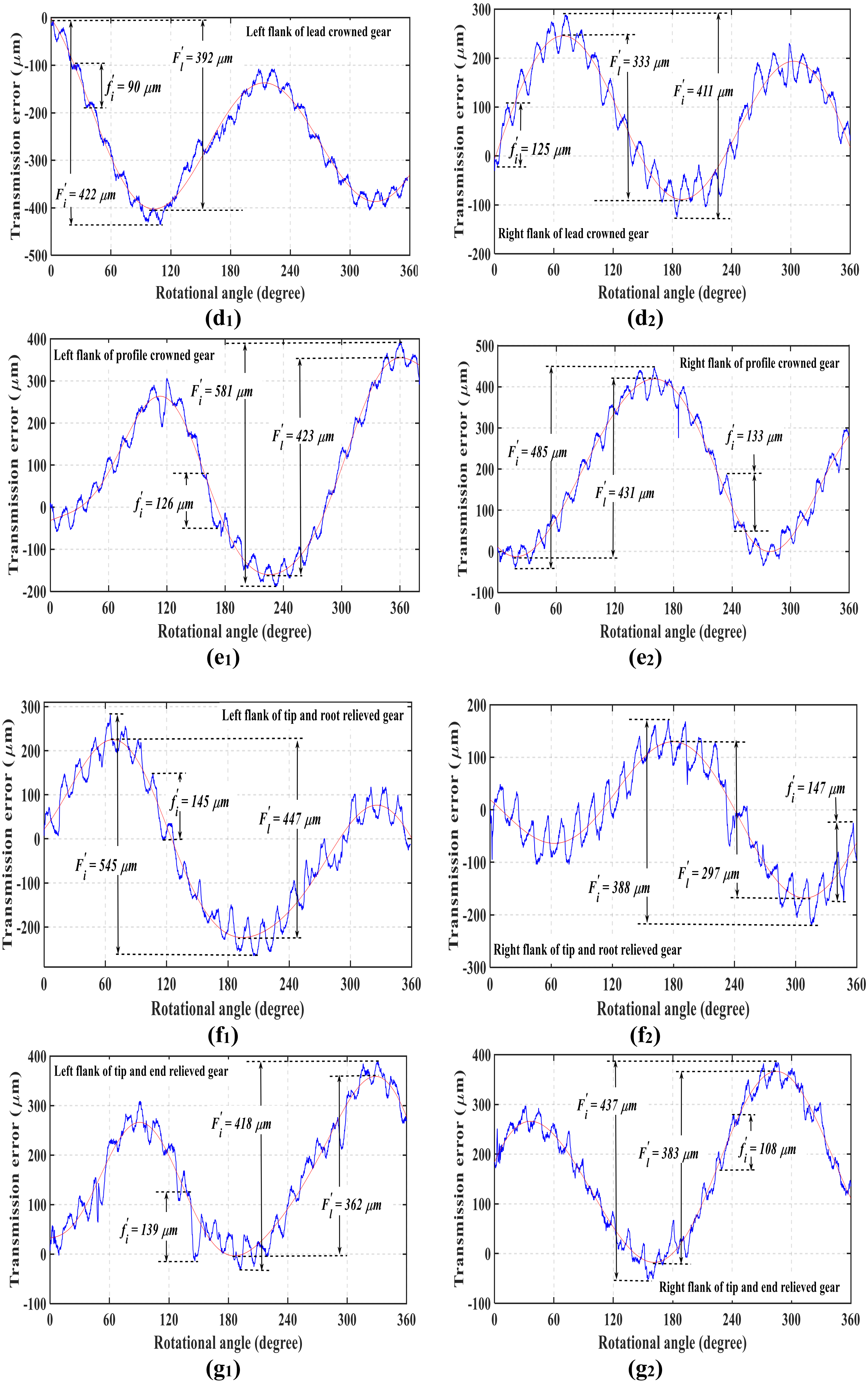
Left flank of lead crowned gear
F'l = 392 μm
f'i = 90 μm
F'i = 422 μm
(d1)
Right flank of lead crowned gear
F'l = 333 μm
F'i = 411 μm
f'i = 125 μm
(d2)
Left flank of profile crowned gear
F'i = 581 μm
F'l = 423 μm
f'i = 126 μm
(e1)
Right flank of profile crowned gear
F'i = 485 μm
F'l = 431 μm
f'i = 133 μm
(e2)
Left flank of tip and root relieved gear
f'i = 145 μm
F'l = 447 μm
F'i = 545 μm
(f1)
Right flank of tip and root relieved gear
f'i = 147 μm
F'l = 297 μm
F'i = 388 μm
(f2)
Left flank of tip and end relieved gear
F'i = 418 μm
F'l = 362 μm
f'i = 139 μm
(g1)
Right flank of tip and end relieved gear
F'i = 437 μm
F'l = 383 μm
f'i = 108 μm
(g2)
Transmission error (μm)
Rotational angle (degree)

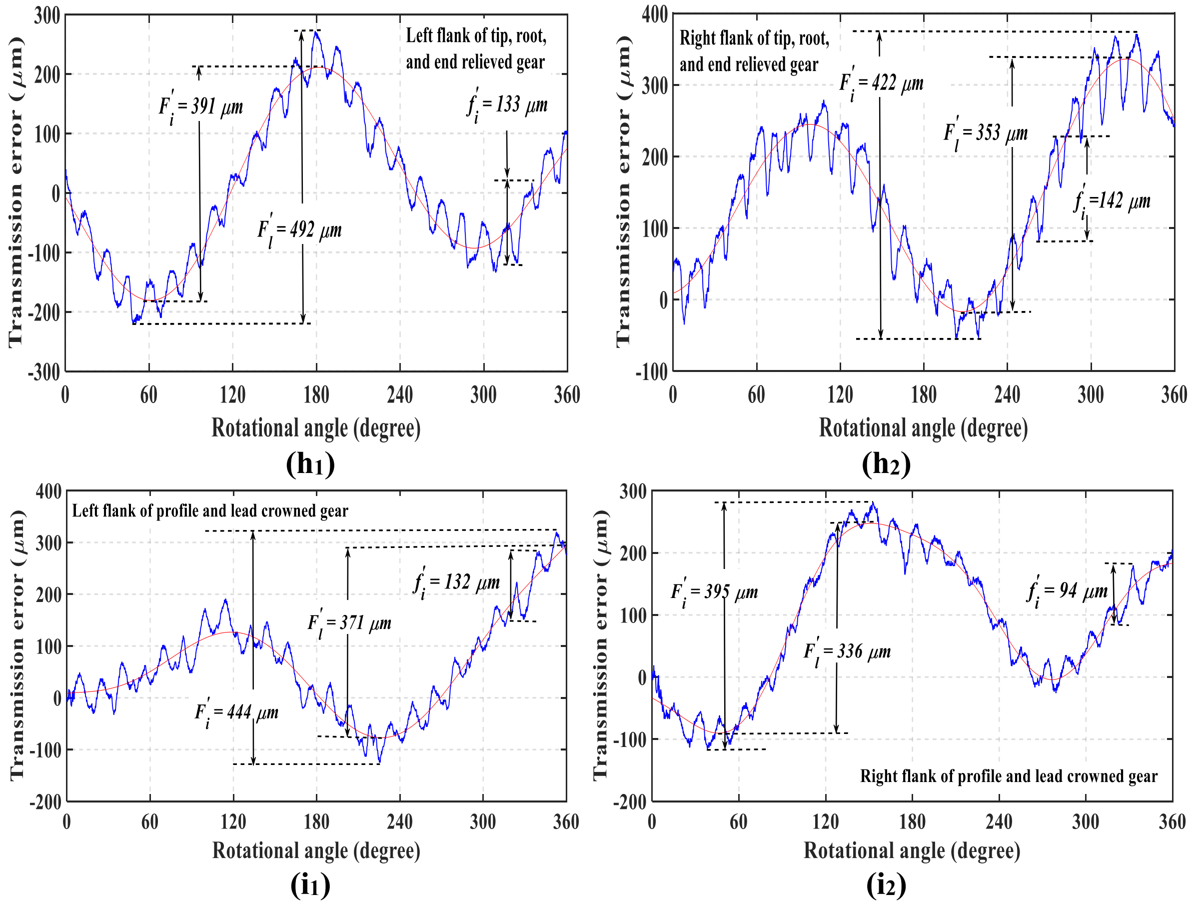

Fig. 6.15: Results of single flank roll testing for workpiece spur gear: (a_1) left flank (LF) and (a_2) right flank (RF) of workpiece spur gear before any flank modification i.e., unmodified gear, (b_1) LF and (b_2) RF of tip relieved gear, (c_1) LF and (c_2) RF of end relieved gear, (d_1) LF and (d_2) RF of lead crowned gear, (e_1) LF and (e_2) RF of profile crowned gear, (f_1) LF and (f_2) RF of tip and root relieved gear, (g_1) LF and (g_2) RF of tip and end relieved gear, (h_1) LF and (h_2) RF of tip, root, end relieved gear, and (i_1) LF and (i_2) RF of profile and lead crowned gear.

Table 6.10: Parameters obtained for unmodified and flank modified workpiece spur gears from graphs of their single flank roll testing [LF: left flank; RF: right flank].

Name of flank modification(s) imparted to workpiece gear	Total transmission error 'F_i'' (μm)			Tooth-to-tooth transmission error 'f_i'' (μm)			Longwave transmission error 'F_l'' (μm)		
	LF	RF	Avg.	LF	RF	Avg.	LF	RF	Avg.
Unmodified gear (UM)	612	514	563	131	151	141	534	440	487
Gear-1: Tip relief (TR)	423	438	431	137	102	120	338	378	358
Gear-2: End relief (ER)	448	411	430	124	*83*	*104*	335	361	*348*
Gear-3: Lead crowning (LC)	422	411	*417*	*90*	125	108	392	333	363
Gear-4: Profile crowning (PC)	*581*	*485*	*533*	126	133	130	423	431	427
Gear-5: Tip and root relief (TRR)	545	*388*	467	145	147	146	447	297	372
Gear-6: Tip and end relief (TER)	*418*	437	428	139	108	124	362	383	373
Gear-7: Tip, root, and end relief (TRER)	492	422	457	133	142	138	391	353	372
Gear-8: Profile and lead crowning (PLC)	444	395	420	132	94	113	371	336	354

Following are the observations from graphs presented in Fig. 6.15 and Table 6.10 along with and their explanations:

- Average value of total transmission error for unmodified workpiece spur gear is 563 μm. It is reduced for all the eight modified workpiece gears by different amounts. Maximum reduction (i.e., 25.9%) is for lead crowned gear (Gear-3 in Table 6.10 and Figs. 6.15d_1, 6.15d_2) whereas minimum reduction (i.e., 5.3%) is for profile crowned gear (Gear-4 in Table 6.10 and Figs. 6.15e_1, 6.15e_2).
- Average value of tooth-to-tooth transmission error for unmodified gear is 141 μm. It is reduced for all the modified workpiece gears except for tip and root relieved gear (i.e., Gear-5 in Table 6.10 and Fig. 6.15f_1, 6.15f_2) for which it is slightly increased to 146 μm. Maximum reduction (i.e., 26.2%) is for end relieved gear (Gear-2 in Table 6.10 and Figs. 6.15c_1, 6.15c_2) and is closely followed (23.4%) by lead crowned gear (Gear-3 in Table 6.10 and Figs. 6.15d_1, 6.15d_2). Minimum reduction (i.e., 2.1%) is for combined tip, root, and end relieved gear (Gear-7 in Table 6.10 and Figs. 6.15h_1, 6.15h_2).
- Average value of longwave transmission error for unmodified gear is 487 μm. It is reduced for all the 8 flank modified gears. Maximum reduction (i.e., 28.5%) is for end relieved gear (Gear-2 in Table 6.10 and Figs. 6.15c_1, 6.15c_2) and minimum reduction (i.e., 12.3%) is for profile crowned gear (Gear-4 in Table 6.10 and Figs. 6.15e_1, 6.15e_2).
- Total transmission errors, tooth-to-tooth transmission errors, and longwave transmission error are reduced by unequal amounts for left and right flanks of all 8 flank modified workpiece gears due to differences in their microgeometry deviations.
- It can be inferred summarily that average values of total transmission error, tooth-to-tooth transmission error, and longwave transmission error are reduced by imparting non-contact flank modifications to workpiece spur gears by the developed cathode gears and the apparatus via PED process though by different amounts.
- Lead crowned workpiece gear showed maximum reduction for total transmission error. It is due to minimizing contact at the ends of face width in the lead crowned gear. Lead crowning maximizes contact at the center of flank surfaces of workpiece gear tooth, minimizes effects of lead error and misalignment of the gear mounting shaft, and increases load carrying capacity, service life, and operating performance of workpiece gear.
- End relieved workpiece gear showed maximum reductions in tooth-to-tooth transmission error and longwave transmission error. It is due to minimizing contact at both the ends of face width of workpiece gear teeth during meshing with its mating gear.

It reduces the forces generated at the engagement and disengagement of workpiece gear teeth which helps in reduction of tooth-to-tooth transmission error.

- Profile crowned gear gave minimum reduction in total and longwave transmission errors because profile crowning though maximizes contact on areas adjacent to the pitch line along the profile direction but not over the entire face width. Combined tip, root, and end relieved gear showed minimum reduction for tooth-to-tooth transmission error. Since this modification is a combination of partial lead and profile crowning therefore it may be due to advantages of lead crowning being offset by profile crowning.

6.7.2 Analysis of Double Flank Roll Testing Results

Figure 6.16 presents results of double flank testing in the form of graphs showing variation in center-to-center distance between the workpiece gear and the master gear with rotation angle of workpiece gear before any flank modification i.e., unmodified condition (Fig. 6.16a), tip relieved (Fig. 6.16b), end relieved (Fig. 6.16c), lead crowned (Fig. 6.16d), profile crowned (Fig. 6.16e), tip and root relieved (Fig. 6.16f), tip and end relieved (Fig. 6.16g), combined tip, root and end relieved (Fig. 6.16h), and profile and lead crowned (Fig. 6.16i) workpiece gears by the PED process. Computed values of functional performance parameters from double flank roll testing i.e., total composite error '$F_i^{"}$', tooth-to-tooth composite error '$f_i^{"}$', and radial runout '$F_{rf}^{"}$' are shown in each of these graphs and Table 6.11 summarizes them.

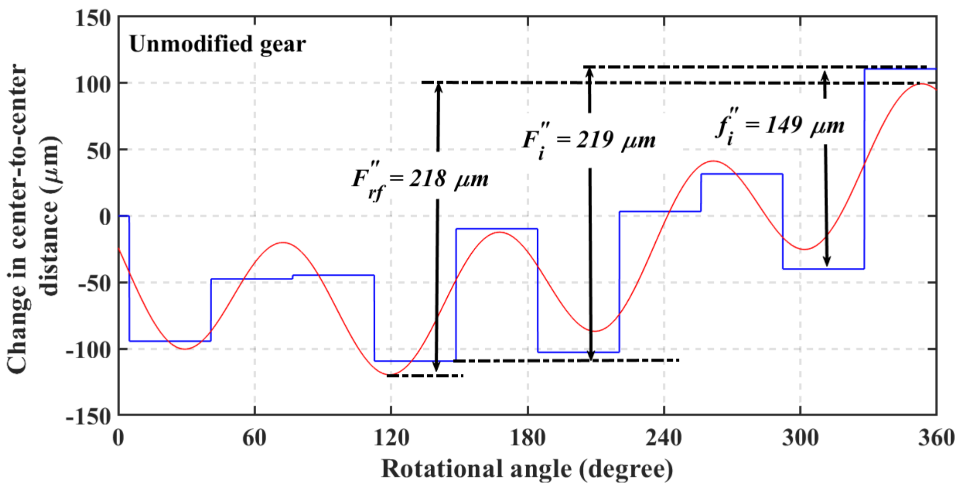

(a)

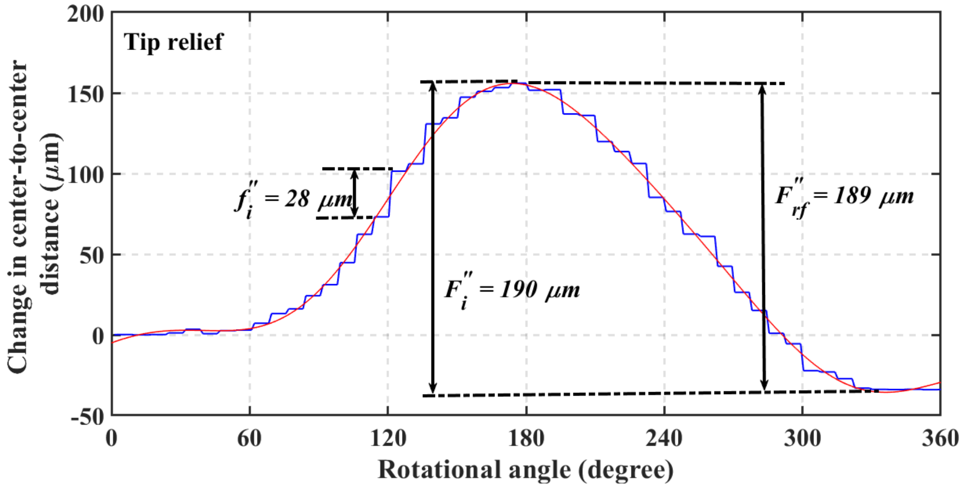

Tip relief
$f_i'' = 28\ \mu m$
$F_i'' = 190\ \mu m$
$F_{rf}'' = 189\ \mu m$
Change in center-to-center distance (μm)
Rotational angle (degree)

(b)

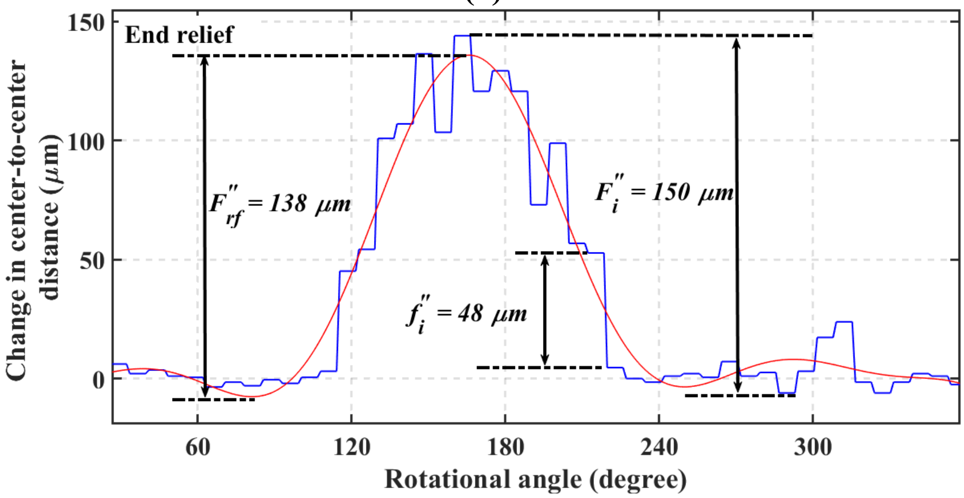

End relief
$F_{rf}'' = 138\ \mu m$
$F_i'' = 150\ \mu m$
$f_i'' = 48\ \mu m$
Change in center-to-center distance (μm)
Rotational angle (degree)

(c)

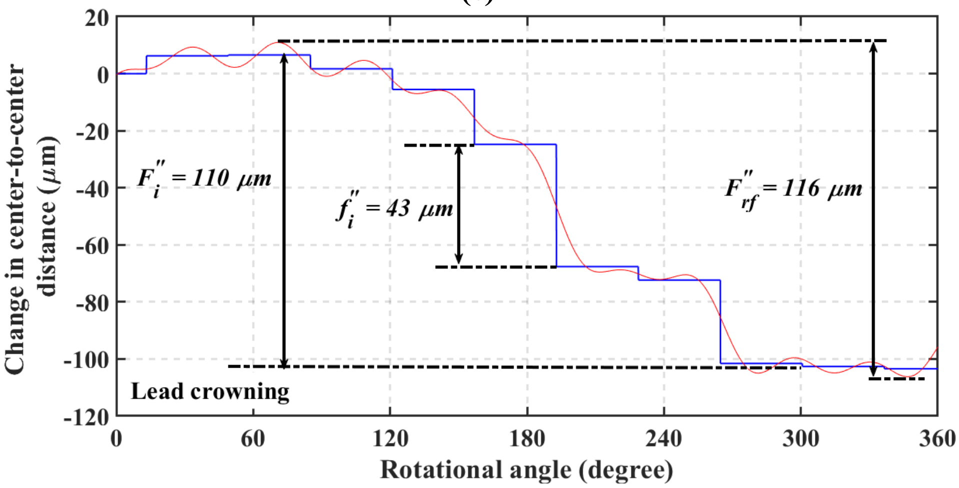

Lead crowning
$F_i'' = 110\ \mu m$
$f_i'' = 43\ \mu m$
$F_{rf}'' = 116\ \mu m$
Change in center-to-center distance (μm)
Rotational angle (degree)

(d)

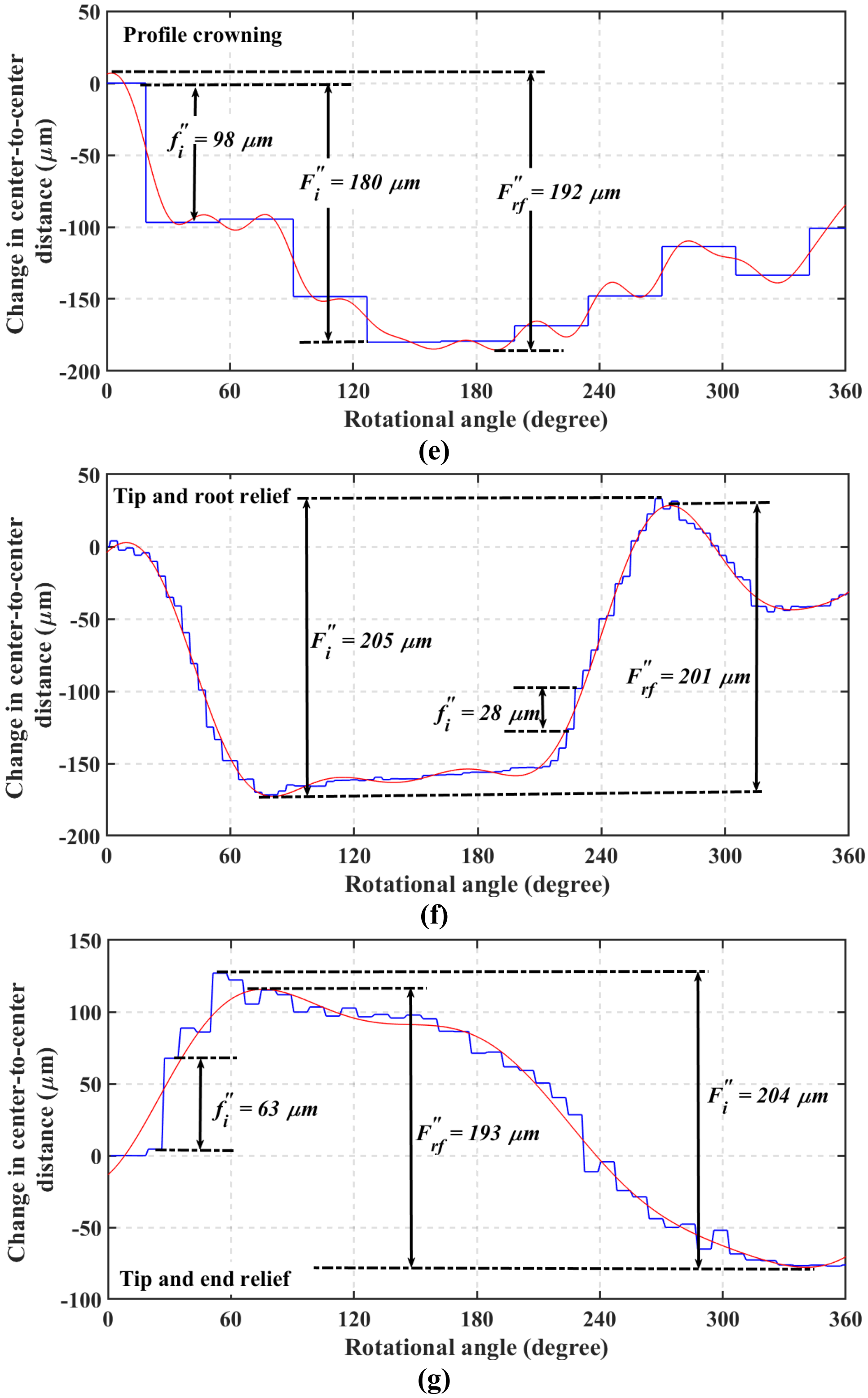

Profile crowning
$f_i'' = 98\ \mu m$
$F_i'' = 180\ \mu m$
$F_{rf}'' = 192\ \mu m$
Change in center-to-center distance (μm)
Rotational angle (degree)
(e)
Tip and root relief
$F_i'' = 205\ \mu m$
$f_i'' = 28\ \mu m$
$F_{rf}'' = 201\ \mu m$
Change in center-to-center distance (μm)
Rotational angle (degree)
(f)
$f_i'' = 63\ \mu m$
$F_{rf}'' = 193\ \mu m$
$F_i'' = 204\ \mu m$
Tip and end relief
Change in center-to-center distance (μm)
Rotational angle (degree)
(g)

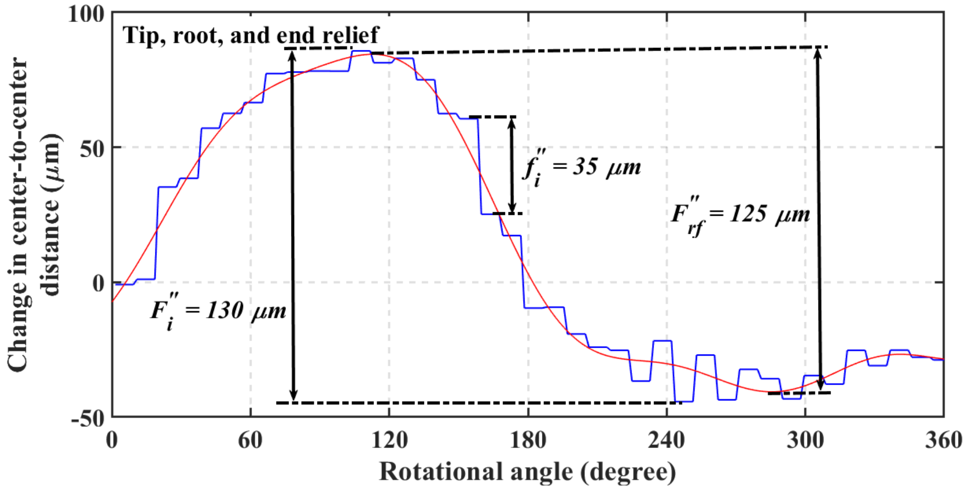

(h)

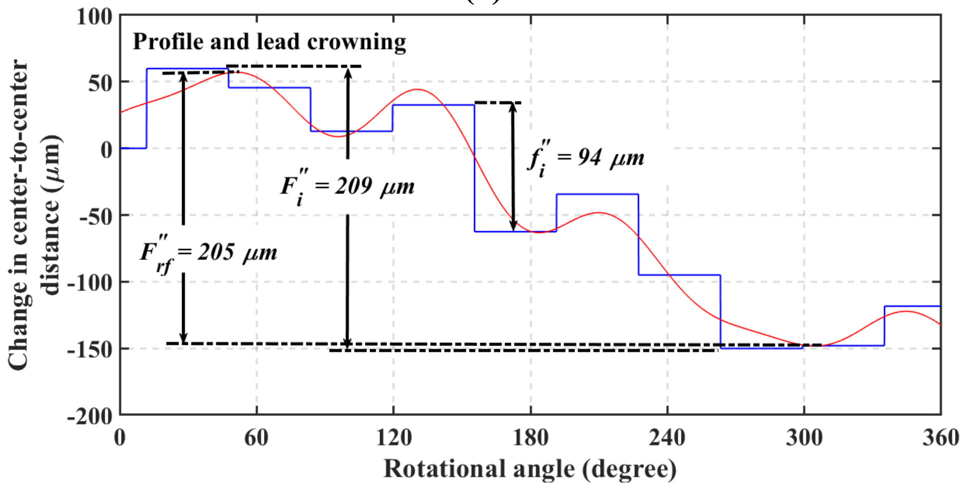

(i)

Fig. 6.16: Results of double flank roll testing of workpiece spur gear: (a) before any flank modification, and after imparting it: (b) tip relief, (c) end relief, (d) lead crowning, (e) profile crowning, (f) tip and root relief, (g) tip and end relief, and (h) tip, root, and end relief, and (i) profile and lead crowning.

Table 6.11: Parameters obtained for unmodified and flank modified workpiece spur gears from graphs of their double flank roll testing.

Name of flank modification(s) imparted to workpiece gear	**Total composite error 'F''_i' (μm)**	**Tooth-to-tooth composite error 'f''_i' (μm)**	**Radial runout 'F''_{rf}' (μm)**
Unmodified gear (UM)	219	149	218
Gear-1: Tip relief (TR)	190	*28*	189
Gear-2: End relief (ER)	150	48	138
Gear-3: Lead crowning (LC)	*110*	43	*116*
Gear-4: Profile crowning (PC)	180	98	192
Gear-5: Tip and root relief (TRR)	205	*28*	201
Gear-6: Tip and end relief (TER)	204	63	193
Gear-7: Tip, root, and end relief (TRER)	130	35	125
Gear-8: Profile and lead crowning (PLC)	209	94	205

Following are observations from graphs presented in Fig. 6.16 and Table 6.11 along with their explanations:

- Total composite error for workpiece gear before imparting any flank modification or in unmodified condition is 219 μm. It is reduced for all the 8 workpiece gears modified by the developed cathode gears and the apparatus via the PED process. Maximum reduction (49.8%) is for lead crowned workpiece gear (Gear-3 in Table 6.11 and Fig. 6.16d). Minimum reduction (4.6%) for profile and lead crowned workpiece gear (Gear-8 in Table 6.11 and Fig. 6.16i).
- Unmodified workpiece gear has 149 μm as tooth-to-tooth composite error. Non-contact flank modifications by the developed cathode gears and the apparatus through the PED process reduced it for all the 8 modified workpiece gears. Tip relieved (Gear-1 in Table 6.11 and Fig. 6.16b) and tip and root relieved (Gear-5 in Table 6.11 and Fig. 6.16f) workpiece gears showed maximum reduction (81.2%) in it whereas profile crowned gear (Gear-4 in Table 6.11 and Fig. 6.16e) shows minimum reduction (34.2%) in it.
- Radial runout of unmodified workpiece gear is 218 μm. It is reduced for all 8 modified workpiece gears. Maximum reduction (i.e., 46.8%) is for lead crowned gear (Gear-3 in Table 6.11 and Fig. 6.16d) and minimum reduction (i.e., 5.9%) is shown by profile and lead crowned gear (Gear-8 in Table 6.11 and Fig. 6.16i).
- Imparting different non-contact flank modifications to the workpiece gears by the developed cathode gears and the apparatus via PED process reduced total composite errors, tooth-to-tooth composite error, and radial runout.
- Lead crowned workpiece gear gave maximum reduction in total composite error and radial runout. It is due to reduction in variation in center-to-center distance enabled by minimization of contact area along the lead direction by lead crowning which mitigates the effects of lead error during motion of a gear pair.
- Tip relieved, and tip and root relieved gear showed maximum reduction in tooth-to-tooth composite error. It is due to ease in loading at start and end of gear tooth meshing which smoothens engagement of the mating gears thus reducing variations in their center-to-center distance and consequently tooth-to-tooth composite error.
- Combined profile and lead crowned gear gave minimum reduction in total composite error and radial runout and profile crowned gear gave minimum reduction in tooth-to-tooth composite error. It is due to undesired effects of profile crowning compensating the advantages of lead crowning.

6.7.3 Analysis of Running Noise and Vibrations

Sixteen full factorial experiments were performed each for the unmodified workpiece gear (i.e., before imparting any flank modification) and the eight modified workpiece gears by varying speed of test gear (i.e., workpiece spur gear) at 300; 600; 900; and 1200 rpm and applying a load of 5; 10; 15; and 20 N i.e., total 144 experiments were performed to measure their running noise in terms of sound pressure by a microphone and vibrations in terms of acceleration through a tri-axial accelerometer. Table 6.12 presents values of sound pressure levels (SPL) for the unmodified workpiece gear (i.e., before imparting any flank modification) and different modified workpiece gears by the PED process and differences in SPL between each modified and unmodified workpiece gear for 300; 600; 900; and 1200 rpm speed of the test (i.e., corresponding workpiece) gear. Table 6.13 presents root mean square (RMS) values of vibrations for the unmodified workpiece gear and different modified workpiece gears by the PED process and differences in RMS value between each modified and unmodified workpiece gear for 300; 600; 900; and 1200 rpm speed of the test gear and Table 6.14 lists these values at gear mesh frequency (GMF). Time domain signal of vibrations were transformed to frequency domain signals through Fast Fourier transform (FFT) to obtain the value of vibrations at gear mesh frequency (GMF). GMF is the characteristic frequency of a gear pair and it is the rate at which their teeth mesh during power and/or motion transmission by a gear pair. It is calculated by multiplying the number of teeth in a gear by its rotational frequency i.e., rotations per second. Figure 6.17 shows frequency domain signals of vibrations of the unmodified and flank modified workpiece gears at 1200 rpm test gear speed and 20 N applied load. Comparison of value of vibrations of unmodified workpiece gear (which is 0.182 m/s^2 from Fig. 6.17a) with those of different flank modified workpiece gears (from Fig. 6.17b to 6.17i) at their GMF (≈ 320 Hz for 1200 rpm) reveals that the end relieved workpiece gear has minimum value of vibrations. Figure 6.18 graphically presents variation in SPL with applied load for the unmodified gear and 8 modified workpiece gears for test gear speed of 300 rpm (Fig. 6.18a); 600 rpm (Fig. 6.18b); 900 rpm (Fig. 6.18c); and 1200 rpm (Fig. 6.18d). Figures 6.19 and 6.20 depict variation of RMS values of vibrations and their values at GMF respectively with applied load for unmodified workpiece gear and 8 flank modified gears for test gear speed of 300 rpm (Fig. 6.19a, Fig. 6.20a); 600 rpm (Fig. 6.19b, Fig. 6.20b); 900 rpm (Fig. 6.19c, Fig. 6.20c); and 1200 rpm (Fig. 6.19d, Fig. 6.20d).

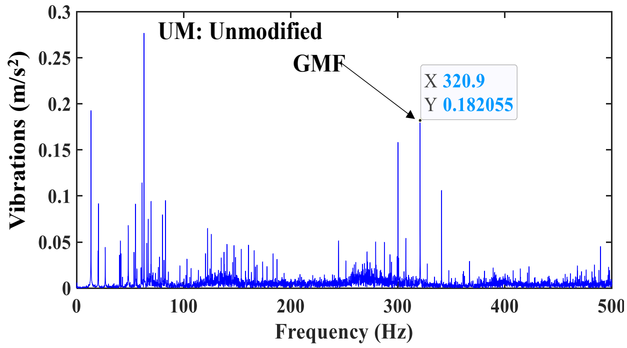
UM: Unmodified
GMF
X 320.9
Y 0.182055
Vibrations (m/s^2)
Frequency (Hz)
0
0.05
0.1
0.15
0.2
0.25
0.3
0
100
200
300
400
500

(a)

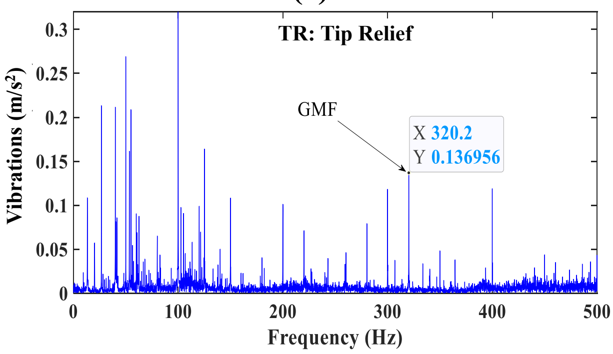
TR: Tip Relief
GMF
X 320.2
Y 0.136956
Vibrations (m/s^2)
Frequency (Hz)
0
0.05
0.1
0.15
0.2
0.25
0.3
0
100
200
300
400
500

(b)

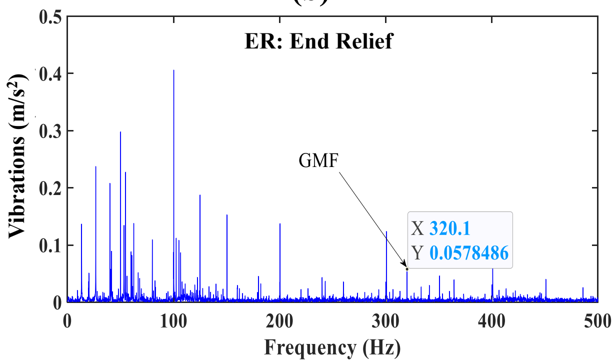
ER: End Relief
GMF
X 320.1
Y 0.0578486
Vibrations (m/s^2)
Frequency (Hz)
0
0.1
0.2
0.3
0.4
0.5
0
100
200
300
400
500

(c)

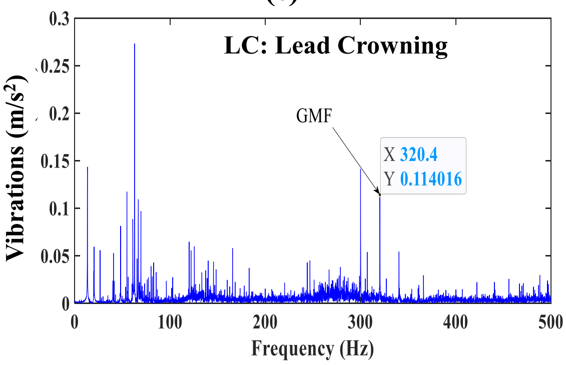
LC: Lead Crowning
GMF
X 320.4
Y 0.114016
Vibrations (m/s^2)
Frequency (Hz)
0
0.05
0.1
0.15
0.2
0.25
0.3
0
100
200
300
400
500

(d)

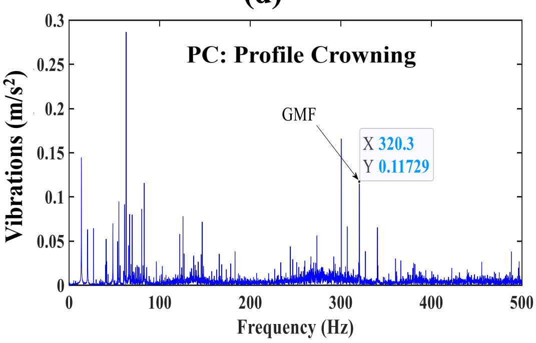
PC: Profile Crowning
GMF
X 320.3
Y 0.11729
Vibrations (m/s^2)
Frequency (Hz)
0
0.05
0.1
0.15
0.2
0.25
0.3
0
100
200
300
400
500

(e)

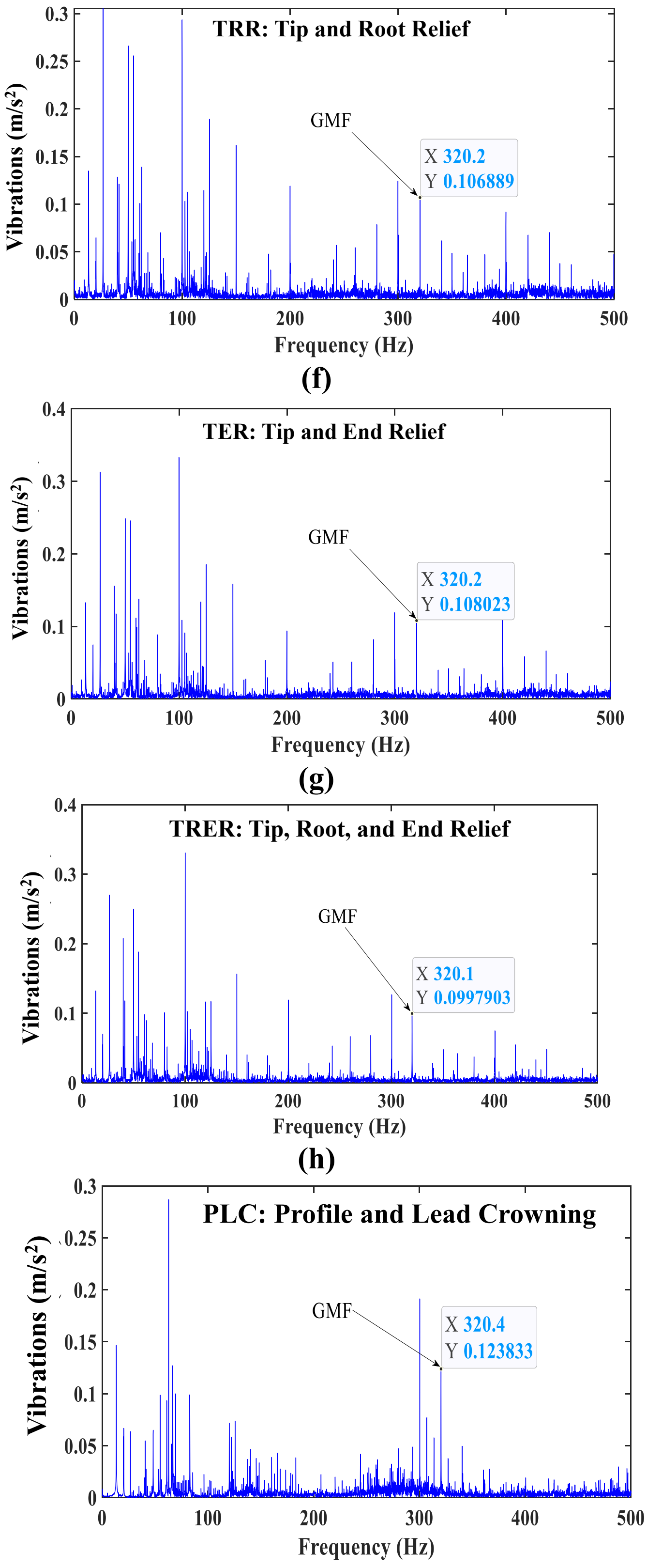

Fig. 6.17: Example of time domain signal in frequency domain using FFT for obtaining the value of vibration at gear mesh frequency (GMF) at 1200 rpm and 20 N applied load for workpiece gear with: (a) unmodified, (b) tip relief, (c) end relief, (d) lead crowning, (e) profile crowning, (f) tip and root relief, (g) tip and end relief, and (h) tip, root, and end relief, and (i) profile and lead crowning.

Table 6.12: Sound pressure level for unmodified and different modified workpiece gears for different rotational speed and applied load.

Exp. No.	Rotational speed (rpm)	Applied load (N)	Sound pressure level (dBA)									Difference in sound pressure levels of unmodified and flank modified workpiece gear (dBA)							
			UM	Gear-1 TR	Gear-2 ER	Gear-3 LC	Gear-4 PC	Gear-5 TRR	Gear-6 TER	Gear-7 TRER	Gear-8 PLC	ΔN_{G1}	ΔN_{G2}	ΔN_{G3}	ΔN_{G4}	ΔN_{G5}	ΔN_{G6}	ΔN_{G7}	ΔN_{G8}
1	300	5	71.1	69.6	69.0	69.6	70.6	70.8	70.4	69.1	71.6	1.5	2.1	1.5	0.5	0.3	0.7	2.0	-0.5
2		10	70.7	70.5	69.1	69.9	71.2	70.8	70.5	69.5	70.6	0.2	1.6	0.8	-0.5	-0.1	0.2	1.2	0.1
3		15	71.1	70.1	69.2	69.3	70.2	71.0	70.4	68.8	70.8	1.0	1.9	1.8	0.9	0.1	0.7	2.3	0.3
4		20	70.1	70.4	69.4	70.5	72.0	71.2	70.6	690	71.4	-0.3	0.7	-0.4	-1.9	-1.1	-0.5	1.1	-1.3
5	600	5	77.3	76.4	75.2	76.7	77.5	76.3	76.2	74.9	77.5	0.9	2.1	0.6	-0.2	1.0	1.1	2.4	-0.2
6		10	77.0	76.9	75.6	76.8	78.0	76.7	76.0	75.7	77.7	0.1	1.4	0.2	-1.0	0.3	1.0	1.3	-0.7
7		15	77.3	77.0	76.2	76.7	77.3	76.4	76.2	75.2	77.8	0.3	1.1	0.6	0.0	0.9	1.1	2.1	-0.5
8		20	77.4	77.4	76.2	76.6	77.4	76.3	76.0	75.8	77.1	0.0	1.2	0.8	0.0	1.1	1.4	1.6	0.3
9	900	5	81.8	79.8	78.0	80.4	80.6	80.4	80.1	78.5	80.8	2.0	3.8	1.4	1.2	1.4	1.7	3.3	1.0
10		10	81.9	80.5	78.1	80.6	79.9	80.2	80.3	77.9	81.0	1.4	3.8	1.3	2.0	1.7	1.6	4.0	0.9
11		15	81.5	81.2	78.7	81.1	80.7	81.0	81.1	79.3	80.5	0.3	2.8	0.4	0.8	0.5	0.4	2.2	1.0
12		20	82.1	81.6	78.4	81.4	80.9	80.9	81.2	79.4	80.9	0.5	3.7	0.7	1.2	1.2	0.9	2.7	1.2
13	1200	5	84.4	81.6	79.4	82.6	83.0	81.6	81.4	79.9	83.3	2.8	5.0	1.8	1.4	2.8	3.0	4.5	1.1
14		10	84.6	82.3	79.8	83.0	83.0	81.5	81.9	80.4	83.6	2.3	4.8	1.6	1.6	3.1	2.7	4.2	1.0
15		15	85.0	82.6	80.6	82.8	83.5	82.5	81.8	80.8	84.0	2.4	4.4	2.2	1.5	2.5	3.2	4.2	1.0
16		20	85.1	83.4	81.0	83.5	83.8	82.7	82.4	81.4	83.5	1.7	4.1	1.6	1.3	2.4	2.7	3.7	1.6

Table 6.13: RMS values of vibrations for the unmodified and different modified workpiece gears for different rotational speed and applied load.

Exp. No.	Rotational speed (rpm)	Applied load (N)	RMS values of vibrations (m/s^2)									Difference in RMS values of vibrations of unmodified and flank modified workpiece gear							
			UM	Gear-1 TR	Gear-2 ER	Gear-3 LC	Gear-4 PC	Gear-5 TRR	Gear-6 TER	Gear-7 TRER	Gear-8 PLC	ΔV_{G1}	ΔV_{G2}	ΔV_{G3}	ΔV_{G4}	ΔV_{G5}	ΔV_{G6}	ΔV_{G7}	ΔV_{G8}
1	300	5	3.53	2.86	2.91	3.13	3.18	2.93	2.92	2.86	3.21	0.67	0.62	0.40	0.35	0.60	0.61	0.67	0.32
2		10	3.53	2.84	2.93	3.13	3.18	2.93	2.93	2.85	3.19	0.69	0.60	0.40	0.35	0.60	0.60	0.68	0.34
3		15	3.52	2.84	2.91	3.09	3.14	2.97	2.95	2.87	3.20	0.68	0.61	0.43	0.38	0.55	0.57	0.65	0.32
4		20	3.50	2.84	2.91	3.11	3.17	2.96	2.97	2.86	3.20	0.66	0.59	0.39	0.33	0.54	0.53	0.64	0.30
5	600	5	4.23	3.12	3.01	3.64	3.93	3.42	3.45	2.89	3.95	1.11	1.22	0.59	0.30	0.81	0.78	1.34	0.28
6		10	4.27	3.17	3.09	3.64	3.88	3.49	3.49	2.95	4.00	1.10	1.18	0.63	0.39	0.78	0.78	1.32	0.27
7		15	4.52	3.16	3.17	3.69	3.94	3.62	3.62	2.98	3.92	1.36	1.35	0.83	0.58	0.90	0.90	1.54	0.60
8		20	4.64	3.26	3.23	3.62	3.90	3.71	3.72	3.03	3.98	1.38	1.41	1.02	0.74	0.93	0.92	1.61	0.66
9	900	5	6.22	4.39	3.45	5.83	4.94	4.18	4.20	3.84	5.38	1.83	2.77	0.39	1.28	2.04	2.02	2.38	0.84
10		10	6.11	4.55	3.54	5.79	4.83	4.33	4.40	3.93	5.39	1.56	2.57	0.32	1.28	1.78	1.71	2.18	0.72
11		15	6.28	4.84	3.66	5.78	4.76	4.65	4.55	4.00	5.44	1.44	2.62	0.50	1.52	1.63	1.73	2.28	0.84
12		20	5.99	5.01	3.74	5.50	4.71	4.82	4.79	4.01	5.44	0.98	2.25	0.49	1.28	1.17	1.20	1.98	0.55
13	1200	5	7.48	5.20	4.09	6.77	6.65	5.01	4.93	4.65	6.30	2.28	3.39	0.71	0.83	2.47	2.55	2.83	1.18
14		10	7.60	5.54	4.23	7.03	6.89	5.23	5.19	4.80	6.54	2.06	3.37	0.57	0.71	2.37	2.41	2.80	1.06
15		15	8.03	5.81	4.39	7.12	7.00	5.41	5.41	4.95	6.69	2.22	3.64	0.91	1.03	2.62	2.62	3.08	1.34
16		20	8.17	5.93	4.40	7.34	7.11	5.68	5.72	5.20	6.99	2.24	3.77	0.83	1.06	2.49	2.45	2.97	1.18

Table 6.14: Values of vibrations for unmodified and different modified workpiece gears at gear mesh frequency (GMF) for different rotational speed and applied load.

Exp. No.	Rotational speed (rpm)	Applied load (N)	Value of vibrations at gear mesh frequency (GMF) (m/s^2)									Difference in values of vibrations at GMF of unmodified and flank modified workpiece gear (m/s^2)							
			UM	**Gear 1 TR**	**Gear 2 ER**	**Gear 3 LC**	**Gear 4 PC**	**Gear 5 TRR**	**Gear 6 TER**	**Gear 7 TRER**	**Gear 8 PLC**	ΔV_{G1}	ΔV_{G2}	ΔV_{G3}	ΔV_{G4}	ΔV_{G5}	ΔV_{G6}	ΔV_{G7}	ΔV_{G8}
1	300	5	0.027	0.019	0.010	0.013	0.020	0.014	0.013	0.021	0.021	0.008	0.017	0.014	0.007	0.013	0.014	0.006	0.006
2		10	0.040	0.018	0.011	0.015	0.017	0.019	0.024	0.014	0.022	0.022	0.029	0.025	0.023	0.021	0.016	0.026	0.018
3		15	0.036	0.024	0.015	0.020	0.017	0.011	0.027	0.024	0.024	0.012	0.021	0.016	0.019	0.025	0.009	0.012	0.012
4		20	0.034	0.021	0.018	0.021	0.025	0.016	0.016	0.025	0.024	0.013	0.016	0.013	0.009	0.018	0.018	0.009	0.010
5	600	5	0.023	0.020	0.016	0.028	0.026	0.011	0.017	0.022	0.012	0.003	0.007	-0.005	-0.003	0.012	0.006	0.001	0.011
6		10	0.023	0.018	0.019	0.025	0.027	0.016	0.014	0.011	0.013	0.005	0.004	-0.002	-0.004	0.007	0.009	0.012	0.010
7		15	0.020	0.027	0.020	0.025	0.021	0.021	0.023	0.014	0.019	-0.007	0.000	-0.005	-0.001	-0.001	-0.003	0.006	0.001
8		20	0.024	0.019	0.019	0.036	0.027	0.022	0.022	0.020	0.016	0.005	0.005	-0.012	-0.003	0.002	0.002	0.004	0.008
9	900	5	0.041	0.060	0.038	0.051	0.042	0.069	0.063	0.053	0.054	-0.019	0.003	-0.010	-0.001	-0.028	-0.022	-0.012	-0.013
10		10	0.053	0.051	0.046	0.043	0.042	0.074	0.069	0.059	0.049	0.002	0.007	0.010	0.011	-0.021	-0.016	-0.006	0.004
11		15	0.042	0.064	0.043	0.039	0.036	0.087	0.082	0.086	0.054	-0.022	-0.001	0.003	0.006	-0.045	-0.040	-0.044	-0.012
12		20	0.044	0.090	0.085	0.037	0.039	0.100	0.094	0.100	0.043	-0.046	-0.041	0.007	0.005	-0.056	-0.050	-0.056	0.001
13	1200	5	0.157	0.080	0.034	0.102	0.107	0.059	0.071	0.087	0.095	*0.077*	0.123	0.055	0.050	*0.098*	*0.086*	0.070	0.062
14		10	0.162	0.098	0.047	0.126	0.112	0.084	0.083	0.094	0.098	0.064	0.115	0.036	0.050	0.078	0.079	0.068	*0.064*
15		15	0.152	0.147	0.052	0.105	0.115	0.077	0.087	0.085	0.105	0.005	0.100	0.047	0.037	0.075	0.065	0.067	0.047
16		20	0.182	0.137	0.058	0.114	0.117	0.107	0.108	0.100	0.124	0.045	*0.124*	*0.068*	*0.065*	0.075	0.074	*0.082*	0.058

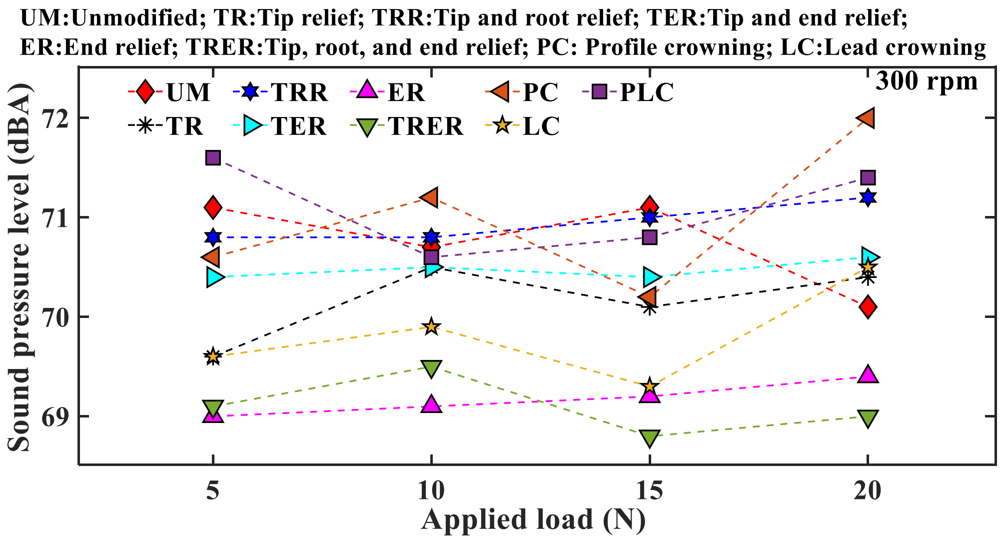
UM:Unmodified; TR:Tip relief; TRR:Tip and root relief; TER:Tip and end relief;
ER:End relief; TRER:Tip, root, and end relief; PC: Profile crowning; LC:Lead crowning
300 rpm
UM
TRR
ER
PC
PLC
TR
TER
TRER
LC
Sound pressure level (dBA)
72
71
70
69
5
10
15
20
Applied load (N)

(a)

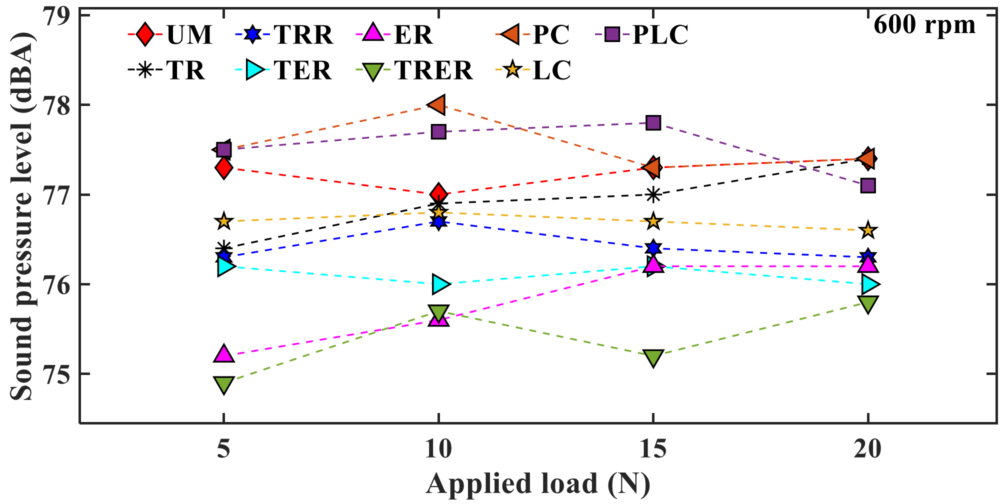
600 rpm
UM
TRR
ER
PC
PLC
TR
TER
TRER
LC
Sound pressure level (dBA)
79
78
77
76
75
5
10
15
20
Applied load (N)

(b)

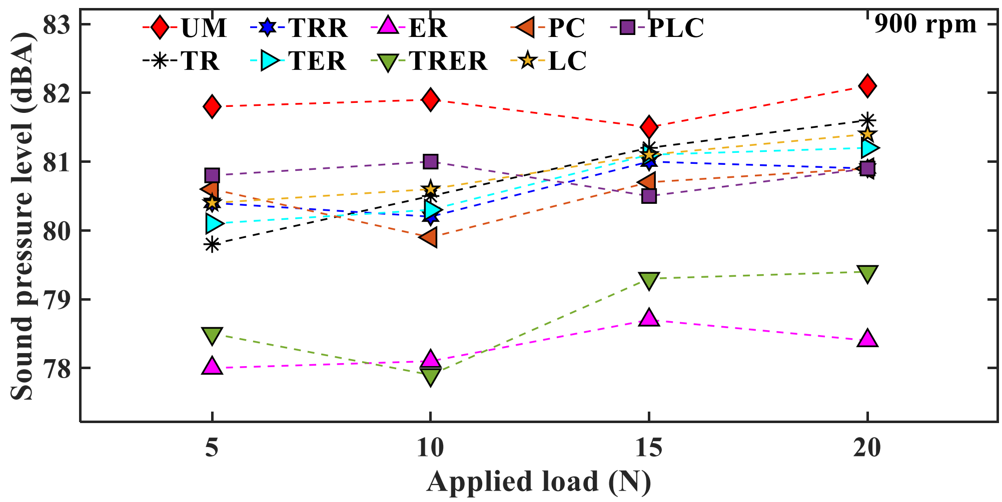
900 rpm
UM
TRR
ER
PC
PLC
TR
TER
TRER
LC
Sound pressure level (dBA)
83
82
81
80
79
78
5
10
15
20
Applied load (N)

(c)

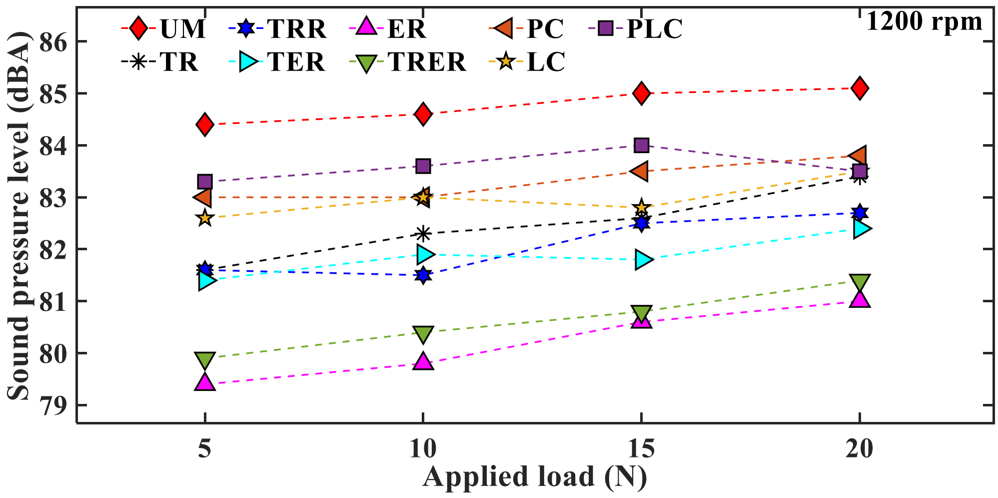

(d)

Fig. 6.18: Variation in sound pressure levels of unmodified and 8 modified workpiece gears with applied load for test gear speed of (a) 300 rpm, (b) 600 rpm, (c) 900 rpm, and (d) 1200 rpm.

UM:Unmodified; TR:Tip relief; TRR:Tip and root relief; TER:Tip and end relief; ER:End relief; TRER:Tip, root, and end relief; PC: Profile crowning; LC:Lead crowning

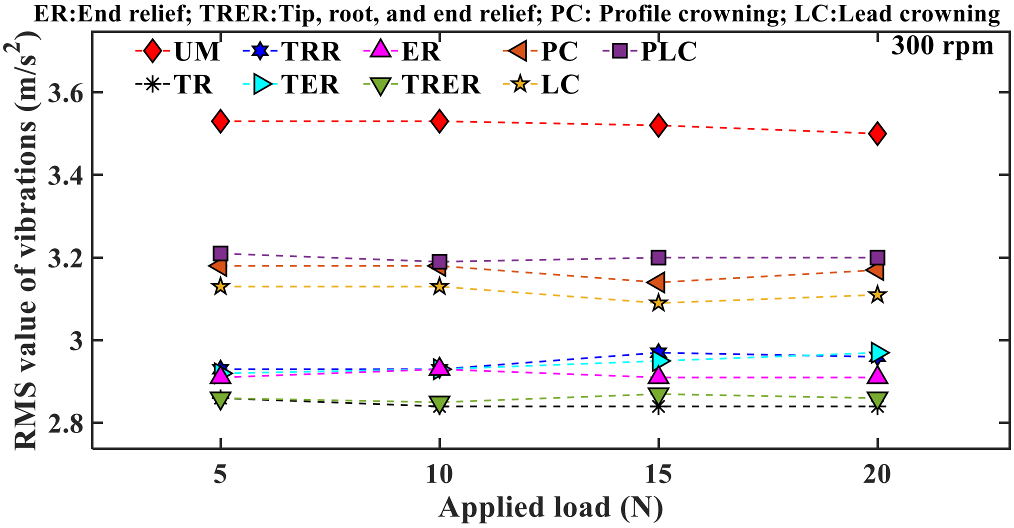

(a)

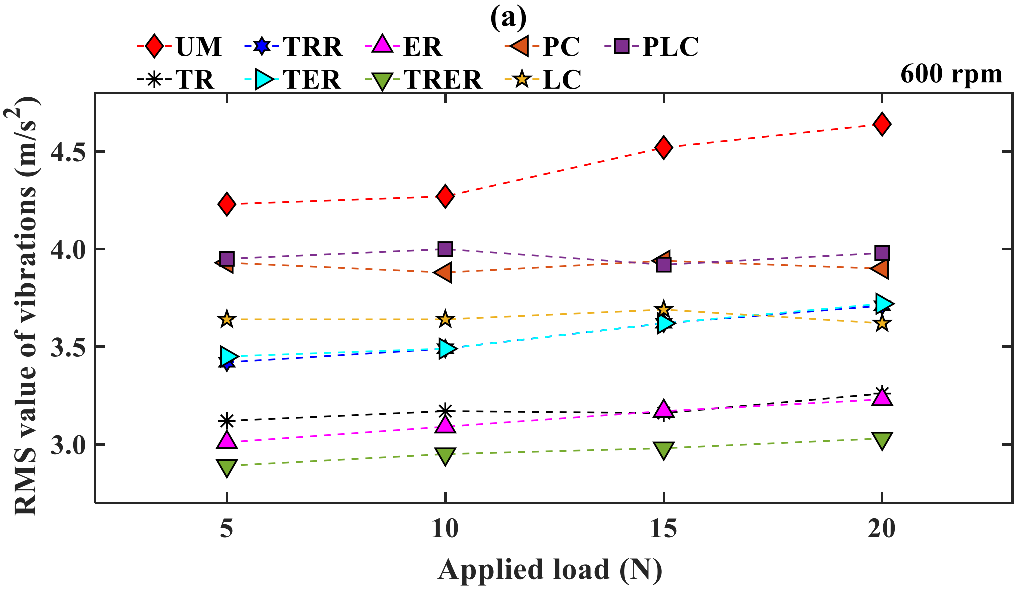

(b)

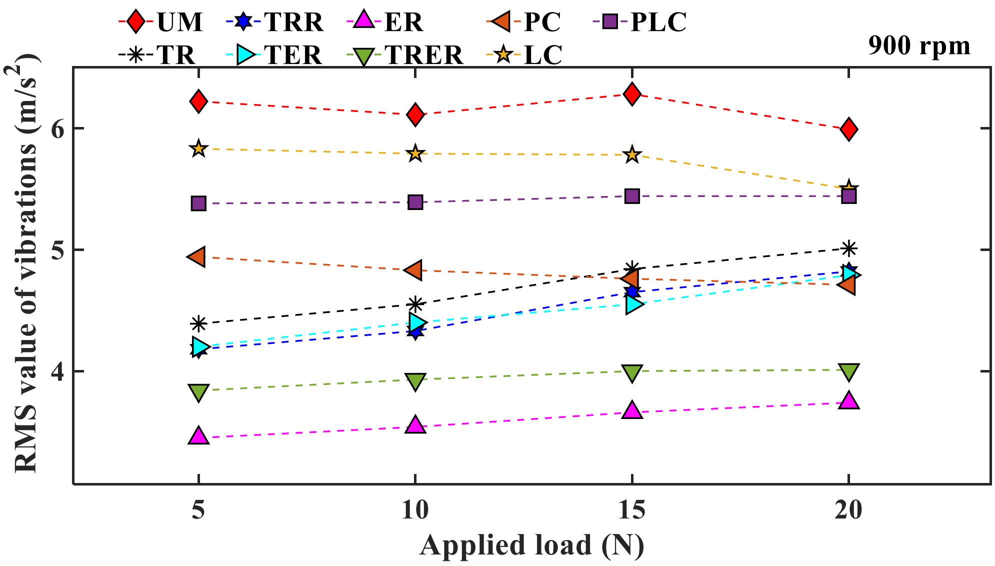

(c)

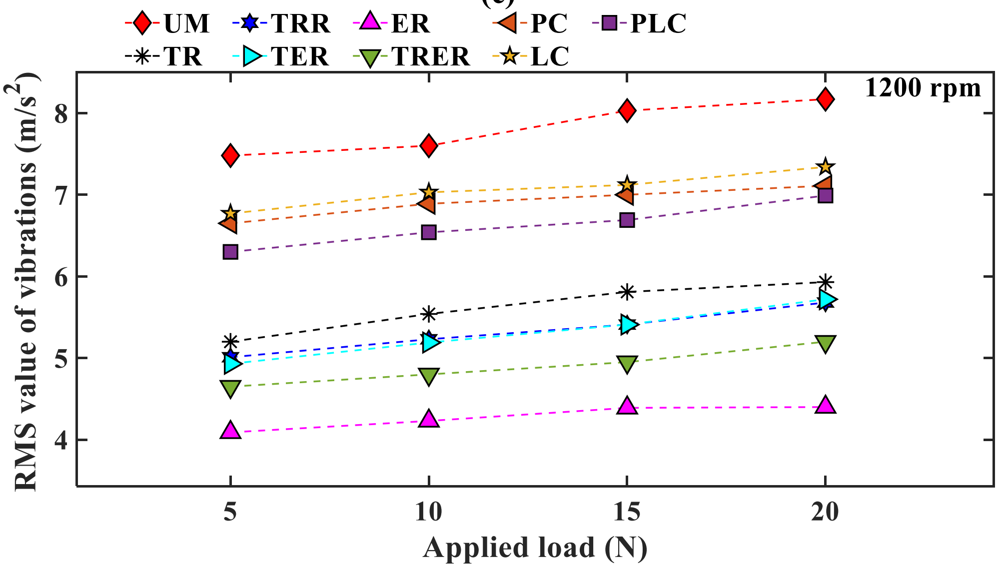

(d)

Fig. 6.19: Variation in RMS value of vibrations of unmodified and 8 modified workpiece spur gears with applied load for workpiece gear speed of (a) 300 rpm, (b) 600 rpm, (c) 900 rpm, and (d) 1200 rpm.

UM:Unmodified; TR:Tip relief; TRR:Tip and root relief; TER:Tip and end relief; ER:End relief; TRER:Tip, root, and end relief; PC: Profile crowning; LC:Lead crowning

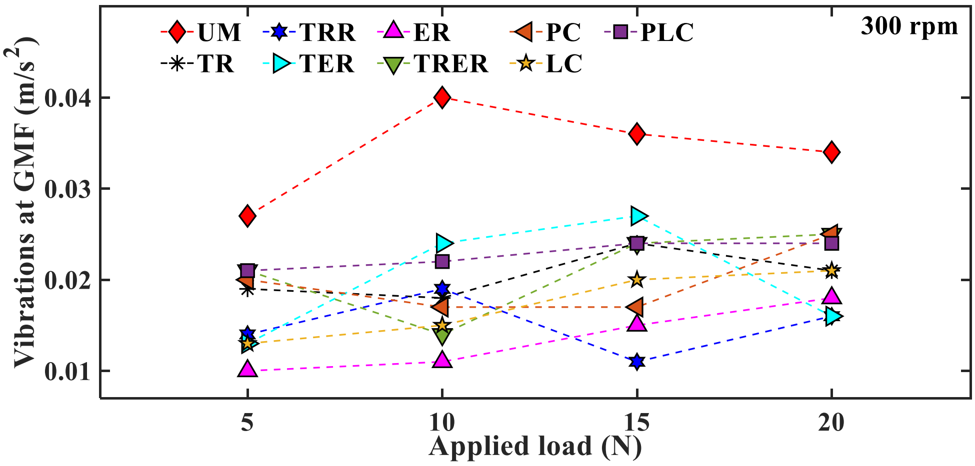

(a)

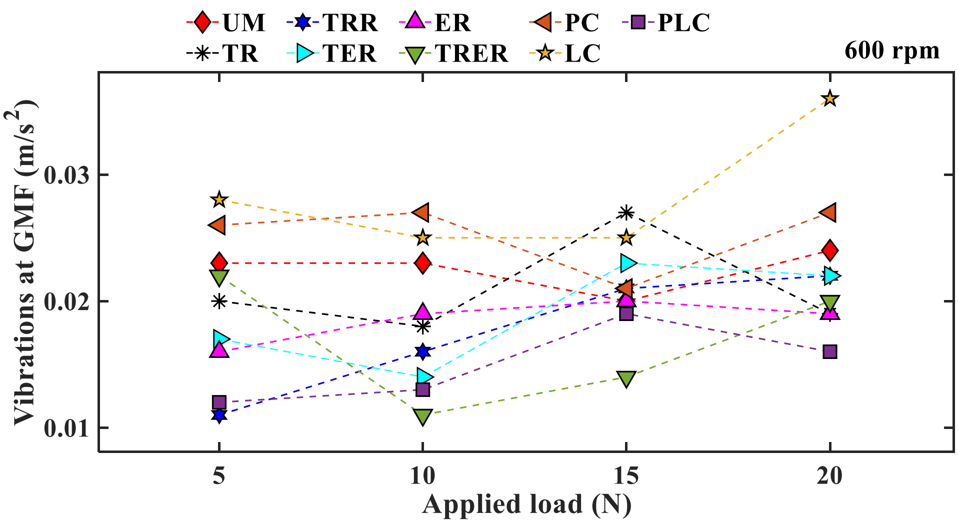

(b)

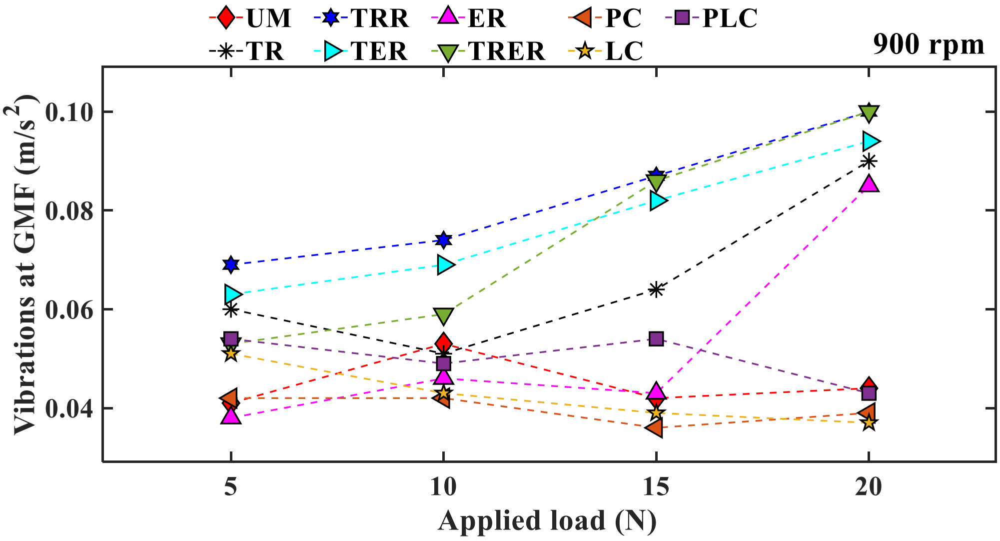

(c)

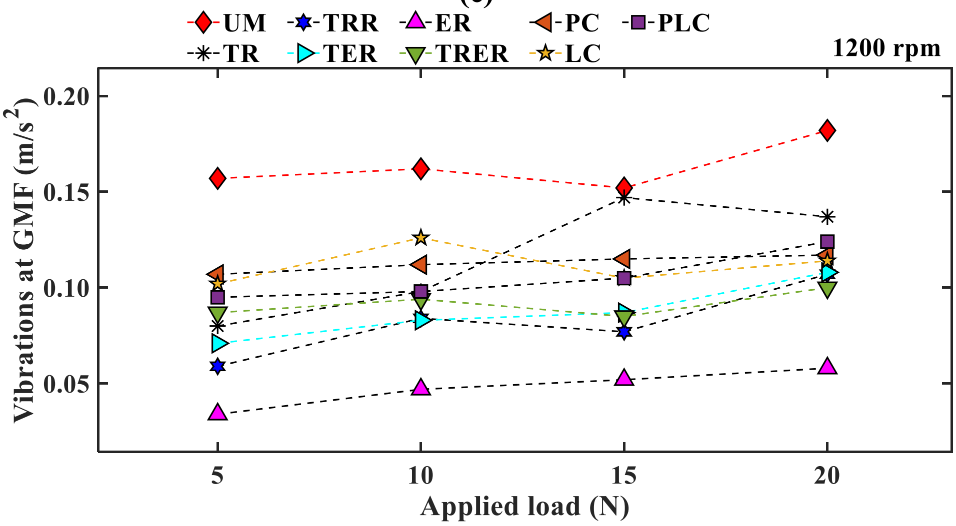

(d)

Fig. 6.20: Variation in values vibrations of unmodified and 8 modified workpiece spur gears with applied load at GMF for test gear speed of (a) 300 rpm, (b) 600 rpm, (c) 900 rpm, and (d) 1200 rpm.

Following are the observations from Figs. 6.18-6.20 and Tables 6.12- 6.14 along with their explanations:

- At 300 rpm of test gear speed (Fig. 6.18a), sound pressure level is reduced (with respect to unmodified gear) for only end relieved and combined tip, root, and end relieved workpiece spur gears for all values of applied load. At 600 rpm speed (Fig. 6.18b), it is reduced for all the modified workpiece gears except profile crowned and combined profile and lead crowned gears for all values of the applied load. But at 900 and 1200 rpm (Figs. 6.18c, 6.18d), it is reduced for all 8 modified gears for all the values of the applied load.
- Maximum reduction in sound pressure level of 5 dBA is achieved for end relieved workpiece gear (Gear-2) in Exp. No. 13 in Table 6.12 for 1200 rpm speed and 5 N applied load due to maximum reduction in tooth-to-tooth and longwave transmission errors for it. Following are the reduction in sound pressure levels for other modified workpiece gears at 1200 rpm for different applied loads: 4.5 dBA for combined tip, root and end relieved workpiece gear (Gear-7) and 2.8 dBA for tip relieved workpiece gear (Gear-1) both in Exp. No. 13; 3.1 dBA for tip and root relieved (Gear-5) and 1.6 dBA for profile crowned (Gear-4) workpiece gears both in Exp. No. 14; 3.2 dBA for tip and end relieved (Gear-6) and 2.2 dBA for lead crowned (Gear-3) workpiece gears both in Exp. No. 15; and 1.6 dBA for profile and lead crowned (Gear-8) workpiece gear in Exp. No. 16.
- RMS values of vibrations are reduced for all the 8 modified gears at all four values of rotational speeds and applied loads (Fig. 6.19). Maximum reduction by an amount of 3.77 m/s^2 is shown by end relieved workpiece gear (Gear-2) at 1200 rpm and 20 N applied load (Table 6.13). It is due to maximum reduction in tooth-to-tooth and longwave transmission errors for this gear. Following are the reductions in RMS values of vibrations for other flank modified workpiece gears (from Table 6.13): 2.28 m/s^2 for tip relieved workpiece gear (Gear-1) in Exp. No. 13; 2.62 m/s^2 for tip and root relieved (Gear-5), 2.62 m/s^2 for tip and end relieved (Gear-6), 3.08 m/s^2 for combined tip, root and end relieved (Gear-7), and 1.34 m/s^2 for profile and lead crowned (Gear-8) workpiece gears all in Exp. No. 15; 1.52 m/s^2 for profile crowned workpiece gear (Gear-4) in Exp. No. 11; and 1.02 m/s^2 for lead crowned workpiece gear (Gear-3) in Exp. No. 8.
- At 300 rpm and 1200 rpm of test gear speed (Fig. 6.20a and Fig. 6.20d), value of vibrations at GMF reduced for all 8 modified workpiece gears for all the values of applied load. At 600 rpm of test gear speed (Fig. 6.20b) the value of vibrations at GMF

reduced for end relieved, combined tip, root, and end relieved, and combined profile and lead crowned gears only. At 900 rpm speed (Fig. 6.20d) the value of vibrations at GMF was not reduced for any flank modifications for all the values of applied load.

- The maximum reductions in value of vibrations at GMF (from Table 6.14) are: 0.077 m/s^2 for tip relieved gear (Gear-1), 0.098 m/s^2 for tip and root relieved gear (Gear-5), 0.086 m/s^2 for tip and end relieved gear (Gear-6) all three in Exp. No. 13; 0.124 m/s^2 for end relieved gear (Gear-2), 0.086 m/s^2 for combined tip, root, and end relieved gear (Gear-7), 0.065 m/s^2 for profile crowned gear (Gear-4), and 0.068 m/s^2 for lead crowned gear (Gear-3) all in Exp. No. 16; and 0.064 m/s^2 for profile and lead crowned gear (Gear-8) in Exp. No. 14. End relieved gear shows the maximum reduction in value of vibrations at GMF. From Fig. 6.20 and Table 6.14 it is evident that modified gears show maximum reduction in value of vibrations at GMF at higher speed of the test gear.
- The amount of reduction in SPL, RMS values of vibrations, and vibrations at GMF for the modified workpiece gears (with reference to the unmodified workpiece gear) increases with rotational speed of the test gear. Influence of the applied load is insignificant on RMS values of vibrations for the different modified workpiece gears, but it affects their SPL particularly at smaller values of rotational speed of the test gear. Signals of SPL from a gearbox has SPL contributions from the gear pairs and other components of the gearbox such as bearings. At smaller speed, the total SPL generated fluctuates instead of making any trend. But at higher speed, the SPL generated by the gears dominates the SPL generated by other components of a gearbox. This may be the reason for the linear trend of SPL with the applied load at higher speed of the test gear.
- RMS values of vibrations reduced for all the speeds of the test gear but vibrations at GMF only reduced at higher speed of the test gear because the RMS value of vibrations is resultant of vibrations from all components of a gearbox. It may happen that the flank modifications are effective for a gear at its higher speed but they help in mitigating the adverse effects of shaft misalignments, manufacturing and assembly errors of a gearbox, hence the vibration generated by all components of a gearbox are reduced for all speeds of the test gear.

The ***next chapter*** summarizes the outcomes of the present research work by presenting its significant achievements, conclusions, and some identified avenues for future research work.

Chapter 7

Conclusions and Scope for the Future Work

This chapter summarizes the outcomes of the present research work by presenting its significant achievements, conclusions, and some identified avenues for future research work.

7.1 Significant Achievements

- Developed cathode gears and unique apparatus to impart non-contact tip relieving, root relieving, end relieving, profile crowning, and twist-free lead crowning by the PED process either individually or their any combination to a spur gear in one setting by engaging it with the corresponding developed cathode gear(s).
- The developed apparatus has provisions to provide rotary motion to the developed cathode gear(s), constant value of reciprocating motion to the spur gear to impart it tip relief, root relief, profile crowning, and variable reciprocating motion for its lead crowning, and no reciprocating motion for end relief.
- The developed cathode gears and apparatus through PED process significantly reduced surface roughness of the modified spur gear flank surfaces and completely removed the hob cutter marks and cracks from them in addition to providing the intended flank modification in non-contact manner.
- Developed generic analytical models for non-contact tip relieving, root relieving, end relieving, and lead crowning of a spur gear. They are very useful in designing or predicting the value of tip relief, root relief, end relief, and lead crowning that can be imparted to a spur gear in a given duration of time or to optimize the parameters of PED process.
- Developed single flank roll tester for cylindrical gears to evaluate total, tooth-to-tooth, and longwave transmission errors which help in minimizing the running noise and vibrations of a spur or helical gear before its actual use in any application.

7.2 Conclusions

Following are the major conclusions drawn from the different work done to meet the identified research objectives of the present work:

7.2.1 Developed Cathode Gears and Apparatus

- Microgeometry results and photographs of the flank modified spur gears confirm that the developed cathode gears and the apparatus via the PED process provided the intended tip relief, root relief, end relief, lead crowning, and profile crowning individually or their any combination to spur gear non-contact manner. This confirms their conceptual design, development, and successful functioning.

- Root relieving of the spur gear needed more modification duration than other flank modifications due to insufficient time available for meshing of spur gear teeth roots with conductive portions of the corresponding cathode gear.
- In some experiments, considerably different values of flank modifications are imparted to left and right flank surfaces of spur gear due to differences in their microgeometry deviations and uncertainty in their tip/root/profile being either positive, negative, or their combination.

7.2.2 Parametric Study for Tip Relief and Profile Crowning

- The value of tip relief increases significantly with modification duration and electrolyte concentration, slightly increases with electrolyte temperature, changes insignificantly with electrolyte flow rate, no change with rotational speed of the cathode gear up to 35 rpm but increases significantly beyond this speed.
- Experimental investigation identified 20 minutes, 2 Molarity, 35ºC, 30 lpm, and 45 rpm as values for modification duration, electrolyte concentration, electrolyte temperature, electrolyte flow rate, and rotational speed of cathode gear respectively to achieve higher values of tip relief.
- Maximum percentage reductions in '*Ra'*, and '*Ry'* (i.e., *PRRa* and *PRRy*) are found for 12 minutes of tip relieving duration, 1.5 and 2 Molarity of electrolyte concentration, 25ºC of electrolyte temperature, 20 lpm of electrolyte flow rate, and 15 rpm of rotational speed of cathode gear.
- Average values of profile crowning increase with voltage and pulse-on time but show a zig-zag trend with pulse-off time.
- Following values were identified for further experiments based upon the experimental results and their analyses: 0.5 Molarity for tip, root and end relieving, and 1.0 Molarity for lead and profile crowning; 30ºC for electrolyte temperature; 20 lpm for electrolyte flow rate, 15 rpm for rotational speed of cathode gear for tip, root, and end relief and 35 rpm for lead and profile crowning, and 12 minutes modification duration for tip relief, end relief, lead crowning, and profile crowning and 20 minutes for root relief.

7.2.3 Developed Analytical Models

- Predictions by the developed analytical models for root relief, tip relief, end relief, and lead crowning closely agree with the corresponding experimental values which is evidenced by minimum values of prediction error of 0.9% for tip relief model, 1.2% for root relief model, 1.4% for end relief model, and 0.5% for lead crowning model. The predicted and experimental values of tip, root, end relief, and lead crowning increase with voltage and pulse-on time and reduce with pulse-off time. Similar trend is observed in the experimental value of profile crowning except with pulse-off time.

- Predicted and experimental values of tip relief, root relief, end relief, and lead crowning increase with voltage and pulse-on time and reduce with pulse-off time.
- The developed models will be very useful in designing or predicting the value of tip, root, end relief, and lead crowning that can be imparted to a spur gear for a given time. Conversely, they can be used for parametric optimization of PED process and to compute the required duration to impart the desired amount of tip/root/end relief or lead crowning to spur gears by the PED process.
- Providing twist-free lead crowning to spur gear flank surfaces by the developed cathode gears and the apparatus is confirmed by comparison of flank surface topography of spur gear before and after its lead crowning.

7.2.4 Surface Finish and Morphology

- Considerable improvements in surface roughness parameters along with complete removal of hob cutter marks and cracks from flank surfaces of the modified spur gears have been achieved after flank modification of spur gears by the developed cathode gears and the apparatus through the PED process. Though surface morphology revealed presence of some micro-pits on the modified gear flank surfaces.
- PED process maximum reduced arithmetical average roughness and maximum height for the combination of applied voltage 18 volts, pulse-on time of 3 ms, and pulse-off time of 4 ms for tip, end relieved, and profile crowned gear; applied voltage 27 volts, pulse-on time of 3 ms, and pulse-off time of 4 ms for root relieved gear; and applied voltage of 18 volts, pulse-on time of 4 ms and pulse-off time of 4 ms for lead crowned gear.

7.2.5 Influence of Workpiece Gear Material Hardness

The developed cathode gears and apparatus through PED process:

- Results in similar values of volumetric MRR for case-hardened and unhardened workpiece spur gears while imparting all 5 flank modifications implying that material removal does not depend on hardness of spur gear material.
- Imparted higher values of tip relief, profile crowning, and lead crowning to the case-hardened spur gears than the corresponding unhardened workpiece spur gears but imparted slightly smaller values of root relief and end relief to case-hardened workpiece spur gear than the corresponding unhardened spur gears.

- Yielded significantly higher values of *'PRRa'* and *'PRRy'* for case-hardened spur gear than the corresponding unhardened spur gear during its tip relieving, end relieving, profile crowning, and lead crowning.
- Resulted in slightly smaller values of *'PRRa'* and *'PRRy'* for case-hardened workpiece spur gear than the corresponding unhardened spur gear during their root relieving.

7.2.6 Comparative Study of Functional Performance Parameters

- Total transmission errors, tooth-to-tooth transmission errors, and longwave transmission errors are reduced for all the eight modified spur gears. Though these values are unequal for left and right flanks of the modified spur gears due to differences in their microgeometry deviations.
- Those flank modifications which minimize contact of face width ends of modified gear during meshing with the mating gear teeth (i.e., lead crowning and end relieving) significantly reduce total, tooth-to-tooth, and longwave transmission errors. It is confirmed by the fact that the lead crowned spur gear showed maximum reduction in total transmission error and the end relieved spur gear showed maximum reductions for tooth-to-tooth and longwave transmission errors.
- Those flank modifications which reduce contact length along the profile and lead direction and smoothen engagement of modified gear with the mating gear (i.e., lead crowing, tip relief, root relief) significantly reduce variation in center-to-center distance, thus reducing total and tooth-to-tooth composite errors of modified workpiece gears. It is again confirmed by the fact that the lead crowned spur gear gave maximum reduction in total composite error and radial runout and that the tip relieved, and tip and root relieved spur gear showed maximum reduction in tooth-to-tooth composite error due to ease in loading at start and end of gear tooth meshing which smoothens engagement.
- Profile crowned gear gave minimum reduction for total and longwave transmission errors because it does not affect contact along the lead direction. Combined root, tip and end relieved gear showed minimum reduction for tooth-to-tooth transmission error because this modification is a combination of partial lead and partial profile crowning therefore, advantages of lead crowning may be offset by the profile crowning.
- Imparting flank modifications to spur gear by non-contact process reduced transmission errors which compensate the gear tooth deflection and assembly errors during the transmission **(Yu and Ting, 2016)**. Hence noise and vibrations are expected to be reduced for all the modified spur gears. It is confirmed by maximum reduction in noise by 5 dBA for end relieved spur gear at 1200 rpm speed and 5 N applied load. Vibrations are reduced for all 8 modified spur gears at all 4 values of rotational speeds and applied loads.

Maximum reduction by 3.77 m/s^2 for end relieved gear at 1200 rpm and 20 N applied load.

7.3 Directions for the Future Work

- Investigation on non-contact flank modifications of helical gears, bevel gears and other types of gears using PED process.
- Flank modifications of gears using other non-contact type processes such as electro-discharge machining.
- Development of theoretical models for non-contact flank modification of helical, bevel and other types of gears.
- Study of providing different shapes (i.e., parabolic, quadratic, cubic, polynomial curve) of non-contact flank modification to workpiece gear flank surfaces by suitably designing the cathode gears and study their effect on functional performance.
- Study of the shape (i.e., quadratic, cubic, polynomial curve) of lead crowning of spur gear by providing different variable reciprocating velocity.
- Finite element simulation for better understanding of the mechanism of providing non-contact flank modification to spur gears by the developed cathode gears using the PED process.
- The cathode gears can be designed in such a way that IEG can be adjusted by using bit type of conductive portion which can be only replaceable part of cathode gear. It helps in providing different IEG variation with same cathode gear and imparting different shape to the gears.

References

Arteta, M.P., Mazo, J.S., Cacho, R.A., Arjol, G.A., **2013**. Double flank roll testing machines intercomparison for worm and worm gear. **Procedia Engineering**, 63, 454-462. https://doi.org/10.1016/j.proeng.2013.08.231

Chong, T.H., Myong, J.H., Kim, K.T., **2001**. Tooth modification of helical gears for minimization of vibration and noise. **International Journal of Precision Engineering and Manufacturing**, 2, 5-11.

Colbourne, J.R., **2012**. The Geometry of Involute Gears. Springer Science & Business Media. DOI: https://doi.org/10.1007/978-1-4612-4764-7

Davis, J.R., **2005**. Gear Materials, Properties, and Manufacture. ASM International.

Fatourehchi, E., Mohammadpour, M., King, P.D., Rahnejat, H., Trimmer, G., Williams, A., **2018**. Microgeometrical tooth profile modification influencing efficiency of planetary hub gears. **International Journal of Powertrains**, 7, 162-179. https://doi.org/10.1504/IJPT.2018.090374

Fong, Z.H., Chen, G.H., **2016**. Gear flank modification using a variable lead grinding worm method on a computer numerical control gear grinding machine. **Trans ASME: Journal of Mechanical Design**, 138, 083302. https://doi.org/10.1115/1.4033919

Ghosh, S.S., Chakraborty, G., **2016**. On optimal tooth profile modification for reduction of vibration and noise in spur gear pairs. **Mechanism and Machine Theory**, 105, 145-163. http://dx.doi.org/10.1016/j.mechmachtheory.2016.06.008

Gimpert, D., **2007**. Gear Inspection: Troubleshooting Tips, Gear Solutions, pp. 36-43.

Guo, E., Hong, R., Huang, X., Fang, C., **2015**. A correction method for power skiving of cylindrical gears lead modification. **Journal of Mechanical Science and Technology**, 29, 4379-4386. https://doi.org/10.1007/s12206-015-0936-x

Guo, Z., Xie, R., Guo, W., Han, W., Gao, F., Zhang, Y., **2023**. A Novel Method for Improving the Skiving Accuracy of Gears with Profile and Lead Modifications, **Machines,** 11, 87. https://doi.org/10.3390/machines11010087

Gupta, K., Jain, N.K., Laubscher, R., **2017**. Advanced Gear Manufacturing and Finishing: Classical and Modern Processes. Academic Press, London. https://doi.org/10.1016/B978-0-12-804460-5.00008-0

Han, J., Zhu, Y., Xia, L., Tian, X., **2018**. A novel gear flank modification methodology on internal gearing power honing gear machine. **Mechanism and Machine Theory**, 121, 669-682. https://doi.org/10.1016/j.mechmachtheory.2017.11.024

He, K., Li, G., Li, X., **2017**. The second envelope method of point-vector and its application on worm wheel grinding modified gear. **The International Journal of Advanced

Manufacturing Technology, 88, 3175-3184. https://doi.org/10.1007/s00170-016-9028-z

Hsu, R.H., Fong, Z.H., **2010**. Analysis of auxiliary crowning in parallel gear shaving. **Mechanism and Machine Theory**, 45, 1298-1313. https://doi.org/10.1016/j.mechmachtheory.2010.04.002

Hsu, R.H., Fong, Z.H., **2011**. Novel variable-tooth-thickness hob for longitudinal crowning in the gear-hobbing process. **Mechanism and Machine Theory**, 46, 1084-1096. https://doi.org/10.1016/j.mechmachtheory.2011.03.007

Hsu, R.H., Wu, Y.R., Tran, V.T., **2019**. Manufacturing helical gears with double-crowning and twist-free tooth flanks using a variable pressure angle shaving cutter. **Proceedings of the Institution of Mechanical Engineers, Part B: Journal of Engineering Manufacture**, 233, 77-86. https://doi.org/10.1177/0954405417718590

ISO Standard, 21771: 2007. Gears - Cylindrical Involute Gears and Gear pairs–Concepts and Geometry. ISO Geneva, Switzerland. https://www.iso.org/standard/35989.html

Jain, N.K., Petare, A.C., **2017**. Review of Gear Finishing Processes, In: Hashmi, S. (Ed.), Comprehensive Materials Finishing. Elsevier Science, Oxford (UK) pp. 93-120. https://doi.org/10.1016/B978-0-12-803581-8.09150-5

Jain, V.K., **2009**. Advanced Machining Processes. Allied publishers.

Jelaska, D.T., **2012**. Gears and gear drives. John Wiley & Sons.

Jia, C., Fang, Z., Yao, L., Zhang, J., **2020**. Tooth flank modification to reduce transmission error and mesh-in impact force in consideration of contact ratio for helical gears. **Proceedings of the Institution of Mechanical Engineers, Part C: Journal of Mechanical Engineering Science**, 235, 4475-4493. https://doi.org/10.1177/0954406220975065

Li, S., **2007**. Effects of machining errors, assembly errors and tooth modifications on loading capacity, load-sharing ratio and transmission error of a pair of spur gears. **Mechanism Machine Theory**, 42, 698-726. https://doi.org/10.1016/j.mechmachtheory.2006.06.002

Lin, H., Chen, Y., Li, X., Li, H., Chen, Q., **2021**. Simulation and experimental research on electrochemical machining of cross groove. **International Journal of Electrochemical Science**, 16, 150959. https://doi.org/10.20964/2021.01.20

Litvin, F.L., Fuentes, A., **2004**. Gear Geometry and Applied Theory. Cambridge University Press. https://doi.org/10.1017/CBO9780511547126

Liu, J.H., Hung, C.H., Chang, S.L., **2009**. Design and manufacture of plunge shaving cutter for shaving gears with tooth modifications. **The International Journal of**

Advanced Manufacturing Technology, 43, 1024-1034. https://doi.org/10.1007/s00170-008-1783-z

Ma, H., Yang, J., Song, R., Zhang, S., Wen, B., **2014**. Effects of tip relief on vibration responses of a geared rotor system. **Journal of Mechanical Engineering Science**, 228, 1132-1154. https://doi.org/10.1177/0954406213500615

Mao, K., **2006**. An approach for powertrain gear transmission error prediction using the non-linear finite element method. **Proceedings of the Institution of Mechanical Engineers, Part D: Journal of Automobile Engineering**, 220, 1455-1463. https://doi.org/10.1243/09544070JAUTO251

Mayank, G., Fuchen, C., Masanori, K., **2018**. Analysis of reactions determining current efficiency in electrochemical machining. **Procedia CIRP**, 68, 511-516. https://doi.org/10.1016/j.procir.2017.12.083

Mithu, M.A.H., Fantoni, G., Ciampi, J., **2011**. A step towards the in-process monitoring for electrochemical microdrilling. **The International Journal of Advanced Manufacturing Technology**, 57, 969-982. https://doi.org/10.1007/s00170-011-3355-x

Neha, G., Shunmugam, M.S., **2017**. Effect of shaft misalignment and mitigation through crowning in spur gear transmission. **International Journal of Computer Aided Engineering and Technology**, 9, 385-407. https://doi.org/10.1504/IJCAET.2017.086919

Pang, G.B., Xu, W.J., Zhou, J.J., Li, D.M., **2010**. Gear finishing and modification compound process by pulse electrochemical finishing with a moving cathode. **Advanced Materials Research**, 126-128, 533-538. https://doi.org/10.4028/www.scientific.net/AMR.126-128.533

Pueo, M., Santolaria, J., Acero, R., Gracia, A., **2017**. A review of tangential composite and radial composite gear inspection. **Precision Engineering**, 50, 522-537. https://doi.org/10.1016/j.precisioneng.2017.05.007

Ren, Z., Fang, Z., Kizaki, T., Feng, Y., Nagata, T., Komatsu, Y., Sugita, N., **2022**. Understanding local cutting features affecting surface integrity of gear flank in gear skiving. **International Journal of Machine Tools Manufacture**, 172, 103818. https://doi.org/10.1016/j.ijmachtools.2021.103818

Terauchi, Y., Nadano, H., Nohara, M., **1982**. On the effect of the tooth profile modification on the dynamic load and the sound level of the spur gear. **Bulletin of JSME**, 25, 1474-1481. https://doi.org/10.1299/jsme1958.25.1474

Tesfahunegn, Y.A., Rosa, F., Gorla, C., **2010**. The effects of the shape of tooth profile modifications on the transmission error, bending, and contact stress of spur gears. **Proceedings of the Institution of Mechanical Engineers, Part C: Journal of Mechanical Engineering Science**, 224, 1749-1758. https://doi.org/10.1243/09544062JMES1844

Tian, X., Zhou, L., Han, J., Xia, L., **2021**. Research on gear flank twist compensation of continuous generating grinding gear based on flexible electronic gearbox. **IEEE Access**, 9, 151080-151088. https://doi.org/10.1109/ACCESS.2021.3126673

Tian, X., Li, D., Huang, X., Liu, H., Han, J., Xia, L., **2022**. A topological flank modification method based on contact trace evaluated genetic algorithm in continuous generating grinding. **Mechanism Machine Theory**, 172, 104820. https://doi.org/10.1016/j.mechmachtheory.2022.104820

Tran, V.T., Hsu, R.H., Tsay, C.B., **2014a**. A novel finish hobbing methodology for longitudinal crowning of a helical gear with twist-free tooth flanks by using dual-lead hob cutters, **Proceedings of ASME's International Mechanical Engineering Congress and Exposition (IMECE) 2014: Systems, Design, and Complexity**. https://doi.org/10.1115/imece2014-36149

Tran, V.T., Hsu, R.H., Tsay, C.B., **2014b**. Study on the anti-twist helical gear tooth flank with longitudinal tooth crowning. **Trans ASME: Journal of Mechanical Design**, 136, 061007. https://doi.org/10.1115/1.4027166

Tran, V.Q., Wu, Y.R., **2018**. Dual lead-crowning for helical gears with long face width on a CNC internal gear honing machine. **Mechanism and Machine Theory**, 130, 170-183. https://doi.org/10.1016/j.mechmachtheory.2018.08.018

Tran, V.Q., Wu, Y.R., **2020**. A novel method for closed-loop topology modification of helical gears using internal-meshing gear honing. **Mechanism and Machine Theory**, 145, 103691. https://doi.org/10.1016/j.mechmachtheory.2019.103691

Wang, W.S., Fong, Z.H., **2008**. A dual face-hobbing method for the cycloidal crowning of spur gears. **Mechanism and Machine Theory**, 43, 1416-1430. https://doi.org/10.1016/j.mechmachtheory.2007.11.007

Wang, H., Zhou, C., Hu, B., Liu, Z., **2020**. Tooth wear prediction of crowned helical gears in point contact. **Proceedings of the Institution of Mechanical Engineers, Part J: Journal of Engineering Tribology**, 234, 947-963. https://doi.org/10.1177/1350650119896467

Wang, H., Tang, L., Zhou, C., Shi, Z., **2021**. Wear life prediction method of crowned double helical gear drive in point contact mixed elastohydrodynamic lubrication. **Wear**, 484, 204041. https://doi.org/10.1016/j.wear.2021.204041

Wu, Y.R., Tran, V.T., **2015**. Lead crowning and anti-twist for tooth flank of a heat treated helical gear on internal CNC honing machine, **Applied Mechanics and Materials**. **Trans Tech Publ**, pp. 554-559. https://doi.org/10.4028/www.scientific.net/AMM.799-800.554

Yang, J., Zhang, H., Li, T., Gao, Z., Nie, S., Wei, B., **2018**. A profile dressing method for grinding worm used for helical gear with higher order modification profile. **The International Journal of Advanced Manufacturing Technology**, 99, 161-168. https://doi.org/10.1007/s00170-018-2459-y

Yi, J., Zheng, J., Yang, T., Xia, D., Hu, D., **2002**. Solving the control problem for electrochemical geartooth-profile modification using an artificial neural network. **The International Journal of Advanced Manufacturing Technology**, 19, 8-13. https://doi.org/10.1007/PL00003970

Yu, B., Ting, K.l., **2016**. Compensated conjugation and gear tooth modification design. **Trans ASME: Journal of Mechanical Design**, 138, 073301. https://doi.org/10.1115/1.4032264

Yu, B., Shi, Z., Lin, J., **2017**. Topology modification method based on external tooth-skipped gear honing. **The International Journal of Advanced Manufacturing Technology**, 92, 4561-4570. https://doi.org/10.1007/s00170-017-0463-2

Yu, B., Kou, H., Zhao, B., Shi, Z., Sun, Y., Wu, G., **2021**. Approximation model for longitudinal-crowned involute helical gears with flank twist in continuous generating grinding. **The International Journal of Advanced Manufacturing Technology**, 114, 3675-3694. https://doi.org/10.1007/s00170-021-07099-y

Zhang, H., Fang, C., Huang, X., **2014**. Accurate tooth lead crowning without twist in cylindrical helical gear grinding. **Advances in Mechanical Engineering**, 6, 496181. https://doi.org/10.1155/2014/496181

Zhao, B., Yu, B., Shi, Z., Sun, Y., Wu, G., **2022**. Research on tooth flank twist based on orthogonal polynomials characterization. **Machines**, 10, 532. https://doi.org/10.3390/machines10070532

Zheng, F., Zhang, M., Zhang, W., Guo, X., **2018**. Research on the tooth modification in gear skiving. **Trans ASME: Journal of Mechanical Design**, 140, 084502. https://doi.org/10.1115/1.4040268

Zou, T., Shaker, M., Angeles, J., Morozov, A., **2017**. An innovative tooth root profile for spur gears and its effect on service life. **Meccanica**, 52, 1825-1841. https://doi.org/10.1007/s11012-016-0519-7

Appendix-A: Spur Gear Geometry Relations Used in Development of Analytical Models for Tip/Root/End Relief and Lead Crowning

A1. Geometry Relations Used in Developing Analytical Model for Tip Relief

Involute function for a pressure angle *'ψ'* is given by Eq. A1a (**Litvin and Fuentes, 2004**) (the concept is shown in Fig. A1). Parametric equations for a point (having cartesian coordinates as *'x'* and *'y'* and gear roll angle as *'θ'* radian) which lies on the involute profile of a gear having *'r_b'* base circle radius are given by Eq. A1b **(Litvin and Fuentes, 2004)**:

$$inv(\psi) = tan\,\psi - \psi \qquad (A1a)$$

$$x = r_b[cos\theta + \theta sin\theta];\;\; y = r_b[sin\,\theta - \theta\,cos\,\theta] \qquad (A1b)$$

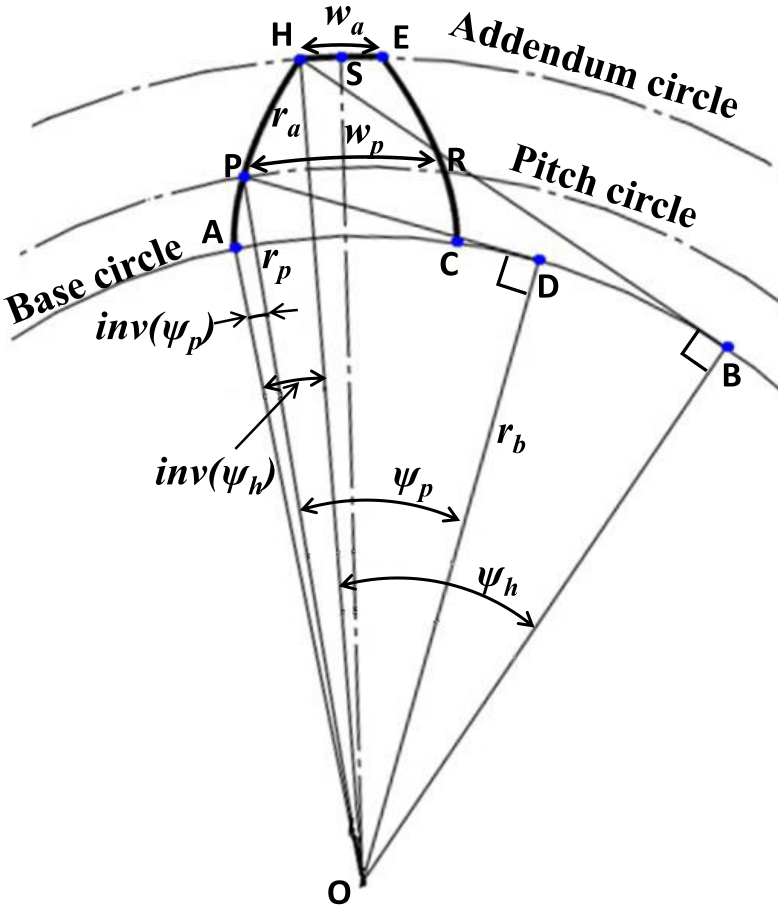

Fig. A1: Geometry of anodic workpiece gear tooth used to calculate different parameters required in development of analytical model for non-contact *tip relief* by the PED process.

Tip relieving of anodic spur gear by the PED process changes the involute profile arc length *'GH'* to *'GE'* (depicted in Fig. 4.3a). The parametric equations (Eq. A1b) for cartesian coordinates and gear roll angles of points '*G' (x_g, y_g, θ_g)* and *'H'* (x_h, y_h, θ_h) lying on the involute profile of anodic workpiece gear are used to compute its involute profile arc length 'L_{tr}' and area of *GHTRG* (shown in Fig. 4.3b) which are given by following equations:

$$L_{tr} = \int_{\theta_g}^{\theta_h} \sqrt{\left[\left(\frac{dx}{d\theta}\right)^2 + \left(\frac{dy}{d\theta}\right)^2\right]}\, d\theta \Rightarrow L_{tr} = \frac{r_b}{2}\left({\theta_h}^2 - {\theta_g}^2\right) \qquad (A2)$$

$$Area\ of\ GHTRG = \int_{x_g}^{x_h} y\, dx = {r_b}^2 \int_{\theta_g}^{\theta_h} [\sin\theta - \theta\cos\theta]\theta\cos\theta\, d\theta \qquad (A3a)$$

Integration of Eq. B3a and substituting of integration limits gives the following expression:

$$Area\ of\ GHTRG = \frac{{r_b}^2}{2}\left(\frac{\sin 2\theta_h - \sin 2\theta_g + {\theta_g}^2 \sin 2\theta_g - {\theta_h}^2 \sin 2\theta_h}{2} + \frac{{\theta_g}^3 - {\theta_h}^3}{3} + \theta_g \cos 2\theta_g - \theta_h \cos 2\theta_h\right) \qquad (A3b)$$

The chordal thickness of anodic workpiece gear tooth along its addendum circle *'w_a'* (mm) (depicted in Fig. A1) is computed by the following expression **(Colbourne, 2012)**:

$$w_a = 2r_a(\angle HOS) = 2r_a(\angle POS + \angle AOP - \angle AOH) = 2r_a\left[\frac{w_p}{2r_p} + inv(\psi_p) - inv(\psi_h)\right] \Rightarrow$$

$$w_a = r_a\left[\frac{w_p}{r_p} + 2\{inv(\psi_p) - inv(\psi_h)\}\right] \qquad (A4)$$

where, *'r_p'* and *'r_a'* are radii (mm) of pitch circle and addendum circle of anodic workpiece gear; *'Ψ_p'* and *'Ψ_h'* are pressure angles (rad) of points '*P*' and *'H'* on the involute profile of anodic spur gear flank surface. The following equation is obtained after substituting expressions for cartesian coordinates of point *'E'* i.e., *'$x_e = r_a \cos(\gamma)$'* and *'$y_e = r_a \sin(\gamma)$'* in Eq. 7b where $\boldsymbol{\gamma = inv(\psi_h) + \frac{C_{\alpha t}}{r_a}}$:

$$\frac{Q_{tr}}{2Zb_t} d = \frac{1}{2}\left[(x_h - x_g) r_a \sin\gamma - (y_h - y_g) r_a \cos\gamma + x_h y_h - x_g y_g\right] - Area\ GHTRG \qquad (A5)$$

Using $\boldsymbol{(x_h - x_g) r_a = R\cos\alpha}$; $\boldsymbol{(y_h - y_g) r_a = R\sin\alpha}$ in Eq. B5 *gives Eq. B6.*

$$\frac{Q_{tr}}{2Zb_t} d = \frac{1}{2}\left[R\sin(\gamma - \alpha) + x_h y_h - x_g y_g\right] - Area\ GHTRG \qquad (A6)$$

where, $\boldsymbol{R = r_a\sqrt{(x_h - x_h)^2 + (y_h - y_g)^2}}$; $\boldsymbol{\alpha = \tan^{-1}\left(\frac{y_h - y_g}{x_h - x_h}\right)}$ $\qquad$ $(\boldsymbol{A7})$

Rearranging terms of Eq. A6 and using Eq. A7 in it gives the following equation for *'γ'*:

$$\gamma = inv(\psi_h) + \frac{C_{\alpha t}}{r_a} = \sin^{-1}\left[\frac{2\left\{\frac{Q_{tr}}{2Zb_t} + Area\ of\ GHTRG\right\} + y_g x_g - x_h y_h}{r_a\sqrt{(x_h - x_g)^2 + (y_h - y_g)^2}}\right] + \tan^{-1}\left(\frac{y_h - y_g}{x_h - x_g}\right) \qquad (A8)$$

Substituting *area of GHTRG* from Eq. A3b in Eq. A8; substituting $\boldsymbol{\gamma = inv(\psi_h) + \frac{C_{\alpha t}}{r_a}}$; and rearranging the terms gives the following expression for '*$C_{\alpha t}$*'.

$$C_{\alpha t} = r_a \left[sin^{-1} \left\{ \frac{\frac{Q_{tr}}{Zb_t} + r_b{}^2 \left(\frac{sin2\theta_h - sin2\theta_g + \theta_g{}^2 sin2\theta_g - \theta_h{}^2 sin2\theta_h}{2} + \frac{\theta_g{}^3 - \theta_h{}^3}{3} + \theta_g cos2\theta_g - \theta_h cos2\theta_g \right)}{r_a \sqrt{(x_h - x_g)^2 + (y_h - y_g)^2}} \right\} + \right.$$

$$\left. tan^{-1} \left(\frac{y_h - y_g}{x_h - x_g} \right) - inv(\psi_h) \right] \qquad (A9a)$$

Eq. A9a can be expressed in a simplified Eq. A9b using the following relations in it:

$$D_{t1} = r_b{}^2 \left[\frac{sin\,2\theta_h - sin\,2\theta_g + \theta_g{}^2\, sin\,2\theta_g - \theta_h{}^2\, sin\,2\theta_h}{2} + \frac{\theta_g{}^3 - \theta_h{}^3}{3} + \theta_g\, cos\,2\theta_g - \theta_h\, cos\,2\theta_h \right] +$$

$$y_g x_g - y_h x_h$$

$$D_{t2} = r_a \sqrt{(x_h - x_g)^2 + (y_h - y_g)^2} \qquad D_{t3} = tan^{-1} \left(\frac{y_h - y_g}{x_h - x_g} \right) - inv(\psi_h)$$

$$\Rightarrow \boldsymbol{C_{\alpha t} = r_a \left[sin^{-1} \left\{ \frac{\frac{Q_{tr}}{Zb_t} + D_{t1}}{D_{t2}} \right\} + D_{t3} \right]} \qquad (\boldsymbol{A9b})$$

A2. Geometry Relation Used in Developing Analytical Model for Root Relief

The length of arcs AC, EG, and 'L_{rf}' can be computed using the geometry depicted in Fig. A2 by the following equations:

$$AC = OA - OC = r_b - \sqrt{OD^2 - DC^2} \Rightarrow AC = r_b - \sqrt{r_d^2 + 2r_d r_{rf}} \qquad (A10)$$

where, 'r_b' and 'r_d' are radii (mm) of the base circle and dedendum circle of the anodic workpiece gear.

$$EG = r_d(\angle GOE) = r_d(\angle ZOA - \angle DOC) \Rightarrow EG = r_d \left(\frac{KA - KJ}{2r_b} - sin^{-1} \frac{CD}{OD = OE + ED} \right) \qquad (A11)$$

where, 'KJ' is the chordal thickness of anodic workpiece gear tooth at base circle 'w_b', and it can be computed using $w_b = r_b \left\{ \frac{w_p}{r_p} + 2inv(\psi_p) \right\}$; and '$KA$' is given by $2\pi r_b/Z$; using these in Eq. A11 gives the following relation:

$$\Rightarrow EG = r_d \left[\frac{\pi}{Z} - \left\{ \frac{w_p}{2r_p} + inv(\psi_p) \right\} - sin^{-1} \left(\frac{r_{rf}}{r_{rf} + r_d} \right) \right] \qquad (A12)$$

$$L_{rf} = EC = r_{rf}(\angle ODC) = r_{rf}\, cos^{-1} \left(\frac{CD}{OD} \right) \Rightarrow L_{rf} = r_{rf}\, cos^{-1} \left(\frac{r_{rf}}{r_d + r_{rf}} \right) \qquad (A13)$$

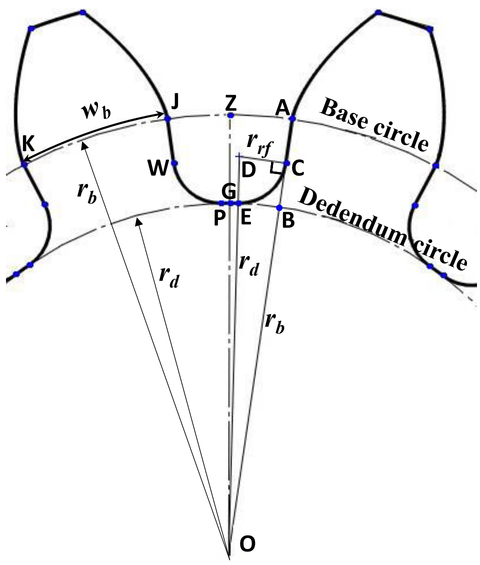

Fig. A2: Geometry of anodic workpiece gear tooth used to calculate different parameters required in the development of analytical model for its *root* relief by the PED process.

The parametric equations (Eq. A1b) for cartesian coordinates and gear roll angles of points '*A' (x_a, y_a, θ_a* with $\theta_a = 0$ since point '*A*' is on the base circle as shown in Fig. 4.5a) and *'Q'* (x_q, y_q, θ_q) lying on the involute profile of anodic spur gear are used to compute its involute profile arc length 'L_{rr}' which will be modified in root relieving and area of *AQTA* (shown in Fig. 4.5b) which are given by following equations:

$$L_{rr} = \int_{\theta_a=0}^{\theta_q} \sqrt{\left[\left(\frac{dx}{d\theta}\right)^2 + \left(\frac{dy}{d\theta}\right)^2\right]} d\theta = \frac{r_b}{2}\left(\theta_q^2 - \theta_a^2\right) = \frac{r_b \theta_q^2}{2} \qquad (A14)$$

$$Area\ of\ AQTA = \int_{x_a}^{x_q} y dx = r_b^2 \int_{\theta_a=0}^{\theta_q} [\sin\theta - \theta\cos\theta]\theta\cos\theta d\theta$$

$$\Rightarrow Area\ of\ AQTA = \frac{r_b^2}{2}\left(\frac{\sin 2\theta_q - \theta_q^2 \sin 2\theta_q}{2} - \frac{\theta_q^3}{3} - \theta_q \cos 2\theta_q\right) \qquad (A15)$$

Areas of RQTSR, and *RASR* are computed using the following expressions (refer to Fig. 4.5b):

$$Area\ of\ RQTSR = \frac{1}{2}(y_q + y_r)(x_q - x_r) = \frac{1}{2}\left\{y_q + r_b \sin\left(\frac{C_{ft}}{r_b}\right)\right\}\left\{x_q - r_b \cos\left(\frac{C_{ft}}{r_b}\right)\right\} \qquad (A16)$$

$$Area\ of RASR = \frac{1}{2}(AS)(RS) = \frac{1}{2}(r_b - x_r)(y_r)$$

$$\Rightarrow Area\ of\ RASR = \frac{1}{2}\left\{r_b - r_b \cos\left(\frac{C_{ft}}{r_b}\right)\right\} r_b \sin\left(\frac{C_{ft}}{r_b}\right) \qquad (A17)$$

where, (x_q, y_q) and (x_r, y_r) are the cartesian coordinates of points *'Q'* and *'R'* respectively; 'C_{ft}' is the amount of root relief imparted to anodic workpiece gear flank surface (mm). Substituting the expression of areas of *AQTA* (Eq. A15)*, RQTSR* (Eq. A16)*,* and *RASR* (Eq. A17) in the following relation (i.e., Eq. 4.14b) and rearranging the terms gives the Eq. A18:

$$\frac{Q_{rr}}{2Zb_t} = Area\ of\ trapezium\ RQTSR - area\ of AQTA - area\ of RASR$$

$$\Rightarrow sin\left(\frac{C_{ft}}{r_b}\right)\left(x_q r_b - r_b^2\right) - y_q r_b\, cos\left(\frac{C_{ft}}{r_b}\right) = \frac{Q_{rr}}{Zb_t} + r_b^2\left(\frac{sin\,2\theta_q}{2} - \theta_q\, cos\,2\theta_q - \frac{\theta_q^2\, sin\,2\theta_q}{2} - \frac{\theta_q^3}{3}\right) - x_q y_q \quad (A18)$$

Using $\boldsymbol{x_q r_b - r_b{}^2 = P\,cos\,\phi}$; **and** $\boldsymbol{y_q r_b = P\,sin\,\phi}$ in Eq. A18 gives Eq. A19:

$$\Rightarrow P\,sin\left(\frac{C_{ft}}{r_b} - \phi\right) = \frac{Q_{rr}}{Zb_t} + r_b^2\left(\frac{sin\,2\theta_q}{2} - \theta_q\, cos\,2\theta_q - \frac{\theta_q^2\, sin\,2\theta_q}{2} - \frac{\theta_q^3}{3}\right) - x_q y_q \quad (A19)$$

where, $P = \sqrt{\left(x_q r_b - r_b{}^2\right)^2 + \left(y_q r_b\right)^2}$; $and\ \phi = tan^{-1}\left(\frac{y_q r_b}{x_q r_b - r_b{}^2}\right)$ $\quad (A20)$

Rearranging terms of Eq. A19 and using Eq. A20 in it gives the following equation for 'C_{ft}':

$$C_{ft} = r_b\left[sin^{-1}\left\{\frac{\frac{Q_{rr}}{Zb_t} + r_b^2\left(\frac{sin\,2\theta_q}{2} - \theta_q\, cos\,2\theta_q - \frac{\theta_q^2\, sin\,2\theta_q}{2} - \frac{\theta_q^3}{3}\right) - x_q y_q}{\sqrt{(x_q r_b - r_b^2)^2 + (y_q r_b)^2}}\right\} + tan^{-1}\left(\frac{y_q r_b}{x_q r_b - r_b^2}\right)\right] \quad (A21)$$

Representing $r_b^2\left(\frac{sin\,2\theta_q}{2} - \theta_q\, cos\,2\theta_q - \frac{\theta_q^2\, sin\,2\theta_q}{2} - \frac{\theta_q^3}{3}\right) - x_q y_q = D_{r1}$;

$\sqrt{\left(x_q r_b - r_b^2\right)^2 + \left(y_q r_b\right)^2} = D_{r2}$ and $tan^{-1}\left(\frac{y_q r_b}{x_q r_b - r_b^2}\right) = D_{r3}$ in Eq. A21 gives the following relation for 'C_{ft}':

$$C_{ft} = r_b\left[sin^{-1}\left\{\frac{\frac{Q_{rr}}{Zb_t} + D_{r1}}{D_{r2}}\right\} + D_{r3}\right] \quad (A22)$$

A3. Geometry Relations Used in Developing Analytical Model for End Relief

End relieving of anodic workpiece gear by the PED process changes the involute profile arc length *'AH'* to *'MN'* (depicted in Fig. 4.6c). The parametric equations (Eq. A1b) for cartesian coordinates and gear roll angles of points '*A*' (x_a, y_a, θ_a) and *'H'* (x_h, y_h, θ_h) lying on the involute profile of anodic workpiece gear are used to compute its involute profile arc length 'L_{er}' which is given by following equations:

$$L_{er} = \int_{\theta_a=0}^{\theta_h} \sqrt{\left[\left(\frac{dx}{d\theta}\right)^2 + \left(\frac{dy}{d\theta}\right)^2\right]}\, d\theta = \frac{r_b}{2}(\theta_h^2 - \theta_a^2) = \frac{r_b}{2}\theta_h^2 \quad (A23)$$

Equation A23 can also be used to compute the involute profile arc length of anodic workpiece gear flank surface *'L_{lc}'* that will be modified in its lead crowning (as depicted in Fig. 4.7b).

A4. Expressions for Lead Crowning Time at Different Positions of the Anodic Workpiece Gear During its Downward/Upward Reciprocating Motion

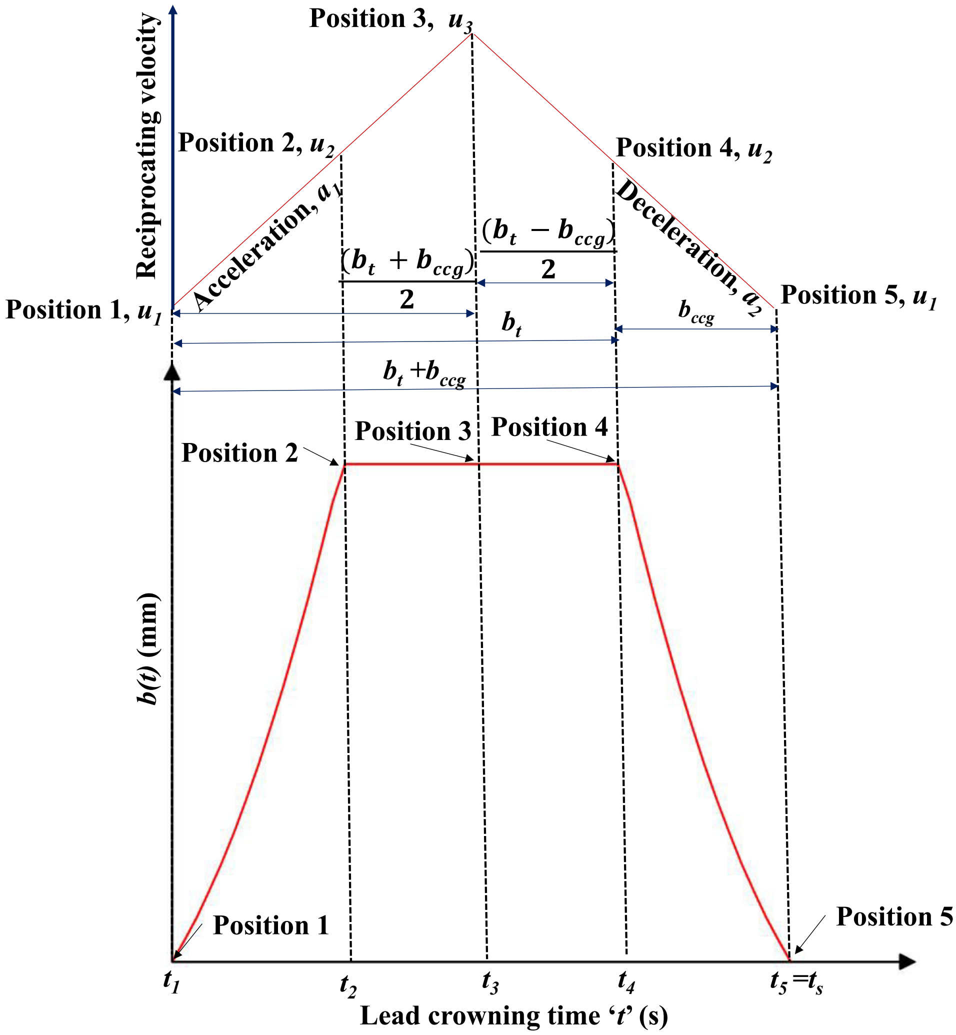

Fig. A3: Graph of variation in '$b(t)$' with lead crowning time combined with graph of variation in reciprocating velocity with distance travelled by workpiece gear.

Acceleration 'a_1' (mm/s^2) during first half of the downward/upward stroke can be obtained by using third equation of motion ($v^2 + u^2 = 2as$):

$$u_3{}^2 - u_1{}^2 = 2a_1\left(\frac{b_t + b_{ccg}}{2}\right) \Rightarrow a_1 = \frac{u_3{}^2 - u_1{}^2}{b_t + b_{ccg}} \qquad (A24)$$

where, 'u_3' is maximum reciprocating velocity and 'u_1' is minimum reciprocating velocity of the anodic workpiece gear (mm/s); 'b_t' is total face width of anodic workpiece gear (mm); 'b_{ccg}' is face width of conductive portion of developed cathode gear for lead crowning (mm).

Similarly, deceleration 'a_2' during second half of the downward/upward stroke:

$$a_2 = \frac{u_1{}^2 - u_3{}^2}{b_t + b_{ccg}} \qquad (A25)$$

Expression for time instant 't_2' using second equation of motion [$s = ut + (1/2)at^2$]:

Distance 'S_{12}' travelled by the workpiece from position 1 and time $t_1 = 0$ to position 2 and time 't_2' is $S_{12} = b_{ccg}$ (Fig. A3). Using second equation of motion following expression is obtained:

$$b_{ccg} = u_1 t_2 + \frac{1}{2} a_1 {t_2}^2 \Rightarrow a_1 {t_2}^2 + 2u_1 t_2 - 2b_{ccg} = 0 \qquad (A26)$$

Solving the equation (A26) for obtaining the expression for 't_2' using Shridhar Acharya formula:

$$t_2 = \frac{-u_1 + \sqrt{{u_1}^2 + 2a_1 b_{ccg}}}{a_1} \qquad (A27)$$

Expression for time instant 't_3' using first equation of motion ($v= u + at$):

$$t_3 = \frac{u_3 - u_1}{a_1} \qquad (A28a)$$

Using expression of 'a_1' from Eq. A24 into Eq. A28a gives the following expression for 't_3':

$$\Rightarrow t_3 = 2\frac{b_t \ + \ b_{ccg}}{u_3 + u_1} \qquad (A28b)$$

Expression for time instant 't_4' using second equation of motion ($s = ut + 0.5at^2$):

Distance 'S_{34}' travelled by the anodic workpiece gear form position 3 to position 4 during 't'_{34}' (Fig. A3) is as follows:

$$S_{34} = \frac{b_t - b_{ccg}}{2} \qquad (A29)$$

Using second equation of motion with distance 'S_{34}', deceleration 'a_2' and time t'_{34} taken by anodic workpiece gear to travel the distance 'S_{34}' gives the following equation:

$$S_{34} = u_3 t'_{34} + \frac{1}{2} a_2 {t'_{34}}^2 \Rightarrow \frac{b_t - b_{ccg}}{2} = u_3 t'_{34} + \frac{1}{2} a_2 {t'_{34}}^2$$

$$\Rightarrow \ a_2 {t'_{34}}^2 + 2u_3 t'_{34} - (b_t - b_{ccg}) = 0 \qquad (A30)$$

Solving the equation (A30) using Shridhar Acharya formula the gives the following equation for t'_{34}:

$$t'_{34} = \frac{-u_3 + \sqrt{{u_3}^2 + a_2(b_t - b_{ccg})}}{a_2} \qquad (A31)$$

From Fig. A3 't_4' can be expressed as $\boldsymbol{t_4 = t_3 + t'_{34}}$ and using expression of time 't_3' from Eq. A28a and t'34 form Eq. A31 give the following equation for time 't_4':

$$t_4 = t_3 + t'_{34} \Rightarrow t_4 = \frac{u_3 - u_1}{a_1} + \left(\frac{-u_3 + \sqrt{{u_3}^2 + a_2(b_t - b_{ccg})}}{a_2} \right) \qquad (A32)$$

Expression for time instant 't_5':

The acceleration and deceleration 'a_1' and 'a_2' are equal in magnitude hence the time 't'_{13}' taken by workpiece gear to travel from position 1 to position 3 (half of the stroke length in first half of upward/downward stroke) is equal to the time 't'_{35}' taken to travel from position 3 to position 5 (the half of the stroke in second half of upward/downward stroke).

$$t'_{13} = t'_{35} = t_3$$

Using expression of 't_3' from Eq. A28 the expression for 't_5' is obtained as follows:

$$t_5 = t'_{13} + t'_{35} = 2t_3 \Rightarrow t_5 = 2\frac{u_3 - u_1}{a_1} \qquad (A33)$$

Time for completion of one stroke during downward/upward stroke of the workpiece gear 't_s' is equal to the time 't_5'.

The expression of lead crowning time of first downward/upward stroke further used to obtain the expression of second upward/downward stroke and n^{th} stroke as mentioned in Table 4.2. The expression for '$b(t)$' can be obtained using second equation of motion ($s = ut + 0.5at^2$).

Appendix-B: Results of Microgeometry Measurement for Different Flank Modifications

B1: For Validation of the Developed Analytical Model for Tip Relief

- **Stage 3a Exp. No. 1 for Tip Relief Model**

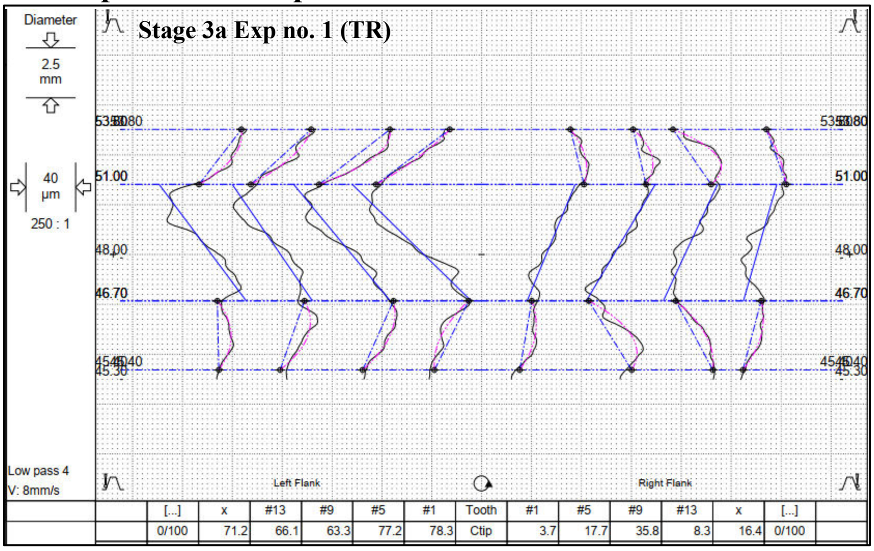

- **Stage 3a Exp. No. 2 for Tip Relief Model**

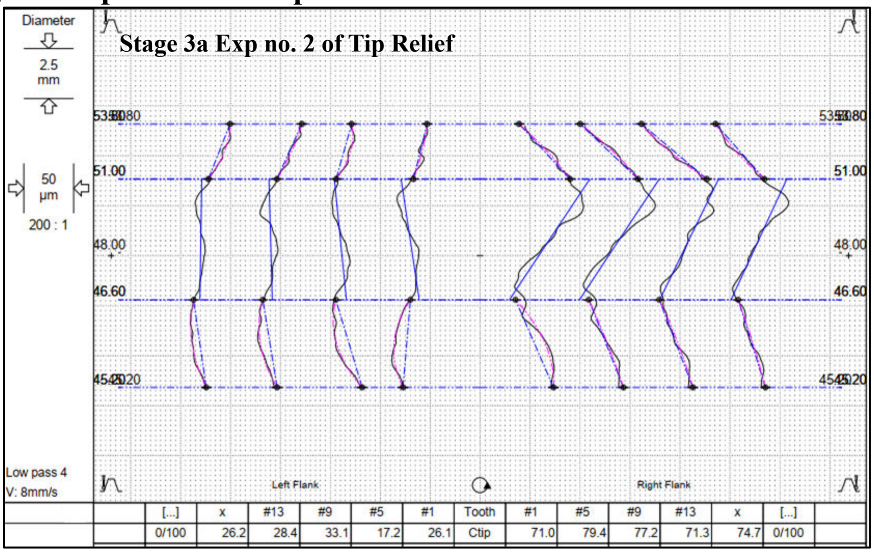

- **Stage 3a Exp. No. 3 for Tip Relief Model**

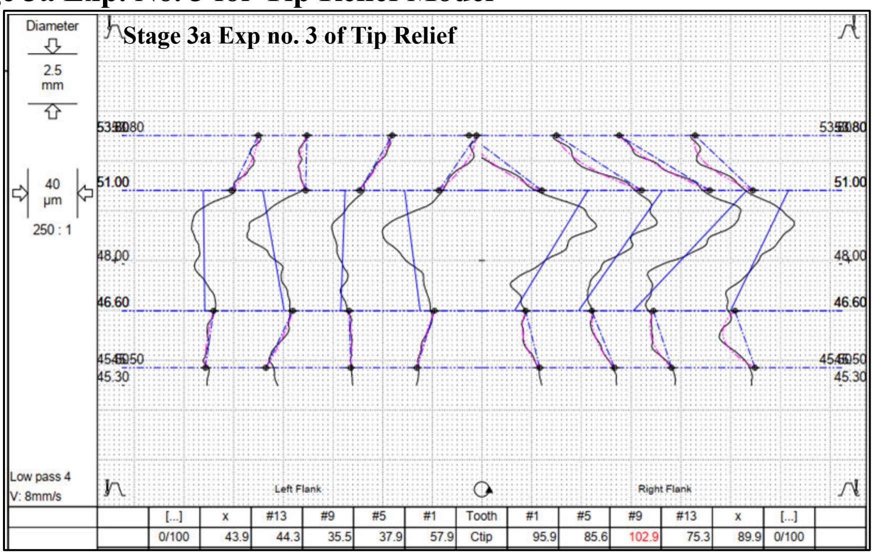

- **Stage 3a Exp. No. 4 for Tip Relief Model**

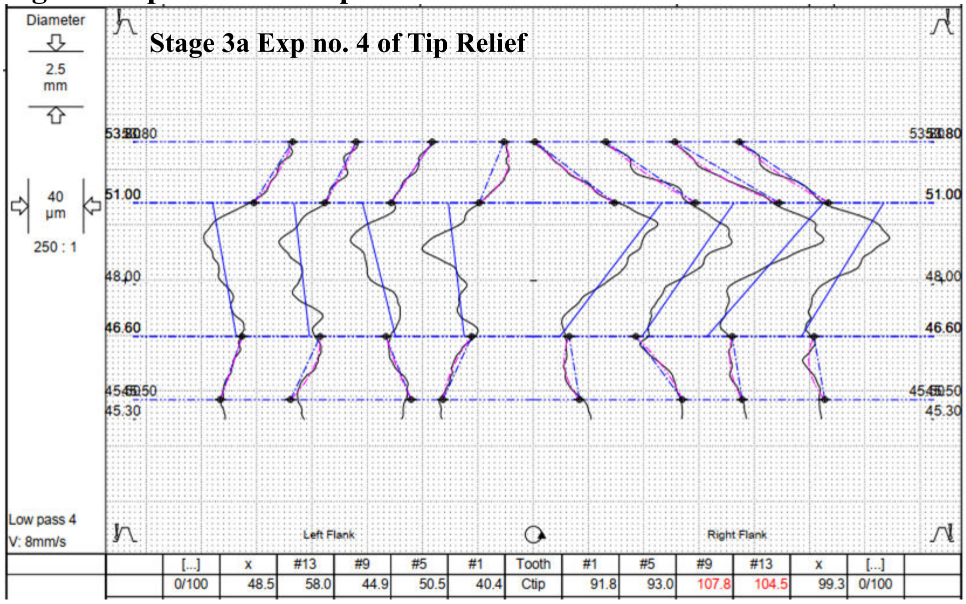

- **Stage 3a Exp. No. 5 for Tip Relief Model**

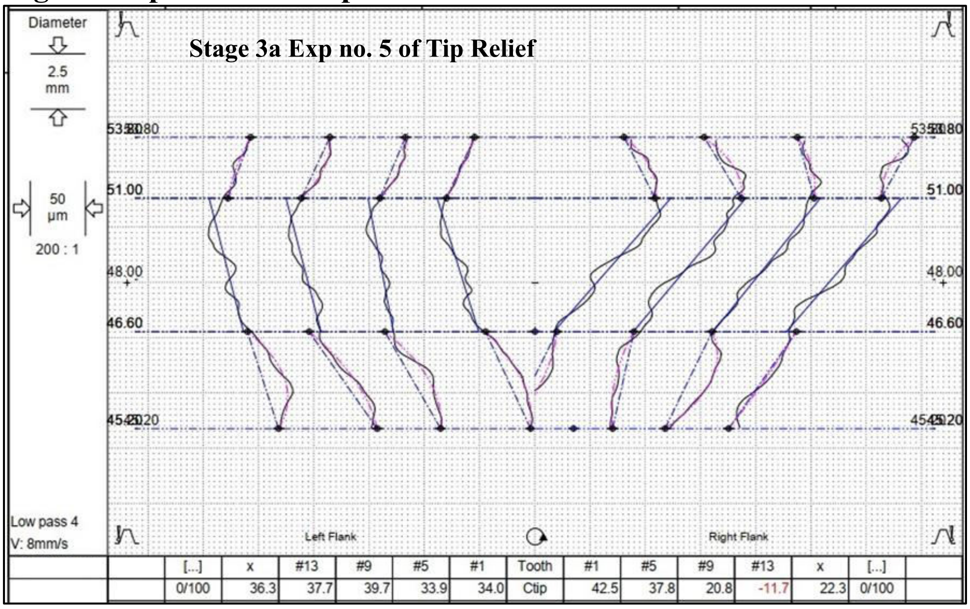

- **Stage 3a Exp. No. 6 for Tip Relief Model**

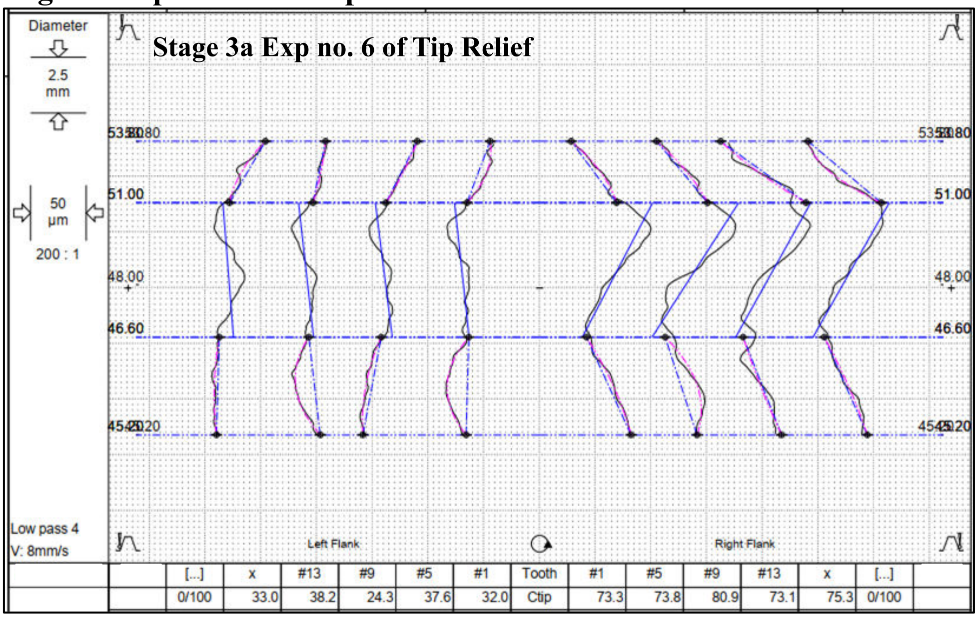

- **Stage 3a Exp. No. 7 for Tip Relief Model**

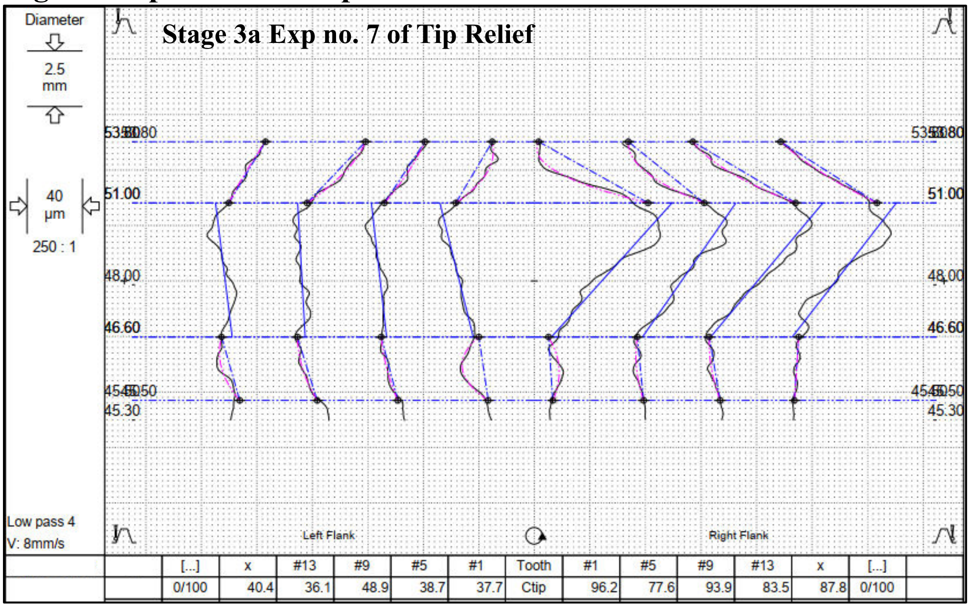

- **Stage 3a Exp. No. 8 for Tip Relief Model**

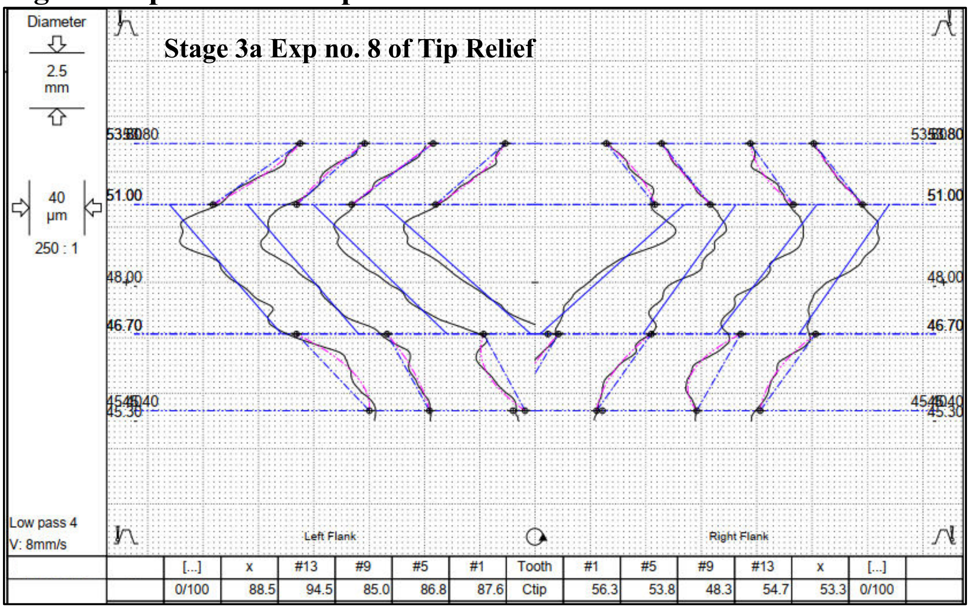

- **Stage 3a Exp. No. 9 for Tip Relief Model**

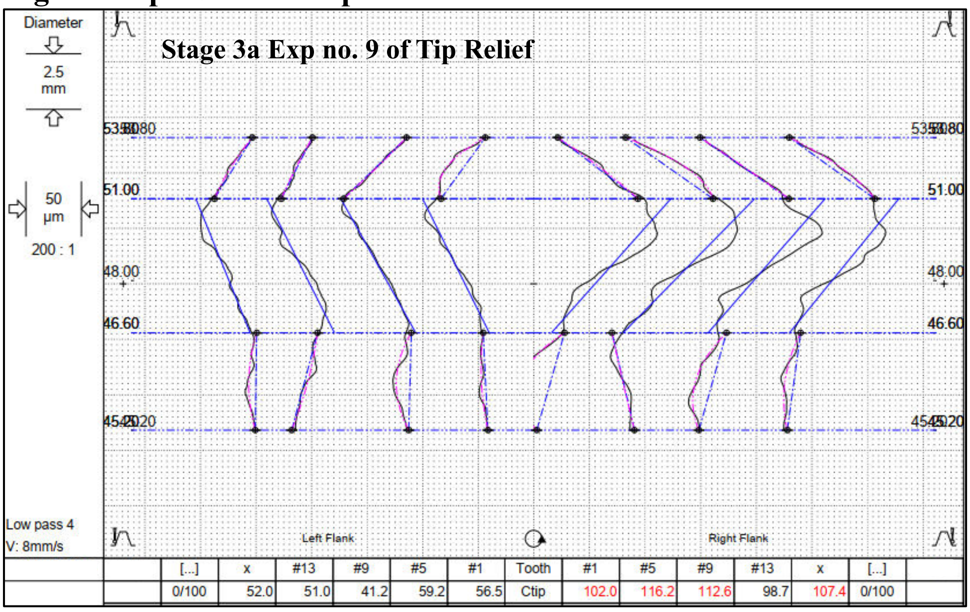

- **Stage 3a Exp. No. 10 for Tip Relief Model**

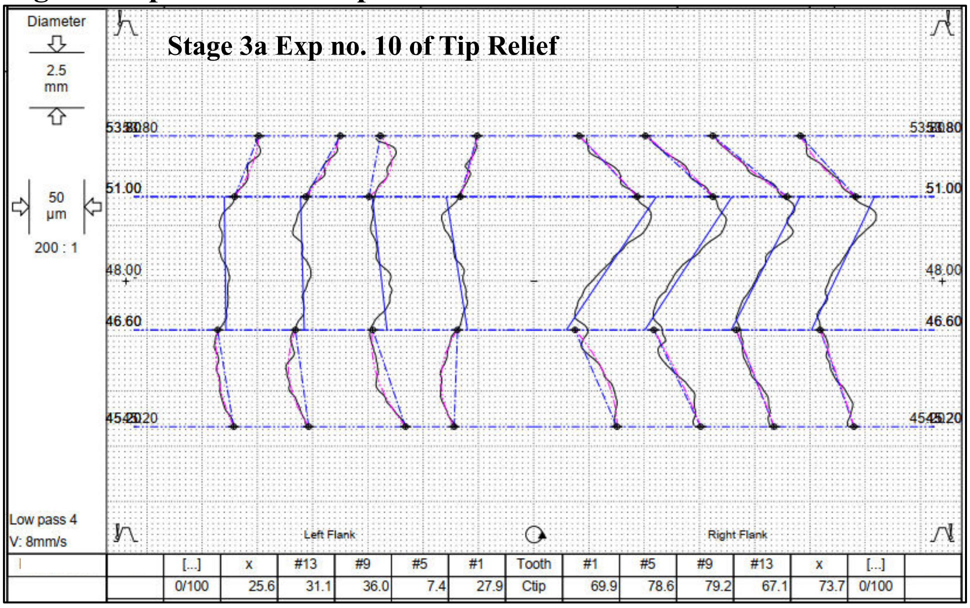

- **Stage 3a Exp. No. 11 for Tip Relief Model**

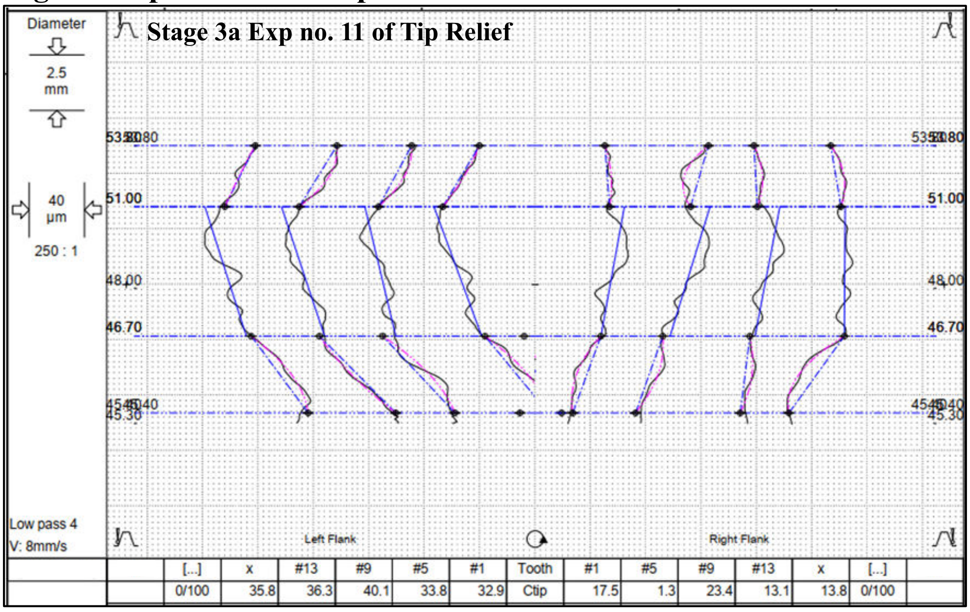

- **Stage 3a Exp. No. 12 for Tip Relief Model**

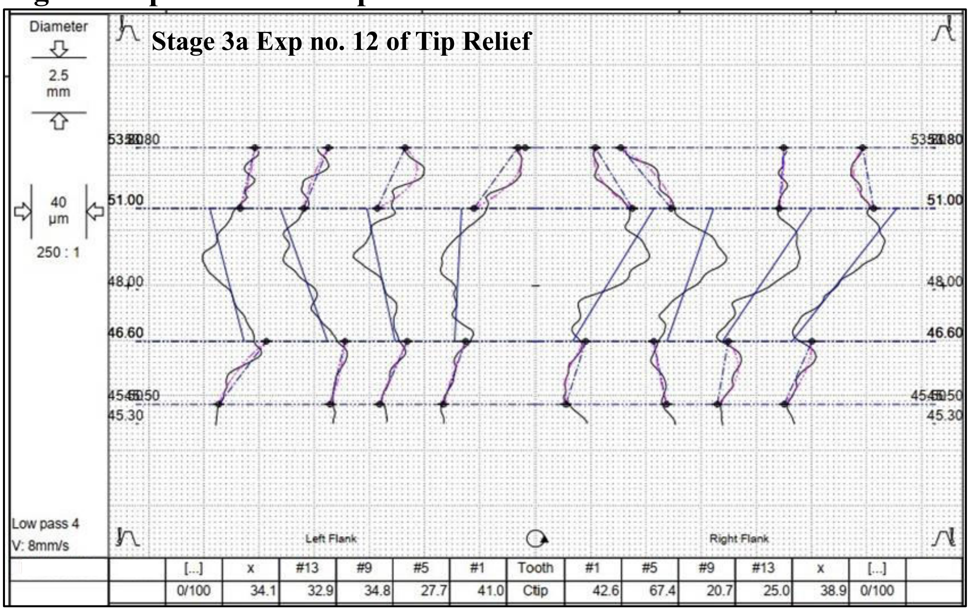

B2: For Validation of the Developed Analytical Model for Root Relief

- **Stage 3a Exp. No. 1 for Root Relief Model**

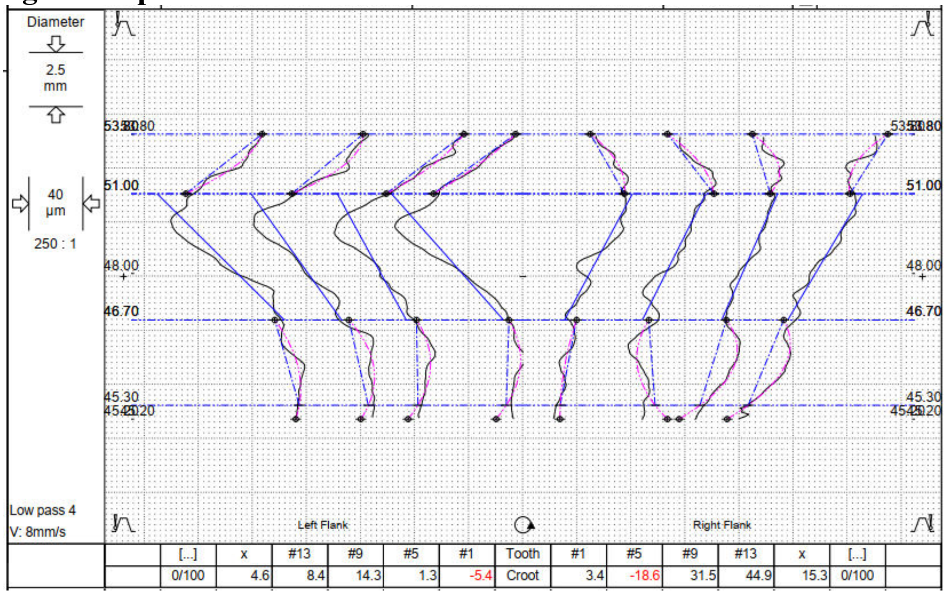

- **Stage 3a Exp. No. 2 for Root Relief Model**

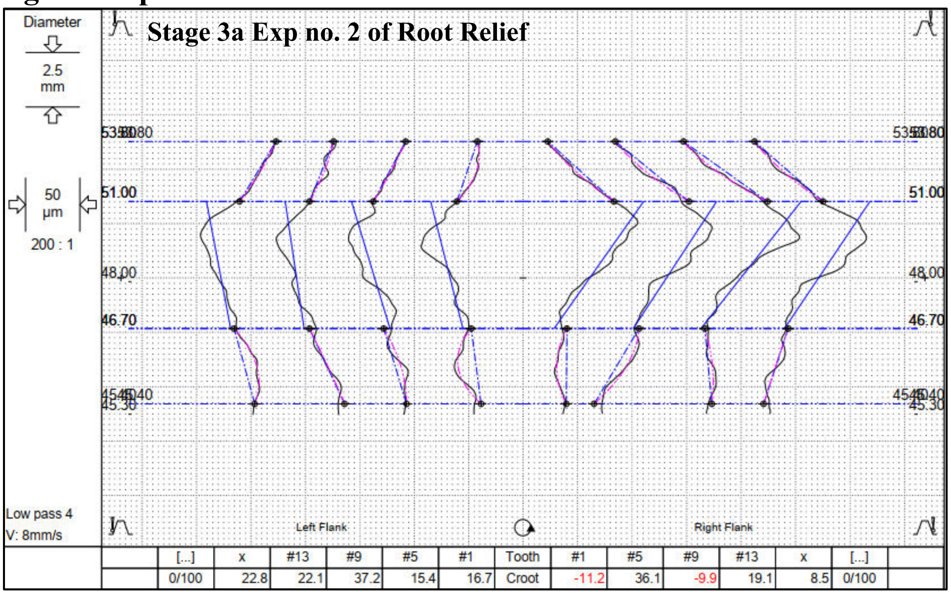

- **Stage 3a Exp. No. 3 for Root Relief Model**

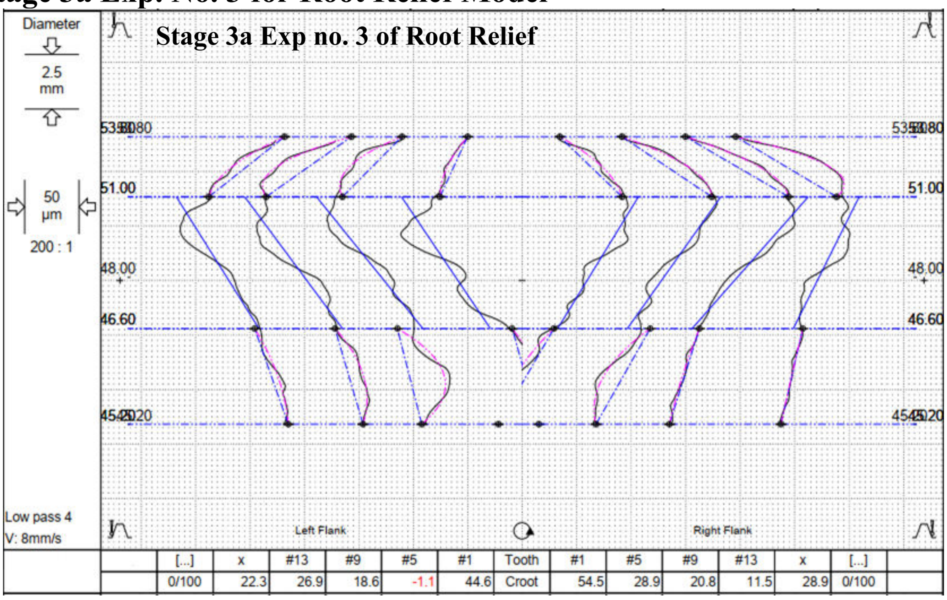

- **Stage 3a Exp. No. 4 for Root Relief Model**

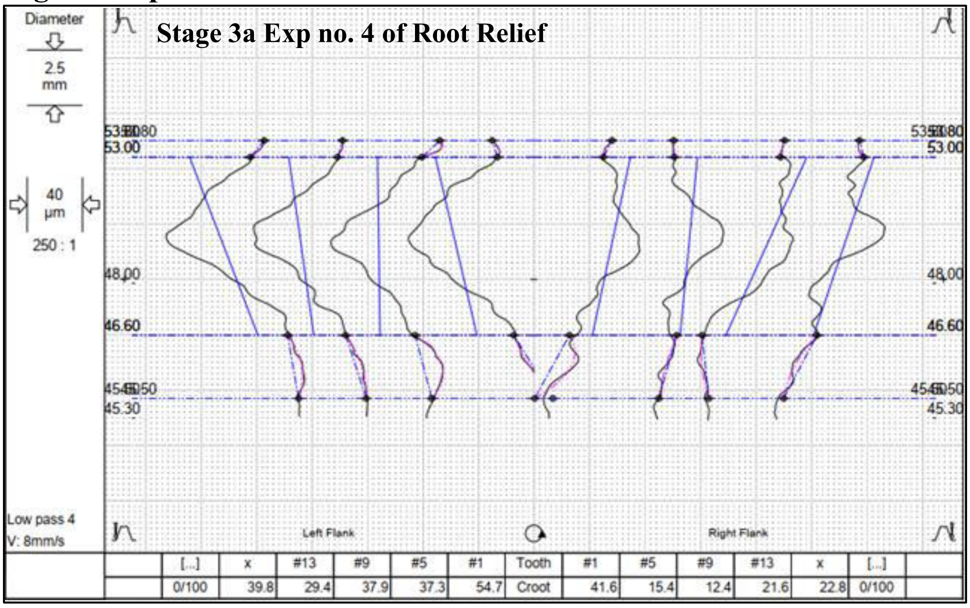

- **Stage 3a Exp. No. 5 for Root Relief Model**

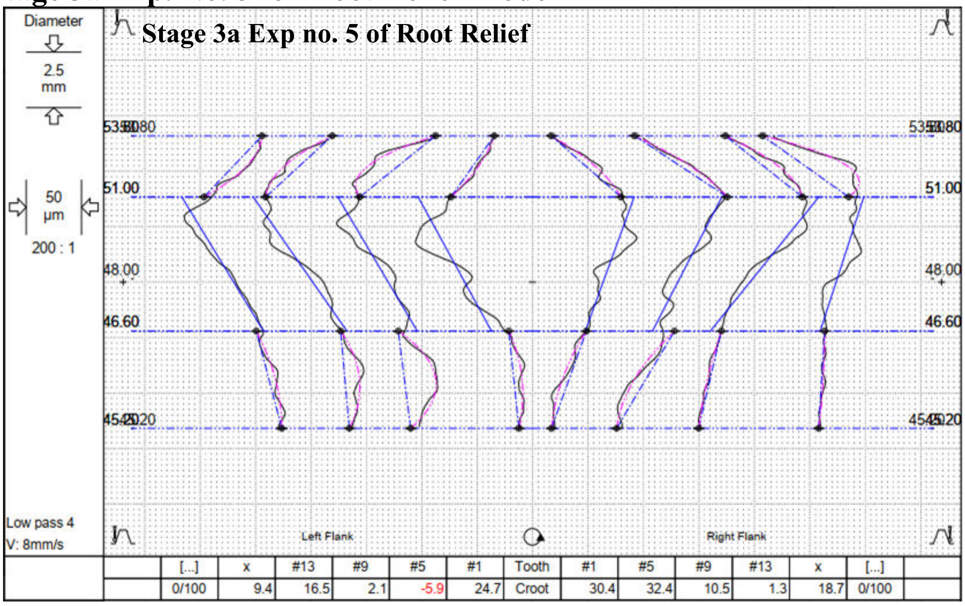

- **Stage 3a Exp. No. 6 for Root Relief Model**

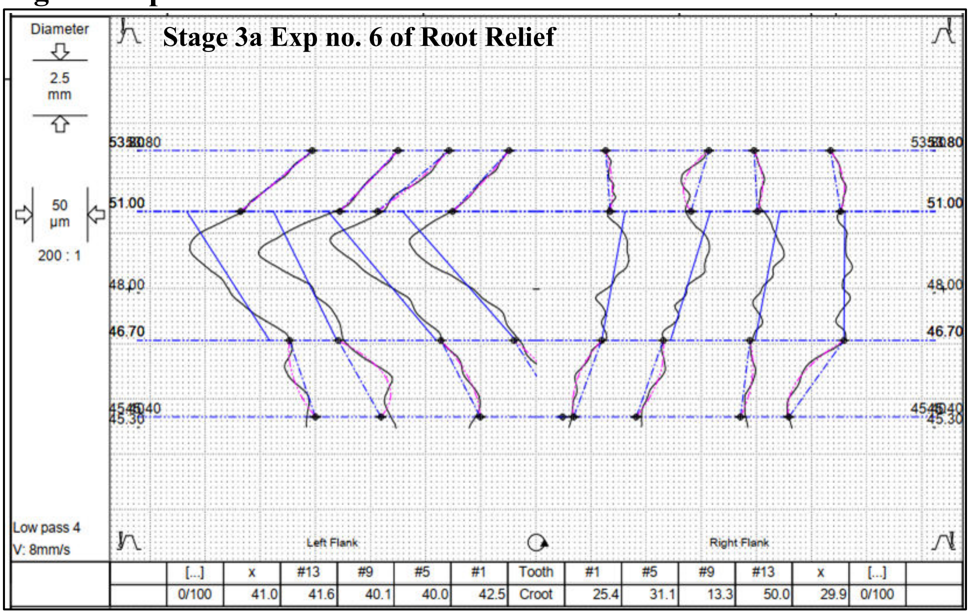

- **Stage 3a Exp. No. 7 for Root Relief Model**

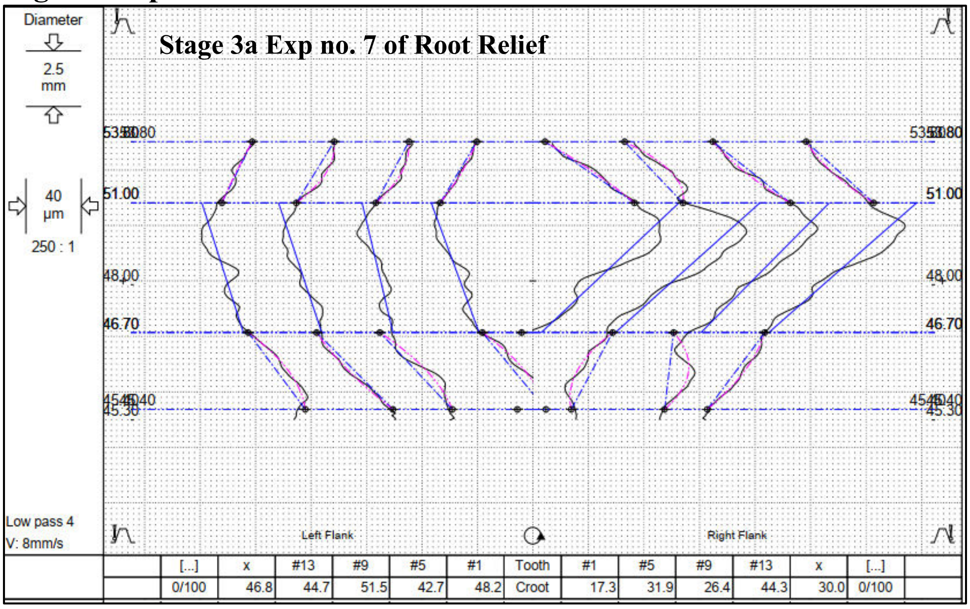

- **Stage 3a Exp. No. 8 for Root Relief Model**

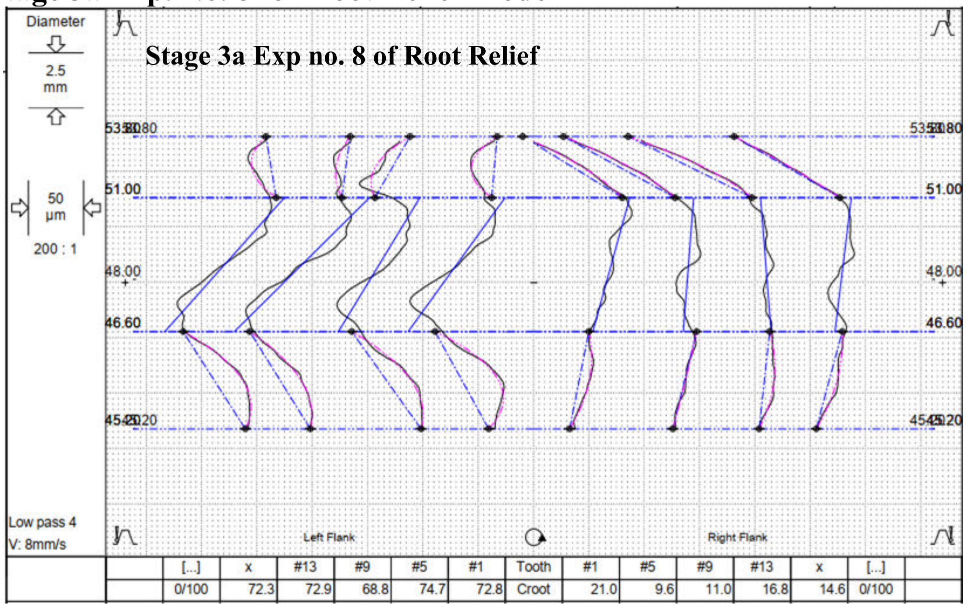

- **Stage 3a Exp. No. 9 for Root Relief Model**

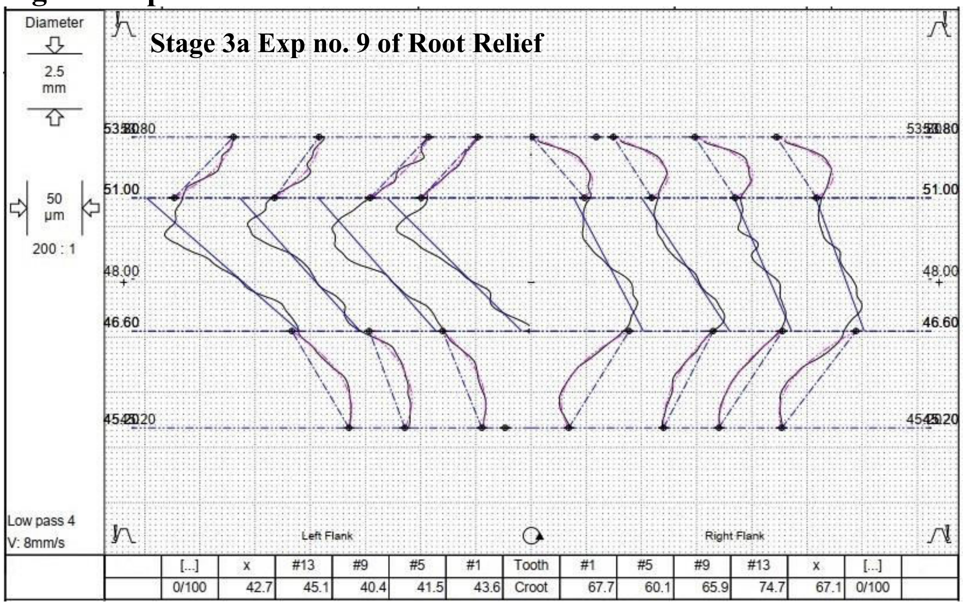

- **Stage 3a Exp. No. 10 for Root Relief Model**

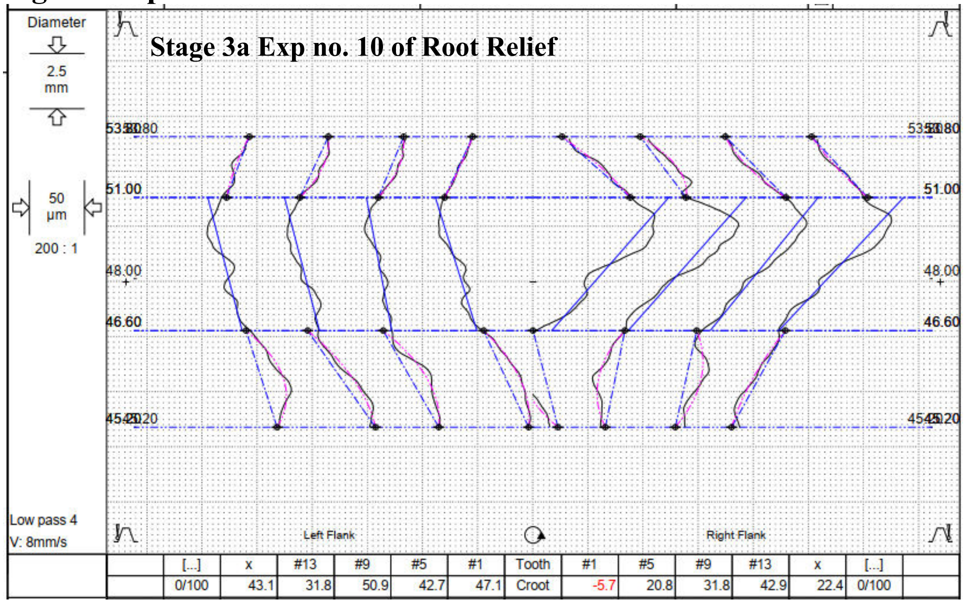

- **Stage 3a Exp. No. 11 for Root Relief Model**

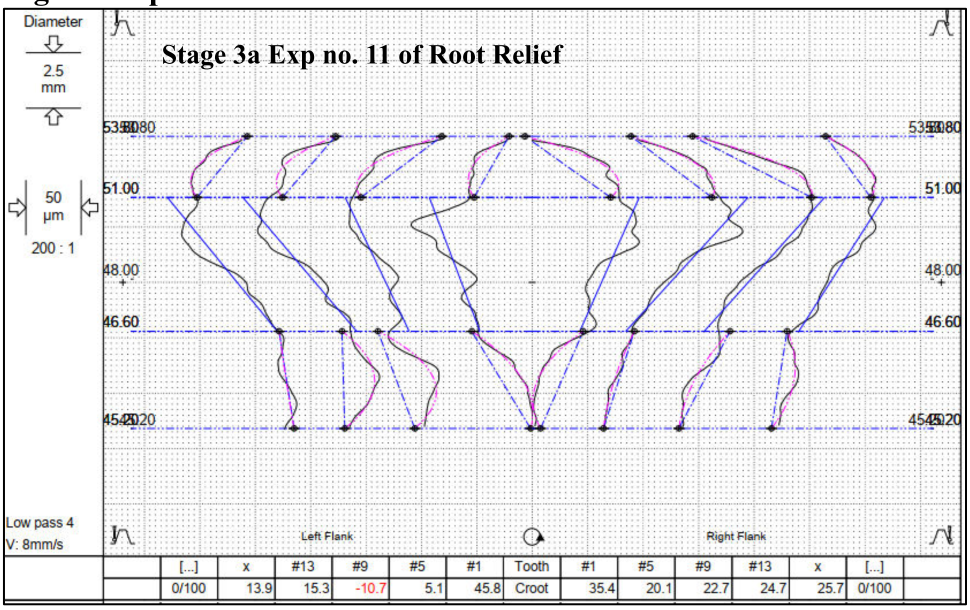

- **Stage 3a Exp. No. 12 for Root Relief Model**

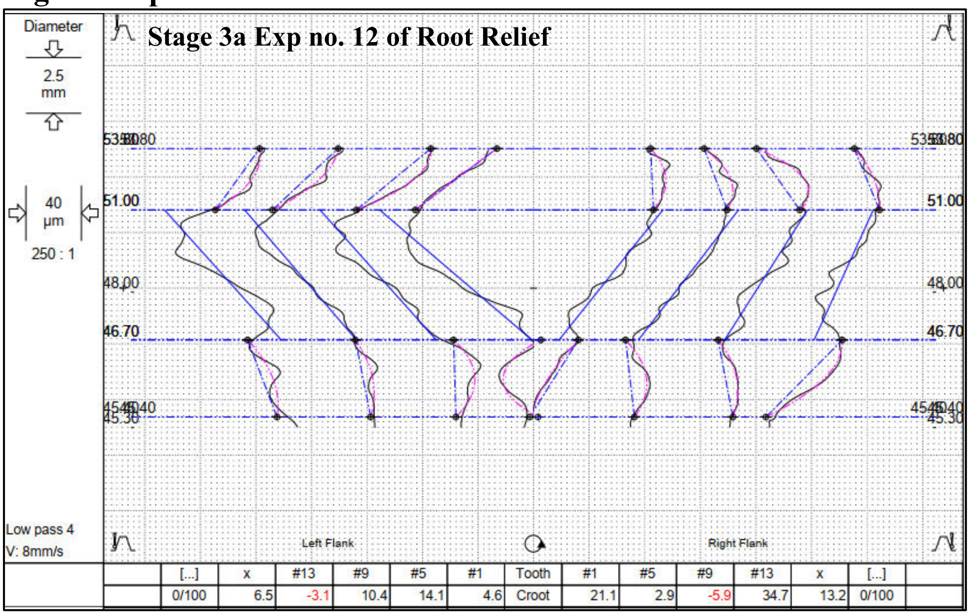

B3: For Validation of the Developed Analytical Model for End Relief

- **Stage 3a Exp. No. 1 for End Relief Model**

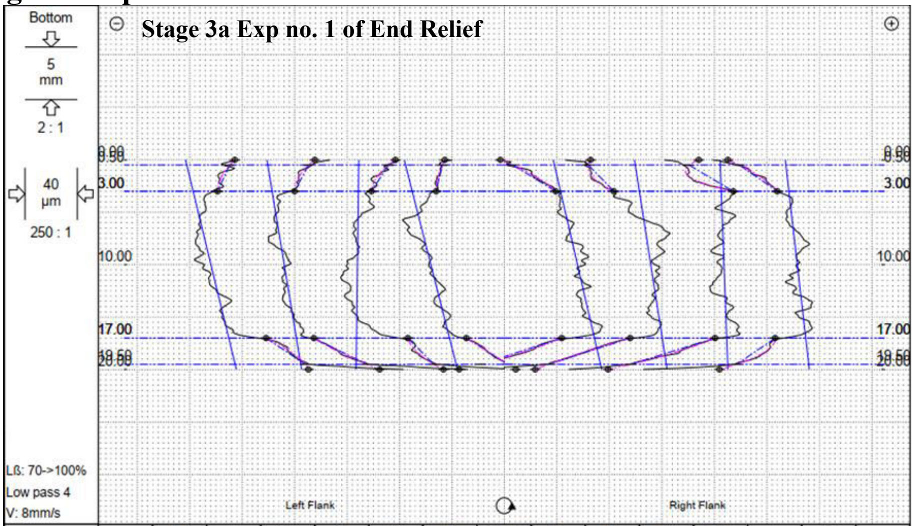

	[...]	x	#13	#9	#5	#1	Tooth	#1	#5	#9	#13	x	[...]
	0/100	29.4	31.8	32.6	28.2	24.8	Cbttm	45.9	37.2	17.2	46.6	36.7	0/100
	0/100	60.4	60.9	63.6	66.3	50.6	Ctop	103.2	97.0	90.6	65.9	89.2	0/100

- **Stage 3a Exp. No. 2 for End Relief Model**

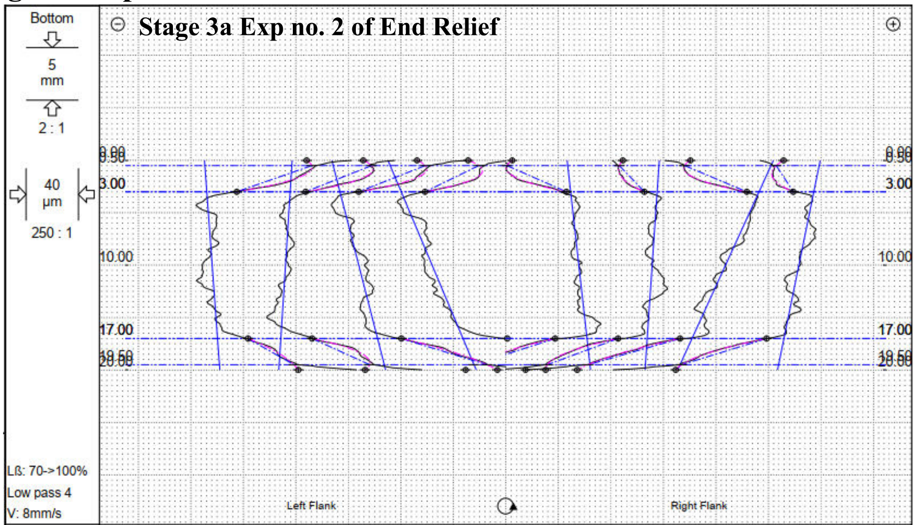

	[...]	x	#13	#9	#5	#1	Tooth	#1	#5	#9	#13	x	[...]
	0/100	60.4	76.2	55.7	58.7	50.9	Cbttm	44.6	26.2	52.3	23.0	36.5	0/100
	0/100	66.3	61.6	64.4	91.4	47.7	Ctop	92.6	77.5	87.7	82.6	85.1	0/100

- **Stage 3a Exp. No. 3 for End Relief Model**

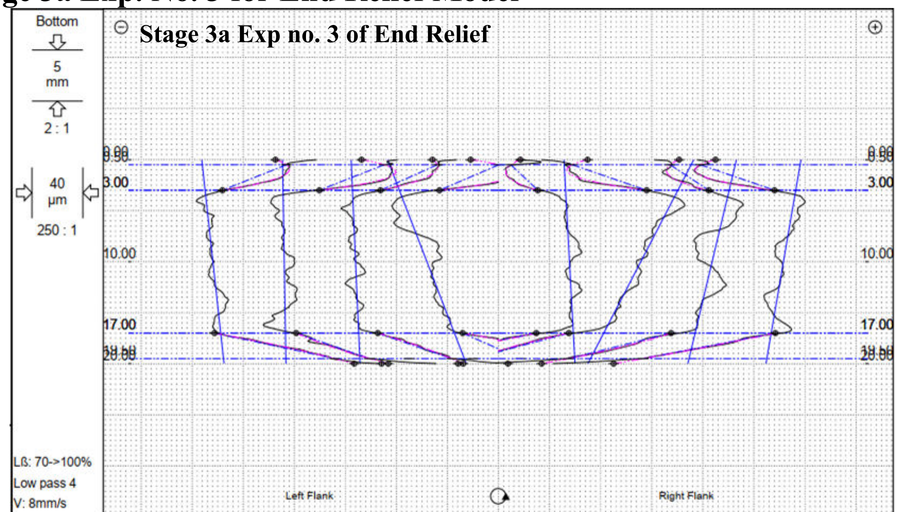

	[...]	x	#13	#9	#5	#1	Tooth	#1	#5	#9	#13	x	[...]
	0/100	58.9	55.1	61.6	62.8	56.0	Cbttm	35.5	70.8	39.2	63.0	52.1	0/100
	0/100	77.4	104.8	80.7	82.0	42.0	Ctop	150.4	114.4	120.5	123.7	127.2	0/100

- **Stage 3a Exp. No. 4 for End Relief Model**

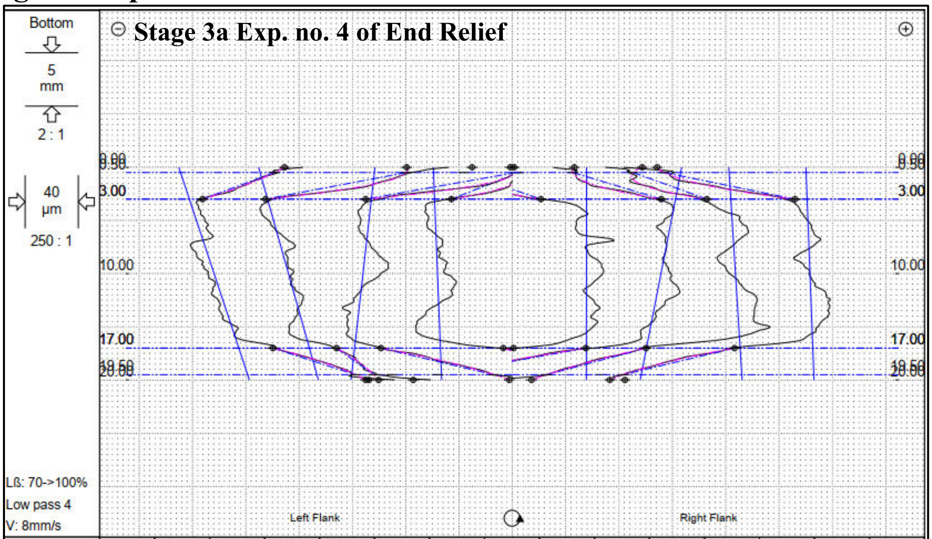

[...]	x	#13	#9	#5	#1	Tooth	#1	#5	#9	#13	x	[...]
0/100	85.0	71.5	104.4	107.2	56.9	Cbttm	86.0	76.1	66.5	112.7	85.3	0/100
0/100	100.4	95.2	51.9	116.0	138.6	Ctop	163.4	175.2	156.7	152.5	161.9	0/100

- **Stage 3a Exp. No. 5 for End Relief Model**

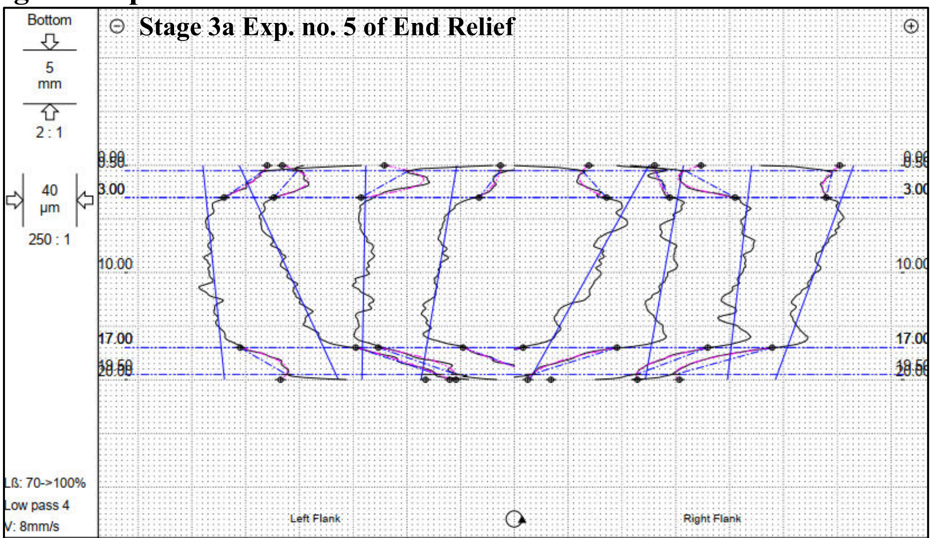

[...]	x	#13	#9	#5	#1	Tooth	#1	#5	#9	#13	x	[...]
0/100	29.3	45.6	21.0	14.3	36.5	Cbttm	31.3	17.2	34.9	1.5	21.2	0/100
0/100	75.1	44.2	94.0	69.5	92.7	Ctop	90.9	91.9	69.8	80.3	83.2	0/100

- **Stage 3a Exp. No. 6 for End Relief Model**

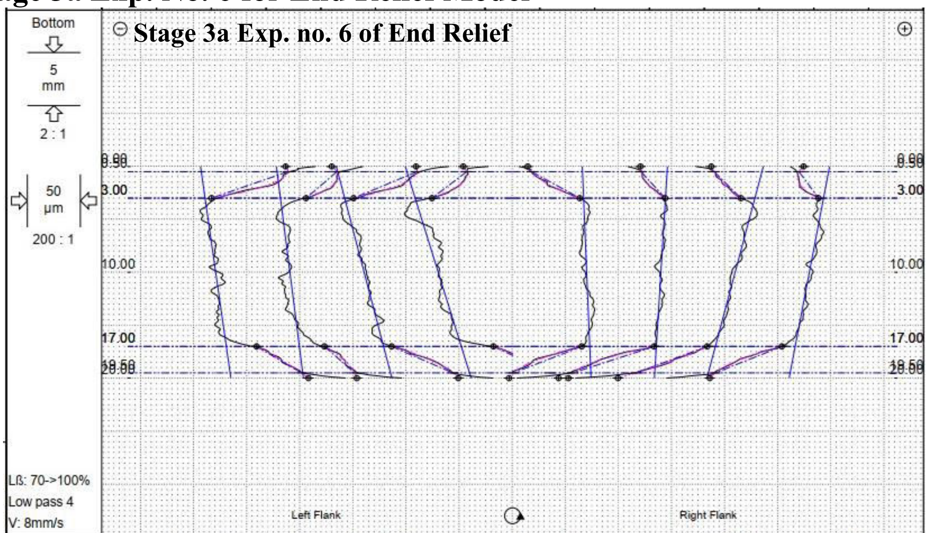

[...]	x	#13	#9	#5	#1	Tooth	#1	#5	#9	#13	x	[...]
0/100	59.2	75.8	48.3	67.2	45.3	Cbttm	52.7	23.7	41.1	18.8	34.1	0/100
0/100	73.4	77.4	54.2	70.3	91.7	Ctop	76.1	83.0	91.8	80.5	82.9	0/100

- **Stage 3a Exp. No. 7 for End Relief Model**

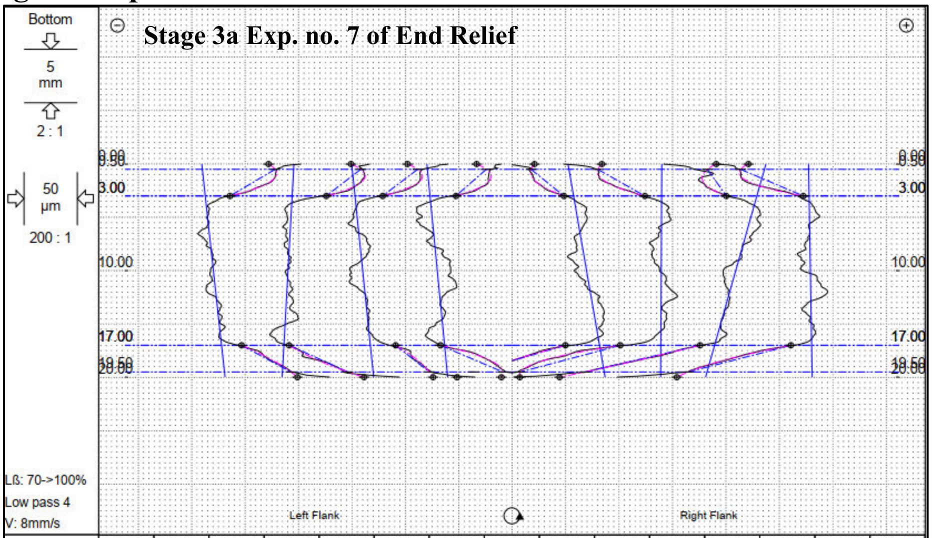

	[...]	x	#13	#9	#5	#1	Tooth	#1	#5	#9	#13	x	[...]
	0/100	51.9	59.3	55.1	49.3	43.7	Cbttm	36.6	55.9	38.0	56.9	46.9	0/100
	0/100	64.6	71.1	75.2	58.9	53.3	Ctop	133.6	132.1	145.4	126.3	134.4	0/100

- **Stage 3a Exp. No. 8 for End Relief Model**

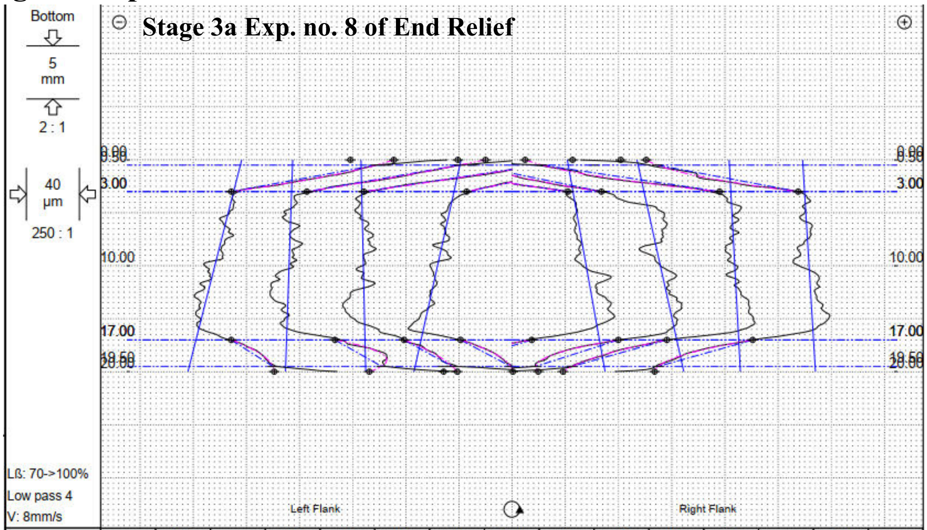

	[...]	x	#13	#9	#5	#1	Tooth	#1	#5	#9	#13	x	[...]
	0/100	137.9	120.7	146.2	158.9	125.6	Cbttm	167.7	140.3	154.9	119.2	145.5	0/100
	0/100	65.0	59.0	62.3	69.5	69.1	Ctop	117.4	104.4	132.3	119.7	118.4	0/100

- **Stage 3a Exp. No. 9 for End Relief Model**

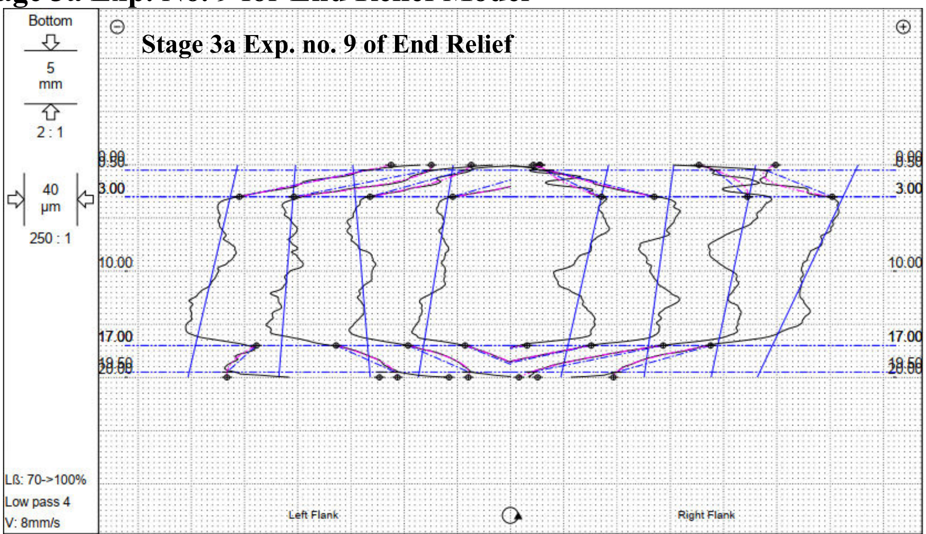

	[...]	x	#13	#9	#5	#1	Tooth	#1	#5	#9	#13	x	[...]
	0/100	95.4	121.0	104.2	87.2	69.1	Cbttm	46.4	102.3	37.6	50.8	59.3	0/100
	0/100	68.1	23.8	87.4	75.7	85.7	Ctop	141.9	150.2	149.6	119.6	140.3	0/100

- **Stage 3a Exp. No. 10 for End Relief Model**

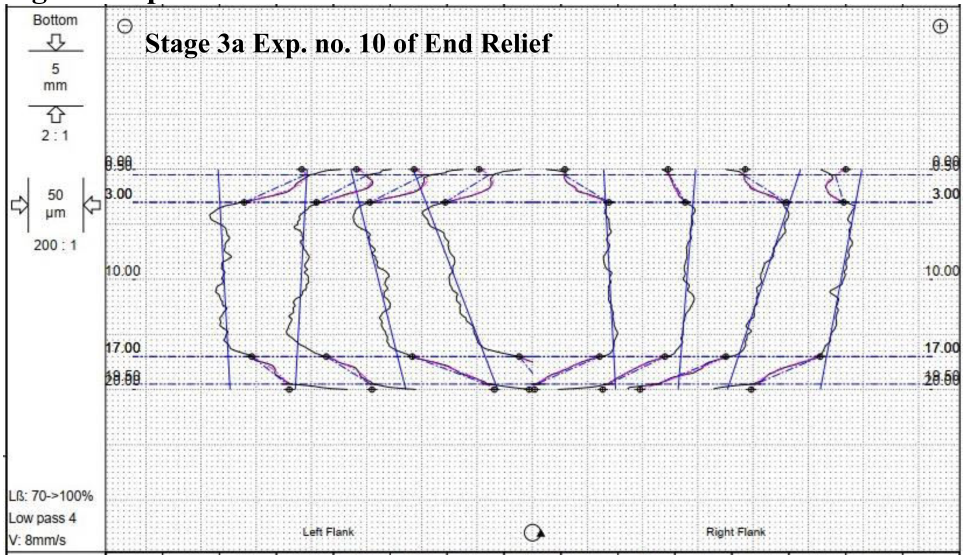

[...]	x	#13	#9	#5	#1	Tooth	#1	#5	#9	#13	x	[...]
0/100	54.7	74.2	46.6	49.9	48.3	Cbttm	36.9	22.6	40.2	8.9	27.1	0/100
0/100	64.0	55.5	67.9	87.9	44.9	Ctop	76.7	70.8	89.2	68.4	76.3	0/100

- **Stage 3a Exp. No. 11 for End Relief Model**

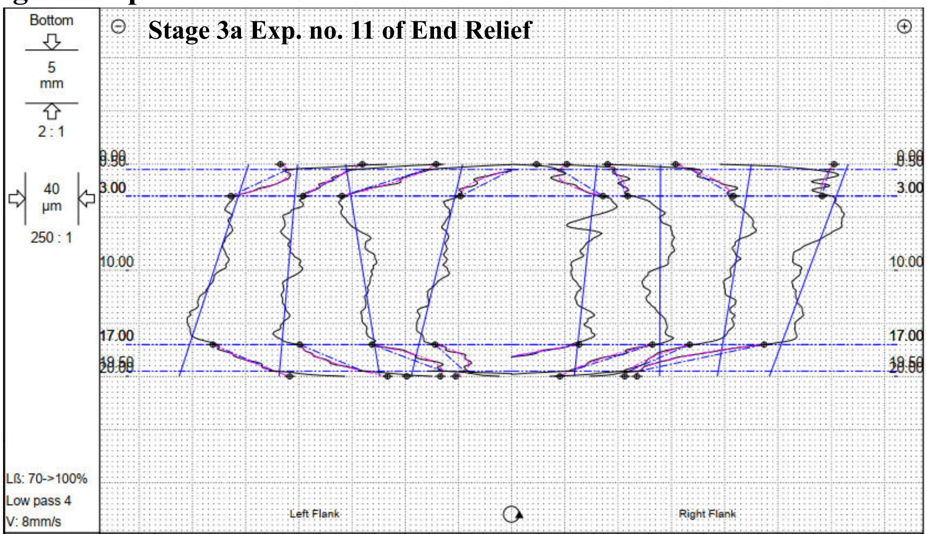

[...]	x	#13	#9	#5	#1	Tooth	#1	#5	#9	#13	x	[...]
0/100	52.1	31.8	50.8	64.3	61.3	Cbttm	20.1	39.7	53.2	1.7	28.6	0/100
0/100	58.0	75.3	79.6	49.5	27.6	Ctop	128.6	75.2	73.6	108.6	96.5	0/100

- **Stage 3a Exp. No. 12 for End Relief Model**

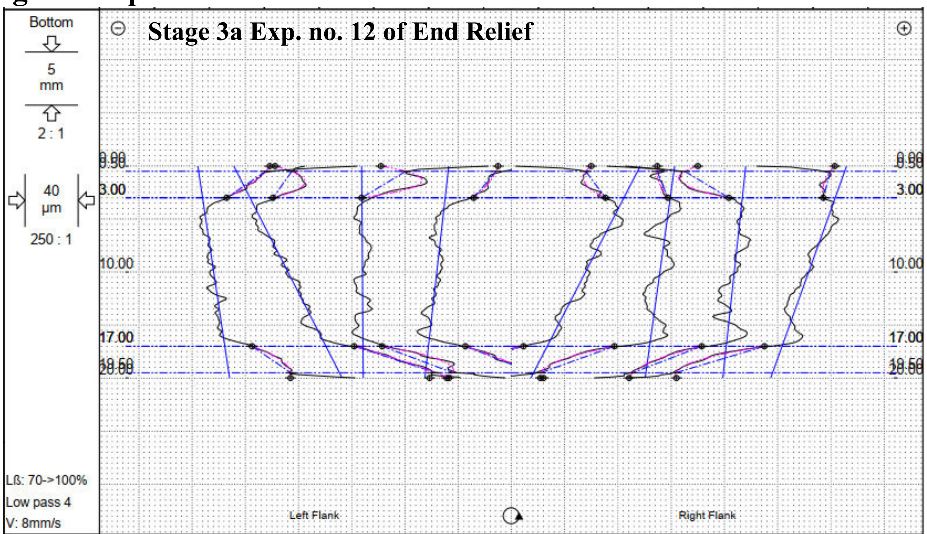

[...]	x	#13	#9	#5	#1	Tooth	#1	#5	#9	#13	x	[...]
0/100	30.9	50.6	18.7	14.4	39.9	Cbttm	24.5	9.7	33.4	.2	16.9	0/100
0/100	72.9	49.5	92.6	63.0	86.7	Ctop	88.5	82.2	73.0	79.4	80.8	0/100

B4: For Validation of the Developed Analytical Model for Lead Crowning

- **Stage 3a Exp. No. 1 for Lead Crowning Model**

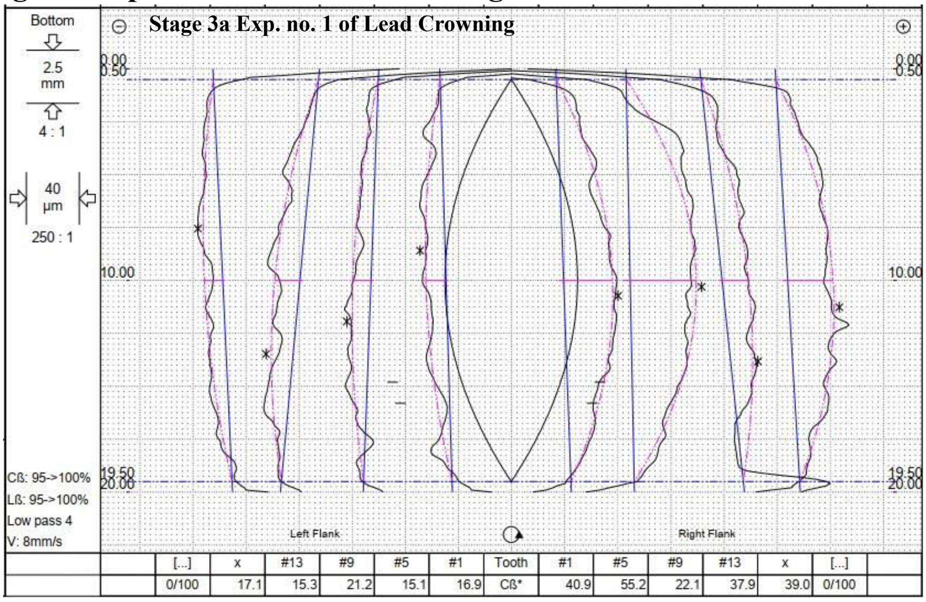

- **Stage 3a Exp. No. 2 for Lead Crowning Model**

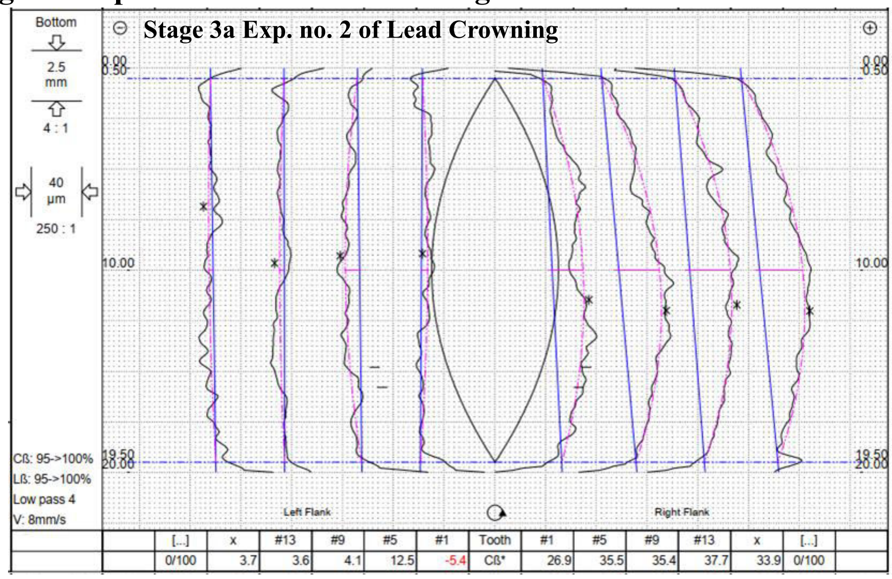

- **Stage 3a Exp. No. 3 for Lead Crowning Model**

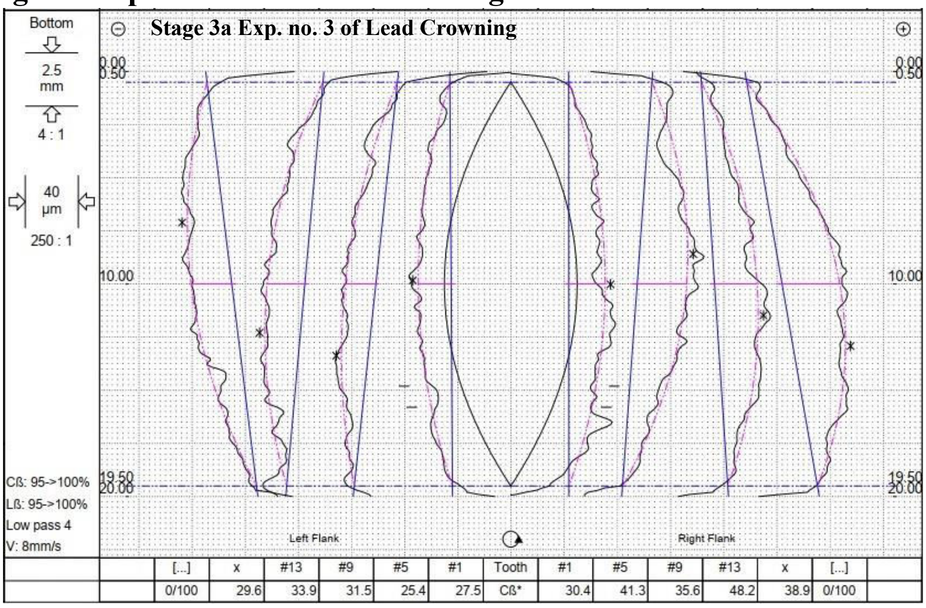

- **Stage 3a Exp. No. 4 for Lead Crowning Model**

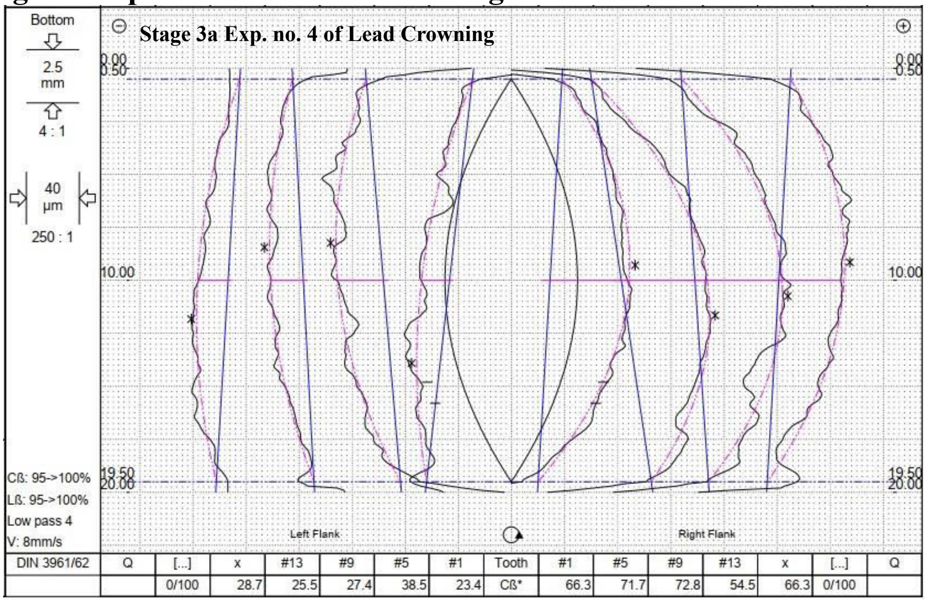

- **Stage 3a Exp. No. 5 for Lead Crowning Model**

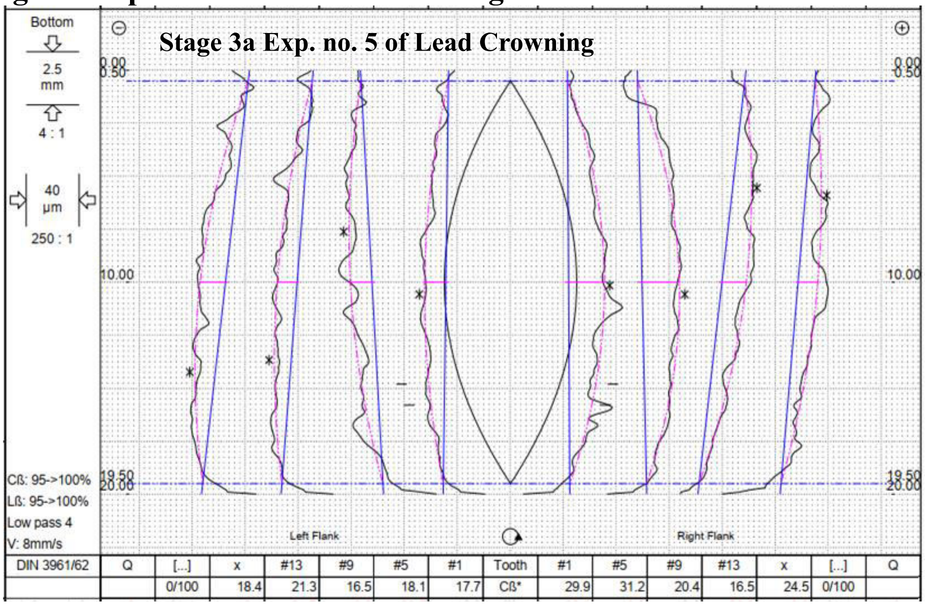

- **Stage 3a Exp. No. 6 for Lead Crowning Model**

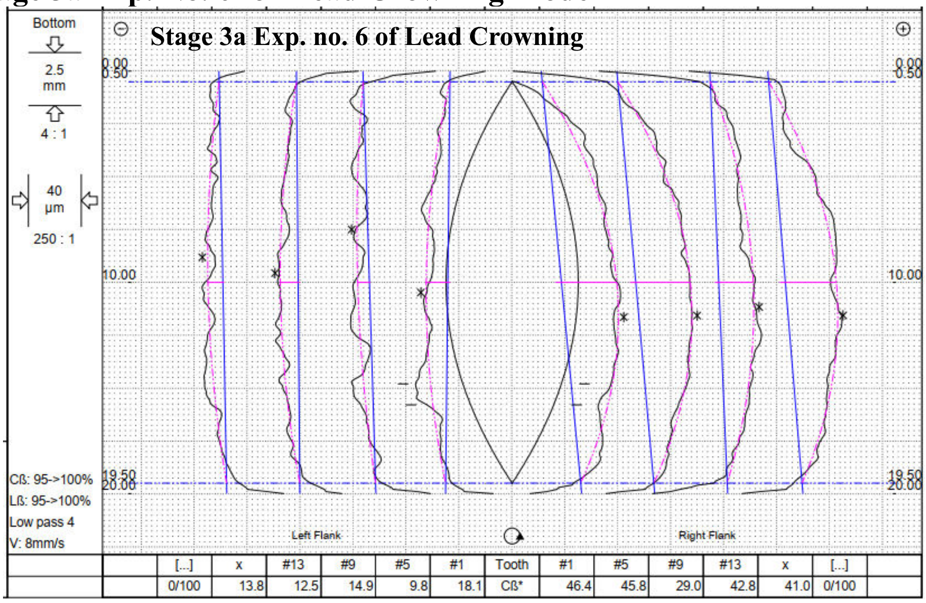

- **Stage 3a Exp. No. 7 for Lead Crowning Model**

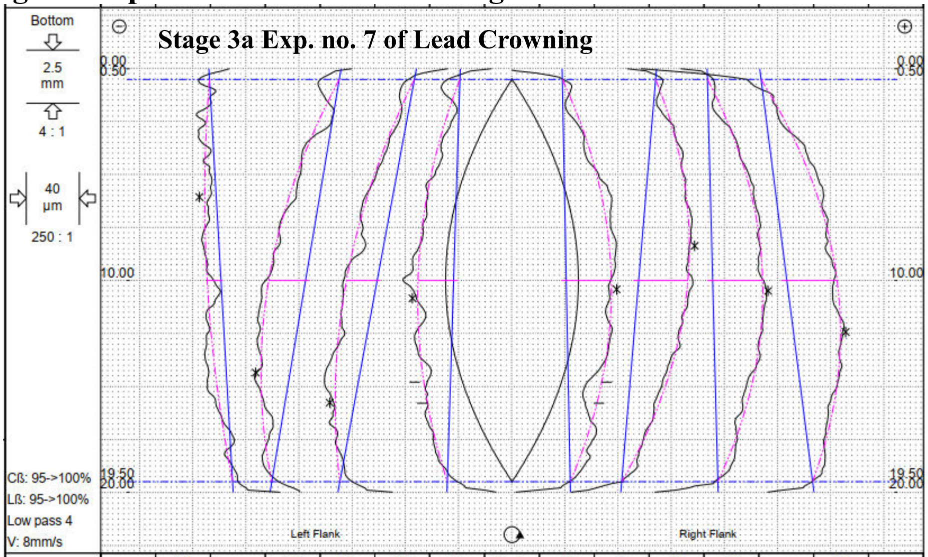

[...]	x	#13	#9	#5	#1	Tooth	#1	#5	#9	#13	x	[...]
0/100	24.4	11.6	30.8	25.6	29.7	Cß*	37.6	41.0	41.8	42.0	40.6	0/100

- **Stage 3a Exp. No. 8 for Lead Crowning Model**

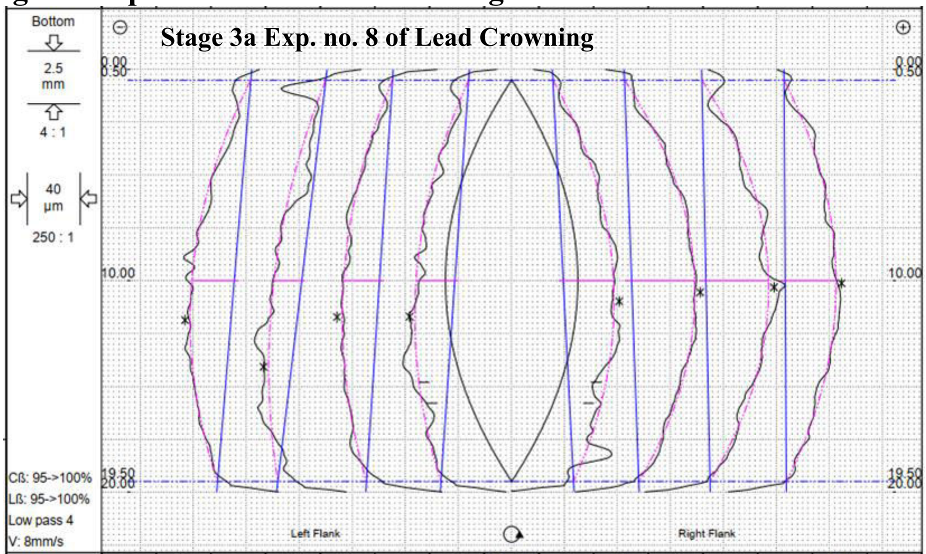

[...]	x	#13	#9	#5	#1	Tooth	#1	#5	#9	#13	x	[...]
0/100	30.3	35.4	23.3	30.0	32.4	Cß*	42.1	52.8	52.5	42.8	47.5	0/100

- **Stage 3a Exp. No. 9 for Lead Crowning Model**

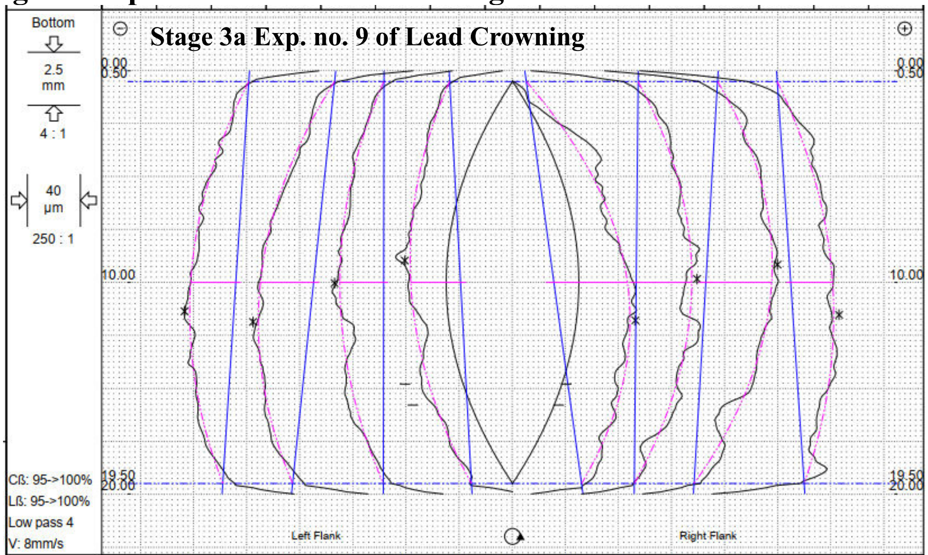

[...]	x	#13	#9	#5	#1	Tooth	#1	#5	#9	#13	x	[...]
0/100	40.1	37.8	44.5	36.6	41.6	Cß*	61.4	46.4	55.0	35.1	49.5	0/100

- **Stage 3a Exp. No. 10 for Lead Crowning Model**

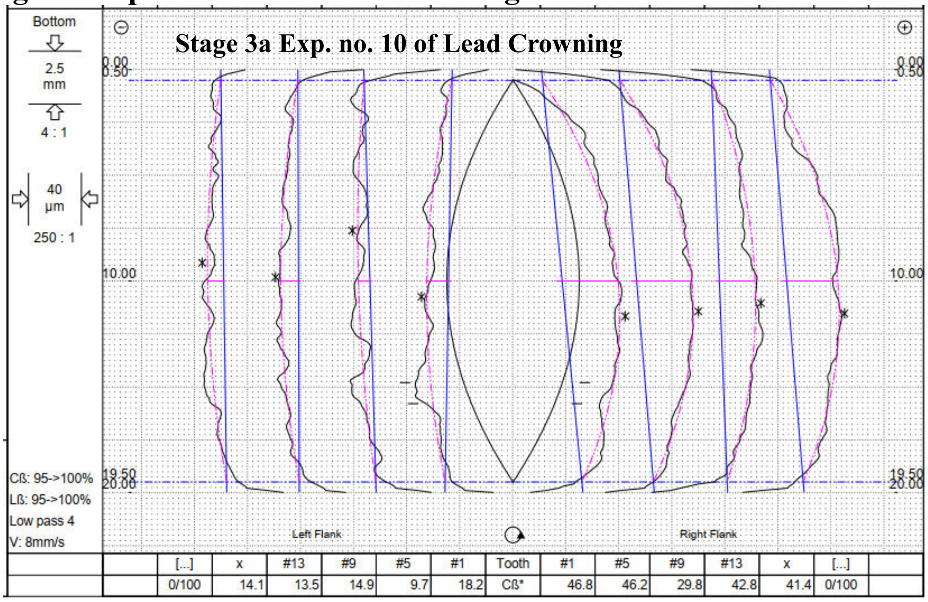

- **Stage 3a Exp. No. 11 for Lead Crowning Model**

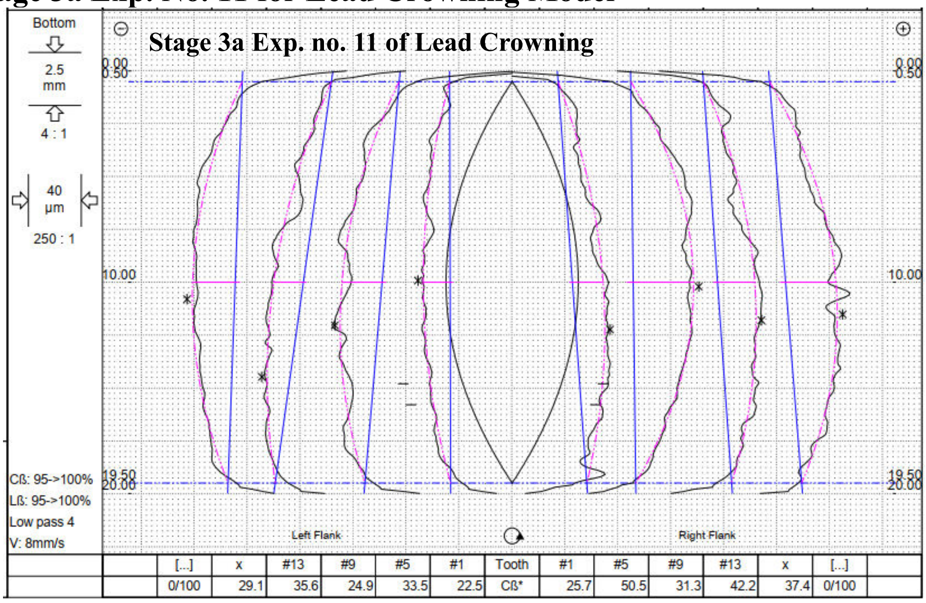

- **Stage 3a Exp. No. 12 for Lead Crowning Model**

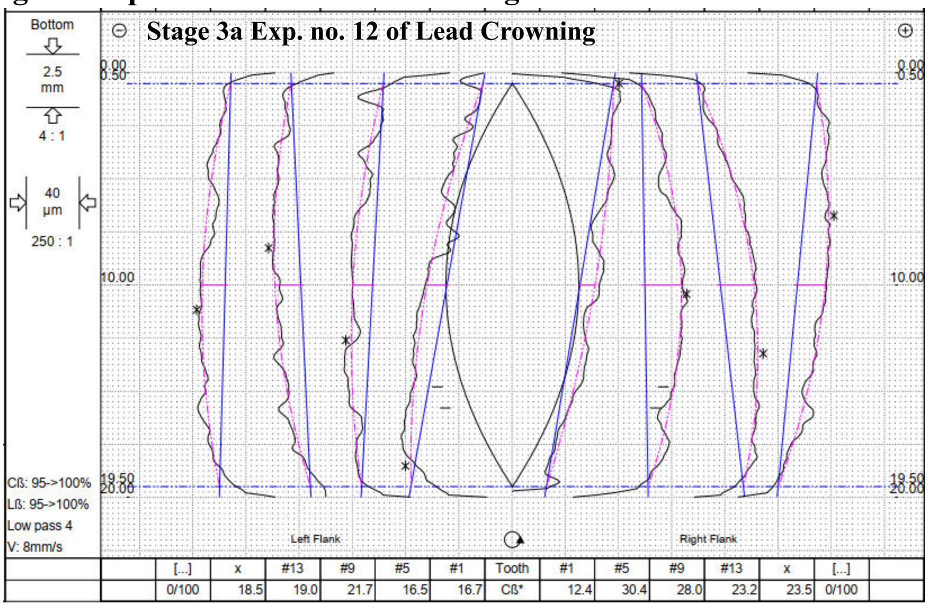

B5: For Effects of PED Process Parameters on Profile Crowning

- **Stage 3a Exp. No. 1 for Profile Crowning**

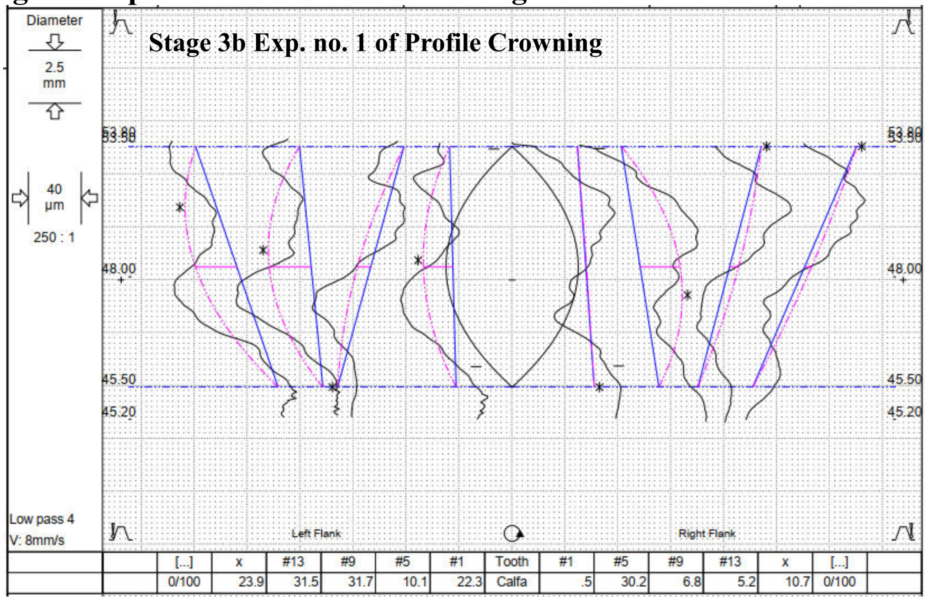

- **Stage 3a Exp. No. 2 for Profile Crowning**

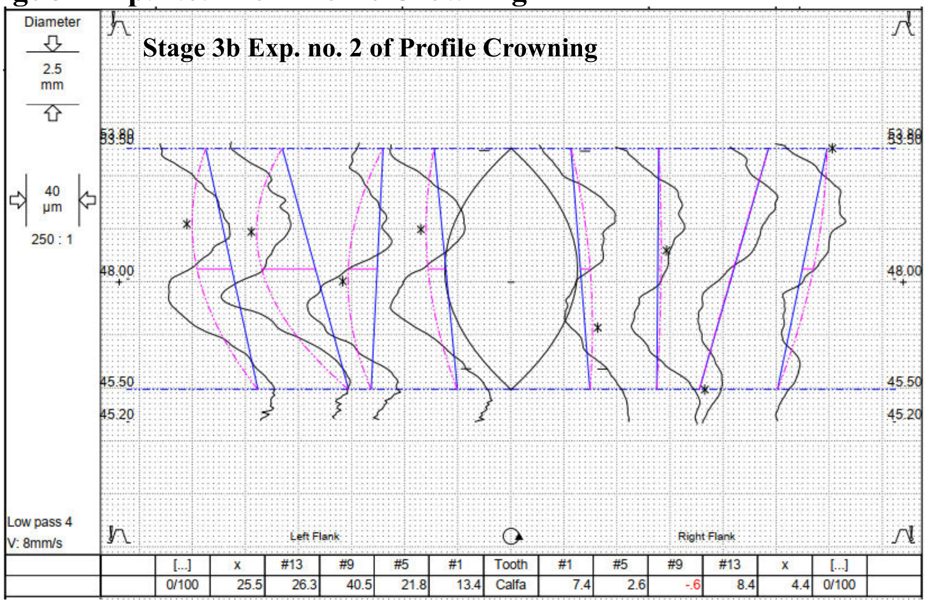

- **Stage 3a Exp. No. 3 for Profile Crowning**

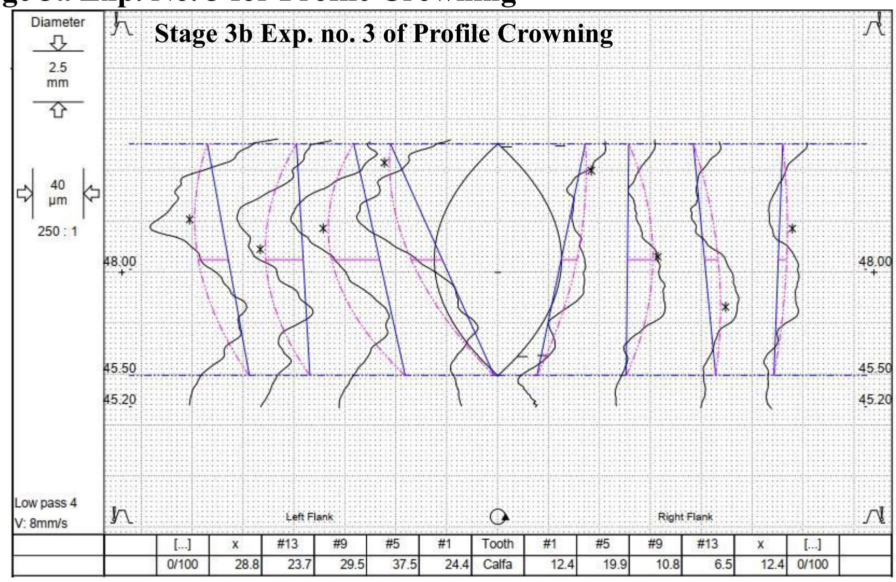

- **Stage 3a Exp. No. 4 for Profile Crowning**

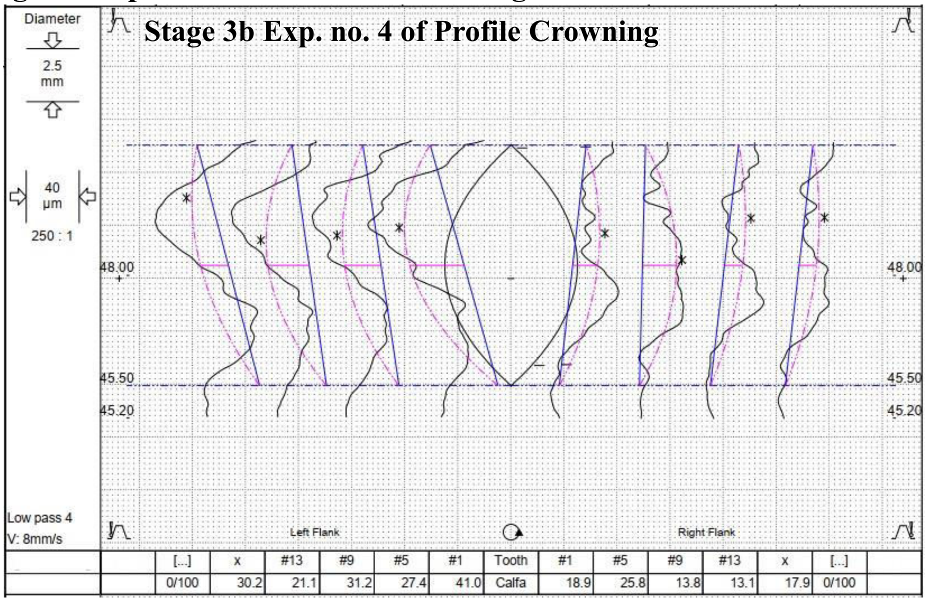

- **Stage 3a Exp. No. 5 for Profile Crowning**

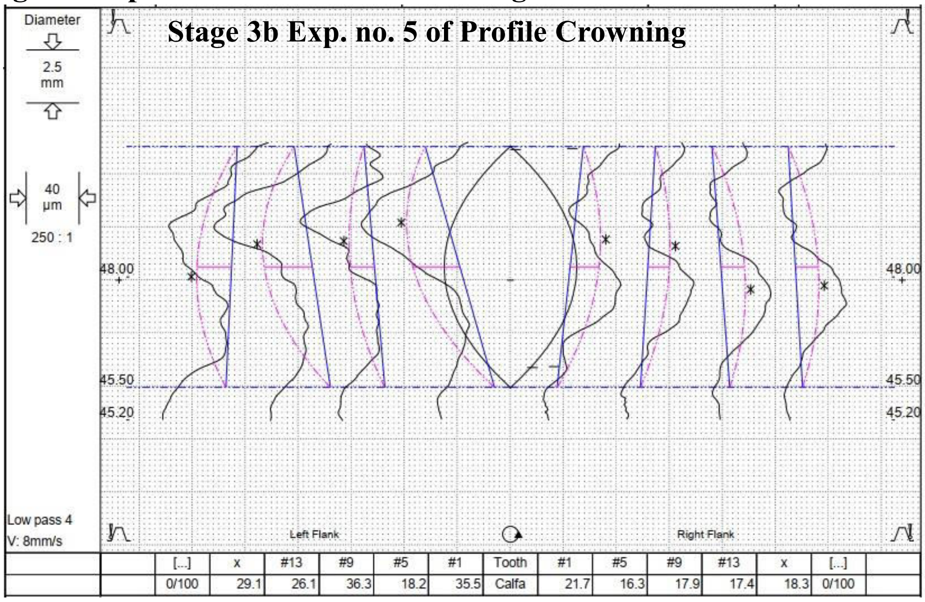

- **Stage 3a Exp. No. 6 for Profile Crowning**

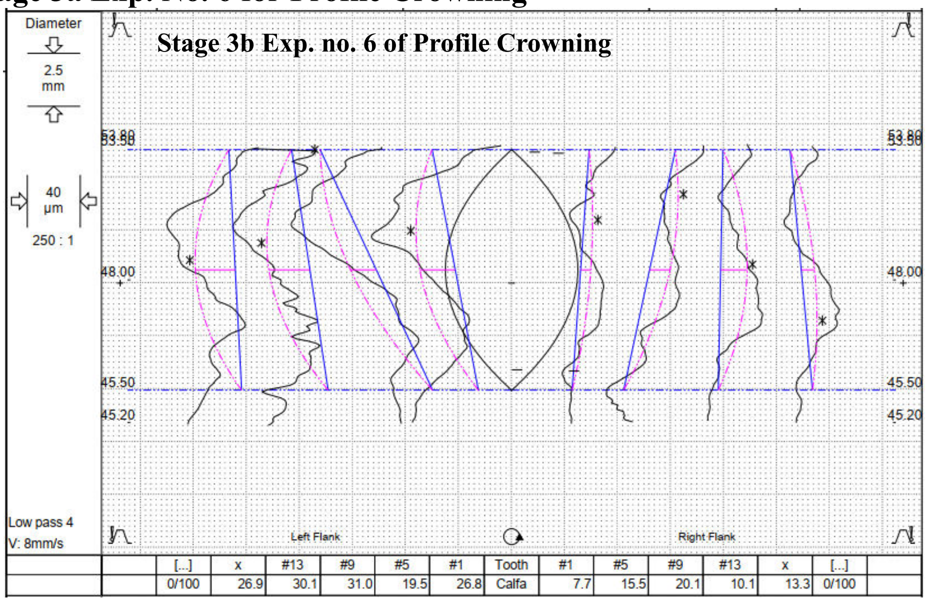

- **Stage 3a Exp. No. 7 for Profile Crowning**

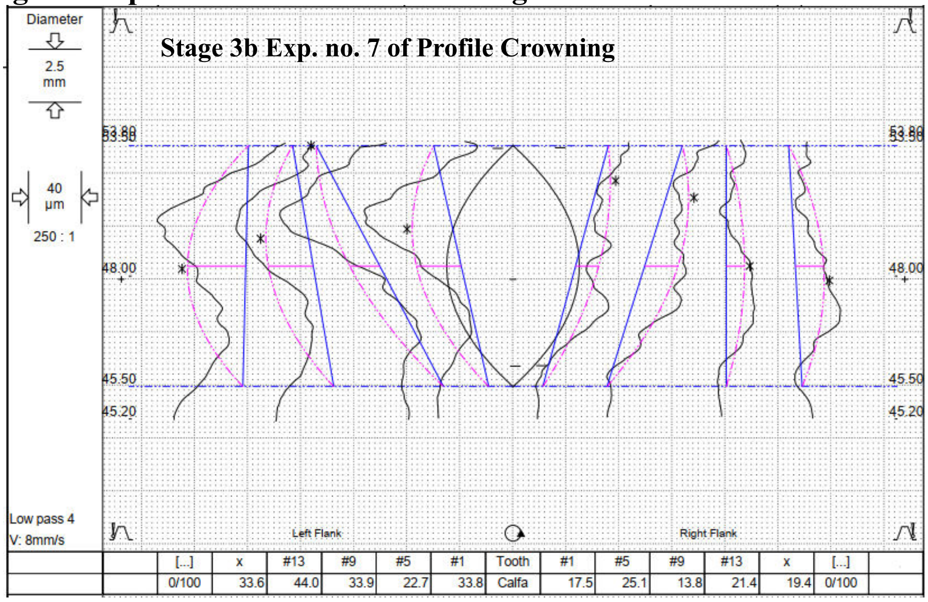

- **Stage 3a Exp. No. 8 for Profile Crowning**

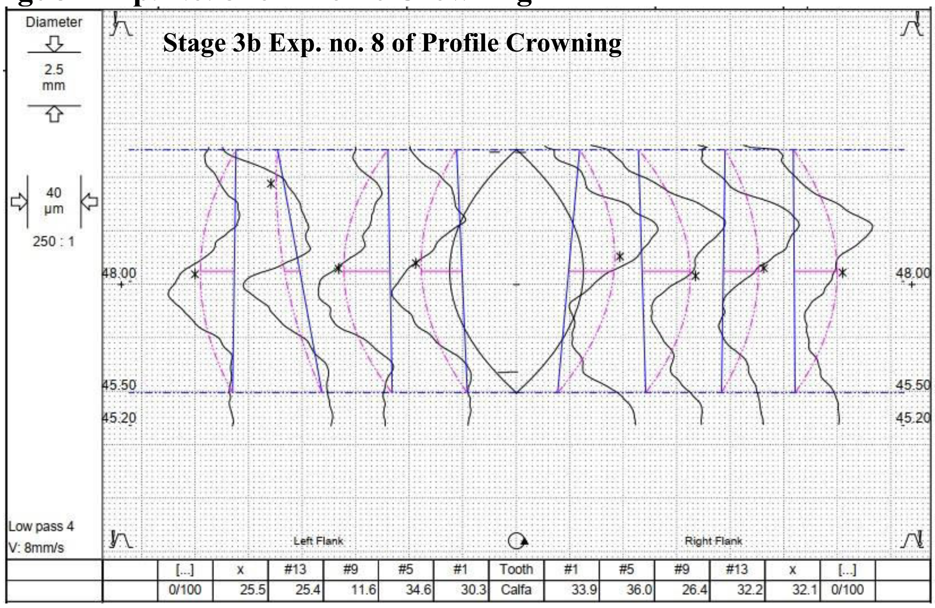

- **Stage 3a Exp. No. 9 for Profile Crowning**

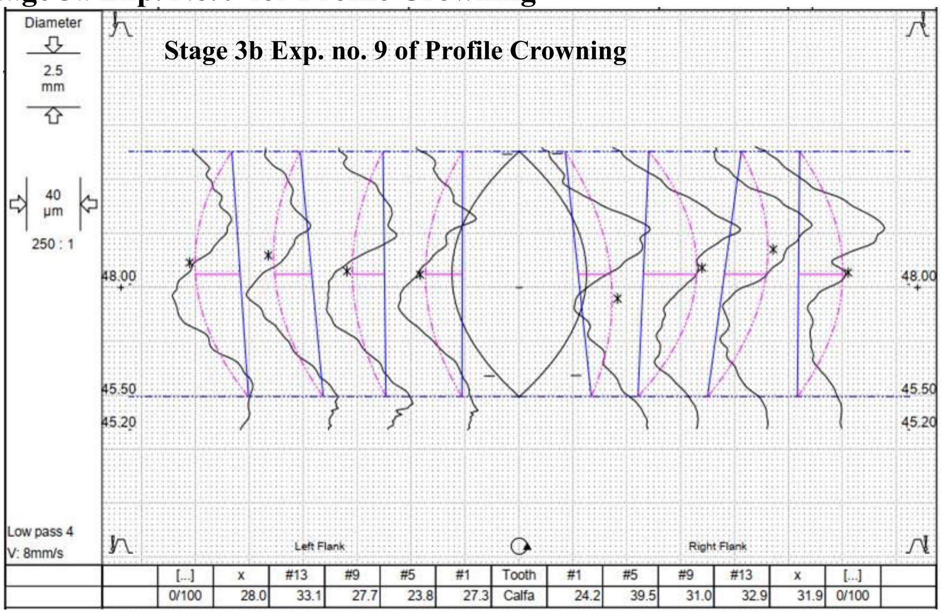

- **Stage 3a Exp. No. 10 for Profile Crowning**

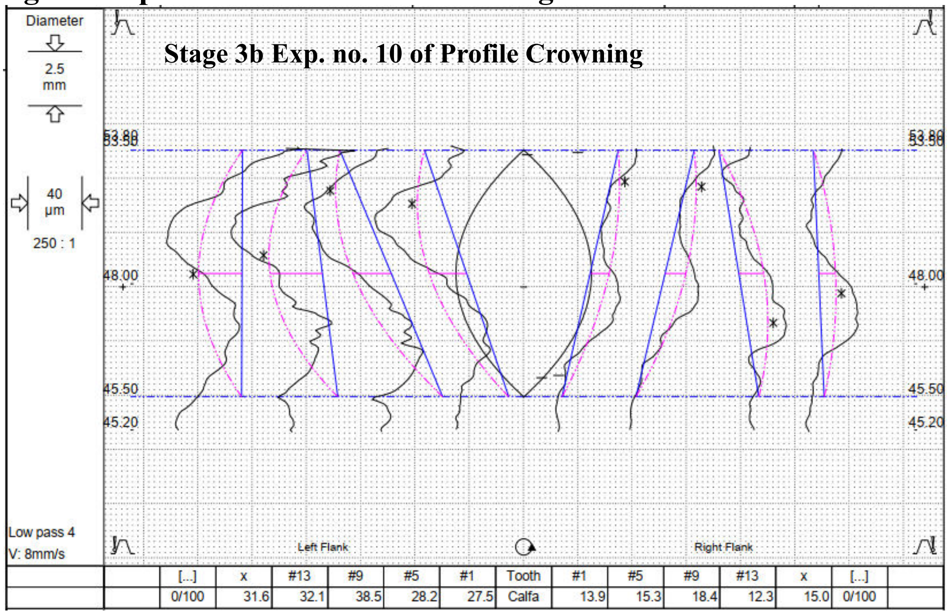

- **Stage 3a Exp. No. 11 for Profile Crowning**

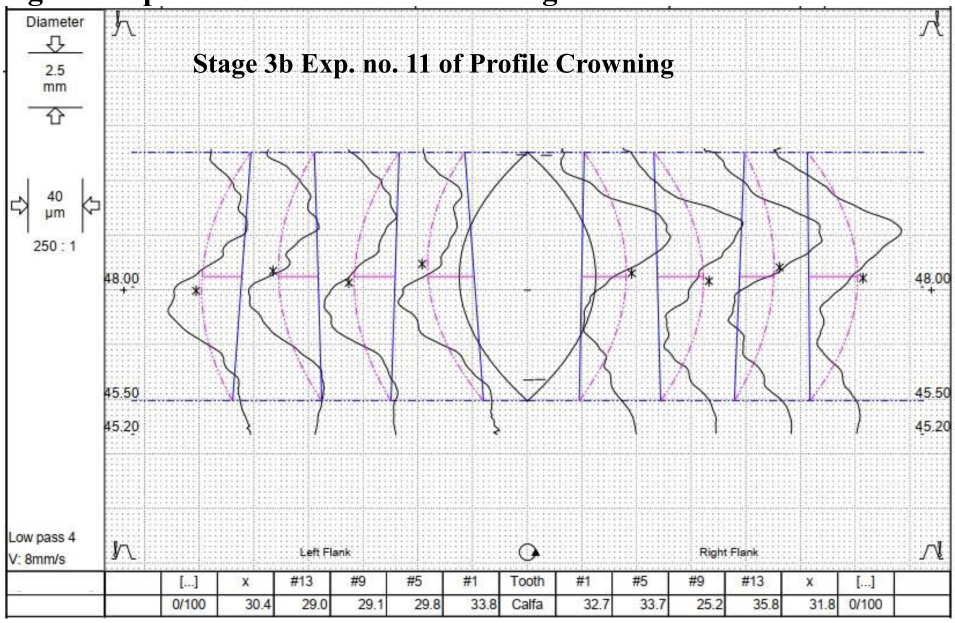

- **Stage 3a Exp. No. 12 for Profile Crowning**

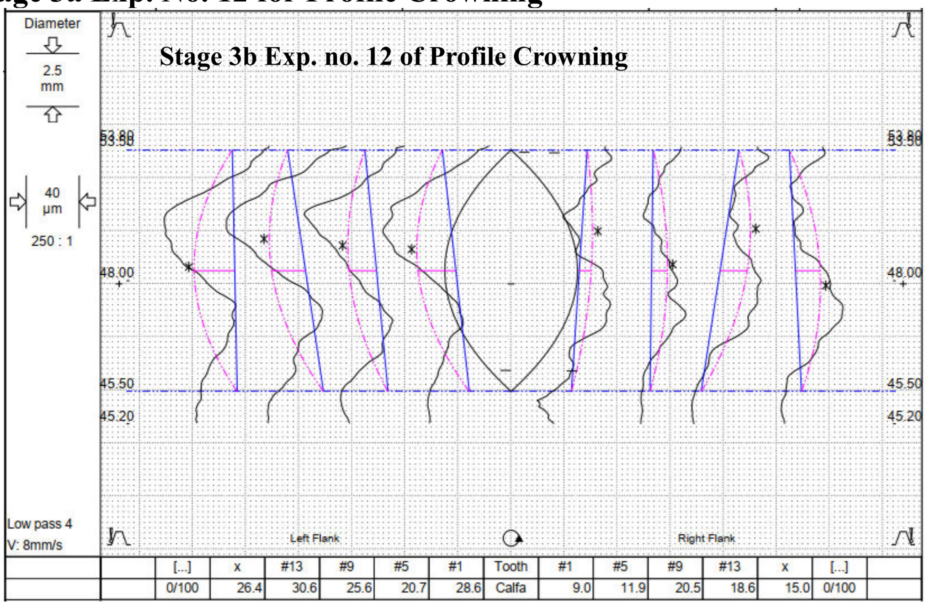

B6: For Effects of Workpiece Gear Material Hardness

- **For Tip relief**

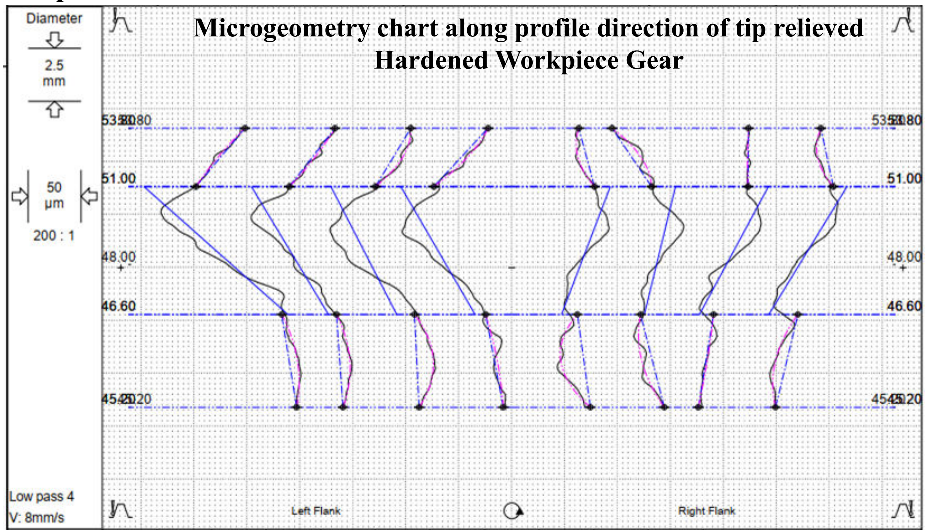

	[...]	x	#13	#9	#5	#1	Tooth	#1	#5	#9	#13	x	[...]
	0/100	83.2	95.6	79.0	75.4	82.7	Ctip	29.7	59.9	18.8	24.7	33.3	0/100

- **For Root Relief**

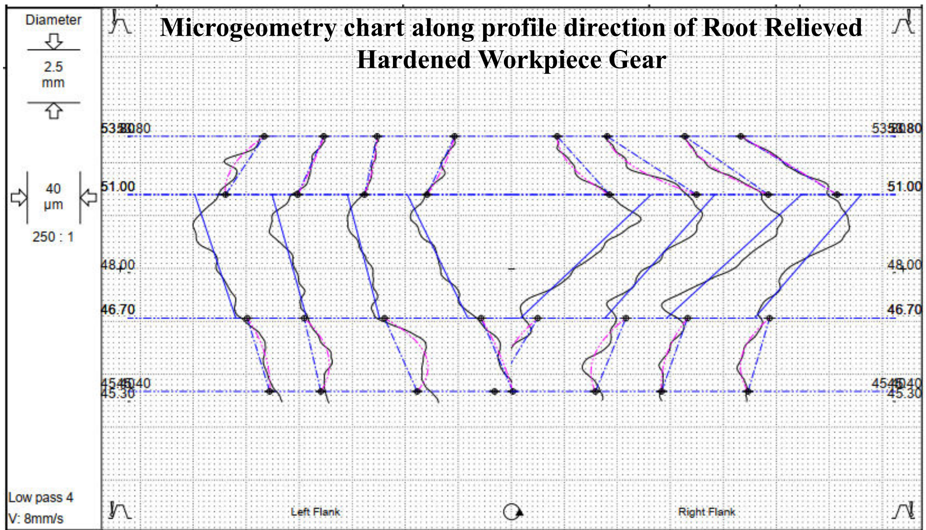

	[...]	x	#13	#9	#5	#1	Tooth	#1	#5	#9	#13	x	[...]
	0/100	24.7	25.6	10.7	28.4	34.0	Croot	19.4	7.1	3.6	5.0	8.8	0/100

- **For End Relief**

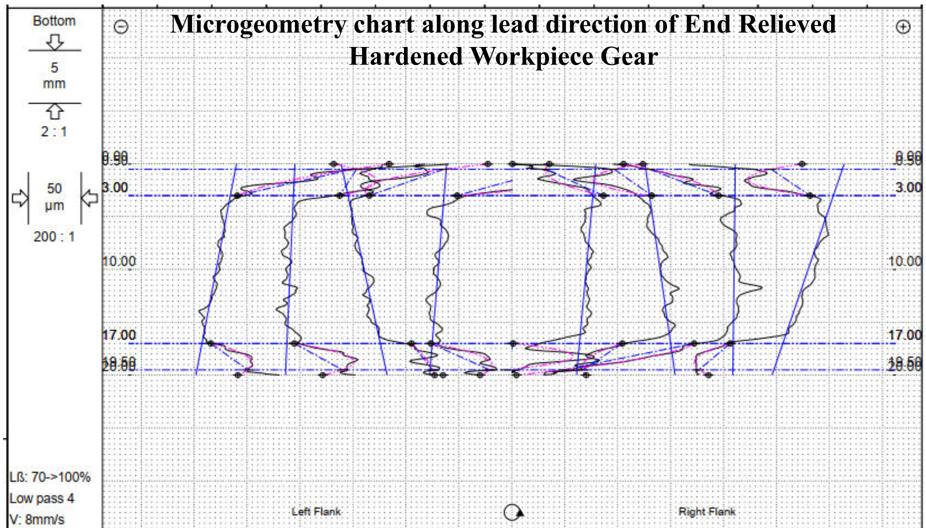

	[...]	x	#13	#9	#5	#1	Tooth	#1	#5	#9	#13	x	[...]
	0/100	96.3	150.1	38.0	132.2	64.8	Cbttm	41.2	6.4	105.3	29.5	45.6	0/100
	0/100	41.1	33.9	33.9	51.3	45.2	Ctop	128.9	79.8	205.0	70.3	121.0	0/100

- **For Lead Crowning**

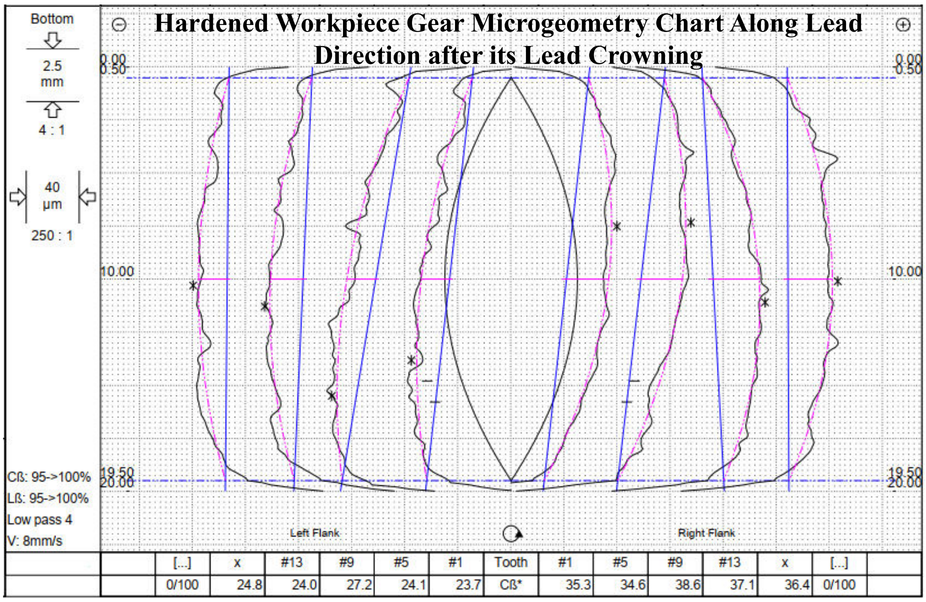

- **For Profile Crowning**

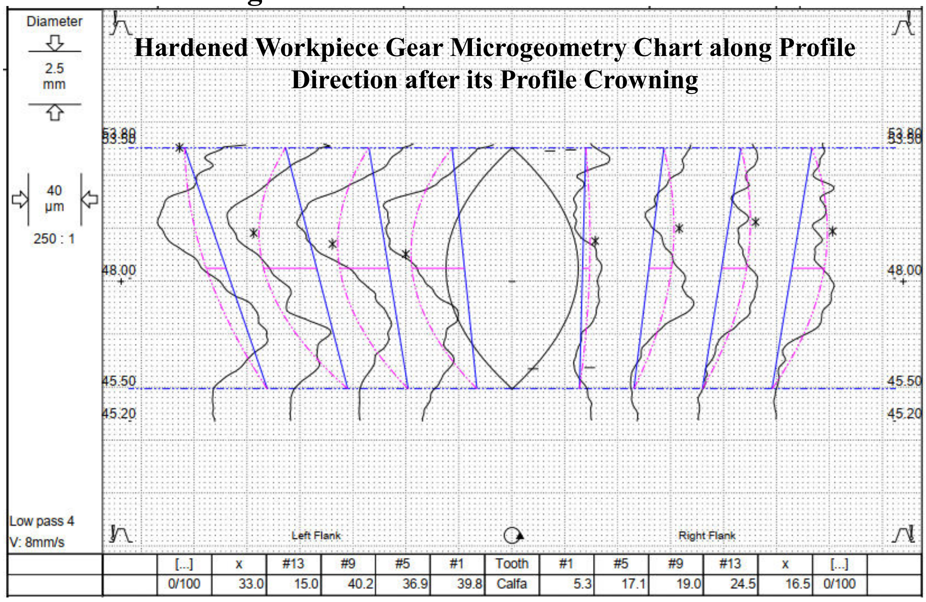

Appendix-C: Details of the Equipment Used in Evaluation of the Responses

- **CNC Gear Metrology Machine (Gear Research LAB, IIT Indore)**

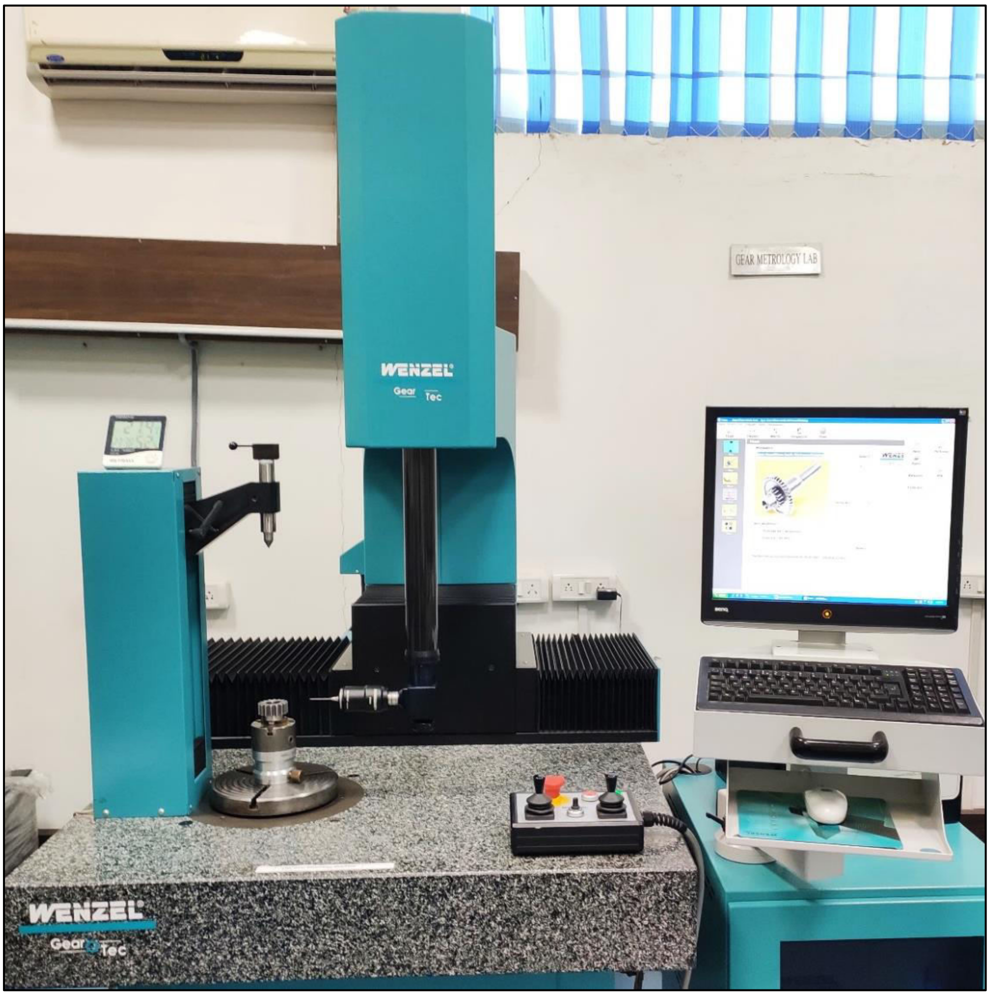

Model	SmartGear 500
Make	WenzelTec Germany
Diameter of work-piece minimum/maximum	5-270 mm
Internal Gear Diameter	> 12 mm
Module range minimum/maximum	0.4-15 mm
Helix angle	< 90°
ISO 10360-2 accuracy for 3D measurement from	$MPE_e = 4.5+L/250$ µm
	$MPE_{thp} = 5.0$ µm
Measurable face width maximum	300 mm
Temperature range	20°C +5k, -3k
Transverse Distance	500 mm
	450 mm
	400 mm
Table diameter	L200 mm

- **3D Surface Roughness cum Contour Tracer (Gear Research LAB, IIT Indore)**

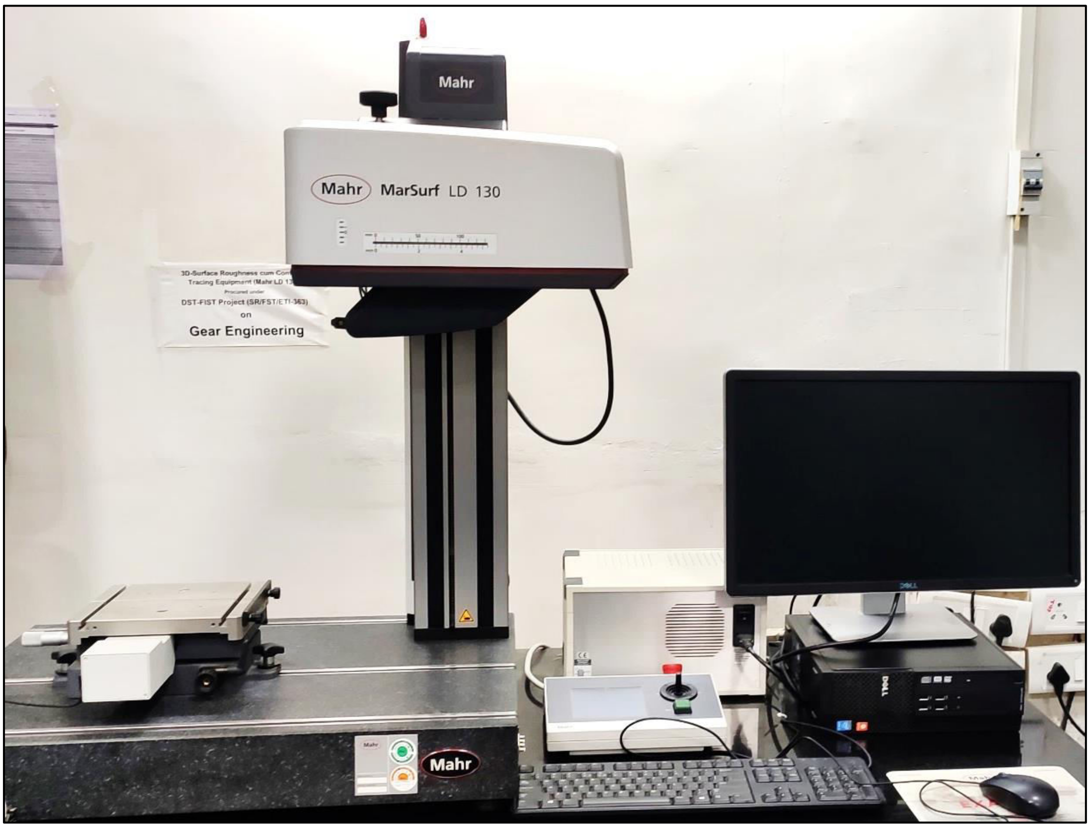

Make	Mahr GmbH
Model	MarSurf LD 130
Resolution	0.8 nm
Positioning speed	0.02 mm/s to 200 mm/s
Measuring speed	0.02 mm/s to 10 mm/s; for roughness measurements 0.1 mm/s to 0.5 mm/s is recommended
Measuring range (mm)	13 mm (100 mm probe arm) 26 mm (200 mm probe arm
Traversing lengths	0.1 mm - 130 mm
Measuring force (N)	0.5 mN to 30 mN, software-adjustable

- **Scanning Electron Microscope (Sophisticated Instrument Centre, IIT Indore)**

Make	Carl Zeiss NTS GmbH, Germany
Model	SUPRA 55
Resolution	1.0 nm @ 15 kV
	1.7 nm @ 1 kV
	4.0 nm @ 0.1 kV
Acceleration Voltage	0.1 - 30 kV
Magnification	12x - 900,000 x
Stages	5-Axes Motorised Eucentric Specimen Stage X = 130 mm, Y = 130mm, Z = 50mm, T = -3 to +70°, R = 360° (continuous)
Standard Detectors	High efficiency In-lens detector Everhart-Thornley Secondary Electron Detector

- **Noise and Vibration Analyzer (Gear Research LAB, IIT Indore)**

Make	OROS, Grenoble, France
Model	OR 35
No. of channel	4
Software	NV Gate 9.0, 3-series
Acquisition data size	24 bit
Input range of signal voltage	± 10 volts

- **Accelerometer**

Make	PCB Pizotronics	
Model	356A16	
Sensitivity	X: 10.52 mV/m/s^2	
	Y: 10.57 mV/m/s^2	
	Z: 10.51 mV/m/s^2	

- **Microphone**

Make	Microtech Gefell GmbH
Model	MV210
Sensitivity	42.9 mv/Pa

Microhardness Tester (Solid Mechanics LAB, IIT Indore)

Make	Walter Uhl techn. Mikroskopie GmbH
Model	UHL-VMH-002
Load range	50 grams – 1000 grams
Dwell time	5-99 second
Stage size	135 x 135 mm
Type of Indenter:	Diamond square base hexagonal pyramid

Appendix-D: Arduino Code for Single Flank Roll Testing

```
//Encoder pins
const int encoderPinA = 2;
const int encoderPinB = 3;
const int encoderPinAbar = 4;
const int encoderPinBbar = 5;
const int encoder2PinA = 6;
const int encoder2PinB = 7;
const int encoder2PinAbar = 8;
const int encoder2PinBbar = 9;

//The number of pulses produced by the encoder within a revolution.
const float PPR = 8192.0;
//When using 2X encoding the value is '2'. In this code 4X encoding is 4
used.
const float decodeNumber = 4.0;
//record the cuurent number of pulses received
volatile float currentPosition = 0.0;
volatile float currentPosition2 = 0.0;

float rotationalAngle = 0.0;
float rotationalAngle2 = 0.0;

void setup() {
  Serial.begin (57600);
  Serial.println("CLEARDATA");
  pinMode (encoderPinA, INPUT_PULLUP);
  pinMode (encoderPinB, INPUT_PULLUP);
  pinMode (encoderPinAbar, INPUT_PULLUP);
  pinMode (encoderPinBbar, INPUT_PULLUP);
  pinMode (encoder2PinA, INPUT_PULLUP);
  pinMode (encoder2PinB, INPUT_PULLUP);
  pinMode (encoder2PinAbar, INPUT_PULLUP);
  pinMode (encoder2PinBbar, INPUT_PULLUP);
  attachInterrupt (digitalPinToInterrupt (encoderPinA), doEncoderA,
CHANGE);
  attachInterrupt (digitalPinToInterrupt (encoderPinB), doEncoderB,
CHANGE);
  attachInterrupt (digitalPinToInterrupt (encoder2PinA), doEncoder2A,
CHANGE);
  attachInterrupt (digitalPinToInterrupt (encoder2PinB), doEncoder2B,
CHANGE);
}
void loop() {
  rotationalAngle = (360.0*currentPosition)/(PPR*decodeNumber);
  rotationalAngle2 = (360.0*currentPosition2)/(PPR*decodeNumber);

  Serial.print(rotationalAngle,6);//upto 6 decimal place
  Serial.print(";");
  Serial.print(currentPosition);
  Serial.print(";");
  Serial.print(rotationalAngle2,6);
  Serial.print(";");
  Serial.println(currentPosition2);
  delay(0);
}

void doEncoderA()
{
  if (digitalRead(encoderPinA) != digitalRead(encoderPinAbar))
  {if (digitalRead(encoderPinA) != digitalRead(encoderPinB))
  {
    currentPosition++;
```

```
  }
  else
  {
    currentPosition--;
  }
  }
  else
  {
  }
  }
void doEncoderB()
{
   if (digitalRead(encoderPinB) != digitalRead(encoderPinBbar))
   {
  if (digitalRead(encoderPinA) == digitalRead(encoderPinB))
  {
    currentPosition++;
  }
  else
  {
    currentPosition--;
  }
   }
  else
  {
  }
   }
void doEncoder2A()
{
 if (digitalRead(encoder2PinA) != digitalRead(encoder2PinAbar))
  {if (digitalRead(encoder2PinA) != digitalRead(encoder2PinB))
  {
    currentPosition2++;
  }
  else
  {
    currentPosition2--;
  }
  }
  else
  {
  }
 }
void doEncoder2B()
{
   if (digitalRead(encoder2PinB) != digitalRead(encoder2PinBbar))
   {
  if (digitalRead(encoder2PinA) == digitalRead(encoder2PinB))
  {
    currentPosition2++;
  }
  else
  {
    currentPosition2--;
  }
   }
  else
  {
  }
   }
```